(12)

PREDICTION OF THE AERODYNAMIC CHARACTERISTICS OF CRUCIFORM MISSILES INCLUDING EFFECTS OF ROLL ANGLE AND CONTROL DEFLECTION

by

Daniel J. Lesieutre
Michael R. Mendenhall
Susana M. Nazario
Michael J. Hemsch

NIELSEN ENGINEERING AND RESEARCH, INC.

OFFICES: 510 CLYDE AVENUE / MOUNTAIN VIEW, CALIFORNIA 94043 / TELEPHONE (415) 968-9457

COPY NO. 33

(12)

PREDICTION OF THE AERODYNAMIC CHARACTERISTICS OF CRUCIFORM MISSILES INCLUDING EFFECTS OF ROLL ANGLE AND CONTROL DEFLECTION

by

Daniel J. Lesieutre
Michael R. Mendenhall
Susana M. Nazario
Michael J. Hemsch

NEAR TR-360

PREDICTION OF THE AERODYNAMIC CHARACTERISTICS OF CRUCIFORM MISSILES INCLUDING EFFECTS OF ROLL ANGLE AND CONTROL DEFLECTION

Daniel J. Lesieutre
Michael R. Mendenhall
Susana M. Nazario
Nielsen Engineering & Research, Inc.
Mountain View, CA 94043-2287

and

Michael J. Hemsch
PRC Kentron, Inc.
Hampton, VA 23666

1 August 1986

Final Report for Period 6 June 1980 - 30 May 1986

Prepared for
OFFICE OF NAVAL RESEARCH
Arlington, VA 22217

UNCLASSIFIED

SECURITY CLASSIFICATION OF THIS PAGE

REPORT DOCUMENTATION PAGE

1a. REPORT SECURITY CLASSIFICATION UNCLASSIFIED	1b. RESTRICTIVE MARKINGS
2a. SECURITY CLASSIFICATION AUTHORITY	3. DISTRIBUTION/AVAILABILITY OF REPORT Approved for public release; distribution unlimited
2b. DECLASSIFICATION/DOWNGRADING SCHEDULE	
4. PERFORMING ORGANIZATION REPORT NUMBER(S) NEAR TR-360	5. MONITORING ORGANIZATION REPORT NUMBER(S)
6a. NAME OF PERFORMING ORGANIZATION Nielsen Engineering & Research, Inc. 6b. OFFICE SYMBOL (If applicable)	7a. NAME OF MONITORING ORGANIZATION Office of Naval Research
6c. ADDRESS (City, State, and ZIP Code) 510 Clyde Avenue Mountain View, CA 94043-2287	7b. ADDRESS (City, State, and ZIP Code) 800 North Quincy Street Arlington, VA 22217-5000
8a. NAME OF FUNDING/SPONSORING ORGANIZATION 8b. OFFICE SYMBOL (If applicable)	9. PROCUREMENT INSTRUMENT IDENTIFICATION NUMBER N00014-80-C-0700
8c. ADDRESS (City, State, and ZIP Code)	10. SOURCE OF FUNDING NUMBERS PROGRAM ELEMENT NO. / PROJECT NO. / TASK NO. / WORK UNIT ACCESSION NO.

11. TITLE (Include Security Classification)
"Prediction of the Aerodynamic Characteristics of Cruciform Missiles Including Effects of Roll Angle and Control Deflection"(U)

12 PERSONAL AUTHOR(S) Daniel J. Lesieutre, Michael R. Mendenhall, Susana M. Nazario, and Michael J. Hemsch(PRC Kentron)

13a. TYPE OF REPORT	13b. TIME COVERED	14. DATE OF REPORT (Year, Month, Day)	15. PAGE COUNT
Final Report	FROM 80/06/16 TO 86/05/30	86 August 1	172 pages

16. SUPPLEMENTARY NOTATION
A missile-fin data

17 COSATI CODES			18. SUBJECT TERMS (Continue on reverse if necessary and identify by block number)
FIELD	GROUP	SUB-GROUP	Missile Aerodynamics; ~~Guided Missiles~~; Aerodynamic Empirical Techniques; Missile Aerodynamic Loads; Wind Tunnel Tests; Computer Codes,
20	04		
16	04		

19. ABSTRACT (Continue on reverse if necessary and identify by block number)

Under a tri-service cooperative effort sponsored by the Air Force, Army, and Navy with extensive participation by NASA, a missile-fin data base for a wide range of configurations and flow conditions was obtained. These data were incorporated into an engineering method for predicting the aerodynamic characteristics of typical cruciform configurations over a wide range of angles of attack, fin deflection angles, roll angles, and Mach numbers. This ~~final~~ report documents the test programs, describes the new code, MISSILE 3, and presents comparisons of independent experiment and predicted results to verify the code. A user's manual for the code is included. Keywords:

20 DISTRIBUTION/AVAILABILITY OF ABSTRACT ☐ UNCLASSIFIED/UNLIMITED ☒ SAME AS RPT ☐ DTIC USERS	21 ABSTRACT SECURITY CLASSIFICATION UNCLASSIFIED
22a NAME OF RESPONSIBLE INDIVIDUAL Michael R. Mendenhall	22b TELEPHONE (Include Area Code) (415) 968-9457 / 22c. OFFICE SYMBOL

DD FORM 1473, 84 MAR — 83 APR edition may be used until exhausted. All other editions are obsolete.

SECURITY CLASSIFICATION OF THIS PAGE

UNCLASSIFIED

A

TABLE OF CONTENTS

TABLE OF CONTENTS (Concluded)

SUMMARY

Under a tri-service cooperative effort sponsored by the Air Force, Army, and Navy with extensive participation by NASA, a missile-fin data base for a wide range of configurations and flow conditions was obtained. These data were incorporated into an engineering method for predicting the aerodynamic characteristics of typical cruciform missile configurations over a wide range of angles of attack, fin deflection angles, roll angles, and Mach numbers. This final report documents the test programs, describes the new code MISSILE 3, and presents comparisons of independent experiment and predicted results to verify the code. A user's manual for the code is included.

FOREWORD

This is the final technical report on the work performed under Contract N00014-80-C-0700 from 16 June 1980 to 30 July 1986. Dr. Robert Whitehead of the Office of Naval Research acted as the Scientific Officer for this effort and his excellent work in this capacity contributed significantly to the success of the program. A number of other individuals and their organizations played an important part in the success of this investigation, and it is important to the authors that these people be recognized. In alphabetical order, they are:

Dr. Donald C. Daniel - AFATL
Mr. Ramond A. Deep - Army MICOM
Mr. Vernon O. Hoehne - AFWAL
Mr. Dale E. Hutchins - NAVAIR
Mr. Charles M. Jackson, Jr. - NASA/Langley Research Center
Dr. Lionel Pasiuk - NAVSEA
Mr. Wallace C. Sawyer - NASA/Langley Research Center
Dr. Leon H. Schindel - NSWC
Mr. Edward Sears - AFATL
Mr. David S. Shaw - NASA/Langley Research Center
Dr. Donald J. Spring - Army MICOM
Mr. William C. Volz - NAVAIR retired
Mr. W. D. Washington - Army MICOM

Sincere thanks go to the wind tunnel staff at both the NASA Ames and Langley Research Centers for their cooperation and help during the test program.

A special acknowledgement is due Dr. Jack N. Nielsen, Chief Scientist at the NASA/Ames Research Center. He conceived the idea of a cooperative program involving the three services and NASA, brought together the key individuals necessary to make it happen, and directed the work in its early stages while he was President of NEAR, Inc.

It is also noteworthy that Dr. Michael J. Hemsch, co-author, was intimately involved with the succesful conduct of the work while at NEAR, Inc., and, even after moving to PRC Kentron, he played an essential role in the completion of the effort.

Michael R. Mendenhall
August 1, 1986

INTRODUCTION

Under Office of Naval Research Contract No. N00014-80-C-0700, Nielsen Engineering & Research, Inc., (NEAR) conducted an investigation to obtain an extensive missile-fin data base for use in broadly applicable engineering prediction programs for calculating the aerodynamic characteristics of body-tail and canard-body-tail missiles. The data base was incorporated into a specific computer program called PROGRAM MISSILE 3 which is valid for angles of attack up to 45°, arbitrary roll angles, fin deflection angles between -40° and 40°, Mach numbers between 0.6 and 4.5, and fin aspect ratios between 0.25 and 4.0.

The investigation reported herein is a tri-services cooperative effort sponsored by the Air Force, Army, and Navy with extensive participation by NASA/Ames Research Center and NASA/Langley Research Center. The first year's work involved: (1) selection of the test model design, test parameters and testing sequence, (2) preliminary investigation of the optimum approach for data handling, that is, preparing the data for and incorporating it into PROGRAM MISSILE 3, and (3) revising the equivalent angle-of-attack formulation (Refs. 1 and 2) to incorporate the new fin deflection data base. The results of that work are described in the first year's report (Ref. 3). The second year's work consisted of (1) support of the ongoing wind tunnel tests, (2) preparation for processing the data to be incorporated into the data base, (3) continued improvement of the methods used in MISSILE 3, and (4) continued code development. The results of that work are described in the second year's report (Ref. 4). The third year's work continued the activities of the second year and are contained in the third year report (Ref. 5). The fourth year's work consisted of organizing the experimental data base, implementing a revised equivalent angle of attack formulation, and incorporating both of these into the computer code MISSILE 3. This report summarizes the previous work and presents the new code MISSILE 3.

An engineering data base method for performance prediction and preliminary design of missiles with cruciform fin sections has been developed. The method uses a newly available systematic data base which covers a Mach number range from 0.6 to 4.5 and fin aspect ratios from 0.25 to 4.0, angles of attack up to 45°, and arbitrary roll angles. It employs the equivalent angle of attack concept to include the effects of vorticity and geometric scaling. The equivalent angle of attack method has been modified somewhat from that used in the previous MISSILE programs described in References 1 and 2.

The report is divided into two major parts: Experimental Program and Technical Approach, and a User's Manual. The Experimental Program and Technical Approach sections describe the experimental tests, the data base, the equivalent angle of attack methodology, and the fin and body vortex models. It is not the purpose of this report to present and document the entire tri-service data base. The incorporation of the data base into the engineering prediction method is the primary objective. The User's Manual section provides instruction for the use of the FORTRAN computer code MISLE3. This includes a program description, program limitations, error messages, input preparation, and sample cases. The report concludes with comparisons to independent experimental data, conclusions and recommendations.

OVERVIEW OF EXPERIMENTAL PROGRAM

The overall objective of the test program was to obtain a high quality systematic fin force and moment data base for use in high angle of attack missile aerodynamics computer programs based on engineering methods. The data obtained fall into two categories: (1) fin loads without fin deflection for all fins in the data base (stability data), and (2) fin loads with fin deflection for a control fin set (control data). The model design and test conditions were based on use of Langley Remote Control Missile Roll Rig and are intended to reflect as completely as possible the range of flight conditions and fin designs employed by modern high-performance missiles. The Langley model is 2.5 inches in diameter and allows independent, remote control of four control surfaces and model roll angle. By interchanging modular components, canard, wing, or tail control may be used. For the tests, a 0.25 inch shell was added to the body to accommodate a three-component balance and associated wiring for each of the four fins. Hence, the diameter of the cylindrical portion of the body was 3.0 inches. All of the data obtained for the data base was for a body-tail configuration.

Multiple tunnel entries were made. Intermediate and high Mach number (2.5 - 4.5) tests were conducted in the NASA/Langley Unitary Plan Tunnel, and low and intermediate Mach number (0.6 - 2.0) tests were conducted in the 6- by 6-foot Supersonic Tunnel at NASA/Ames. These tests were performed between 1982 and 1984.

GENERAL DESCRIPTION OF MISSILE 3 CODE

The range of parameters for MISSILE 3 are described in this section. The Mach number range of the data base is from 0.6 to 4.5. Test Mach numbers of 0.6, 0.8, 0.9, and 1.2 provide detailed loads for the transonic speed regime. This greatly improves the predictions in the transonic regime compared to previous MISSILE programs (Refs. 1 and 2) which contained data at M_∞ = 0.8 and 1.2. The supersonic Mach numbers in the data base are: 1.5, 2.0, 2.5, 3.0, 3.5, and 4.5.

The body angle of attack range is $0° < \alpha_c < 45°$. Test angles of attack were: $\alpha_c = 0, 2, 5, 10, \ldots, 40, 45°$. The fin control deflection angles varied from -40° to 40° in ten-degree increments. The body roll angle range is 0° to 90°. The data base contains loads for $-90° < \phi_f < 90°$ in ten-degree increments, where ϕ_f is the fin orientation angle.

The fin aspect ratio range* of the data base is 0.25 to 4; this greatly extends the range allowed by previous MISSILE codes. The test fins had aspect ratios of 0.25, 0.5, 1, 2, and 4, and the taper ratio range is from 0 to 1. The fins with aspect ratios of 1, 2 and 4 were deflectable. Trailing edge sweep and/or forward swept leading edges are not permitted. The test fins had body radius to semispan ratios (a/s_m) of 0.5. The method and the data base consider cruciform sections with identical fins only.

Figure 1 shows the angle of attack, aspect ratio, and Mach number range of the systematic data base, and the range of parameters allowed by MISSILE 3 are summarized below:

$0.6 < M_\infty < 4.5$
$0^0 < \alpha_c < 45^0$
$0^0 < \phi < 90°$
$0.25 < AR < 4.0$
$0.0 < \lambda < 1.0$
4 fins per section
all fins in a section are identical
symmetrical airfoil sections only
no fin trailing edge sweep
axisymmetric bodies

TABLE 1. Range of Parameters

*Fin aspect ratio is the aspect ratio of two fins joined at the rootchord.

The data base used for MISSILE 3 is much larger than that used in MISSILE 2A. The MISSILE 2A data base contains experimental data for Mach numbers from 0.8 to 3.0 and fin aspect ratios from 0.5 to 2.0 (AR to 3.5 for $M_\infty < 1.2$). Descriptions and development of the MISSILE series analysis methods can be found in References 1, 2, 6, 7, and 8.

The equivalent angle-of-attack concept and the data base used in MISSILE 3 predict missile performance similar to MISSILE 2A. However, the range of applicability is much larger, so performance can be investigated over a larger operating range. MISSILE 3 allows multiple Mach number cases in a single run, a convenience not available with MISSILE 2A. MISSILE 3 has also proven to be more economical than MISSILE 2A, even though a larger data base is included. MISSILE 3 has been compared to independent experimental data for several geometries and operating conditions, and it has provided satisfactory results. Further comparisons with experiment are needed to determine the full range of operation of the method and to locate areas which require further improvement.

OVERVIEW OF THE ENGINEERING METHOD

This section of the report describes the data base and methodology used by MISSILE 3. The missile configurations allowed by MISSILE 3 are cruciform canard-body-tail, canard-body, and body-tail configurations. The missile is divided into four sections for modeling purposes; the nose and forebody, the canard section, the afterbody, and the tail section as shown in Figure 2. For a body-tail configuration, everything forward of the fin section is the forebody.

The coordinate system and fin numbering system used by MISSILE 3 are shown in Figure 3. The x-axis is along the body centerline and positive aft, and the z-axis is in the wind plane and normal to the body axis (positive up). The y-axis is perpendicular to the plane containing the body axis and the wind vector and is positive to the right looking forward. The fins are numbered clockwise, viewed from the rear, with fin 1 always in the first quadrant; this is opposite to previous MISSILE codes which numbers the fins counterclockwise. The normal force for fins 1 and 3 is positive up and to the left, and the normal force for fins 2 and 4 is positive up and to the right. (See Figure 3(c).) Fin deflections are positive when they tend to increase the fin incidence, and hinge moments are positive when they tend to rotate the fins so as to increase the fin incidence. Fin bending moments for fins 1 and 2 are positive when they give positive contributions to the rolling moment, and bending moments for fins 3 and 4 are positive when they give negative contributions to the rolling moment.

Data Base Description

The data base consists of fin data and wing-alone data. The fin data contain normal-force coefficient, axial center-of-pressure, and spanwise center-of-pressure information with and without fin deflections for fins with aspect ratios of 0.25 to 4. The fin data base is divided into stability (no control deflections) and control data, and each of these sections are further divided into normal-force coefficient and center-of-pressure locations. The wing-alone data contain normal-force coefficient information as a function of angle of attack and Mach number. The fin data base is discussed first, followed by the wing-alone data base.

Fin Stability Data Base

The data for the fin data base come from tests performed at NASA Ames and NASA Langley Research Centers as part of the Tri-Services effort (Ref. 9). The forces and moments for the fins depicted in Figure 4 were obtained by force balance measurements. All test fins have body radius to fin semi-span ratios, a/s_m, of 0.5. These tests provide normal-force, hinge-moment, and bending-moment coefficients for Mach numbers between 0.6 and 4.5, angles of attack up to 45°, and roll angles from -90° to 90°. The hinge-moment and bending-moment coefficients were reduced to provide the fin centers-of-pressures, $\bar{x}/C_R$ and $\bar{y}/s$. Table 2 below depicts the aspect ratio and taper ratio domain of the stability data base.

		TAPER RATIO, λ		
		0	1/2	1
Aspect Ratio	1/4	I	12	II
	1/2	31	32	33
	1	III	42	IV
	2	51	52	53
	4	V	62	VI

(oval) = region of interpolation

TABLE 2. Aspect Ratio and Taper Ratio Range of the Stability Data Base

The numbers in Table 2 are the test fin designation numbers (Fig. 4(a)), and the Roman numerals represent regions of interpolation.

The test Mach numbers are:

$$M_\infty = 0.6,\ 0.8,\ 0.9,\ 1.2,\ 1.5,\ 2.0,\ 2.5,\ 3.0,\ 3.5,\ 4.5.$$

The test angles of attack are:

$$\alpha_c = 0,\ 2,\ 5,\ 10,\ 15,\ 20,\ 25,\ 30,\ 35,\ 40,\ 45°.$$

The fin orientation angles are:

$$\phi = -90,\ -80, \ldots,\ -10,\ 0,\ 10, \ldots, 80,\ 90°.$$

Fin Normal-Force Coefficient.- The fin normal-force coefficient, CNF, is a function of aspect ratio, taper ratio, Mach number, included angle of attack, and angle of roll. Methods were developed to interpolate in these parameters to obtain specific values of $CNF(AR, \lambda, M_\infty, \alpha_c, \phi)$. For example, linear interpolation in the Mach number parameter for normal-force coefficient results in

$$CN(M_\infty) = CN(M_1) + \frac{M_\infty - M_1}{M_2 - M_1}\left[CN(M_2) - CN(M_1)\right] \qquad (1)$$

where M_1 and M_2 are the Mach numbers in the data base which enclose the desired M_∞.

Interpolation in the aspect ratio and taper ratio directions is considered separately in the six distinct regions depicted in Table 2, and the general formulas for interpolation in these regions follow.

In Region I, the value of CN is the point in the AR-λ domain which lies on the plane formed by fins 12, 31, and 32; therefore,

Region I: $0.0 < \lambda < 0.5$; $0.25 < AR < 0.50$

$$CN_I = CN32 - 2(0.5-\lambda)(CN32 - CN31) - 4(0.5-AR)(CN32-CN12) \qquad (2)$$

In Region II, the value of CN is the point in the AR-λ domain which lies on the plane formed by fins 12, 32, and 33; therefore,

Region II: $0.0 < \lambda < 0.25; \quad 0.25 < AR < 0.50$

$$CN_{II} = CN32 + 2(\lambda-0.5)(CN33-CN32) - 4(0.5-AR)(CN32-CN12) \quad (3)$$

In Region III, the value of CN is estimated first as the point in the AR-λ domain which lies on the plane formed by fins 31, 32, and 42, and secondly as the point in the AR-λ domain which lies on the plane formed by fins 42, 52, and 51. Since it is unlikely that these two planes intersect at the desired point, the interpolated value of CN is taken as an AR-weighted combination of the two estimates. This method was chosen over a three point method, as described above for Regions I and II, because it uses more information and should provide a better result. Therefore,

Region III: $0.0 < \lambda < 0.5; \quad 0.50 < AR < 2.0$

$$CN_{III} = [CN32 - 2(0.5-\lambda)(CN32-CN31) + 2(AR-0.5)(CN42-CN32)]\frac{2-AR}{1.5}$$

$$+[CN52 - 2(0.5-\lambda)(CN52-CN51) - (2-AR)(CN52-CN42)]\frac{AR-0.5}{1.5} \quad (4)$$

In Region IV, the value of CN is estimated first as the point in the AR-λ domain which lies on the plane formed by fins 32, 33, and 42, and secondly as the point which lies on the plane formed by fins 42, 52, and 53. As in Region III the interpolated value of CN is taken as an AR-weighted combination of the two estimates. Therefore, Region IV: $0.0 < \lambda < 1.0; \quad 0.50 < AR < 2.0$

$$CN_{IV} = [CN32 + 2(\lambda-0.5)(CN33-CN32) + 2(AR-0.5)(CN42-CN32)]\frac{2-AR}{1.5}$$

$$+ [CN52 + 2(\lambda-0.5)(CN53-CN52) - (2-AR)(CN52-CN42)]\frac{AR-0.5}{1.5} \quad (5)$$

In Region V, the value of CN is the point in the AR-λ domain which lies on the plane formed by fins 51, 52, and 62. Thus,

Region V: $0.0 < \lambda < 0.5; \quad 2.0 < AR < 4.0$

$$CN_V = CN52 - 2(0.5-\lambda)(CN52-CN51) + 0.5(AR-2)(CN62-CN52) \quad (6)$$

In Region VI, the value of CN is the point in the AR-λ domain which lies on the plane formed by fins 52, 53, and 62. Thus,

Region VI: $0.0 < \lambda < 1.0; \quad 2.0 < AR < 4.0$

$$CN_{VI} = CN52 + 2(\lambda-.5)(CN53-CN52) + 0.5(AR-2)(CN62-CN52) \quad (7)$$

Figure 5 illustrates representative examples of the normal-force coefficient versus angle of attack for several Mach numbers and roll angles for fin 52. Because of the overwhelming size of the data base, only limited examples are presented in this report.

Fin Center-of-Pressure.- To predict the fin hinge- and bending-moment coefficients and the missile's rolling- and pitching-moment coefficients, it is necessary to determine the axial and lateral positions of the fin center-of-pressure. When body vortex-induced effects on the loads are removed, the fin center-of-pressure locations depend primarily on the fin normal-force coefficient and therefore are insensitive to roll angle. This is discussed below. The data base is used to obtain the center-of-pressure location associated with nonvortex loads. The effects of vorticity in the flow field are added with the equivalent angle of attack.

The test results provide normal-force, hinge-moment and bending-moment coefficients for each test fin as a function of M_∞, α_c and ϕ. These data are reduced to obtain $\bar{x}/C_R$ and $\bar{y}/s$ in the following manner:

$$\frac{\bar{x}(M_\infty, \alpha_c, \phi)}{C_R} = \frac{x_{HL}}{C_R} - \frac{C_{HM}(M_\infty, \alpha_c, \phi)}{C_N(M_\infty, \alpha_c, \phi)} \tag{8}$$

$$\frac{\bar{y}(M_\infty, \alpha_c, \phi)}{s} = \frac{C_{BM}(M_\infty, \alpha_c, \phi)}{C_N(M_\infty, \alpha_c, \phi)} \tag{9}$$

In order to obtain the centers-of-pressures as a function of $|CN|$ without vortex effects, fin 2 on the windward side of the body is considered because the vortex-induced loads are quite small. The measured center-of-pressure for this case is almost entirely free of vortex effects. A piecewise linear least squares fit to the $\bar{x}(M_\infty, \alpha_c, \phi)/C_R$ and $\bar{y}(M_\infty, \alpha_c, \phi)/s$ versus $CN(M_\infty, \alpha_c, \phi)$ data is used to obtain a single curve fit of the fin 2 data for $\phi = 0°$ to $80°$. Figure 6 depicts typical fits of the $\bar{x}/C_R$ and $\bar{y}/s$ data points which are composed of roll angles from 0° to 80°. As with the normal-force coefficient, only limited representative examples from the data base are shown. Generally the center-of-pressure correlated very well with $|C_N|$ for all fins and Mach numbers.

With the dependence on α_c and ϕ reduced to a dependence on $|C_N|$, $\overline{x}/C_R$ and $\overline{y}/s$ depend only on AR, λ, M_∞ and $|C_N|$. The interpolation procedure in the M_∞-$|C_N|$ directions is a bicubic spline, and the interpolation procedure in the aspect ratio and taper ratio directions is the same as that used for the fin normal-force coefficient presented in the previous section.

Fin Control Data Base

The control data base is made up of two parts: transonic normal-force coefficient data and the effect of control fin deflection on the x and y centers-of-pressures. The experimental tests provided normal-force, hinge-moment, and bending-moment coefficients for Mach numbers between 0.6 and 4.5, angles of attack up to 45°, roll angles from -90° to 90°, and deflection angles of -40° to 40°. The hinge-moment and bending-moment coefficients provide the fin centers-of-pressures, $\overline{x}/C_R$ and $\overline{y}/s$. Deflected fin data was only obtained for fins with aspect ratios greater than or equal to 1.0. The following table depicts the aspect ratio and taper ratio domain of the control data base:

		TAPER RATIO, λ		
		0	1/2	1
Aspect	1	III	42	IV
Ratio, AR	2	51	52	53
	4	V	62	VI

⬭ - Region of interpolation

TABLE 3. Aspect Ratio and Taper Ratio Range of the Control Data Base

The numbers in Table 2 are the test fin designation numbers. The missing fins denoted by Roman numerals are considered with interpolation schemes to be described.

The test Mach numbers are:

$M_\infty = 0.8,\ 1.2,\ 2.0,\ 3.0,\ 4.5.$

The test angles of attack are:

$\alpha_c = 0,\ 2,\ 5,\ 10,\ 15,\ 20,\ 25,\ 30,\ 35,\ 40,\ 45°.$

The fin orientation angles are:

$\phi = -90,\ -80, \ldots,\ -10,\ 0,\ 10, \ldots, 80,\ 90°.$

The test deflection angles are:

$\delta = -40,\ -30,\ \ldots,\ 30,\ 40°.$

Fin Control Transonic Normal-Force Coefficient.- The fin normal-force coefficient, CNF, is known as a function of aspect ratio, taper ratio, Mach number, included angle of attack, angle of roll, and deflection angle. Methods are developed to interpolate in these directions to obtain $CNF(AR, \lambda, M_\infty, \alpha_c, \phi, \delta)$. Linear interpolation is used in the Mach number and in the deflection angle parameters. Interpolation in the aspect ratio and taper ratio directions is considered in four regions for the control data as depicted in Table 3, and the general formulas for interpolation in these regions follow.

In Region III, the value of CN is the point in the AR-λ domain which lies on the plane formed by fins 42, 51, and 52; thus,

Region III: $0.0 \leq \lambda \leq 0.5$; $1.0 \leq AR \leq 2.0$

$$CN_{III} = CN52 - 2(0.5-\lambda)(CN52-CN51) - (2-AR)(CN52-CN42) \quad (10)$$

In Region IV, the value of CN is the point in the AR-λ domain which lies on the plane formed by fins 42, 52, and 53; therefore,

Region IV: $0.0 < \lambda < 1.0; \quad 1.0 < AR < 2.0$

$$CN_{IV} = CN52 + 2(\lambda-0.5)(CN53-CN52) - (2-AR)(CN52-CN42) \qquad (11)$$

In Region V, the value of CN is the point in the AR-λ domain which lies on the plane formed by fins 51, 52, and 62; therefore,

Region V: $0.0 < \lambda < 0.5; \quad 2.0 < AR < 4.0$

$$CN_{V} = CN52 - 2(0.5-\lambda)(CN52-CN51) + 0.5(AR-2)(CN62-CN52) \qquad (12)$$

In Region VI, the value of CN is the point in the AR-λ domain which lies on the plane formed by fins 52, 53, and 62; thus,

Region VI: $0.0 < \lambda < 1.0; \quad 2.0 < AR < 4.0$

$$CN_{VI} = CN52 + 2(\lambda-0.5)(CN53-CN52) + 0.5(AR-2)(CN62-CN52) \qquad (13)$$

Figure 7 illustrates representative examples of the fin normal-force coefficient versus angle of attack for several Mach numbers and deflection angles.

Fin Control Center-of-Pressure.- Prediction of the fin hinge- and bending-moment coefficients and the missile's rolling- and pitching-moment coefficients require that the effect of control deflections on the axial and lateral position of the fin center-of-pressure be determined. The data base is used to obtain the center-of-pressure location associated with nonvortex loads. By examining fin 2 at $\phi = 0$, the effect of control deflection on the center-of-pressure locations is obtained.

The test results provide normal-force, hinge-moment, and bending-moment coefficients for each test fin as a function of M_∞, α_c, ϕ, and δ. The $\phi = 0$ data are reduced to obtain $\bar{x}/C_R$ and $\bar{y}/s$ in the following manner:

$$\frac{\bar{x}(M_\infty, \alpha_c, \delta)}{C_R} = \frac{x_{HL}}{C_R} - \frac{C_{HM}(M_\infty, \alpha_c, \delta)}{C_N(M_\infty, \alpha_c, \delta)} \tag{14}$$

$$\frac{\bar{y}(M_\infty, \alpha_c, \delta)}{s} = \frac{C_{BM}(M_\infty, \alpha_c, \delta)}{C_N(M_\infty, \alpha_c, \delta)} \tag{15}$$

The center-of-pressure data are plotted versus $|C_N|$ for each fin. The $-40° < \delta < 40°$ data for each fin is plotted on the same graph for each Mach number, and these data are fit with a piecewise linear curve. Representative examples of these fits are shown in Figure 8. The dependence on α_c and δ is reduced to a dependence on $|C_N|$, and $\bar{x}/C_R$ and $\bar{y}/s$ depend only on AR, λ, M_∞ and $|C_N|$. The interpolation procedure in the AR-λ parameters is the same as that used for the fin transonic normal-force coefficient described in the previous section.

Wing-Alone Data Base

A wing-alone data base, required by the equivalent angle of attack method, is composed of normal-force coefficient data for a range of angles of attack and Mach number. The aspect ratio and taper ratio range for this data base are the same as those for the fin stability data base described above. The wing-alone curves were generated from various sources (Refs. 10 and 11) and from manipulation of the tri-service control data base for positive fin deflection. Representative examples of the wing-alone results are shown in Figure 9.

Nose Vortex Shedding

The forebody vortex model used in the previous MISSILE prediction methods is described in Reference 2 and is used by MISSILE 3. It is a semi-empirical model (Ref. 12) which is based on measurements on various bodies for $\alpha_c < 20°$ and $M_\infty < 2$. Several investigators have demonstrated that the body vortices for such flow are symmetrical, and this finding is incorporated into the low angle of attack model. For angles of attack greater than 20°, the data on body vortices are sparse; consequently, a method based on a multi-vortex tracking code (Ref. 13) was used to calculate a nose vortex numerical data base for bodies at high angles of attack. These results are included in MISSILE 2A and they are currently used in MISSILE 3. Reference 1 describes the development of the nose vortex data base.

Afterbody Vortex Shedding and Tracking

Following the general vortex cloud approach used in References 13, 14, and 15, the three-dimensional steady flow over the afterbody is assumed to be equivalent to a two-dimensional, unsteady, separated flow. The two-dimensional solution is carried out in the crossflow plane where the flow about the body in the presence of discrete vortices is obtained. At each time step, corresponding to an interval of the length on the body, a new vortex pair is shed into the flow field from separation points. The discrete vortices forming the wake are allowed to move under the influences of the freestream flow, the body, and the other vortices (including fin vortices) in the field.

The calculation procedure is carried out in the following manner along the afterbody following the canard section. Starting at the crossflow plane located at the canard trailing edge, the boundary layer in the crossflow plane is forced to separate at points on the body determined from the crossflow Mach number. Figure 10 shows the variation of the separation angle with crossflow Mach number as obtained from References 16, 17, and 18. The equations for the separation line used in MISSILE 3 are:

$$\text{if } M_\infty \sin\alpha_c < 0.8 \qquad \theta_s = 90° \tag{16}$$

$$\text{if } .8 < M_\infty \sin\alpha_c < 1.2 \qquad \theta_s = 20° \, (2.5\, M_\infty \sin\alpha_c - 2) + 90° \tag{17}$$

$$\text{if } M_\infty \sin\alpha_c > 1.2 \qquad \theta_s = 110° \tag{18}$$

The trailing vortices from the canard fins are placed in the flow field, and vortices are shed from the afterbody at the predicted separation points. The strength of the body separation vortices is determined from the vorticity transport in the boundary layer. The paths taken by these free vortices are calculated by integration of the equations of motion of each vortex in a stepwise fashion using a variable step size differential equation solver. A detailed development of the multiple vortex tracking procedure can be found in References 13 and 14. At following downstream crossflow planes, the canard vortices and the free vortices being shed from the body are allowed to influence the body pressure distribution and the motion of other vortices in the field. This procedure is carried out over the entire length of the afterbody; to the tail leading edge for a canard-body-tail configuration and to the base for a canard-body configuration.

Since this method is only used on the afterbody where the body is required to be a constant radius cylinder, the effects of changing body radius or noncylindrical bodies are not considered. These effects could be included in MISSILE 3 at a later date if it is desirable.

Equivalent Angle of Attack

Data bases, such as the one used in MISSILE 3, provide a foundation for preliminary design and prediction methods, but they do not encompass all geometries and flow conditions. For example, all the fins in the new data base have radius to semi-span ratios, a/s_m, of 0.5 and they are located at various positions on the test body. In order to investigate missiles with different radius to span ratios and fin locations different from those in the data base, it is necessary to have a method which geometrically scales the data base and takes into account different vortical flow fields. The equivalent angle of attack concept is used in MISSILE 3 to accomplish these tasks, and it is discussed briefly in this section. The equivalent angle of attack concept is presented in References 19 and 20; however the current method is slightly different from the previous methods.

Scaling Effects

The first step in the equivalent angle of attack approach is to determine the fin normal-force coefficient from the data base for each AR, λ, M_∞, α_c, and ϕ_i combination of interest. This is done for each of the four fins and is denoted as $CNF_{i,o}$. The subscript "i" denotes fin number, i=1,2,3,4, and the subscript "o" indicates the value corresponds to $a/s_m = 0.5$. If the cross-flow Mach number, $M_\infty \sin\alpha_c$, exceeds unity, it is necessary to adjust the reference of $CNF_{i,o}$ to the average local dynamic pressure, $\bar{q}_{\ell_{i,o}}$. This correction is necessary because of the presence of a body bow shock which significantly changes the dynamic pressure near the fins. Details are presented in the Appendix. The correction is based on predicted flow field results from the Euler code SWINT (Ref. 21).

The next step is to determine the equivalent angle of attack for the fin in the data base, $\alpha_{eq_{i,o}}$. If the crossflow Mach number exceeds unity, it is necessary to use the fin average local Mach number, $\overline{M}_{\ell_{i,o}}$, because of the presence of the bow shock. As above, the correction is based on predicted flow field results from program SWINT. For the fin local Mach number and the normal-force coefficient of interest given by $CNF_{i,o} \cdot (q_\infty/\overline{q}_\ell)_{i,o}$, the equivalent angle of attack, $\alpha_{eq_{i,o}}$, is calculated from the wing-alone tables as indicated in the following sketch.

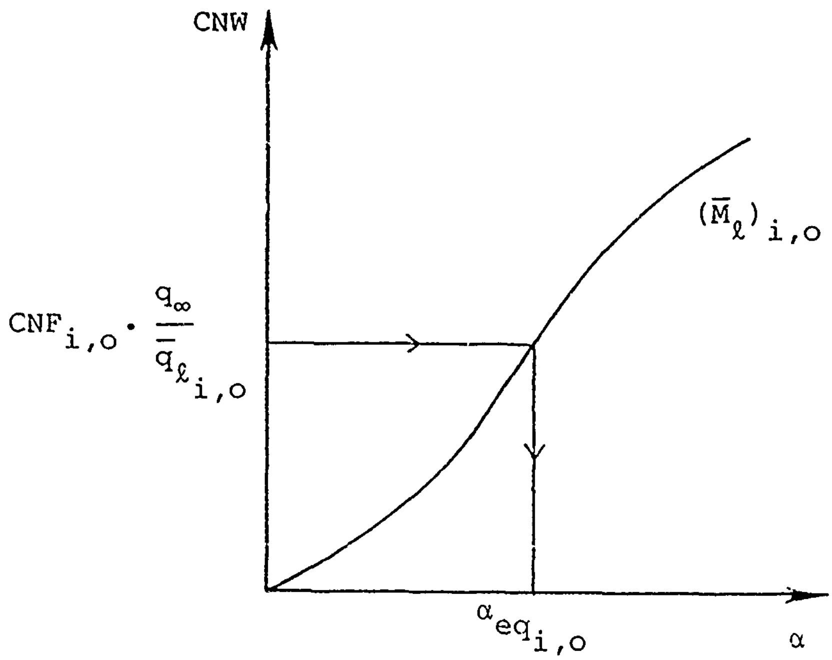

Once $\alpha_{eq_{i,o}}$ is determined, the next step is to remove the vortex-induced effects for the test conditions of the data base; that is, the nose and forebody flow field and the body radius to semi-span ratio, a/s_m. These adjustments are necessary so that the vortex field for the actual geometry and flow conditions can be included later. The fins in the data base are located on a cylindrical body at various axial stations aft of a 3-caliber ogive nose. A semi-empirical method, based on 3-caliber ogive nose and cylinder, is used to obtain the body vortex strength and location for the test fin locations. This method is the same as that used for the nose vortex model described earlier. With the strength and location of the forebody vortex known, the effect of the vortex field on the equivalent angle of attack is obtained in the same manner as the previous MISSILE programs. The increment in the equivalent angle of attack due to the body vortex system is obtained from reverse flow theorems as described in Reference 1 (Appendix B). The following equation is solved for the vortex free equivalent angle of attack, $\hat{\alpha}_{eq_{i,o}}$, for each fin ϕ_i.

$$\tan\hat{\alpha}_{eq_{i,o}} = \tan\alpha_{eq_{i,o}} - \tan(\Delta\alpha_{eq})_{v,i,o} \tag{19}$$

Once the vortex-free equivalent angle of attack is found, the results are scaled to the a/s_m of the actual fin. If it is assumed that K_W, the Beskin upwash factor, is given by

$$K_W = \frac{\tan\hat{\alpha}_{eq_{i,o}}}{\tan\alpha_c \cos\phi} \tag{20}$$

and that K_W is linear with respect to a/s_m as predicted by slender body theory. Then the scaling with a/s_m is given by

$$\tan\hat{\alpha}_{eq_{i,1}} = 2\frac{a}{s_m}\tan\hat{\alpha}_{eq_{i,o}} - (2\frac{a}{s_m} - 1)\tan\alpha_c\cos\phi_i \tag{21}$$

The subscript 1 denotes the a/s_m of interest, and the ^ indicates the absence of vortices. With $\hat{\alpha}_{eq_{i,1}}$ known, the actual vortical flow field may be included. If the first fin section is under consideration, the vortex field due to the nose and forebody must be added. If the second fin set is being considered, the vortex field from both the first fin set and the afterbody must be included. The equivalent angle of attack for the fin geometry and flow conditions of interest for no fin deflections is given by

$$\tan \alpha_{eq_{i,1}} = \tan \hat{\alpha}_{eq_{i,1}} + \tan(\Delta\alpha_{eq})_{v,i,1} \tag{22}$$

The next step is to determine the fin loads without deflections. To calculate the fin normal force, the wing-alone normal-force coefficient is found corresponding to $\alpha_{eq_{i,1}}$ and $\overline{M}_{\ell_{i,1}}$. Quantity $\overline{M}_{\ell_{i,1}}$ is the average local Mach number for the a/s_m of interest. With $CNW_{i,1}$ and the average local dynamic pressure, $\overline{q}_{\ell_{i,1}}$, the fin normal-force coefficient is calculated as

$$CNF_{i,1} = CNW_{i,1} \, (\overline{q}_{\ell}/q_{\infty})_{i,1} \tag{23}$$

The bending-moment coefficient acting on the fins with no control effects is calculated from the normal-force coefficient and the $\overline{y}/s$ center of pressure in the stability data base. The vortex-free fin normal-force coefficient, $\hat{CNF}_{i,1}$, is calculated in the same manner as $CNF_{i,1}$ except $\hat{\alpha}_{eq_{i,1}}$ is used. From the stability spanwise center-of-pressure data base, $(\overline{y}/s)_{i,1}$ is found corresponding to $\hat{CNW}_{i,1}$ and $\overline{M}_{\ell_{i,1}}$ for the fin geometry of interest. The bending-moment coefficient is given by

$$CBMF_{i,1} = \hat{CNF}_{i,1}(\overline{y}/s)_{i,1} + (CNF_{i,1} - \hat{CNF}_{i,1})(\overline{y}/s)_{v,i} \tag{24}$$

where $(\overline{y}/s)_{v,i}$ is the point of action of the normal force due to the vorticity in the flow field as determined by reverse flow theorems (Ref. 1).

The hinge-moment coefficient acting on the fins with no control effects is calculated using the normal-force coefficient and the $\bar{x}/C_R$ from the stability data base. $(\bar{x}/C_R)_{i,1}$ is found from the data base corresponding to $\hat{CNW}_{i,1}$ and $\bar{M}_{\ell_{i,1}}$. The effect of vortices on the axial center-of-pressure is found by the method of Nielsen and Goodwin (Ref. 22). This method assumes the effects of vortices on the center-of-pressure cause it to move along a lifting line (constant percent chord). Given $(\bar{y}/s)_{v,i}$ from reverse flow theorems, $(\bar{x}/C_R)_{v,i}$ is given by

$$(\bar{x}/C_R)_{v,i} = \tau + (1-\tau)(1-\lambda)(\bar{y}/s)_{v,i} \tag{25}$$

where

$$\tau = \frac{(\bar{x}/C_R)_{i,1} - (1-\lambda)(\bar{y}/s)_{i,1}}{1 - (1-\lambda)(\bar{y}/s)_{i,i}} \tag{26}$$

The hinge-moment coefficients for the fins are calculated as

$$\begin{aligned} CHMF_{i,1} &= \left[\frac{x_{HL}}{C_R} - \left(\frac{\bar{x}}{C_R}\right)_{i,1}\right] \hat{CNF}_{i,1} \\ &+ \left[\frac{x_{HL}}{C_R} - \left(\frac{\bar{x}}{C_R}\right)_{v,i}\right] (CNF_{i,1} - \hat{CNF}_{i,1}) \end{aligned} \tag{27}$$

This completes the equivalent angle of attack formulation and the corresponding fin loads for no control deflections.

Fin Deflection Effects

The effect of fin deflection on the equivalent angle of attack is presented in this section. For Mach numbers greater than 1.5, interference effects and control effectiveness are handled by slender body theory and proper use of $\bar{\alpha}_{\ell}$, and $\bar{M}_{\ell}$. For Mach numbers less than 1.2, control effectiveness is obtained from the transonic normal-force coefficient control data base, and interference effects between fins are obtained from slender body theory. For $1.2 < M_\infty < 1.5$, a combination of the two methods is used. The procedure used herein is justified by the correlations presented in Reference 19.

The equivalent angles of attack with fin deflection for each fin for $M_\infty > 1.5$ are given by

$$\alpha_{eq_{1,2}} = \alpha_{eq_{1,1}} + \Lambda_{SELF}\delta_1 - \Lambda_{ADJ}(\bar{q}_\ell/q_\infty)_{2,1}\lambda_{ADJ}\delta_2 + \Lambda_{OPP}(\bar{q}_\ell/q_\infty)_{3,1}\lambda_{OPP}\delta_3 + \Lambda_{ADJ}(\bar{q}_\ell/q_\infty)_{4,1}\lambda_{ADJ}\delta_4 \tag{28}$$

$$\alpha_{eq_{2,2}} = \alpha_{eq_{2,1}} - \Lambda_{ADJ}(\bar{q}_\ell/q_\infty)_{1,1}\lambda_{ADJ}\delta_1 + \Lambda_{SELF}\delta_2 + \Lambda_{ADJ}(\bar{q}_\ell/q_\infty)_{3,1}\lambda_{ADJ}\delta_3 + \Lambda_{OPP}(\bar{q}_\ell/q_\infty)_{4,1}\lambda_{OPP}\delta_4 \tag{29}$$

$$\alpha_{eq_{3,2}} = \alpha_{eq_{3,1}} + \Lambda_{OPP}(\bar{q}_\ell/q_\infty)_{1,1}\lambda_{OPP}\delta_1 + \Lambda_{ADJ}(\bar{q}_\ell/q_\infty)_{2,1}\lambda_{ADJ}\delta_2 + \Lambda_{SELF}\delta_3 - \Lambda_{ADJ}(\bar{q}_\ell/q_\infty)_{4,1}\lambda_{ADJ}\delta_4 \tag{30}$$

$$\alpha_{eq_{4,2}} = \alpha_{eq_{4,1}} + \Lambda_{ADJ}(\bar{q}_\ell/q_\infty)_{1,1}\lambda_{ADJ}\delta_1 + \Lambda_{OPP}(\bar{q}_\ell/q_\infty)_{2,1}\lambda_{OPP}\delta_2 - \Lambda_{ADJ}(\bar{q}_\ell/q_\infty)_{3,1}\lambda_{ADJ}\delta_3 + \Lambda_{SELF}\delta_4 \tag{31}$$

For $M_\infty < 1.2$, the equivalent angle of attack due to control deflection is given by the previous expressions except the $\Lambda_{SELF}\delta_i$ terms are replaced by $\Delta\alpha_{eq_{i,\delta}}$ terms which are calculated from the transonic normal-force coefficient control data base. To calculate $\Delta\alpha_{eq_{i,\delta}}$, the normal-force coefficients with and without deflection, CNF_{i,o,δ_i} and $CNF_{i,o,\delta_i=0}$, are found from the data base for the M_∞, α_c, A_R, λ, and δ_i combination of interest. These values are corrected to the average local test dynamic pressure as previously described. The corrected values of CNF and the average local test Mach number are used to calculate the equivalent angles of attack, $\alpha_{eq_{i,\delta}}$ and $\alpha_{eq_{i,\delta=0}}$. The change in the equivalent angle of attack of fin i due to its deflection is scaled with a/s_m using slender-body theory and is given by

$$\Delta\alpha_{eq_{i,\delta}} = (\alpha_{eq_{i,\delta}} - \alpha_{eq_{i,\delta=0}})\frac{\Lambda_{SELF,a/s_m}}{\Lambda_{SELF,a/s_m=.5}} \tag{32}$$

Given the equivalent angle of attack, the loads on the fins are calculated. The normal-force coefficient is calculated in the same manner as the nondeflected normal-force coefficient. The wing-alone normal-force coefficient is found corresponding to $\alpha_{eq_{i,2}}$ and the average fin local Mach number, $\overline{M}_{\ell_{i,1}}$. With $CNW_{i,2}$ and the average local dynamic pressure, $\overline{q}_{\ell_{i,1}}$, the fin normal-force coefficient is

$$CNF_{i,2} = CNW_{i,2}(\overline{q}_\ell/q_\infty)_{i,1} \tag{33}$$

The effect of control deflection on the bending- and hinge-moment coefficients is calculated from the control $\overline{y}/s$ and $\overline{x}/C_R$ data bases. The wing-alone vortex-free normal-force coefficient for the deflected fin is approximated by

$$\hat{CNW}_{i,2} = CNW_{i,2} - (CNW_{i,1} - \hat{CNW}_{i,1}) \tag{34}$$

From the control spanwise center-of-pressure data base, $(\bar{y}/s)_{i,2,c}$ is found corresponding to $\hat{CNW}_{i,2}$ and $\bar{M}_{\ell_{i,1}}$ for the fin of interest.

$$(\bar{y}/s)_{i,2} = [(\bar{y}/s)_{i,2,c} - (\bar{y}/s)_{i,1,c}] + (\bar{y}/s)_{i,1} \tag{35}$$

where $(\bar{y}/s)_{i,1,c}$ is the control spanwise center of pressure corresponding to $\hat{CNW}_{i,1}$ and $\bar{M}_{\ell_{i,1}}$. $(\bar{y}/s)_{i,2}$ is the spanwise fin center of pressure with control and vortex effects included.

The bending-moment coefficient is

$$CBMF_{i,2} = [\hat{CNF}_{i,2}(\bar{y}/s)_{i,2} - \hat{CNF}_{i,1}(y/s)_{i,1}] + CBMF_{i,1} \tag{36}$$

where from Equation (33)

$$\hat{CNF}_{i,2} = \hat{CNW}_{i,2}(\bar{q}_\ell/q_\infty)_{i,1}$$

The hinge-moment coefficients are calculated from the control $\bar{x}/C_R$ tables. $(\bar{x}/C_R)_{i,1,c}$ is found corresponding to $\hat{CNW}_{i,1}$ and $\bar{M}_{\ell_{i,1}}$, and $(\bar{x}/C_R)_{i,2,c}$ is found corresponding to $\hat{CNW}_{i,2}$ and $\bar{M}_{\ell_{i,1}}$. The axial center-of-pressure with fin deflection is given by

$$(\bar{x}/C_r)_{i,2} = [(\bar{x}/C_R)_{i,2,c} - (\bar{x}/C_R)_{i,1,c}] + (\bar{x}/C_R)_{i,1} \tag{37}$$

The hinge-moment coefficient is then given by

$$\begin{aligned} CHMF_{i,2} = {} & [x_{HL}/C_R - (\bar{x}/C_R)_{i,2}]\ \hat{CNF}_{i,2} \\ & - [x_{HL}/C_R - (\bar{x}/C_R)_{i,1}]\ \hat{CNF}_{i,1} + CHMF_{i,1} \end{aligned} \tag{38}$$

This completes the equivalent angle of attack method implemented within MISSILE 3.

Body Loads

The body force calculation used in MISSILE 3 is the same as that used in MISSILE 2A. These calculations provide a very rough estimate to the forces and moments, and it is recommended the user input body forces if better estimates are available.

The nose forces on the body are found from a combination of potential and crossflow drag theories. Potential forces are included by specifying the normal-force coefficient slope, $dC_N/d\alpha$. The crossflow drag term is included to approximate viscous and vortex loads. The formulation for these loads is found in Reference 4.

The afterbody forces are calculated by a combination of crossflow drag theory and pressure integrations. The crossflow drag term is used to approximate the normal force, and the side force is calculated by integration of the pressure distribution on the afterbody. These formulations are presented in Reference 2.

MISLE3 DESCRIPTION AND USER'S GUIDE

MISLE3 is an aerodynamic engineering prediction method for preliminary design of axisymmetric missiles with one or two cruciform fin sections. The foundations of the method are an experimental data base and the equivalent angle of attack concept. The equivalent angle of attack methodology manipulates the data base results to predict fin loadings for configurations and flow conditions not in the data base. The range of parameters permitted in MISLE3 are: $0° \leq \alpha_c \leq 45°$, $0.6 \leq M_\infty \leq 4.5$, $-40° \leq \delta \leq 40°$, and $0° \leq \phi \leq 90°$.

The following sections are a user's manual for the program MISLE3. Included are descriptions of the program, the calculation procedure, input preparation, sample input and output cases which illustrate various program features, and program limitations.

Program Description

This section provides a general description of program MISLE3 and its various subroutines. The code is written in modular form so that as improvements or additions to the data base or methodology become available they are easy to incorporate. The flow of the calculation is described herein, and detailed comments are provided throughout the code to assist the user in understanding the order of calculation.

The computer code consists of the program MISLE3 and 60 subprograms. The overall flow map of the program is shown in Figure 11 where the general relationship between the subroutines and external references can be seen. Communication between the program modules is handled by argument lists and named common blocks. A cross reference table for the calling relationship between the program subroutines is shown in Figure 12, and a similar table for the named common blocks is shown in Figure 13.

The program is written in standard FORTRAN 77. Execution for a single case on a VAX 11/750 can vary from 1.5 minutes to more than 5 minutes depending on the geometry, the flow conditions, and the number of shed vortices on the afterbody. MISLE3 spends a significant amount of time setting up tables in which to interpolate. This time is independent of the number of cases being run; therefore, the code is much more efficient for multiple cases.

Subroutine Description

This section briefly describes the main program MISLE3 and its various subroutines.

MISLE3	The main program for calculating the forces and moments on missiles with cruciform fin sections.
ALFEQ	Interpolates in the wing-alone normal-force coefficient table to determine the equivalent angle of attack corresponding to CNF and the Mach number of interest.
BLOCK DATA	Initializes the named common blocks CNFD, CNFS and PREPRO.
BODY3	Sheds and tracks vortices in the midbody section at high angles of attack and computes loads on the midbody section.
BVTEX	Computes symmetric body nose vortex strength and position.
CCL	Computes the slender-body theory span loading for fin-fin interference.
CHRT8	Calculates $\beta(dC_L/d\alpha)$ for supersonic Mach numbers; Chart 8 of NACA Report 1307, Reference 23.
CH1416	Calculates the body center of pressure due to a wing or tail; Charts 14, 15 and 16 of NACA Report 1307, Reference 23.

EQ4	Calculates $K_{B(W)}\ \beta(1 + \lambda)\ (s_m - 1)\ (dC_L/d\alpha)$ from Equation 4 of AIAA Journal, Vol. 20, No. 6, June 1982, Page 856, Reference 24.
EQ5	Calculates $K_{B(W)}\ \beta(1 + \lambda)\ (s_m - 1)\ (dC_L/d\alpha)$ from Equation 5 of AIAA Journal, Vol. 20, No. 6, June 1982, Page 856, Reference 24.
EQ6	Calculates $K_{B(W)}\ \beta(1 + \lambda)\ (s_m - 1)\ (dC_L/d\alpha)$ from Equation 6 of AIAA Journal, Vol. 20, No. 6, June 1982, Page 856, Reference 24.
EQ7	Calculates $K_{B(W)}\ \beta(1 + \lambda)\ (s_m - 1)\ (dC_L/d\alpha)$ from Equation 7 of AIAA Journal, Vol. 20, No. 6, June 1982, Page 856, Reference 24.
DFEQKM	Integrates a system of N first order differential equations from X to X + DX with error control by using a Kutta-Merson integration scheme. This routine is used for the vortex tracking on the afterbody.
FINLDS	Computes the loads on a fin section.
FINSHD	Computes the strengths and locations of the trailing vortices from the first fin set.
FTRACK	Calculates the derivatives needed for the ordinary differential equation solver DFEQKM for tracking the shed vorticity.
GVEL	Computes the velocity induced by a set of NV free vortices at an arbitrary field point.

INFLU	Determines the region of influence of one fin of a cruciform set on another for $M_\infty > 1$.
INTFAC	Calculates the fin-body interference factors, $K_{B(W)}$ and $K_{W(B)}$ and the body center of pressure, XB.
INPT	Reads in and prints out all input data for MISLE3.
INTDG1	Computes the transformed geometry for an interdigitated tail fin section. Used only when the body bank angle exceeds 45°.
INTDG2	Transforms loads for interdigitated tails back into the original coordinate system. Used only when the body bank angle exceeds 45°.
LAMIJ	Computes the slender-body theory fin deflection factors given the slender-body theory span loading for fin-fin interference.
LNTRP	Performs a 1-dimensional linear interpolation.
LIN2D	Performs a 2-dimensional linear interpolation.
NOSE	Calculates the loads on the body nose.
PROSS	Sets up tables of wing-alone normal-force coefficient and fin centers of pressures for the geometry of interest.
QLML	Calculates $(\overline{q}_\ell/q_\infty)$ and $(\overline{M}_\ell/M_\infty)$ as a function of $M_\infty\sin(\alpha_c)$ for each fin. $M_\infty\sin(\alpha_c) > 1$. This is based on calculations performed using the Euler code SWINT, Reference 21.

REVFLO	Computes the weighted average of the vortex-induced upwash on each fin and its point of action.
SETCNS	Interpolates in the fin stability data base to produce a table of CNF(B) for no fin deflection for the geometries of interest and for the Mach number of interest. Also sets up a table of transonic normal-force coefficient with fin deflection if $M_\infty < 1.2$.
SIMP1	Computes an integral to a given tolerance using Simpson's rule and a given function for the integrand.
SIMSON	Computes an integral using Simpson's rule and a given array of ordinate values.
TRACK	Tracks vortices from X to X + DX.
VELBOD	Computes the velocity induced on a body by a set of NV free vortices.
VORADD	Computes the initial positions and strengths of the shed body vorticity.
WNGCND	Interpolates in the CNDxx tables (transonic control normal-force coefficient data base) in the aspect ratio and taper ratio directions.
CND42	Transonic control normal-force coefficient data for FIN 42, AR = 1.0, $\lambda = 0.5$, as a function of M_∞, α_c, ϕ, and δ.

CND51 — Transonic control normal-force coefficient data for FIN 51, AR = 2.0, $\lambda = 0.0$, as a function of M_∞, α_c, ϕ, and δ.

CND52 — Transonic control normal-force coefficient data for FIN 52, AR = 2.0, $\lambda = 0.5$, as a function of M_∞, α_c, ϕ, and δ.

CND53 — Transonic control normal-force coefficient data for FIN 53, AR = 2.0, $\lambda = 1.0$, as a function of M_∞, α_c, ϕ, and δ.

CND62 — Transonic control normal-force coefficient data for FIN 62, AR = 4.0, $\lambda = 0.5$, as a function of M_∞, α_c, ϕ, and δ.

WNGCNT — Interpolates in the CNTxx tables (stability normal-force coefficient data base) in the aspect ratio and taper ratio directions.

CNT12 — Stability normal-force coefficient data for FIN 12, AR = 0.25, $\lambda = 0.5$, as a function of M_∞, α_c and ϕ.

CNT31 — Stability normal-force coefficient data for FIN 31, AR = 0.5, $\lambda = 0.0$, as a function of M_∞, α_c and ϕ.

CNT32 — Stability normal-force coefficient data for FIN 32, AR = 0.5, $\lambda = 0.5$, as a function of M_∞, α_c and ϕ.

CNT33 — Stability normal-force coefficient data for FIN 33, AR = 0.5, $\lambda = 1.0$, as a function of M_∞, α_c and ϕ.

CNT42 — Stability normal-force coefficient data for FIN 42, AR = 1.0, $\lambda = 0.5$, as a function of M_∞, α_c and ϕ.

CNT51	Stability normal-force coefficient data for FIN 51, AR = 2.0, λ = 0.0, as a function of M_∞, α_c and ϕ.
CNT52	Stability normal-force coefficient data for FIN 52, AR = 2.0, λ = 0.5, as a function of M_∞, α_c and ϕ.
CNT53	Stability normal-force coefficient data for FIN 53, AR = 2.0, λ = 1.0, as a function of M_∞, α_c and ϕ.
CNT62	Stability normal-force coefficient data for FIN 62, AR = 4.0, λ = 0.5, as a function of M_∞, α_c and ϕ.
WNGCNW	Constructs a table of wing-alone normal-force coefficients as a function of M_∞ and α_c.
XBAR	Computes the vortex-free axial location of the fin center of pressure (stability data base).
XBARC	Computes the vortex-free axial location of the fin center of pressure for fin deflection.
XCPWB	Calculates the body longitudinal center-of-pressure location in the presence of wings or tails. $\beta AR(1 + \lambda)(1 + 1/M_\infty) > 4$ and $M_\infty > 1$.
YBAR	Computes the vortex-free spanwise location of the fin center of pressure (stability data base).
YBARC	Computes the vortex-free spanwise location of the fin center of pressure for fin deflection.

Program Restrictions and Limitations

The major restrictions in MISLE3 were discussed previously, but these are summarized in this section for completeness. Additional limitations and suggestions based on the authors' experience with the code are also included.

The scope of the data base imposes the following restrictions on the flow conditions and the geometries that can be analyzed:

$0.6 < M_{\infty} < 4.5$
$0° < \alpha_c < 45°$
$0° < \phi < 90°$
$0.25 < AR < 4.0$
$0 < \lambda < 1$
4 fins per section
All fins in a section are identical
Symmetric airfoils only
No trailing edge sweep
Axisymmetric bodies

Figure 1 illustrates the angle of attack, aspect ratio, and Mach number range of the systematic data base.

While the data base in MISLE3 is limited to the above restrictions, the program will allow certain of these restrictions to be violated, but it will print out a warning message. These messages are discussed in the following section. It is recommended that the user stay within the aforementioned limits for general usage of the code, and any excursions outside these limits should be made cautiously.

Error Messages and Stops

The code MISLE3 has numerous internal error messages of varying degrees of importance. The severest error message is a FATAL which results in a numbered program STOP. A WARNING message is printed out if a condition is violated but is not considered severe enough to stop execution of the code and prevent the remainder of the cases from being run. The error messages and their location in the code are described, and suggestions to eliminate the problems are presented.

STOP 10 — This is a FATAL error which occurs if the number of input Mach numbers, NMACH, exceeds 5 or the number of total cases, NMACH*NCOND, exceeds 100. One of the two following messages will be printed:

"FATAL 10 **** NUMBER OF MACH NUMBERS EXCEEDS 5 ****"

"FATAL 10 **** TOTAL NUMBER OF CASES (NMACH*NCOND) EXCEEDS 100 ****"

The user should check the input and resubmit the job. Subroutine INPT.

STOP 20 — This is a FATAL error which occurs if the tip chord of a fin is larger than the root chord. One of the two following messages will be printed along with the quantities in question:

"FATAL 20 **** TIP CHORD EXCEEDS ROOT CHORD FOR FIN SET 1 ****"

"FATAL 20 **** TIP CHORD EXCEEDS ROOT CHORD FOR FIN SET 2 ****"

Subroutine INPT.

STOP 30 — This is a FATAL error which occurs when a fin is not fully on the body or when the rear fin section overlaps the front fin section. One of the four following messages is printed along with the quantities in question:

"FATAL 30 **** LEADING EDGE OF FIN SET 1 LESS THAN XZERO ****"

"FATAL 30 **** TRAILING EDGE OF FIN SET 1 EXCEEDS XBASE"

"FATAL 30 **** LEADING EDGE OF FIN SET 2 LESS THAN TRAILING EDGE OF OF FIN SET 1 ****"

"FATAL 30 **** TRAILING EDGE OF FIN SET 2 EXCEEDS XBASE"

Subroutine INPT.

STOP 40 This FATAL error occurs if any of the input Mach numbers are less than 0.6 or greater than 4.5. One of two following messages is printed:

"FATAL 40 **** MACH NUMBER LESS THAN .6 ****"

"FATAL 40 **** MACH NUMBER EXCEEDS 4.5 ****"

STOP 50 This FATAL error occurs if any of the input fins have aspect ratios less than 0.25 or exceeding 4.0. One of the four following messages is printed along with the quantities in question:

"FATAL 50 **** ASPECT RATIO FOR FIN SET 1 LESS THAN .25 ****"

"FATAL 50 **** ASPECT RATIO FOR FIN SET 1 EXCEEDS 4.0 ****"

"FATAL 50 **** ASPECT RATIO FOR FIN SET 2 LESS THAN .25 ****"

"FATAL 50 **** ASPECT RATIO FOR FIN SET 2 EXCEEDS 4.0 ****"

Program MISLE3.

WARNING 60 This WARNING occurs if any of the input angles of attack exceed 45 degrees. A program STOP is not used here since the user may be running a series of angles of attack. The program will skip over any conditions for which this warning occurs. The following error message is printed:

"WARNING 60 **** ANGLE OF ATTACK EXCEEDS 45 DEGREES"

Program MISLE3.

WARNING 70 This WARNING occurs if any of the input angles of attack exceed 30 degrees when the Mach number is less than 0.8. A program STOP is not used here since the user may be running a series of angles of attack and several Mach numbers. The program will skip over conditions for which this warning occurs. The following error message is printed:

"WARNING 40 **** ANGLE OF ATTACK EXCEEDS 30 DEGREES FOR MACH NUMBER LESS THAN .8 ****". The points that violate the conditions are printed.

Program MISLE3.

WARNING 80 This WARNING occurs if the aspect ratio, Mach number, and angle of attack combination are outside the data base values illustrated in the preceding sketch. One of the two following messages is printed along with the parameters of interest:

WARNING 80 **** ASPECT RATIO, MACH NUMBER, ANGLE OF ATTACK COMBINATION OUTSIDE OF DATA BASE FOR FIN SET 1 ****"

WARNING 80 **** ASPECT RATIO, MACH NUMBER, ANGLE OF ATTACK COMBINATION OUTSIDE OF DATA BASE FOR FIN SET 2 ****"

Program MISLE3.

Input Description

This section describes the input data and format required by program MISLE3. MISLE3 uses list-directed input to eliminate the tediousness of input preparation. MISLE3 does not require any specific knowledge of the dimensional unit of measure, but the user must be consistent throughout and not mix units. The remainder of this section describes the order of input and the input variables.

Item 1 is a single card containing an integer specifying the number of title cards to be input.

Item	Variable	Description
1	NCARD	Number of title cards used to identify the run; NCARD $\geq$ 1.

Item 2 is a set of NCARD title cards used to identify the run. These cards are limited to an 80 column field.

Item 3 is a single card containing the program control variables.

Item	Variable	Description
3	NFIN	Number of fin sets; NFIN = 1 or 2.
	NCOND	Number of attitude conditions (α_c, ϕ, δ_i combinations) for which calculations are to be made; NCOND $\leq$ 100. Note that NMACH*NCOND $\leq$ 100.

NMACH — Number of Mach numbers for which NCOND conditions are to be run; NMACH < 5. Note that NMACH*NCOND < 100.

NXAB — Number of axial body stations, aft of the first set of fins, at which body vortices are to be shed. Also, the number of items at which vortex information will be output if OUTP=.T. NXAB < 40. Note that (2*NXAB+4*NSHED) < 100. NXAB should be chosen such that the spacing between stations is less than D/2.

NSET — Number of the fin set used for control.
= 1, First fin set used for control
= 2, Second fin set used for control

NSHED — Number of trailing vortices shed per fin from the forward (first) set of fins; 1 < NSHED < 10. This option is provided for closely coupled canard and tail fins. NSHED = 1 is sufficient if there is a long afterbody between the fin sections.

LTAIL — Logical variable concering interdigitation of the rear (second) set of fins with respect to the first set.
= F, Second fin set in line with the first set.
= T, Second fin set is rolled 45° clockwise (viewed from rear) with respect to the first set.

E5	Accuracy criterion for vortex tracking. Suggested value, E5 < .001.
BSHED	Logical variable concerning shedding of body vortices in segment after the first fin set. = F, No shedding of body vortices. = T, Body vortices shed at the NXAB stations if separation conditions are met.
OUTP	Logical variable concerning intermediate output. If OUTP is true vortex tracking information for diagnostic purposes is printed. = F, No intermediate output. = T, Intermediate output will be printed.
DEFLEC	Logical variable concerning fin deflection. = F, Fins are not deflected. = T, NSET fin set has deflected fins.

Item 4 is a single card containing the reference information for the runs. There is not a specific unit of measure used in MISLE3, but the user must be consistent.

Item	Variable	Description
4	SROUT	Reference area, dimensional.
	LROUT	Reference length, dimensional.
	XMC	Moment center of missile, dimensional.

D	Diameter of missile, dimensional.
XZERO	Axial location of the nose tip, dimensional.
XBASE	Axial location of missile base, dimensional.

Item 5 is a single card containing the geometric information for the first set of fins.

Item	Variable	Description
5	SPAN(1)	Exposed fin semispan, dimensional.
	XLE(1)	Axial location of the leading edge of the fin root chord, dimensional.
	HL(1)	Axial distance from the leading edge of the fin root chord to the fin hinge line, dimensional.
	CT(1)	Fin tip chord, dimensional.
	CR(1)	Fin root chord, dimensional.

Item 6 is a single card containing the geometric information for the second set of fins and is included only if NFIN = 2.

Omit item 6 if NFIN $\neq$ 2.

Item	Variable	Descript'on
6	SPAN(2)	Exposed fin semispan, dimensional.

XLE(2)	Axial location of the leading edge of the fin root chord, dimensional.
HL(2)	Axial distance from the leading edge of the fin root chord to the fin hinge line, dimensional.
CT(2)	Fin tip chord, dimensional.
CR(2)	Fin root chord, dimensional.

Item 7 is a set of NCOND cards specifying the attitude conditions. $1 < I < NCOND$.

Item	Variable	Description
7	ALFAC(I)	Body angle of attack; angle between the wind vector and the body axis in degrees. $0° < \alpha_c < 45°$.
	PHI(I)	Bank angle in degrees; angle between the Z-axis and the hinge line of fin 1 of the first fin set; angle measured clockwise (looking forward). $0° < \phi < 90°$.
	DELTA(1,I)	Deflection of fin 1 in degrees; positive if it produces a counterclockwise rolling moment (looking forward). $-40° < \delta < 40°$.
	DELTA(2,I)	Deflection of fin 2 in degrees; positive if it produces a counterclockwise rolling moment (looking forward). $-40° < \delta < 40°$.

DELTA(3,I) Deflection of fin 3 in degrees; positive if it produces a clockwise rolling moment (looking forward). $-40° < \delta < 40°$.

DELTA(4,I) Deflection of fin 4 in degrees; positive if it produces a clockwise rolling moment (looking forward). $-40° < \delta < 40°$.

Item 8 is a single card containing the Mach numbers for the run; $1 < I < NMACH$.

Item	Variable	Description
8	FMACH(I)	Freestream Mach number; $1 < I < NMACH$ $0.6 < M_\infty < 4.5$.

Item 9 is a single card containing an integer flag, IFLB, which determines whether the body loads are input or calculated.

Item	Variable	Description
9	IFLB	= 0 Body loads are input in item 10.
		= 1 Body loads are calculated; nose information must be input in Items 11 - 15.

Item 10 is a set of NMACH*NCOND cards containing the input loads; $1 < IJ < NMACH*NCOND$, one set of loads per card. These values should be nondimensionalized with respect to the input reference area and length.

Omit item 10 if IFLB > 0.

Item	Variable	Description
10	CZB(IJ)	Z-direction force coefficient of the body alone (normal force) for condition IJ, where IJ = I+(J-1)*NCOND, $1 < I < \mathrm{NCOND}$, $1 < J < \mathrm{NMACH}$. The inner loop is on I (attitude conditions), and the outer loop is on J (Mach numbers).
	CMYB(IJ)	Moment coefficient around y-axis of the body alone (pitching moment) for condition IJ.
	CXB(IJ)	X-direction force coefficient of the body alone (axial force) for condition IJ.

Omit items 11-15 if IFLB < 0.

Item 11 is a single card containing an integer flag, IDCN, which determines whether the potential normal-force coefficient slope $dC_N/d\alpha$ for the body alone is input. If DCNDA is not to be input in Item 12, it is set to its default value of 2.0.

Item	Variable		Description
11	IDCN	= 0	The default value of DCNDA is used, DCNDA = 2.0.
		= 1	DCNDA is input in Item 12.

Item 12 is a single card containing the potential normal-force coefficient slope for the body alone, DCNDA.

Omit Item 12 if IDCN < 0.

Item	Variable	Description
12	DCNDA	Potential normal-force coefficient slope, $dC_N/d\alpha$, in radians.

Item 13 is a single card containing the number of points specifying the nose geometry, NNOSE.

Item	Variable	Description
13	NNOSE	Number of points specifying the body nose.

Items 14 and 15 are two sets of NNOSE values specifying the body nose; XNOSE(I), RNOSE(I), 1 < I < NNOSE.

Item	Variable	Description
14	XNOSE(I)	x-location at which the body radius is specified, dimensional. 1 < I < NNOSE.
15	RNOSE(I)	Body radius at XNOSE(I), dimensional. 1 < I < NNOSE.

Sample Input Cases

In this section, two sample input cases are described to illustrate the various program options available in MISLE3. Their purpose is to illustrate the available features and options and to provide sample inputs which will help users prepare input for specific cases. An effort has been made to simplify the input requirement of MISSILE 3 compared to MISSILE 2A. Figure 14 shows the geometric inputs required by MISSILE 3.

Sample Case 1, Figure 15, is a test case based on the AIM9 wind tunnel model with king size tail fins (Ref. 25). This case will also be used as the sample output case in the next section. It is recommended that this case be run initially to provide a check with the results presented in the following section.

Input Item 1, NCARD, indicates two title cards are to be input. The following two cards are the required title cards for the run.

Input Item 3 contains various program control options. NFIN = 2 indicates that the missile has two cruciform fin sections. NCOND = 3 indicates that 3 attitude conditions are specified in Item 7. Results for these three conditions are calculated for each input Mach number. NMACH = 1 specifies one Mach number is input in Item 8. Vortices after the first fin set are shed and tracked at 25 stations, NXAB, along the afterbody ahead of the second fin section. NSET = 1 indicates that if a fin set is deflected for control effects, it will be fin set 1. NSHED = 1 specifies one trailing vortex per fin is shed from the first fin set. The second fin set is not interdigitated 45 degrees with respect to the front set, LTAIL = F. The accuracy criterion for the vortex tracking, E5, is 0.001. The logical variable BSHED is set to T so that vortices are shed from the afterbody if the separation conditions are met. OUTP = F indicates that vortex tracking output along the afterbody is not output. The final variable in Item 3, DEFLEC = F, indicates there are no deflected fins.

Input Item 4 contains the reference information for the run. These items are dimensional, and for this case the unit of measure is centimeters. The reference area, SROUT, is the maximum crossectional area of the missile; the reference length, LROUT, is the maximum diameter; and the moment center, XMC, is 46.04 centimeters from the nose. The maximum diameter is 4.234 centimeters. The axial location of the nose tip is 0.0, and the axial location of the missile base is 102.319 cm.

Input Item 5 contains the geometry and location of the first fin set. The exposed semispan, SPAN(1), is 7.24 centimeters. The root chord leading edge, XLE(1), is located at axial station 15.80, and HL(1) indicates the hinge line is 6.35 centimeters aft of the root chord leading edge. The tip and root chords, CT(1) and CR(1), are 3.338 and 11.123 centimeters, respectively.

Input Item 6 is the same as item five except the geometry and location of the second fin set is input: SPAN(2) = 9.04, XLE(2) = 80.729, HL(2) = 10.795, CT(2) = 12.55, and CR(2) = 12.59. All these values are specified in centimeters. The hinge line for this fin set is arbitrary because it will not be deflected in this run.

Input Item 7 contains the NCOND attitude conditions for which results are to be obtained. For this sample case, an angle of attack sweep is demonstrated. The first attitude condition for the body is 2.0° angle of attack and 45° roll angle. There are no deflections for this case, but values must be input because the code uses list-directed input and expects input values. The four values of deflection angles are input 0.0. The second and third attitude conditions are identical to the first except the angle of attack is changed to 5.0° and 10.0°, respectively.

Input Item 8 contains the run MACH numbers. For this case, a single Mach number is set to 2.50.

Input Item 9, IFLB, is a single integer flag indicating whether the body forces are to be input or calculated by MISLE3. For this case they are calculated, IFLB = 1. Input Item 10 is not required since the body forces are calculated.

Input Item 11, IDCN, is a single integer flag indicating whether the potential normal-force coefficient slope, $dC_N/d\alpha$, is input or defaulted by the program. IDCN = 1 indicates that DCNDA is to be input in Item 12. Item 12, DCNDA, is the potential normal-force coefficient and is set to 2.0.

Items 13 through 15 contain the body nose geometry required for the body force calculation. NNOSE = 31 in Item 13 specifies 31 points are used to define the body nose. The 31 axial stations, XNOSE(I), where the nose radius is defined are input in Item 14. The nose radii, RNOSE(I), at the 31 axial station specified in Item 14, are input in Item 15. Item 15 completes the input for Sample Case 1.

Sample Case 2, Figure 16, is a test case based on the Army Generalized Missile (Ref. 26) for multiple Mach numbers and deflections. Input Item 1, NCARD, indicates three title cards are input. The following three cards in item 2 are the title cards for the run.

Input Item 3 contains various program control options. NFIN = 2 indicates that the missile has two cruciform fin sections. NCOND = 4 specifies four attitude conditions are input in item 7. Results for these four conditions are calculated for each input Mach number. NMACH = 2 indicates two Mach numbers are input in Item 8. Body vortices after the first fin set are shed and tracked at 10 stations, NXAB, along the afterbody ahead of the second fin section. NSET = 1 identifies fin set 1 as control fins. NSHED = 1 indicates one trailing vortex per fin is shed from the first fin set. The second fin set is not interdigitated 45 degrees with respect to the front set, since LTAIL = F. The accuracy criterion for the vortex tracking, E5, is 0.001. The logical variable BSHED is true so that vortices are shed from the afterbody if the separation conditions are met. OUTP = T indicates the vortex tracking input along the afterbody is printed. The final variable in Item 3, DEFLEC = T, indicates that fins of fin set 1 are deflected for control effects.

Input Item 4 contains the reference information for the run. These items are dimensional, and for this case the unit of measure is inches. The reference area, SROUT, is the maximum crossectional area of the missile, the reference length, LROUT, is the maximum diameter, and the moment center, XMC, is 26.0 inches from the nose. The maximum diameter is D = 5.0 inches. The axial location of the nose tip is 0.0, and the axial location of the missile base is 52.00 inches.

Input Item 5 contains the geometry and location of the first fin set. The exposed semispan, SPAN(1), is 3.75 inches. The root chord leading edge, XLE(1), is located at axial station 12.72, and HL(1) positions the hinge line 2.28 inches aft of the root chord leading edge. The tip and root chords, CT(1) and CR(1), are 0.25 and 4.00 inches, respectively.

Input item 6 is similar to item 5, except the geometry and location of the second fin set is input. SPAN(2) = 3.50, XLE(2) = 43.00, HL(2) = 3.00, CT(2) = 3.50, and CR(2) = 7.00 define the geometry of fin set 2. These values are also specified in inches.

Input Item 7 contains the NCOND attitude conditions for which results are to be obtained. For this sample case, two roll angles with and without pitch control deflection are considered. For the first attitude condition, the body angle of attack is 8.0°, the roll angle is 0.0°, and the deflections are 0.0°. The second case is the same as one except fins 2 and 4 are deflected 15° for pitch control. Case 3 is the same as case 1 except that the roll angle is 45°, and case 4 is the same as case 3 except all the fins are deflected 15°.

Input Item 8 contains the run Mach numbers. For this case there are two, 1.30 and 1.75.

Input Item 9, IFLB, is a single integer flag indicating whether the body forces are to be input or calculated by MISLE3. For this case they are input, IFLB = 0. Input item 10 is a set of NMACH*NCON cards containing the axial-force, normal-force, and pitching-moment coefficients for the body alone. All the values are input as zero for this case.

Output Description

A typical output file from MISLE3 is described in this section. In general, the output quantities from MISLE3 are labeled and each page is headed with appropriate descriptive information. The output from Sample Case 1 requires four pages which are described in this section and shown in Figure 17.

The first output page contains the MISSILE 3 header to indicate the version number and creation date, the summary/title cards for the run, and an echo of the input. The program control variables, reference information, fin geometries, attitude conditions, Mach numbers, and body nose information are all printed for checking purposes. Along with the echo of the input fin geometry, the calculated aspect ratio and taper ratio are printed.

The results from MISLE3 start on output page 2 which contains the output for the first attitude condition. The run number, Mach number, body angle of attack, and roll angle are printed on the second line. The next block of output contains the component and overall loads acting on the missile. The nose loads include components from the potential normal-force coefficient slope, $dC_N/d\alpha$, and from a crossflow drag term. Fin section 1 loads are the sum of the loads on the individual fins of fin set 1 along with the body carryover loads. The afterbody loads are due to the presence of fin and body vortices over the afterbody. Fin section 2 loads are a sum of the individual fin loads and the body carryover loads. The total loads on the missile are the sum of the component loads.

The next block of output on page 2 contains the individual fin loads for both fin sets. The four fins of fin set 1 are given first followed by fin set 2. The deflection angle, if nonzero, is printed followed by the equivalent angle of attack, the normal-force coefficient, the hinge-moment coefficient, the bending-moment coefficient, and the rolling moment coefficient. This completes the output for the first attitude condition.

The output for attitude conditions 2 and 3 are contained on pages 3 and 4, respectively, and have the same format as output page 2. This completes the output description.

RESULTS

This section presents results obtained with the engineering prediction method MISSILE 3. Comparisons of the results to experimental data are made for code verification and to indicate necessary improvements. This section is divided into two sections; Body-Tail configurations and Canard-Body-Tail configurations.

Body-Tail Configurations

Two independent comparisons with experimental data on body-tail geometries are discussed in this section. The first configuration is a 2.5-caliber ogive nose followed by 10.9 diameter cylindrical body (Ref. 27). The tail fins, located 11.2 diameters aft of the nose tip, have an aspect ratio of 2.81, a taper ratio of 0.423, and a body radius to fin semi-span ratio of 0.25. This missile is depicted in Figure 18.

Comparisons of measured and predicted aerodynamic characteristics at $M_\infty = 1.6$ are shown in Figure 19 - 22. Figure 19(a) illustrates the overall normal-force coefficient and the pitching-moment coefficient at zero roll angle with no fin deflections. The normal force is in good agreement with experiment at low and moderate angles of attack and slightly underpredicted at high angles of attack. The pitching moment is also in good agreement for low and moderate angles of attack but overpredicted at high angles of attack above 12 degrees. The predicted loads on fin 2 are compared with experiment in Figure 19(b). The fin normal-force coefficient comparison indicates good agreement for fin loads, but the hinge-moment coefficient comparison is not as good. Hinge moments are sensitive to thickness distribution, and for this case the fins have a wedge leading edge then a flat constant thickness section followed by a wedge trailing edge. The data base fins in MISLE3 are all double wedge sections. The fin bending-moment coefficients are in good agreement with experiment.

Figures 20(a) and 20(b) show results for $M_\infty = 1.6$ at zero roll angle with fins 2 and 4 deflected -15 degrees for nose up pitch control. The overall normal force in Figure 20(a) and the fin normal force in Figure 20(b) are in good agreement with measured loads; however, the pitching moment comparisons in Figure

20(a) indicates an overprediction of complete configuration pitching moment. Since the fin normal force is predicted well, the difference in the pitching moment arises from an error in the body load distribution. The fin loads are small due to the negative deflection angle and the positive angle of attack; therefore, the error in the body load distribution dominates the pitching moment. This is not the case when the fin is highly loaded in the undeflected case shown in Figure 19. The error in the body load distribution arises from using the crossflow drag formulation for the normal force on the body. This correlation predicts overall normal force well but does not provide a force which varies along the body.

Figure 21 compares results for $M_\infty = 1.6$ at 45 degrees roll without fin deflections. Figure 21(a), (b), and (c) indicate the normal force on the fins and body are in good agreement with experiment. The results for the lee side fins in Figure 21(b) show that the effect of the body wake on the fins is handled well by the program for this case. Figure 21(c) indicates an underprediction of normal force on the windward side fins. Bending moments are generally in good agreement for this case.

Figure 22 compares results for $M_\infty = 1.6$ at 45 degrees roll with -15 fin deflection on all four fins for positive pitch control. The results are similar to the results for pitch control at zero roll angle in Figure 20. The overall and fin normal forces agree well with experiment, but the pitching moment is overpredicted. This is attributed to a deficiency in the body load distribution. It is apparent from Figures 20(b), 22(b), and 22(c) that the effect of control deflection on the fin bending-moment coefficient is in error for this fin.

Figures 23 - 26 show comparisons of measured and predicted results on the same missile model for a Mach number of 3.7.

Generally the results are similar to the $M_\infty = 1.6$ results described above. The overall and fin normal forces are in good agreement, and the pitching moment is overpredicted when fins are deflected such that the fin normal force is near zero or when the body loads are large with respect to the fin loads.

An overall view of the body-tail comparisons in Figure 19 - 26 indicate that MISSILE 3 predicts the missile and fin loads well. There is a deficiency in the body load distribution model, and the user should input body loads if a better body model or if correlations from experiment are available.

The second body-tail model considered with MISSILE 3 is shown in Figure 27 (Ref. 28). The body is a 1.5-caliber ogive nose followed by a 15-diameter cylindrical afterbody. The fin aspect ratio is 2.57, the taper ratio is 0.4, and the body radius to fin semi-span ratio is 0.25. This investigation did not provide any fin loads, but total configuration normal force and pitching moment for Mach numbers of 0.7, 0.9, 1.42, 2.01, and 3.08 are available for comparison purposes.

The measured and predicted normal-force and pitching-moment coefficients are compared in Figures 28(a)-(e) for zero roll angle and no fin deflections. The $M_\infty = 0.7$ and 0.9 results in Figures 28(a) and (b) indicate that normal force is predicted well at low to moderate angles of attack, but they are overpredicted at moderate to high angles. Since fin loads are not available for this case, it is not apparent why the predicted normal force is too large. It is possible that the normal force is sensitive to fin cross section geometry in the transonic regime. The test fins have wedge leading edges, a flat constant thickness section, and a wedge trailing edge. The data base fins are double wedge sections.

Figures 28(c) through (e) illustrate results at supersonic Mach numbers of 1.42, 2.01, and 3.08, respectively. These results are similar to the previous supersonic body-tail results described in Figures 18 - 26. The predicted normal-force coefficient is in good agreement with experiment for all cases, but the pitching moment is overpredicted at moderate to high angles of attack. The error in the body load distribution is likely the cause of the pitching moment error, and the error is even larger for this particular case since an extremely long body is involved.

Canard-Body-Tail Results

Comparisons of measured and predicted characteristics on three canard-body-tail models are described in this section. The first configuration is a canard-controlled missile, similar to the Sidewinder missile, presented in Reference 25 and depicted in Figure 29. The body is a 2.25-caliber ogive nose followed by a 21.9-diameter cylindrical body. The canard fins have an aspect ratio of 2.00, a taper ratio of 0.30, and a body radius to fin semi-span ratio of 0.226. The canard leading edge is located 3.73 diameters aft of the nose tip. The tail fins under consideration have an aspect ratio of 1.06, a taper ratio of 0.58, and a body radius to fin semi-span ratio of 0.19. The tail fins are located 12.7 diameters aft of the canard trailing edge. Overall loads on the model at several supersonic Mach numbers are available, but only results for $M_\infty = 2.5$ are presented here. Reference 25 also provides comparisons to MISSILE 2A which are also included herein.

Measured and predicted normal-force and pitching-moment coefficients at $M_\infty = 2.5$ for zero roll angle and without control deflections are shown in Figure 30. MISSILE 3 underpredicts the normal force at high angles of attack; however, for α_c greater than 23.6 degrees, the crossflow Mach number exceeds unity and the correction for local dynamic pressure and local Mach number activate as described in the equivalent angle of attack section. This correction tends to increase the normal force to a level comparable to projected experimental results. Since this correction helps the calculation, an effort should be made to extend the correction down to the critical crossflow Mach number for a circular cylinder. This corresponds to a crossflow Mach number of approximately 0.5 which occurs at an angle of attack of 11.54 degrees in this case. The correction also improves the pitching moment results.

Figure 31 shows a comparison of control deflection effects. Canard fins 2 and 4 are deflected +5 degrees for positive pitch control. The normal-force coefficient is underpredicted at high angles of attack, but the crossflow correction in the equivalent angle of attack formulation increases it when the crossflow Mach number exceeds unity.

Figure 32 compares measured and predicted results on a rolled configuration without fin deflection. As with the previous comparisons, the normal-force coefficient is underpredicted. In general, the MISSILE 2A results are in better agreement with experiment over the entire range of angle of attack.

The next model considered is the Army Generalized Missile of Reference 26 shown in Figure 33. This model consists of a 3-caliber rounded ogive nose and a 7.4-diameter cylindrical afterbody. The canard fins have an aspect ratio of 3.53, a taper ratio of 0.0625, and a body-radius to fin semi-span ratio of 0.42. The tail fins have an aspect ratio of 1.33, a taper ratio of 0.5, and a body radius to fin semi-span ratio of 0.42. The experimental test for this missile provides overall loads and detailed canard and tail fin loads. Results for a Mach number of 1.75 are presented in this report.

Figure 34(a) illstrates the comparicon of measured and predicted overall normal-force and pitching-moment coefficients on the model. The normal force is slightly underpredicted at high angles of attack, and the pitching moment is overpredicted in the same flow regions. Figure 34(b) indicates the loads on the canard fins are underpredicted for high angles of attack. This is due primarily to the nose vortex flow model interaction with the canard fins. In the body-tail case the nose and forebody vortex model did not cause this type of an interference effect since the vortex system is further away from the body and fins because of the long forebody. The close proximity of the nose vortex and the canard fins results in the error in the canard force. The error is even more apparent in the roll cases which follow.

The tail fin loads predicted by MISSILE 3 in Figure 34(c) agree extremely well with the experimental data. Based on the above comparisons, the error in the overall pitching-moment coefficient in Figure 34(c) must be due primarily to an error in the body load distribution since the tail fin loads are in good agreement with experiment and the canard fin loads are underpredicted.

Figure 35 illustrates the effect of canard control deflection on the forces and moments on the unrolled model. Canard fins 2 and 4 are deflected to +15 degrees for positive pitch control. These results are similar to those described for the undeflected fin case. The normal force is in good agreement with experiment except at high angles of attack where it is slightly underpredicted as seen in Figure 35(a). The canard fin loads are underpredicted, Figure 35(b), as in the undeflected case shown in

Figure 34(b). The tail fin loads in Figure 35(c) are in good agreement with the measured results. In general, the hinge-moment coefficients are in fair agreement with experiment, and the bending-moment coefficients agree very well with experiment.

Figure 36 shows the effect on the fin loads of rolling the model 45 degrees. Figure 36(a) indicates the predicted normal force is in good agreement with experiment except at high angles of attack where it is underpredicted. The lee side canard loads shown in Figure 36(b) indicate the individual fin normal forces are dramatically underpredicted. This is likely due to the proximity of the nose vortex system to the lee side canard fins. This effect was seen in the unrolled case, but it was not as dramatic. The windward canard fin loads are seen in Figure 36(c), and these results indicate that the windward fin loads are in satisfactory agreement with experiment. Figure 36(d) illustrates the lee side tail fin loads. The normal force is predicted well for low to moderate angles of attack, but at higher angles of attack, the normal force is underpredicted due to the afterbody wake. The vortex wake also causes a large discrepancy in the tail fin hinge moment. The windward side tail fin loads are in good agreement with experiment as seen in Figure 36(e).

The effects of canard fin deflection on the loads for the model rolled 45 degrees are shown in Figure 37. These results are similar to the undeflected case discussed above.

The final comparison with experiment is for the canard-body-tail model shown in Figure 38 (Ref. 28). The body is a 1.5-caliber ogive nose followed by a 15-diameter cylindrical body. The canard fins have an aspect ratio of 0.857, a taper ratio of 0.4, and a body radius to fin semi-span ratio of 0.25. The tail fins have an aspect ratio of 2.57, a taper ratio of 0.4, and a body radius to fin semi-span ratio of 0.25. Overall model loads

The second objective was to include the new data base into a computer code to provide an engineering prediction method for the aerodynamic characteristics of typical missile configurations over a wide range of flow conditions. Part of this effort included improvements to the equivalent-angle-of-attack method, investigation of efficient means of manipulating large data bases, incorporation of correction methods for local Mach number and dynamic pressure in regions of supersonic crossflow, and investigation of improved vortex-induced effects.

Both the above objectives were accomplished succesfully. A large body of experimental data was collected from four separate tunnel entries, and these data are resident at the NASA/Langley Research Center. The magnitude of the data base is such that it was impossible to analyze and correlate all the information for this investigation. An engineering prediction method in the form of a code, MISSILE 3, was developed, and verification was accomplished by comparison with independent experimental results. The general result from this effort is that an improved prediction method for the normal force, hinge moment, and bending moment of a wide range of missile fins over a wide range of flow conditions is now available.

In conclusion, the extensive comparisons of measured and predicted aerodynamic characteristics presented in this report for verification purposes prompt the following observations. The new code, MISSILE 3, is capable of predicting the performance characteristics of typical missile configurations under an extensive range of flow conditions, and it has application as a preliminary design method. Generally, predicted individual fin loads are in good agreement with experiment, and loading distributions are adequately predicted for preliminary design purposes. Fortunately, this was the prime objective for the new MISSILE 3 code. The simplified body load prediction method is for Mach numbers 0.7, 0.9, 1.42, 2.01, and 3.08 are available. As with the body-tail results from this same reference, no individual fin loads were measured.

Figures 39(a) through (e) illstrate comparisons of measured and predicted overall normal-force and pitching-moment coefficients for the unrolled missile for the Mach number range. The normal force is usually slightly underpredicted with respect to the experimental results. The crossflow Mach number correction in the $M_\infty = 3.08$ condition in Figure 39(e) raises the value of the normal force and improves agreement with experiment. The pitching moment is not predicted well for transonic Mach numbers, but it exhibits trends similar to the other canard-body-tail results for supersonic Mach numbers.

Figures 40(a) through (e) contain the comparisons for normal-force and pitching-moment coefficients for the above model at a roll angle of 45 degrees. The predicted normal force is in good agreement with experiment in all cases. The pitching moment is predicted well in the low and moderate angles of attack range except for the $M_\infty = 0.9$ case.

CONCLUSIONS

The original intended purpose of the multiphase program described in this final report was twofold. The first objective was to obtain an extensive missile-fin data base which would permit development of a broadly applicable engineering predictive method for calculating the aerodynamic characteristics of canard cruciform missiles. Specifically, a systematic data base which extended (1) the geometric fin characteristics of aspect ratio and taper ratio and (2) the flow characteristics of Mach number, angle of attack, deflection angle, and roll angle beyond the current limits of existing experimental data was to be developed.

satisfactory for total normal force, but the distribution of normal force on the body, dominated by vortex shedding characteristics at high angles of attack, is marginal. For this reason, the provision for the input of improved body characteristics is included in the code.

The performance of MISSILE 3 is very similar to that of the previous MISSILE 2A code, but the new code is applicable over a much wider range of geometric and flow parameters. The code is simple and economic to use, and the enclosed user's manual with sample input and output should expedite the learning process associated with a new code. However, it should be noted by prospective users that MISSILE 3 is a newly developed code, not a revised version of MISSILE 2A. There are likely to be subtle errors that were not uncovered during the extensive development phase of the code; therefore, the user is cautioned to carefully test predicted results against common sense and experience before accepting the results. The authors encourage both positive and negative feedback from users of the code.

As noted in various parts of this report, there are certain limitations of the code and suggested improvements that were beyond the scope of the present effort. The next section briefly outlines some of these areas.

RECOMMENDATIONS

The first and most important recommendation is for additional testing and verification of the new MISSILE 3 code to better define the limits of its capability. Extensive comparisons with independent experimental results for a wide range of geometries and flow conditions will help identify the practical range of application of the code and uncover heretofore undetected errors.

Several known areas of needed improvement include the following:

1. Modify the body force distribution calculation to include enhanced vortex shedding characteristics either through empirical means or the inclusion of now-available discrete vortex-methods (Refs. 13 and 14).

2. Improve the fin hinge moment prediction by including additional empirical information and/or correlations for the effects of different airfoil sections.

3. Extend the correction for local Mach number and dynamic pressure effects to include crossflow Mach numbers between 0.5 and 1.0.

4. Extend the correlations for fin control effects through the incorporation of available control data not considered in the current effort.

5. Extend the method to include effects of changing missile afterbody radius.

6. Extend the method to include effects of noncircular cross section missiles.

REFERENCES

1. Nielsen, J. N., Hemsch, M. J., and Smith, C. A.: A Preliminary Method For Calculating the Aerodynamic Characteristics of Cruciform Missiles to High Angles of Attack Including Effects of Roll Angle and Control Deflections. NEAR TR 152, ONR-CR215-226-4F, Nov. 1977.

2. Smith, C. A. and Nielsen, J. N.: Prediction of Aerodynamic Characteristics of Cruciform Missiles to High Angles of Attack Utilizing a Distributed Vortex Wake. NEAR TR 208, Jan. 1980.

3. Hemsch, M. J., and Nielsen, J. N.: Triservice Program for Extending Missile Aerodynamic Data Base and Prediction Program Using Rational Modeling. Interim Report for Period June 16, 1980 to June 15, 1981. NEAR TR 249, Sept., 1981.

4. Hemsch, M. J., and Nielsen, J. N.: Triservice Program for Extending Missile Aerodynamic Data Base and Prediction Program Using Rational Modeling. Interim Report for Period June 16, 1981 to June 15, 1982. NEAR TR 282, Aug., 1982.

5. Hemsch, M. J. and Nielsen J. N.: Triservice Program for Extending Missile Aerodynamics Data Base and Prediction Program Using Rational Modeling. Interim Report for Period June 16, 1982 to June 15, 1983. NEAR TR 305, Aug., 1983.

6. Hemsch, M. J., and Mullen, J., Jr.: Analytical Extension of the MISSILE 1 and MISSILE 2 Computer Programs, March 1982, NEAR TR 272.

7. Hemsch, M. J., Smith, C. A., Nielsen, J. N., and Perkins, S. C., Jr.: Calculation of Component Forces and Moments of

Arbitrary Banked Cruciform Missiles with Control Deflections. Office of Naval Research, Rept. CR215-226-3, 1976 (also NEAR TR 125).

8. Hemsch, M. J., Nielsen, J. N., and Dillenius, M. F. E.: Method for Calculating Induced Rolling Moments for Cruciform Canard Missiles at Angles of Attack up to 20 Degrees. Naval Weapons Center TP 5761, May 1975 (also NEAR TR 85).

9. Private Communication, Mr. David S. Shaw, NASA/Langley Research Center, 1985.

10. Stallings, R. L., Jr. and Lamb, M.: Wing-alone Aerodynamic Characteristics for High Angles of Attack at Supersonic Speeds. NASA TP 1889, Jul. 1981.

11. Baker, W. B., Jr.: Static Aerodynamic Characteristics of a Series of Generalized Slender Bodies With and Without Fins at Mach Numbers from 0.6 to 3.0 and Angles of Attack from 0 to 180 Degs. AEDC-TR-75-124, Vol. II, May 1976.

12. Mendenhall, M. R. and Nielsen, J. N.: Effect of Symmetrical Vortex Shedding on the Longitudinal Aerodynamic Characteristics of Wing-Body-Tail Combinations. NASA CR 2473, 1974.

13. Mendenhall, M. R. and Perkins, Jr., S. C.: Prediction of Vortex Shedding From Circular and Noncircular Bodies in Supersonic Flow, NASA CR 3754, January 1984.

14. Mendenhall, M. R. and Lesieutre D. J.: Prediction of Vortex Shedding from Circular and Noncircular Bodies in Subsonic Flow, NEAR TR 354, November 1985.

15. Spangler, S. B. and Mendenhall, M. R.: Further Studies of Aerodynamic Loads at Spin Entry. Office of Naval Research, Rept. CR212-225-3, 1977.

16. Agnone, A. M., Zakkay, V., Tory, E., and Stallings, R.: Aerodynamics of Slender Finned Bodies at Large Angles of Attack. AIAA Paper No. 77-666, 10th Fluid & Plasmadynamics Conf., Albuquerque, NM, June 1977.

17. Murthy, V. S. and Rose, W. C.: Form Drag, Skin Friction and Vortex Shedding Frequencies for Subsonic and Transonic Cross Flows on Circular Cylinders. AIAA Paper No. 77-687, 10th Fluid & Plasmadynamics Conf., Albuquerque, NM, June 1977.

18. Landrum, E. J.: Wind Tunnel Pressure Data at Mach Numbers from 1.6 to 4.63 for a Series of Bodies of Revolution at Angles of Attack from -4° to 60°, NASA TM X-3558, Oct. 1977.

19. Hemsch, M. J. and Nielsen, J. N.: Extension of Equivalent Angle-of-Attack Method for Nonlinear Flowfields Journal of Spacecraft and Rockets, Vol. 22, No. 3, May-June 1985, pp. 304-308.

20. Hemsch, M. J. and Nielsen, J. N.: Equivalent Angle-of-Attack Method for Estimating Nonlinear Aerodynamics of Missile Fins, Journal of Spacecraft and Rockets, Vol. 20, Jul-Aug. 1983, pp. 356-362.

21. Wardlaw, A. B., Jr., Baltakis, J. P., Solomon, J. M., and Hackerman, L. B.: An Inviscid Computational Method for Tactical Missile Configurations, NSWC TR 81 457, 1981.

22. Nielsen, J. N. and Goodwin, F. K.: Preliminary Method for Estimating Hinge Moments of All-Movable Controls, NEAR TR 268, March 1982.

23. Pitts, C. P., Nielsen J. N. and Kaattari, G. E.: Lift and Center of Pressure of Wing-Body-Tail Combinations at Subsonic, Transonic, and Supersonic Speeds, NACA Report 1307, 1957.

24. Vira, N. R. and Fan, D.: Closed-Form Solutions of Supersonic Wing-Body Interference, AIAA Journal Vol. 20, No. 6, June 1982, p. 256.

25. Blair, A. B., Jr., Allen, J. M., and Hernandez, G.: Effect of Tail Fin Span on Stability and Control Characteristics of a Canard Controlled Missile at Supersonic Mach Numbers, NASA TP 2157, June 1983.

26. Hemsch, M. J., and Nielsen, J. N.: Test Report for Canard Missile Test in Ames 6- by 6-foot Supersonic Wind Tunnel, NEAR TR 72, August 1974.

27. Lamb, M. and Trescot, C. D., Jr.: A Study of Panel Loads and Centers of Pressure of Three Different Cruciform Aft-Tail Control Surfaces of a Wingless Missile From Mach 1.60 to 3.70, NASA TM 81787, May 1980.

28. Gudmundson, S. E. and Torngren, L.: Transonic and Supersonic Wind Tunnel Test or Control Effectiveness on Schematic Missile Configurations, FFA TN 1983-20, 1983.

LIST OF SYMBOLS

a	body radius
AR	aspect ratio of wing-alone formed by joining two fins at their root chords
C_A	axial-force coefficient; axial force/$q_\infty S_R$
C_{BM}	fin bending-moment coefficient; bending moment/$q_\infty S_R l_R$
C_{HM}	fin hinge-moment coefficient; hinge moment/ $q_\infty S_R l_R$
C_l	rolling-moment coefficient; rolling moment/$q_\infty S_R l_R$
C_{Mx}	rolling-moment
C_{My}	pitching-moment
C_{Mz}	yawing-moment
C_m	pitching-moment coefficient; pitching moment/$q_\infty S_R l_R$
C_N	normal-force coefficient; normal force/$q_\infty S_R$
C_{NW}	wing-alone normal-force coefficient; normal force/$q_\infty S_R$
C_R	fin root chord
C_x	force acting along the x-axis, = C_A
C_y	force acting along the y-axis, side force
C_z	force acting along the z-axis, = C_N
D	maximum body diameter
K_W	Beskin upwash factor
l_R	reference length
$\overline{M}_\ell$	average local Mach number
M_∞	freestream Mach number
$\overline{q}_\ell$	average local dynamic pressure
q_∞	freestream dynamic pressure
s	exposed fin semispan
s_m	semispan of fin-body combination
S_R	reference area
v,w	velocity components in the real plane
W	complex potential
x	axis along the missile centerline positive aft
x_{HL}	chordwise location of fin hinge line measured from leading edge of the fin root chord

x_{LE} axial location of the leading edge of the root chord measured from the nose tip

$\bar{x}$ axial location of the fin normal force center-of-pressure measured from the leading edge of the fin root chord

y axis to the right looking forward

$\bar{y}$ spanwise location of the fin normal force center-of-pressure measured outboard from the fin root chord

z axis in the wind plane positive up

α_c included angle of attack; angle between the body axis and the freestream velocity vector.

α_{eq} equivalent angle of attack; that angle of attack of the wing-alone for which its normal force is twice that of the fin

δ fin deflection angle

Λ_{ADJ} slender-body-theory factor for carryover of loading due to deflection to an adjacent fin

Λ_{OPP} slender-body-theory factor for carryover of loading due to deflection to an opposite fin

Λ_{SELF} slender-body-theory factor for effectiveness of fin deflection

λ taper ratio; ratio of fin tip chord to root chord

λ_{ADJ} fraction of the fin planform area affected by the loading on the adjacent fin

λ_{OPP} fraction of the fin planform area affected by the loading on the opposite fin

ϕ roll angle

Subscripts:

i fin position numbered clockwise looking forward; fin 1 of the first fin section is always in the first quadrant

$i,0$ data base value for the i-th fin

i,1 scaled i-th fin value for dimension of interest with no fin deflection

i,2 scaled i-th fin value for dimension of interest with fin deflection included

Superscripts:

^ indicates a quantity which lacks the effects of vorticity in the field

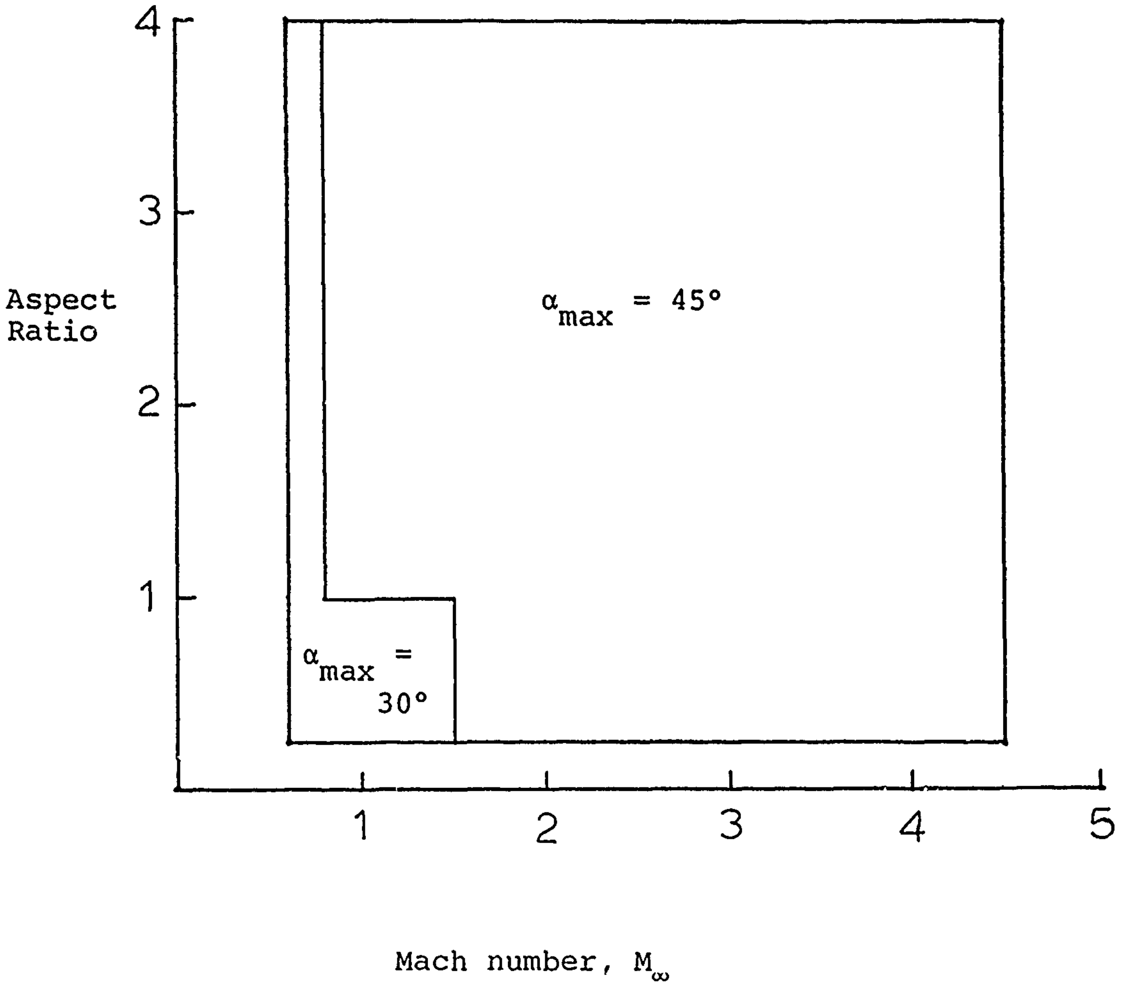

Figure 1.- Mach number, aspect ratio, and angle of attack range of the Tri-Service data base.

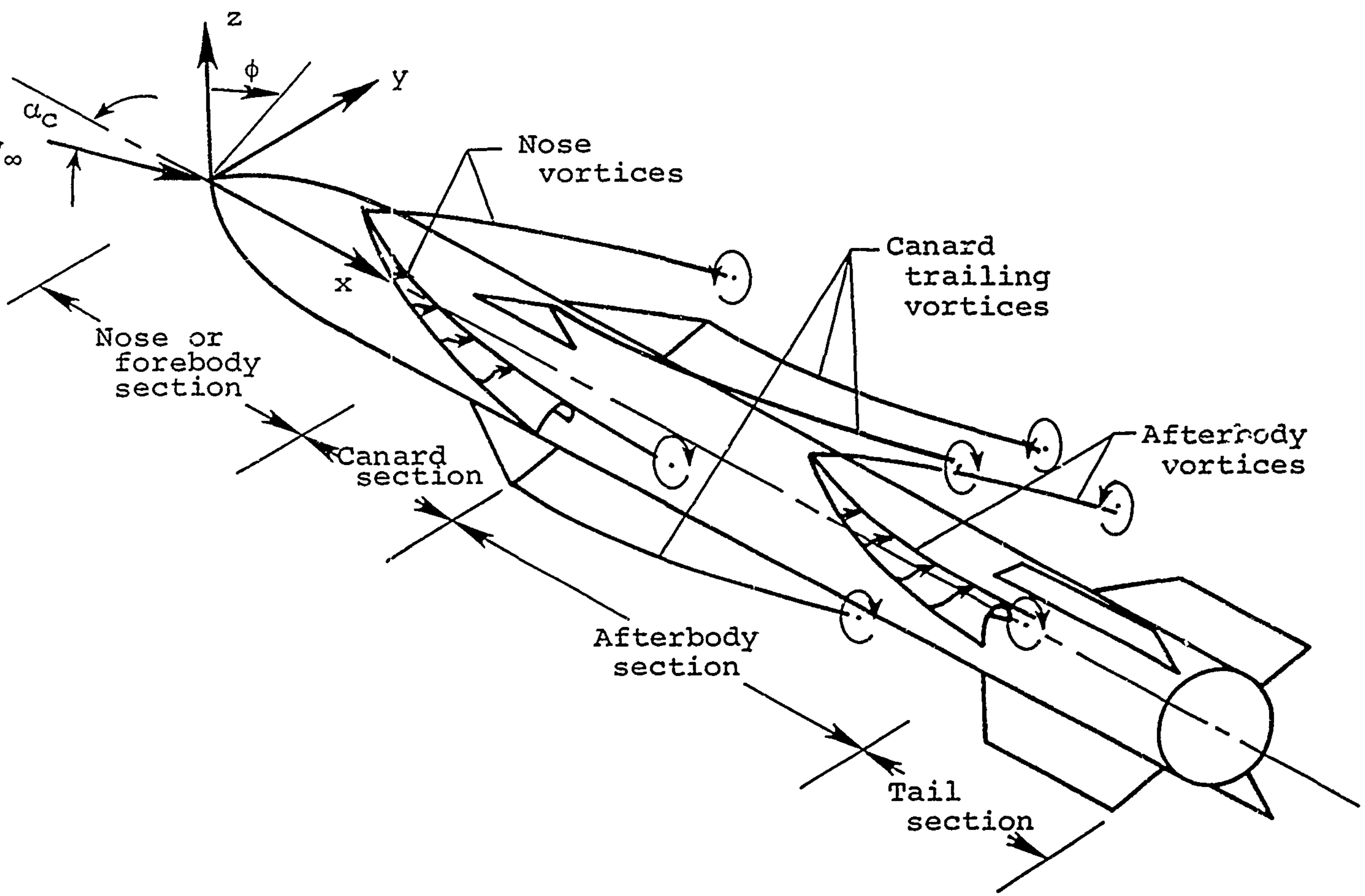

Figure 2.- Banked canard-cruciform missile at angle of attack showing typical vortex field.

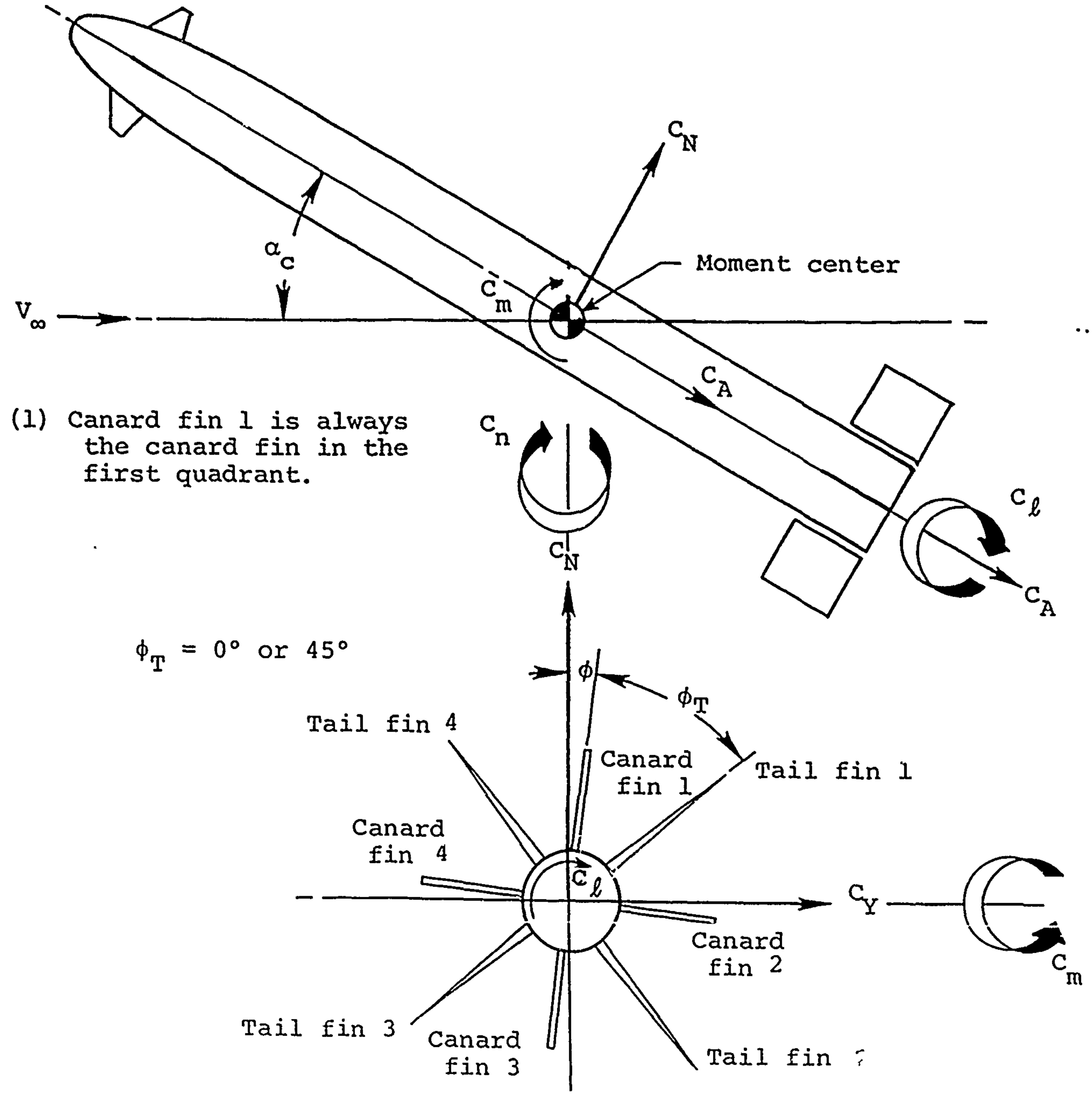

(a) Total loads and fin numbering system.

Figure 3.- Symbols and conventions.

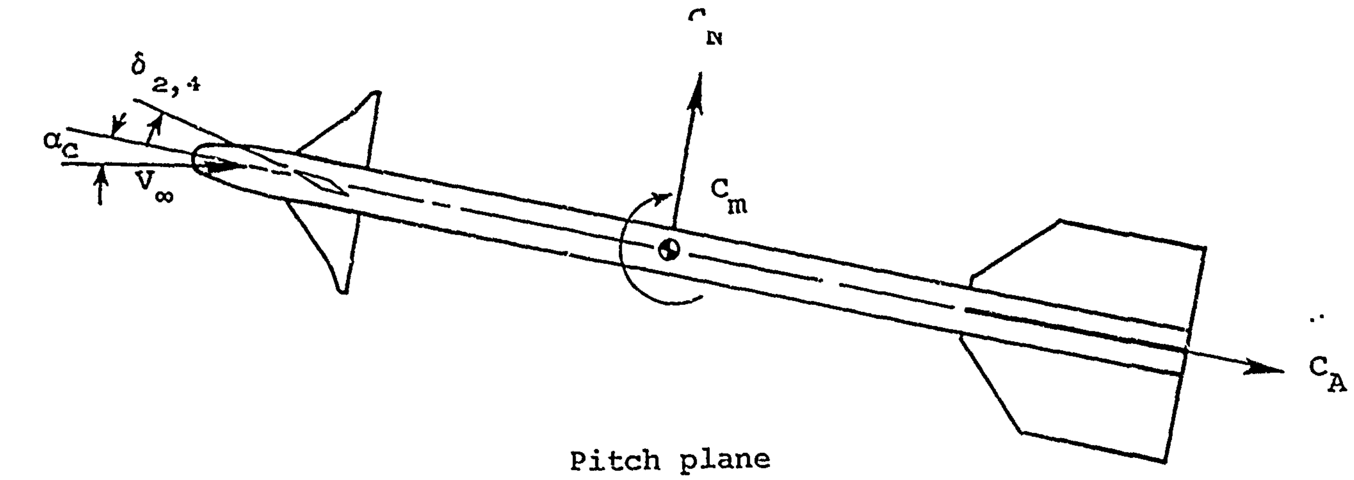

Pitch plane

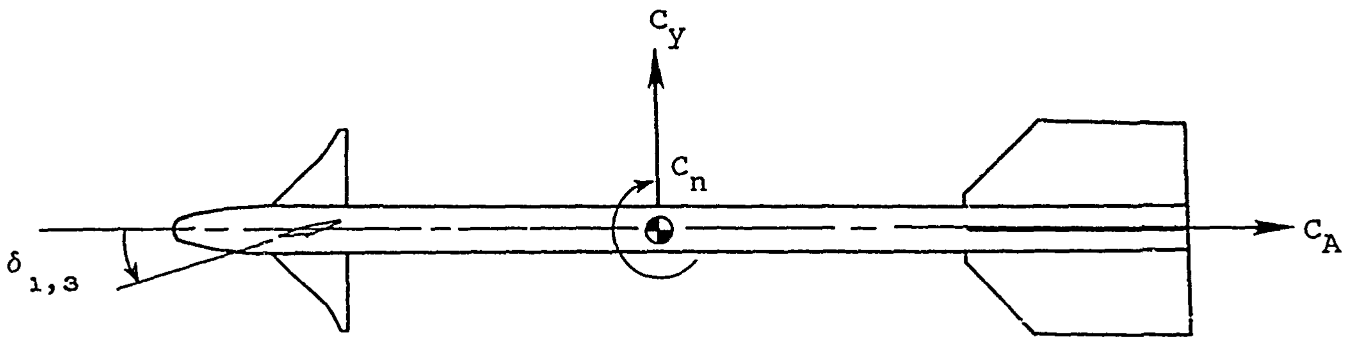

Yaw plane

(b) Sign convention for canard deflection angles.

Figure 3.– Continued.

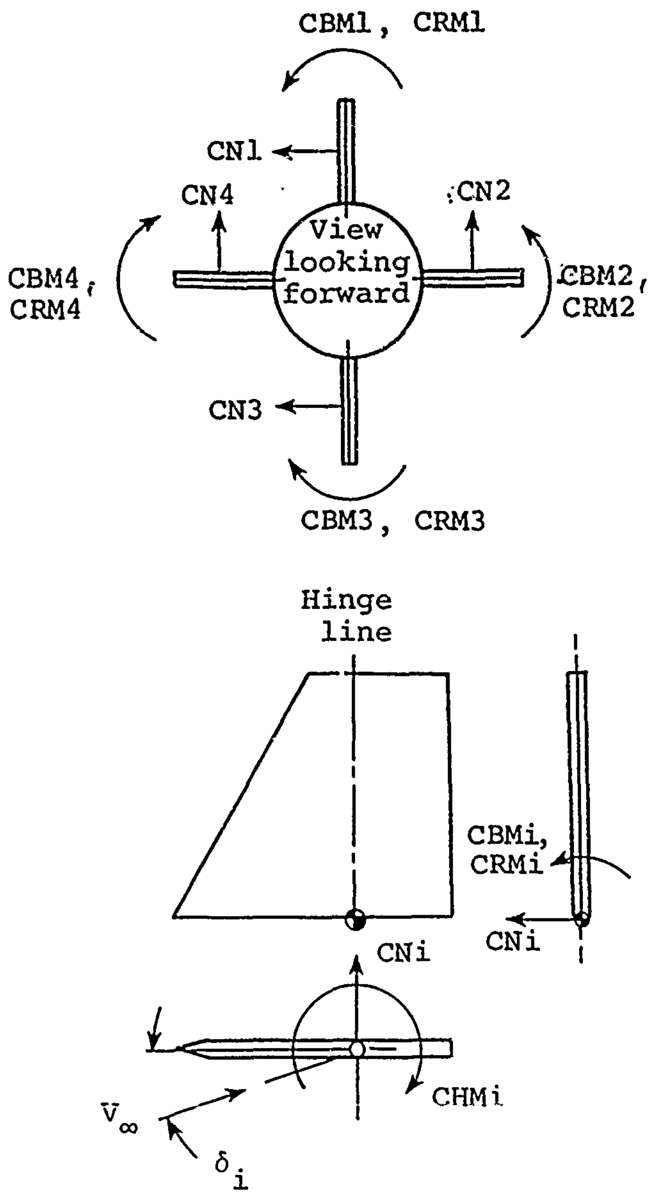

(c) Axis systems and positive sign convention for fins.

Figure 3.- Concluded.

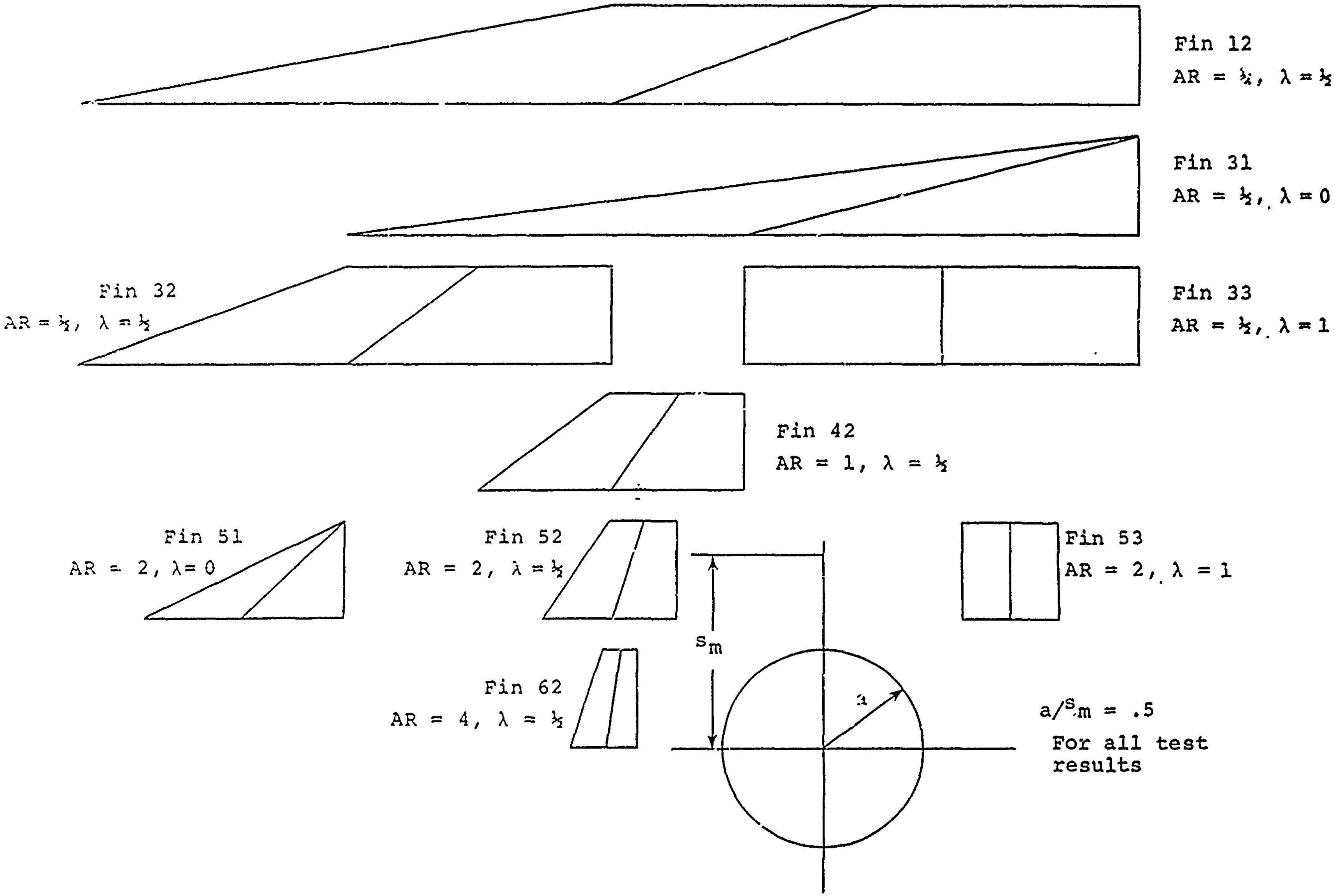

(a) Fin planforms

Figure 4 - Test fin geometries

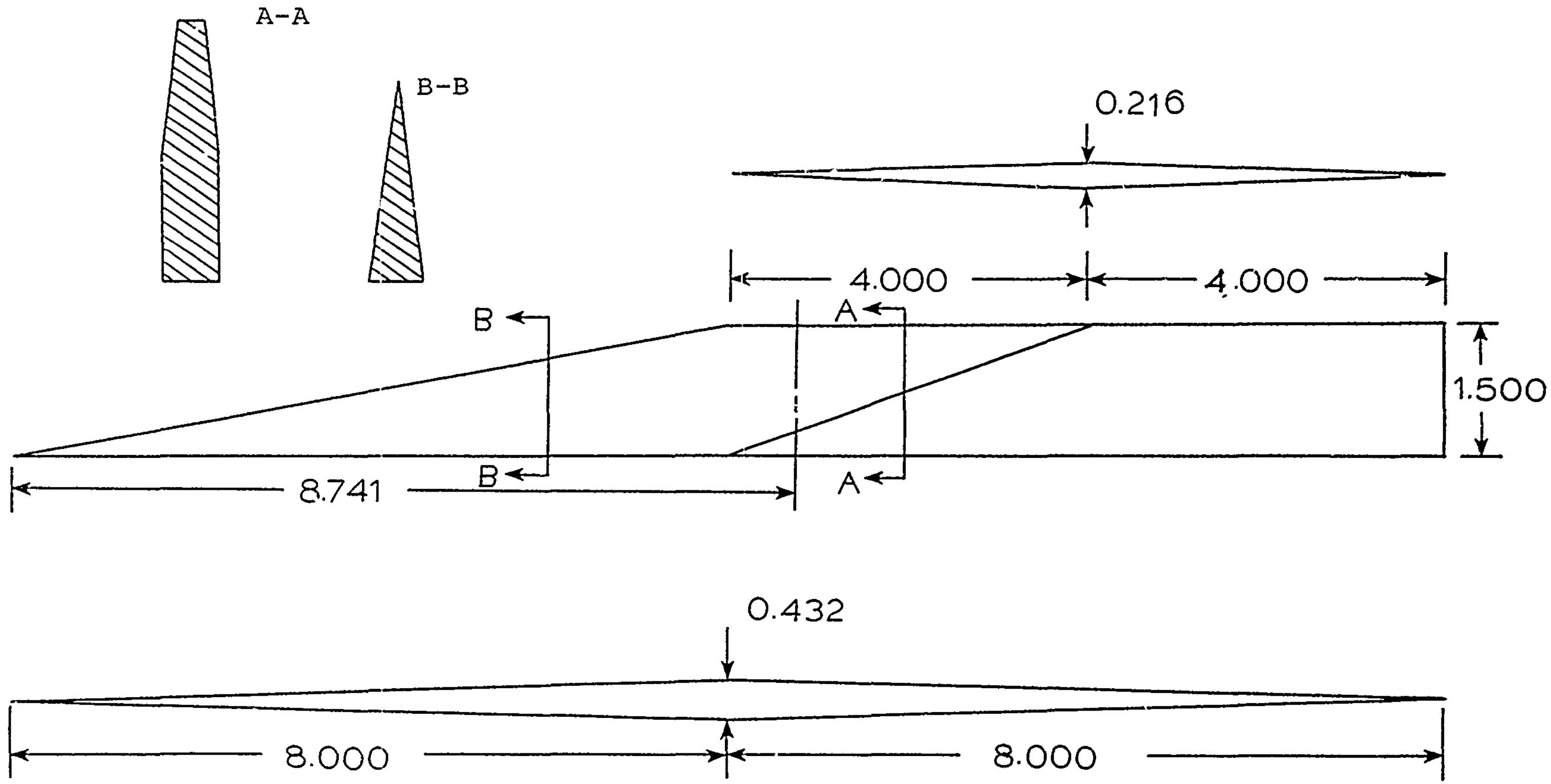

(b) Fin 12; AR = 0.25, λ = 0.5

Figure 4.- Continued.

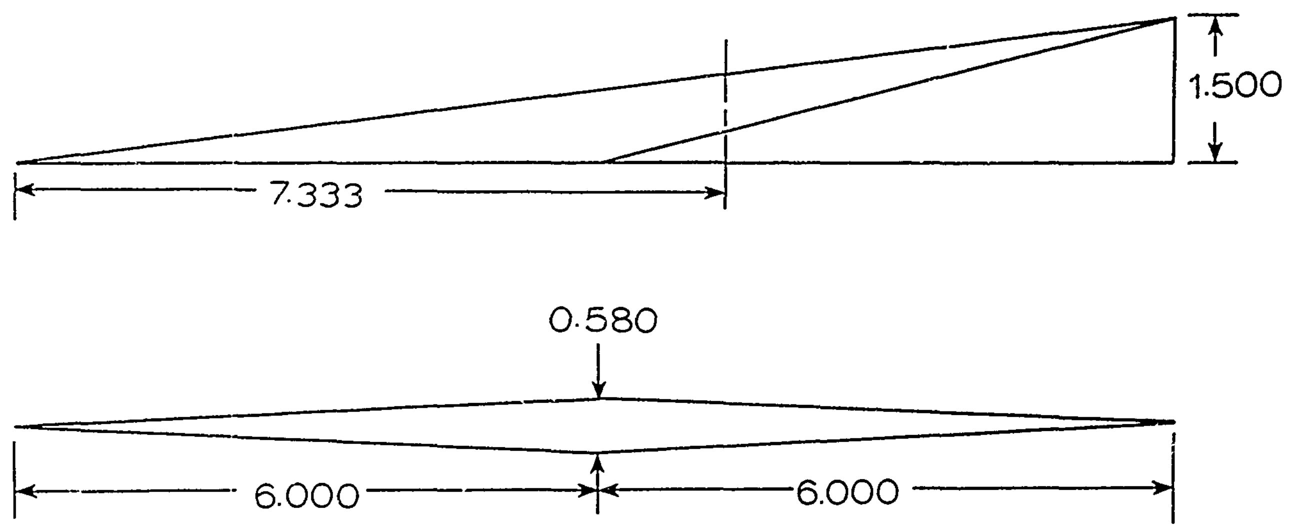

(c) Fin 31; AR = 0.5, λ = 0.0

Figure 4.- Continued.

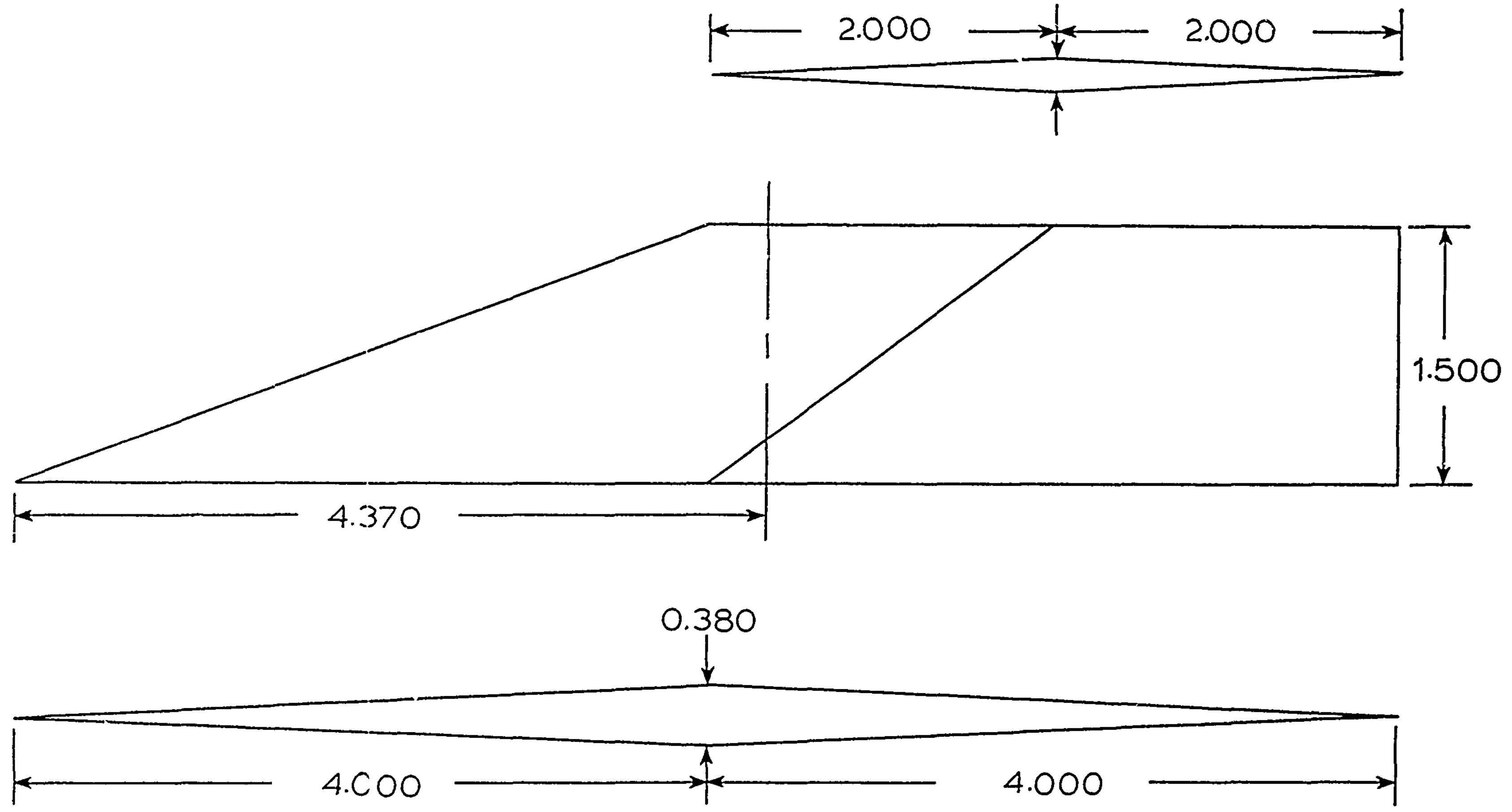

(d) Fin 32; AR = 0.5, λ = 0.5

Figure 4.- Continued.

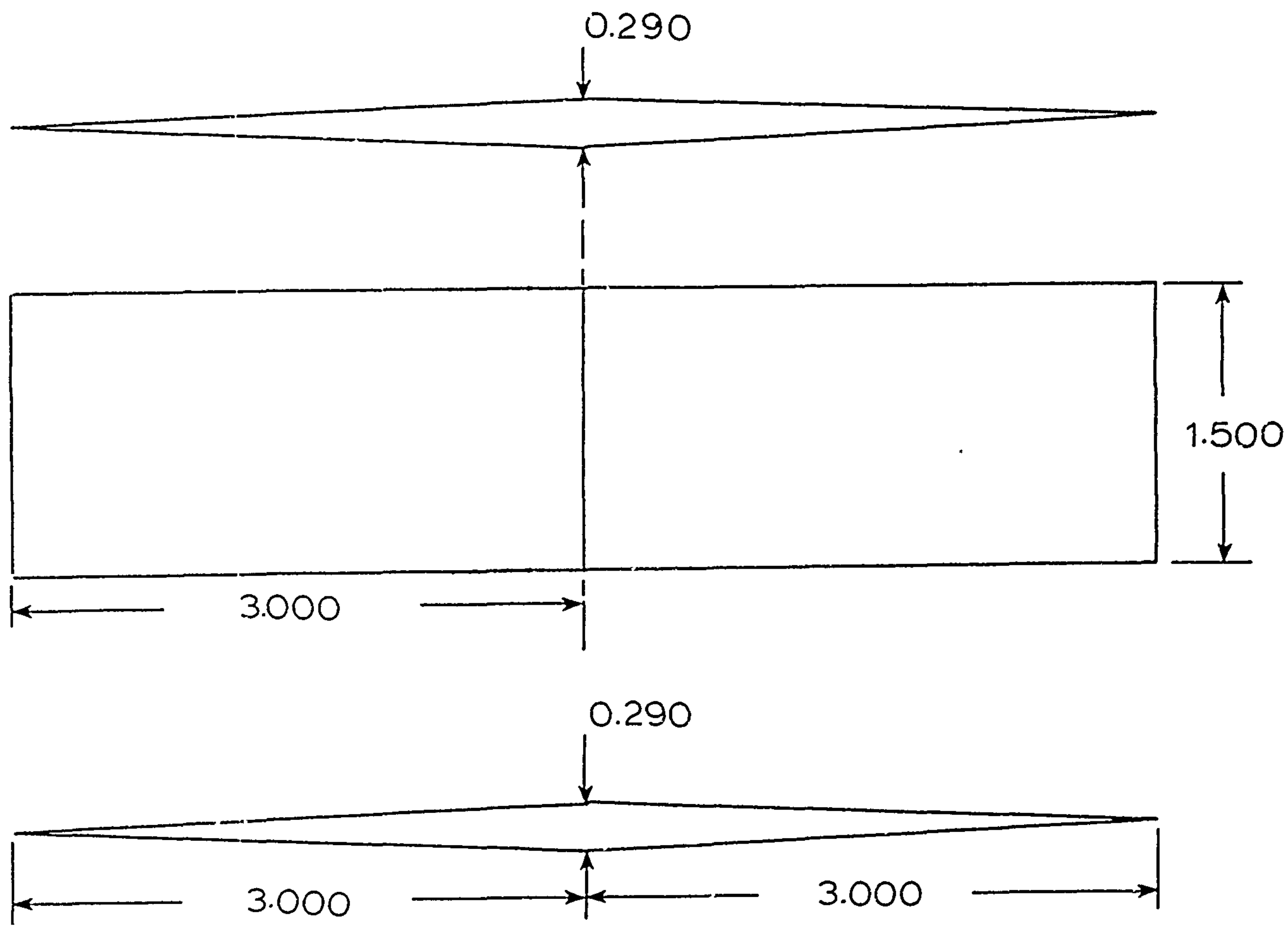

(e) Fin 33; AR = 0.5, λ = 1.0

Figure 4.- Continued.

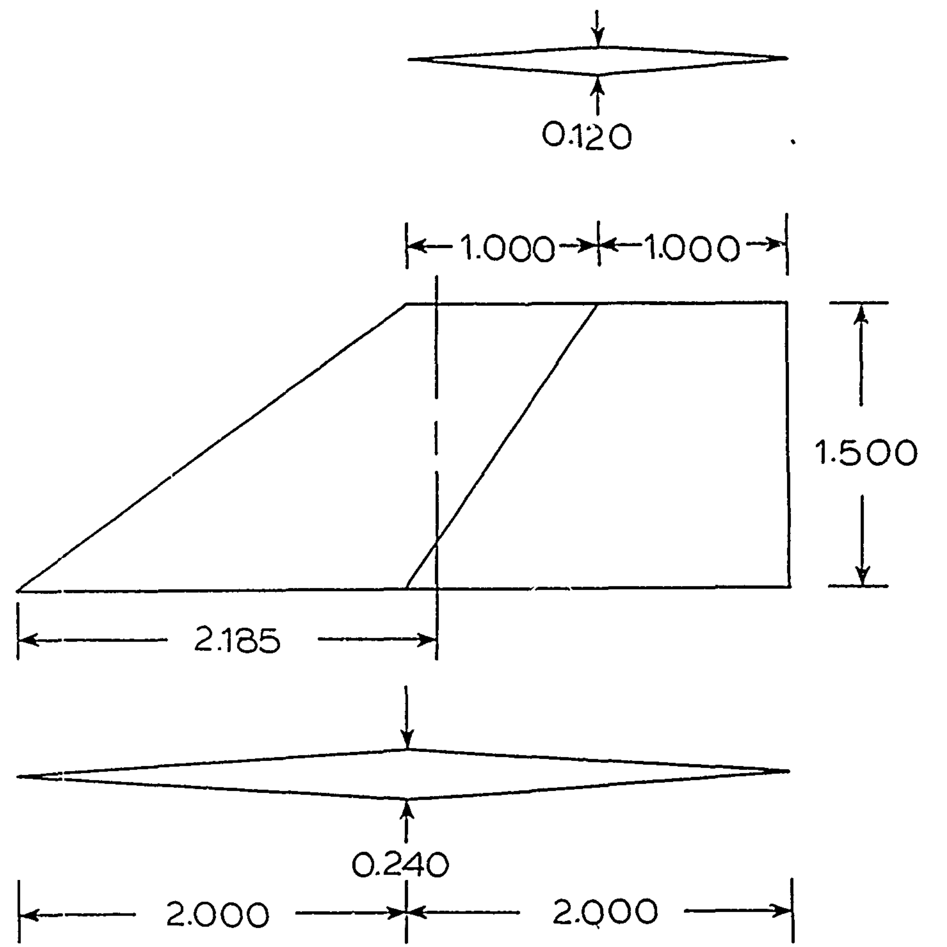

(f) Fin 42; AR = 1, λ = 0.5

Figure 4.- Continued.

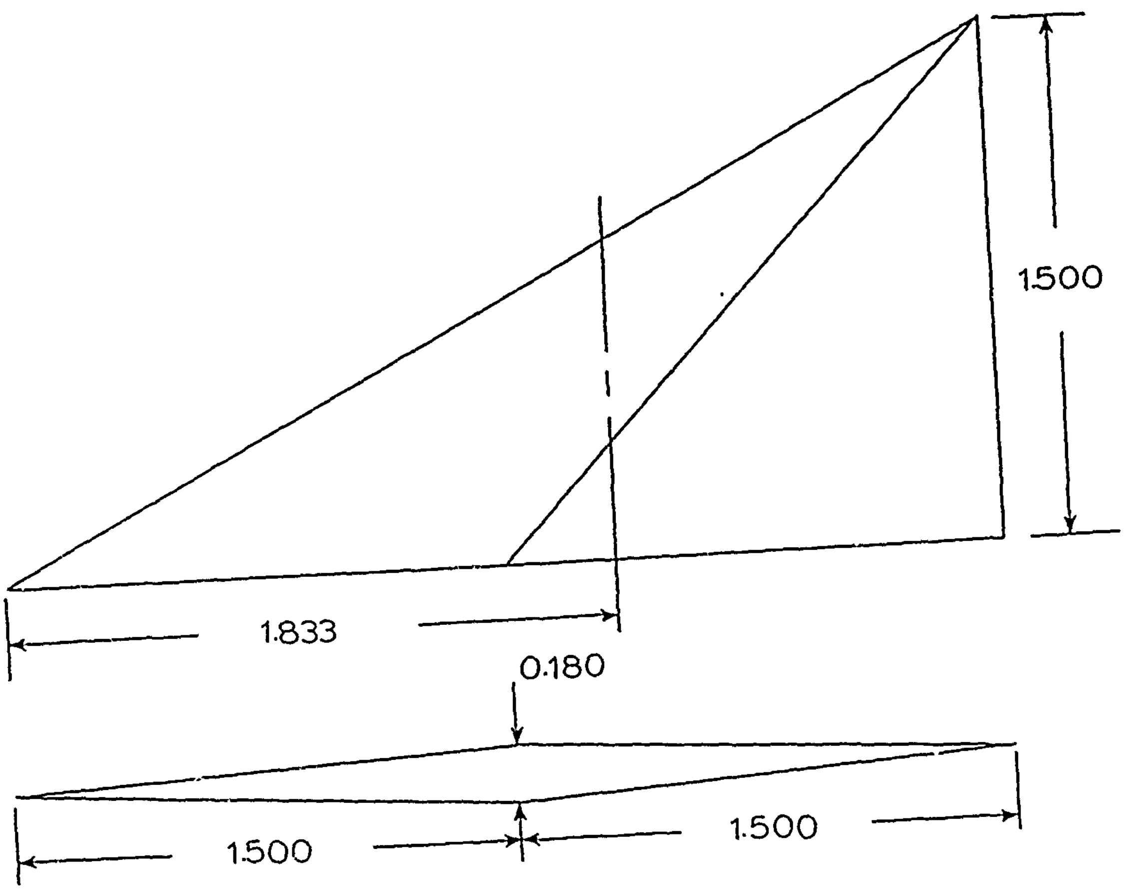

(g) Fin 51; AR = 2.0, λ = 0.0

Figure 4.- Continued.

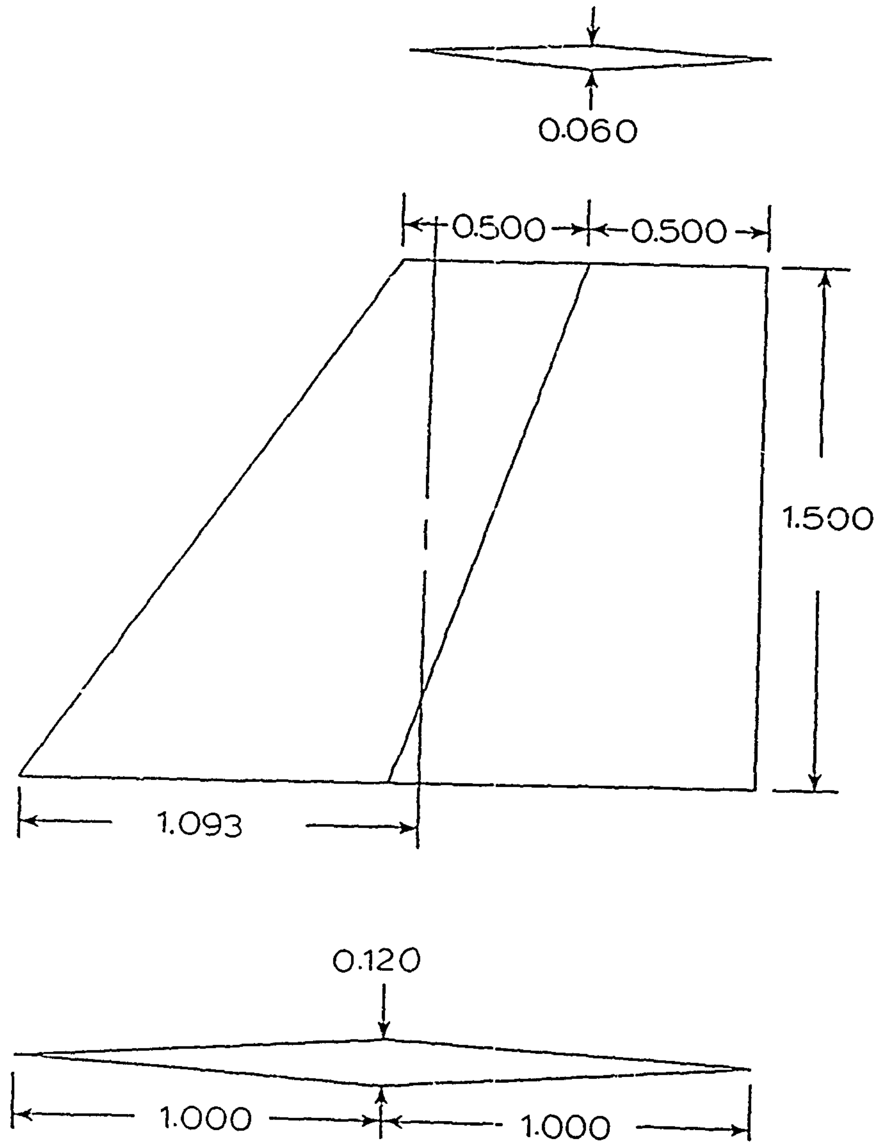

(h) Fin 52; AR = 2.0, λ = 0.5

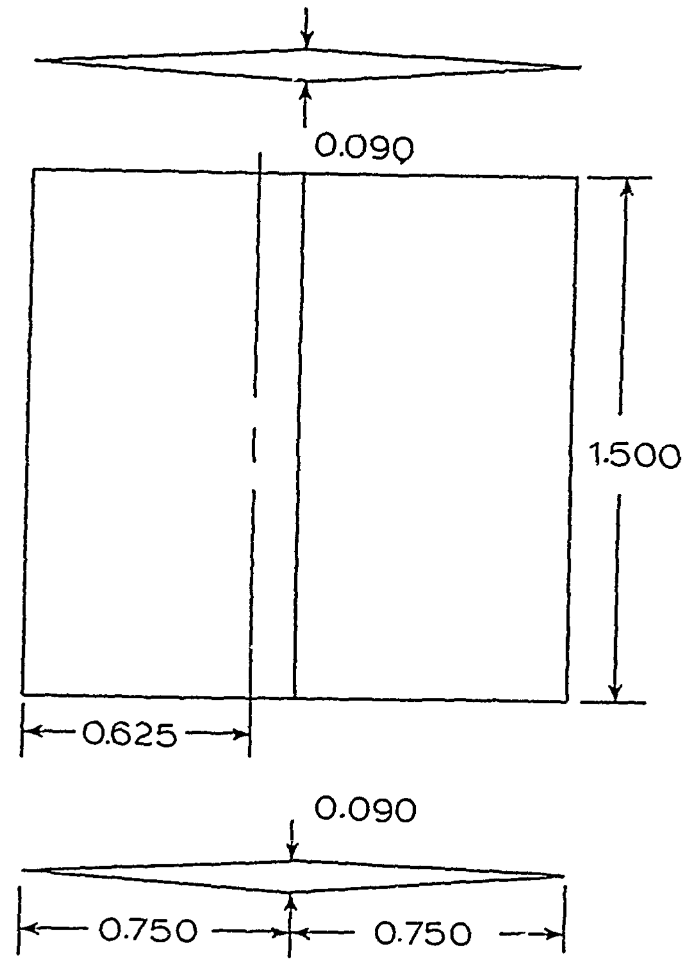

(i) Fin 53; AR = 2.0, λ = 1.0

Figure 4.- Continued.

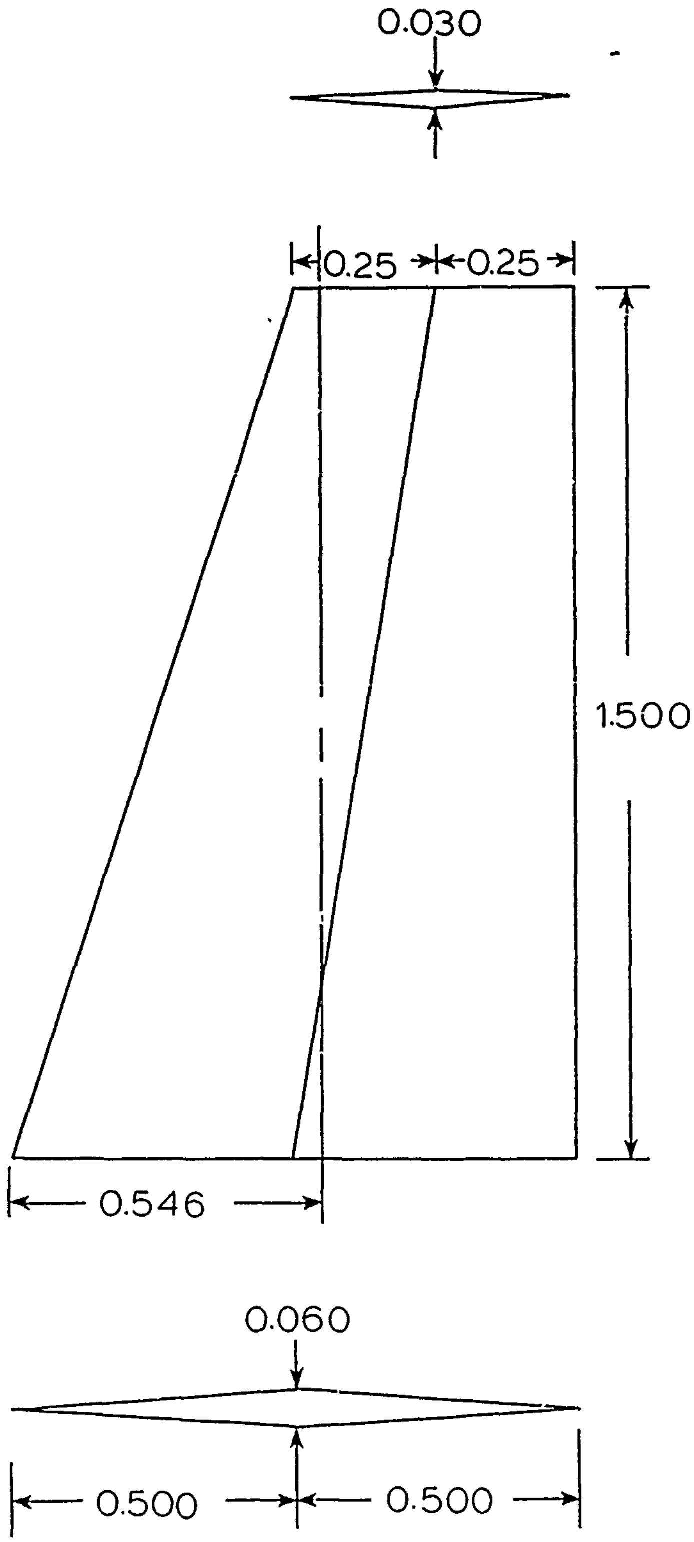

(j) Fin 62; AR = 4.0, λ = 0.5

Figure 4.- Concluded.

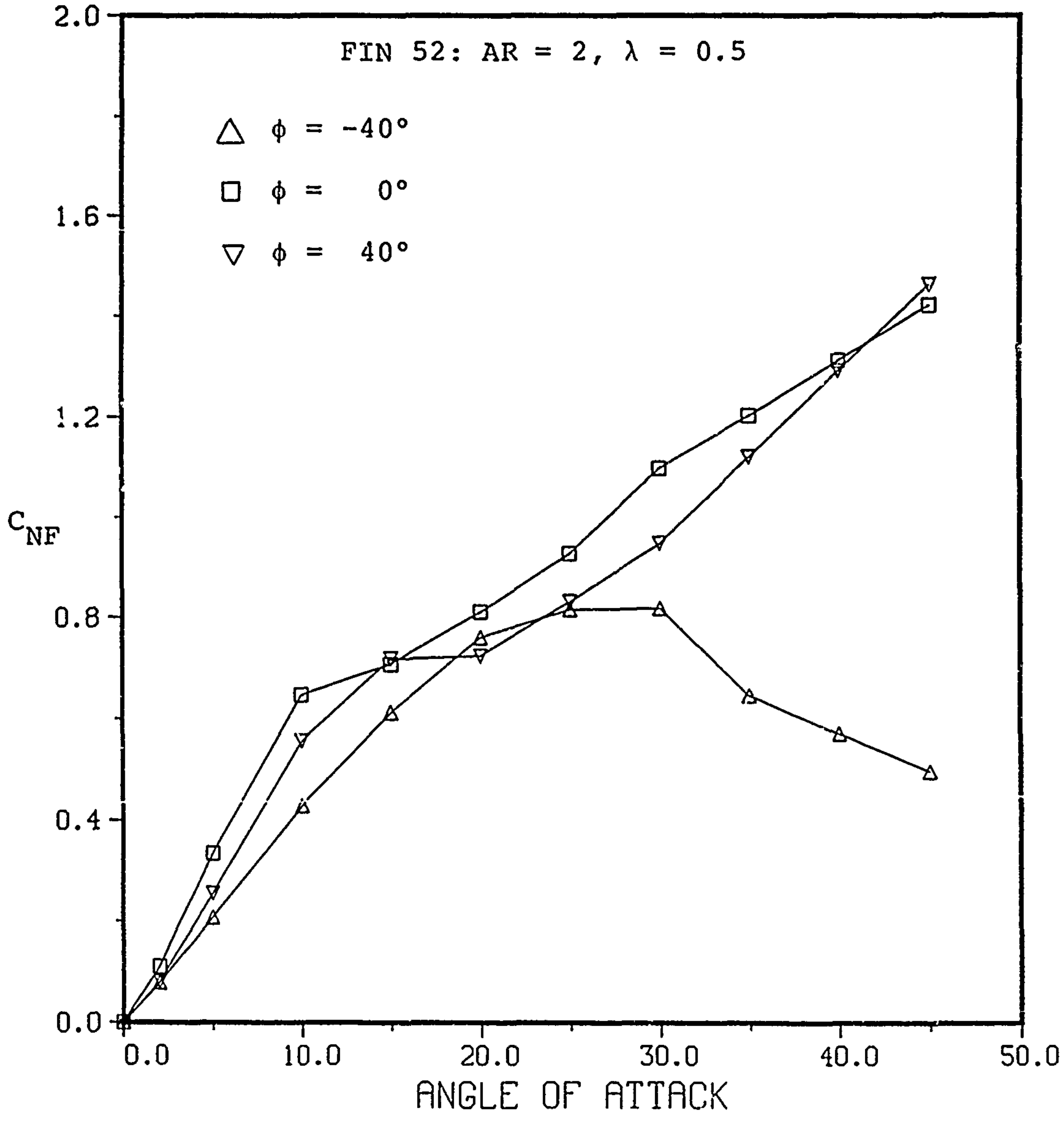

(a) $M_{\infty} = 0.8$

Figure 5.- Stability normal-force coefficient for fin 52; AR = 2, $\lambda = 0.5$.

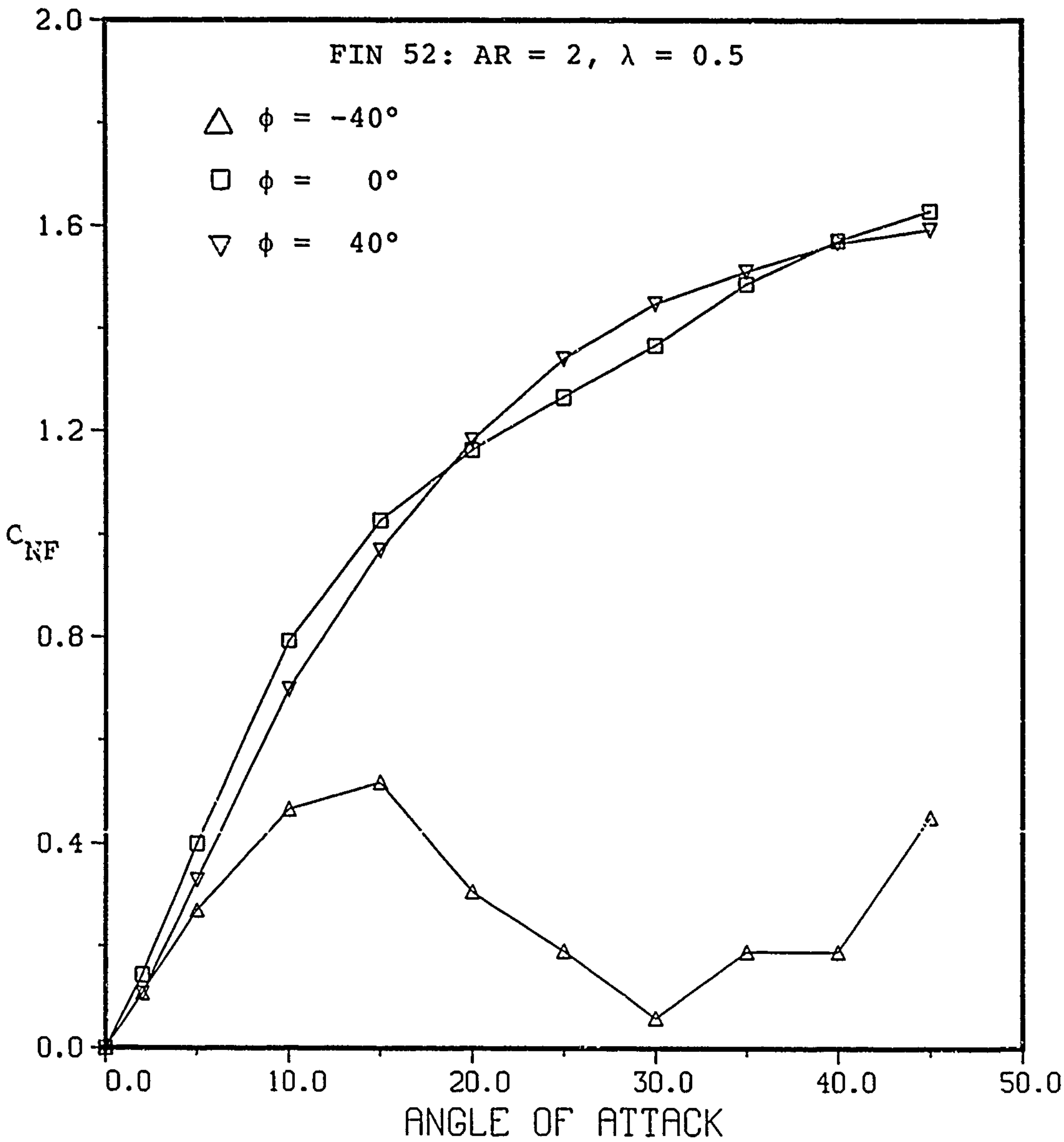

(b) $M_\infty = 1.2$

Figure 5.- Continued.

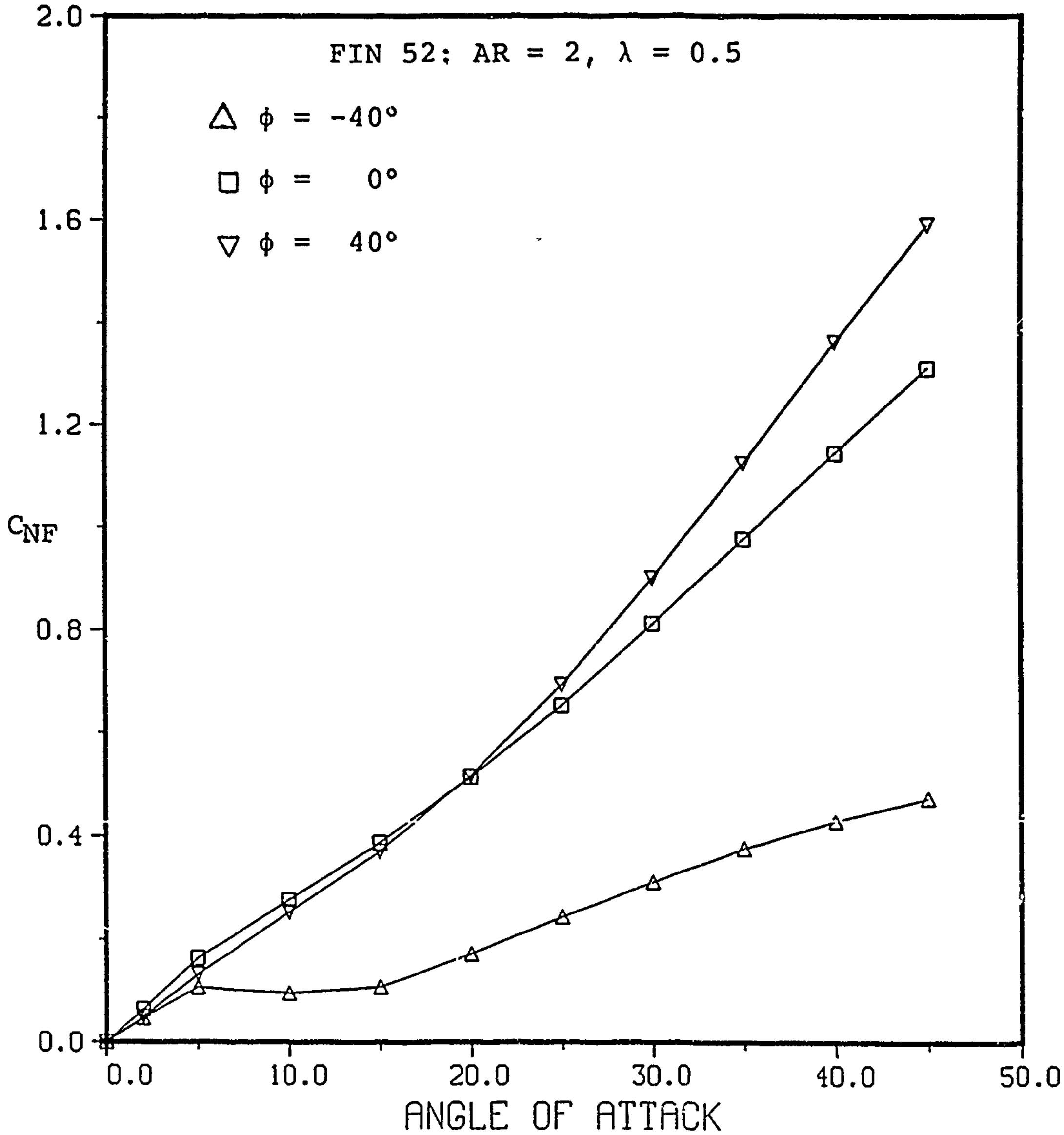

(c) $M_\infty = 3.0$

Figure 5.- Concluded.

FIN 52: AR = 2, λ = 0.5

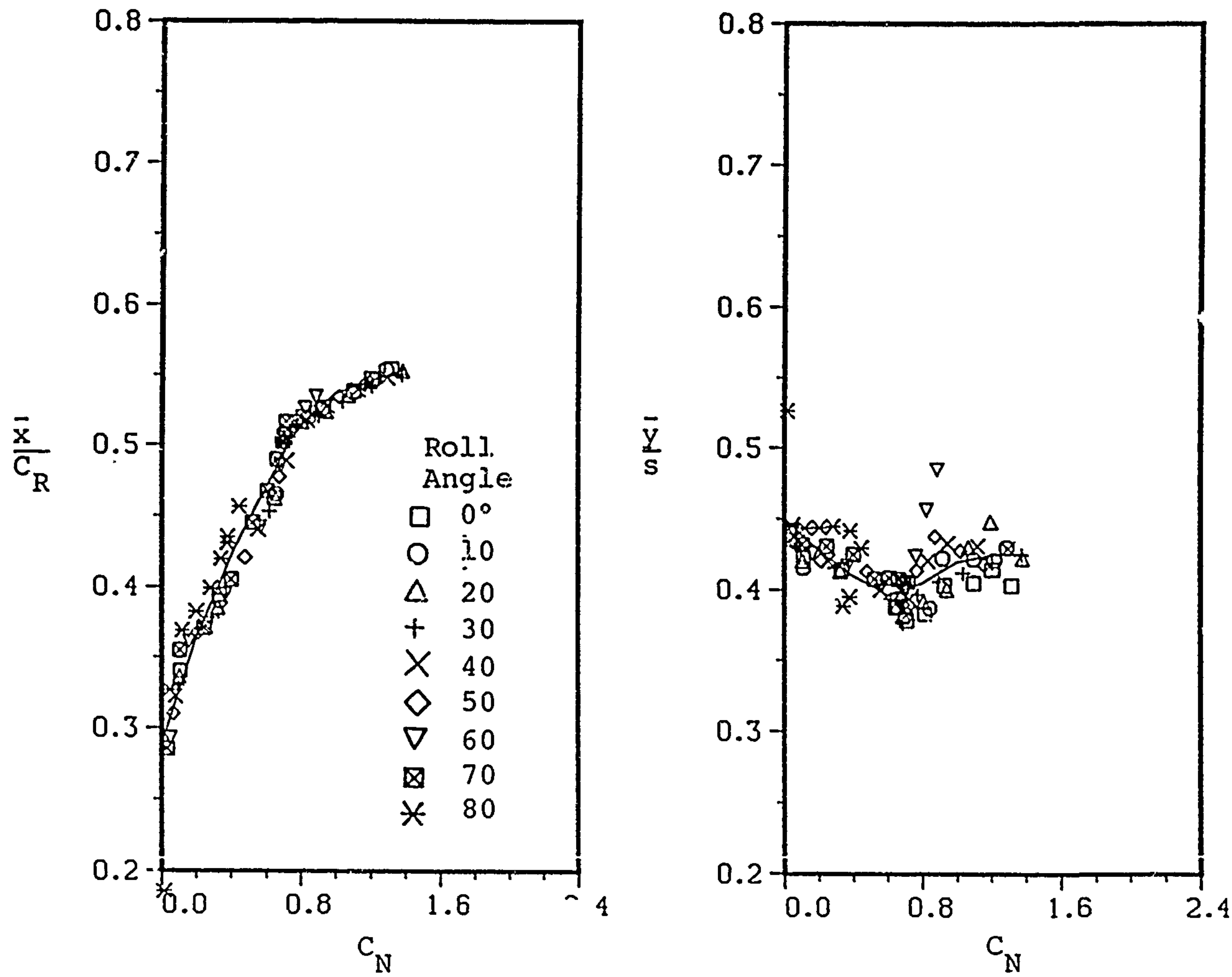

(a) $M_\infty = 0.8$

Figure 6.- $\bar{x}/C_R$ and $\bar{y}/s$ curve fits to the stability data for fin 52.

FIN 52: AR = 2, λ = 0.5

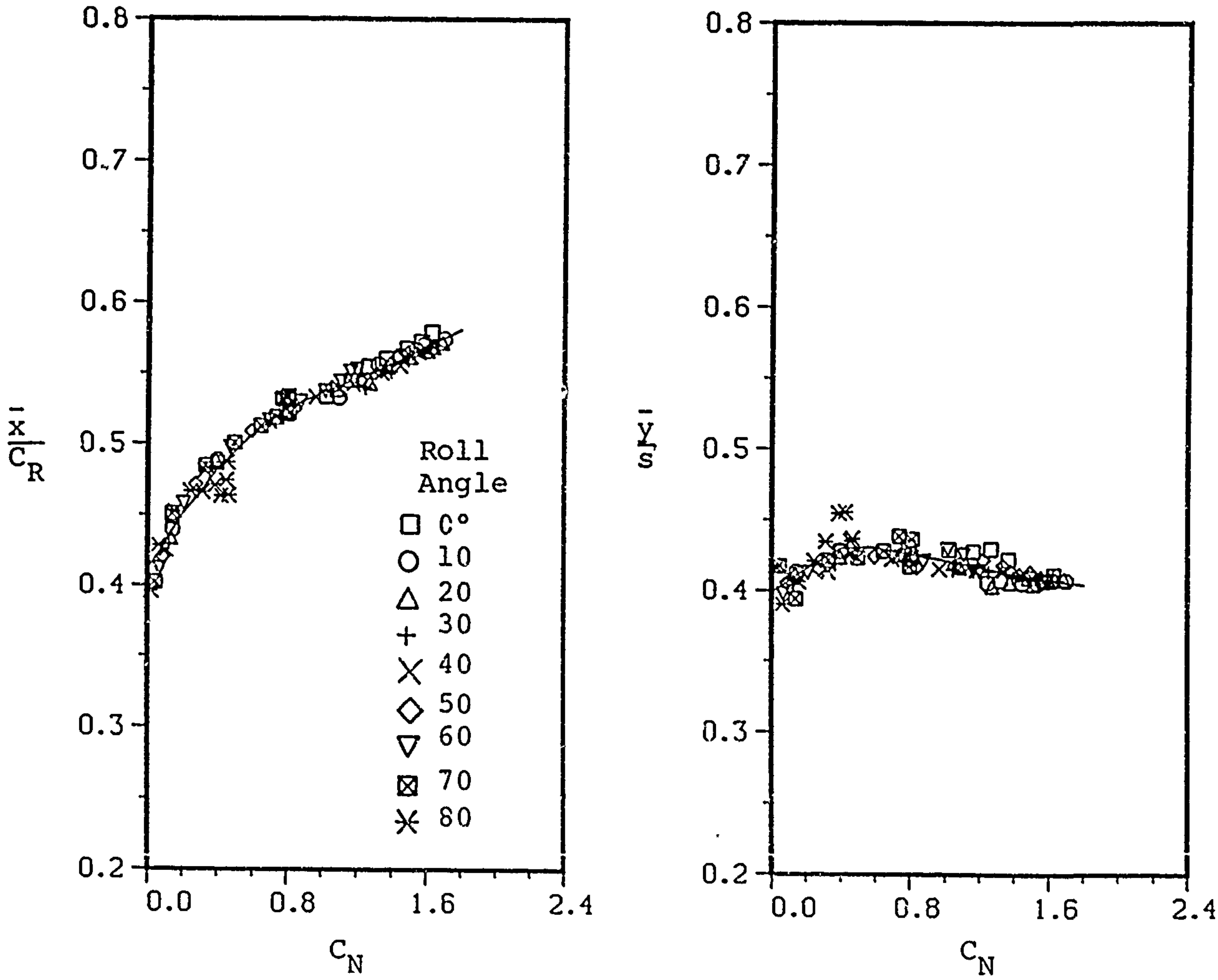

(b) $M_\infty = 1.2$

Figure 6.- Continued.

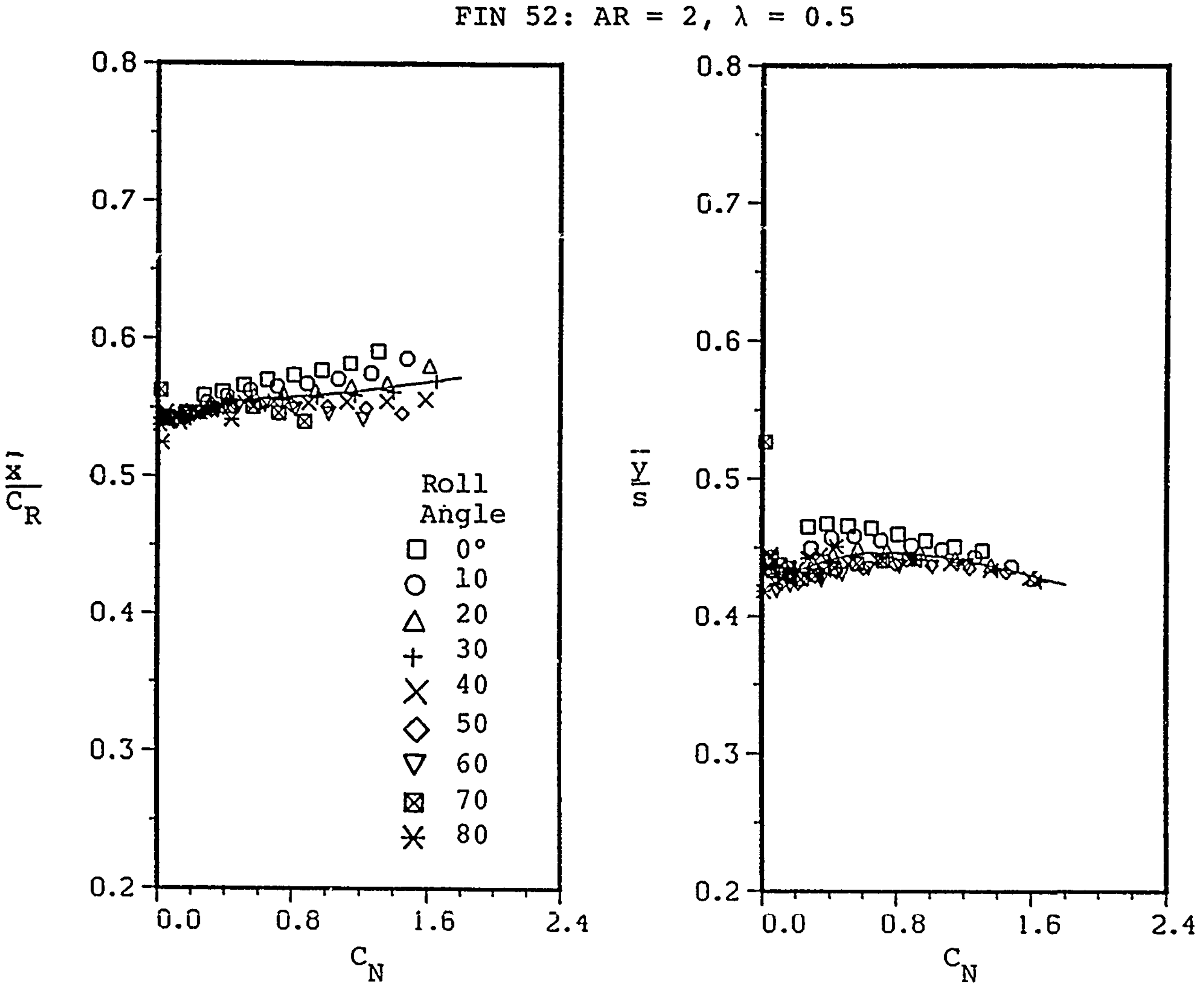

(c) $M_\infty = 3.0$

Figure 6.- Concluded.

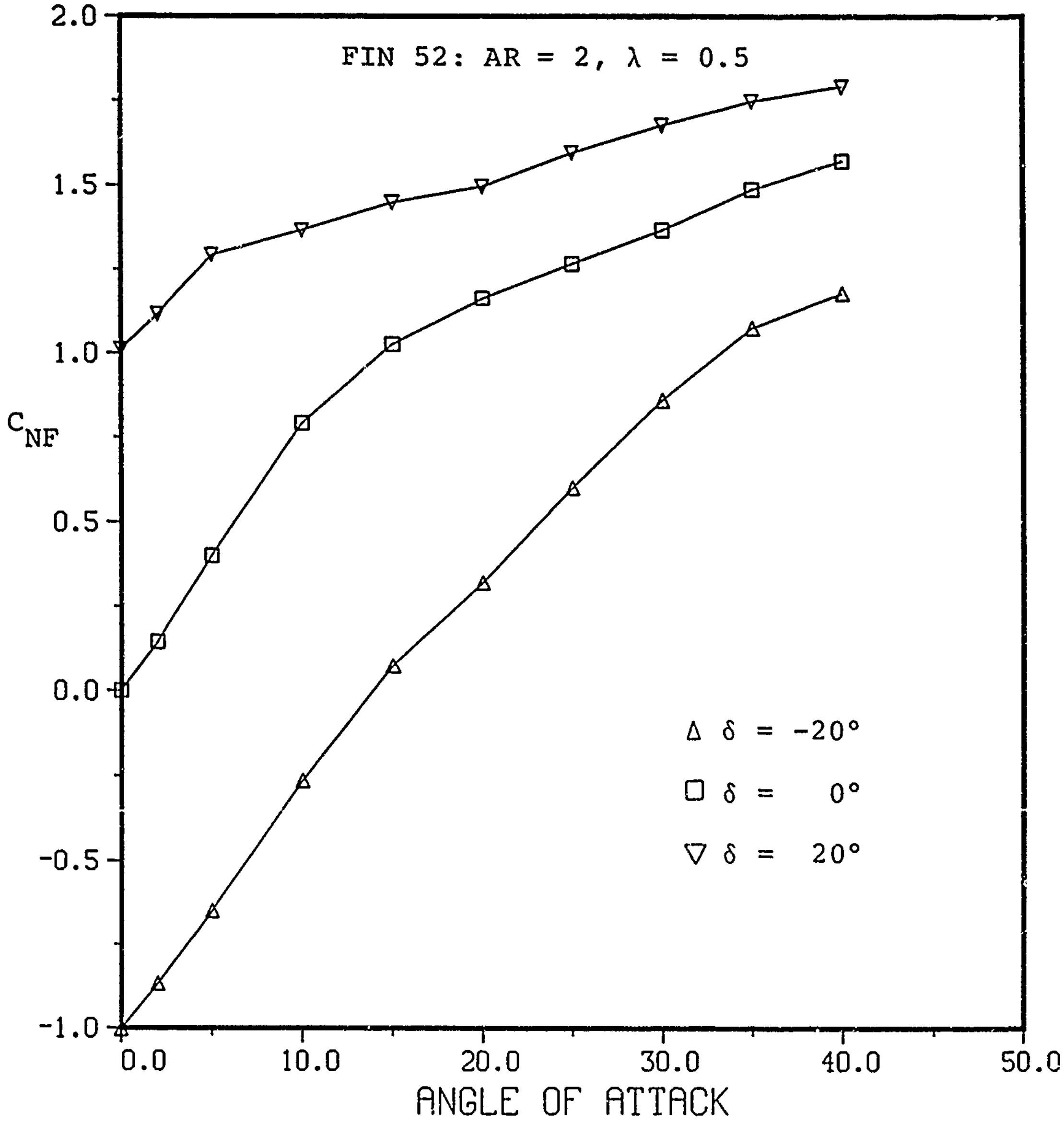

(b) $M_\infty = 1.2$

Figure 7.- Concluded.

FIN 52: AR = 2, λ = 0.5

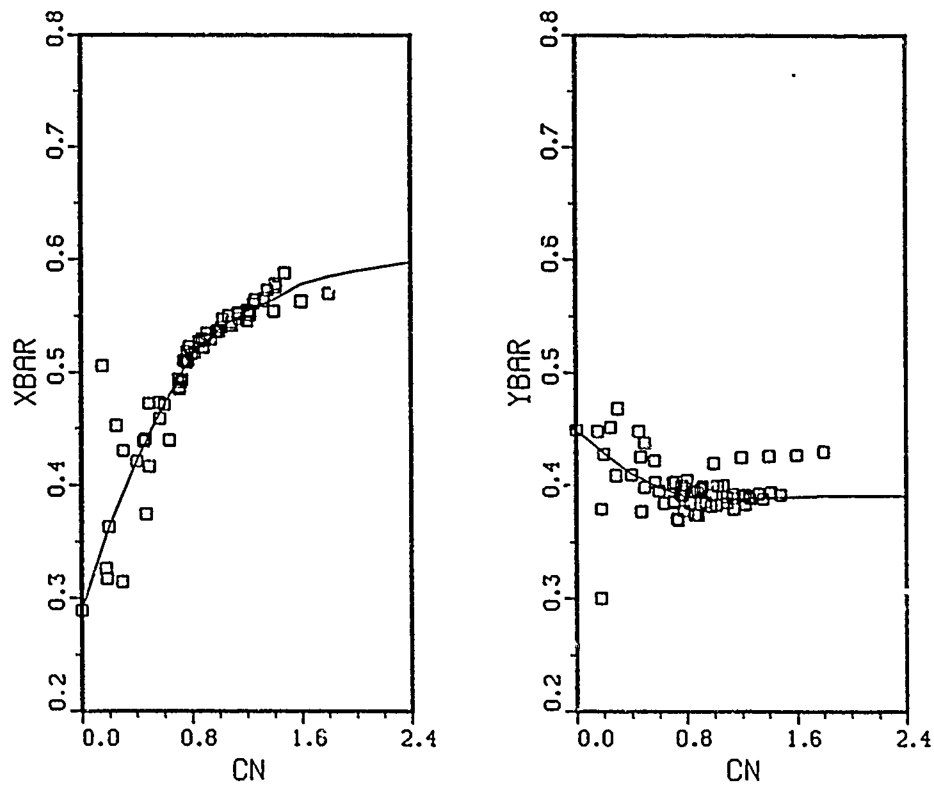

(a) M_∞ = .8

Figure 8.- $\bar{x}/C_R$ and $\bar{y}/s$ curve fits for control deflection effects.

FIN 52: AR = 2, λ = 0.5

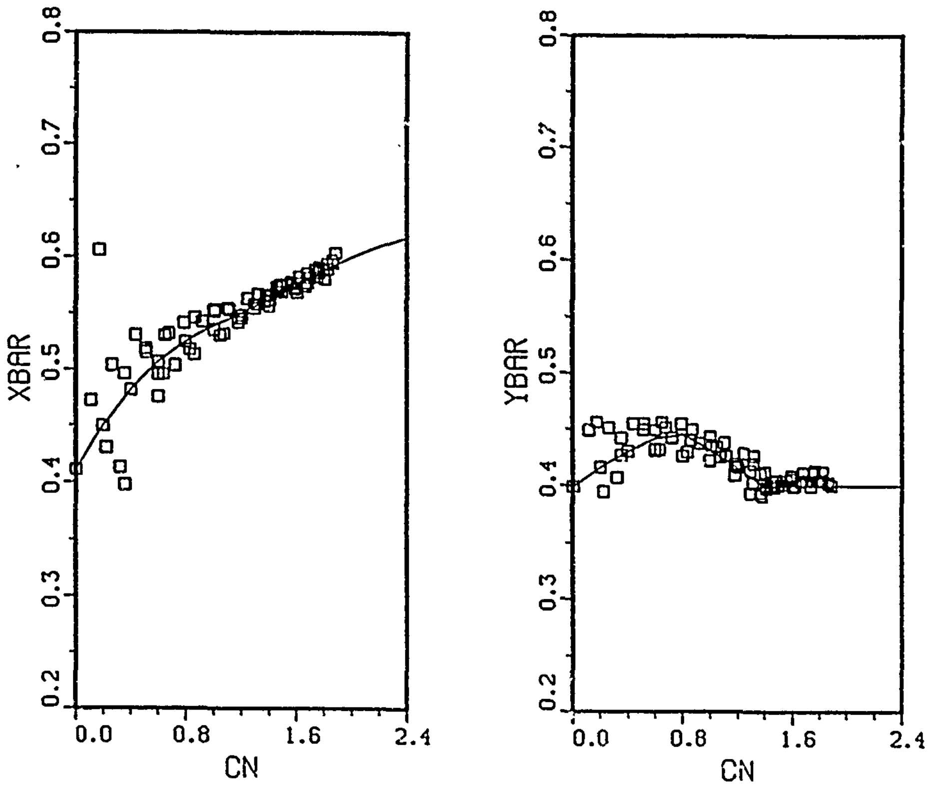

(b) M_∞ = 1.2

Figure 8.- Continued.

FIN 52: AR = 2, λ = 0.5

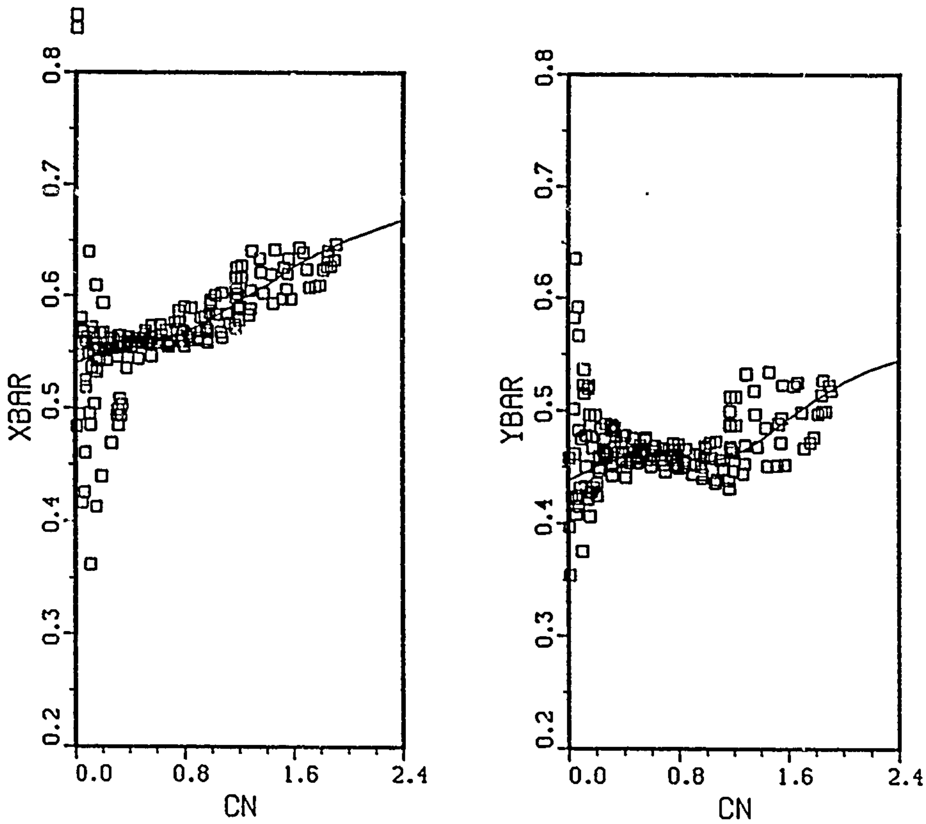

(c) $M_\infty = 3.0$

Figure 8.- Concluded.

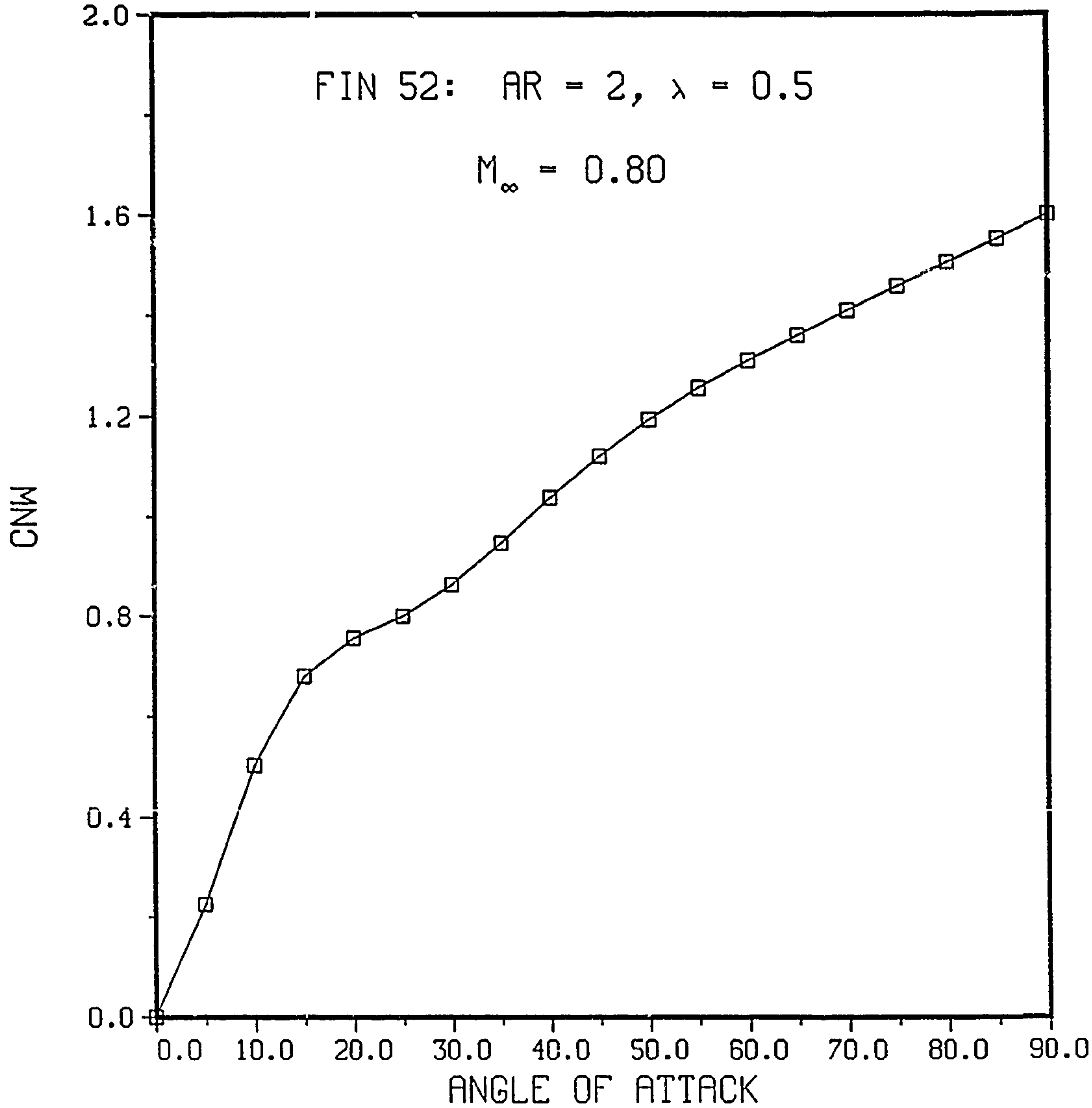

(a) $M_\infty = 0.8$

Figure 9.- Wing-alone normal-force coefficient for Fin 52.

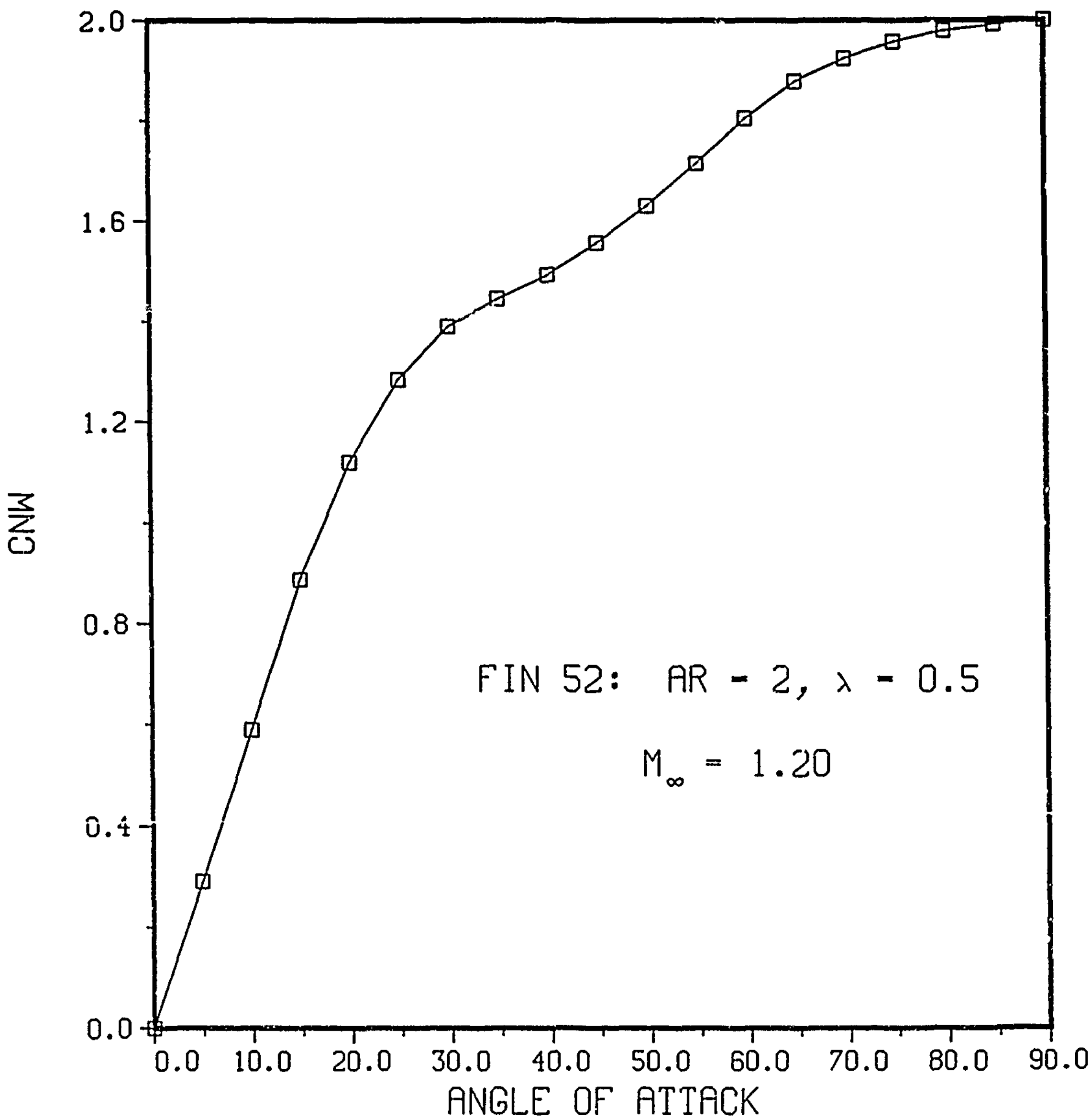

(b) $M_\infty = 1.2$

Figure 9.- Continued.

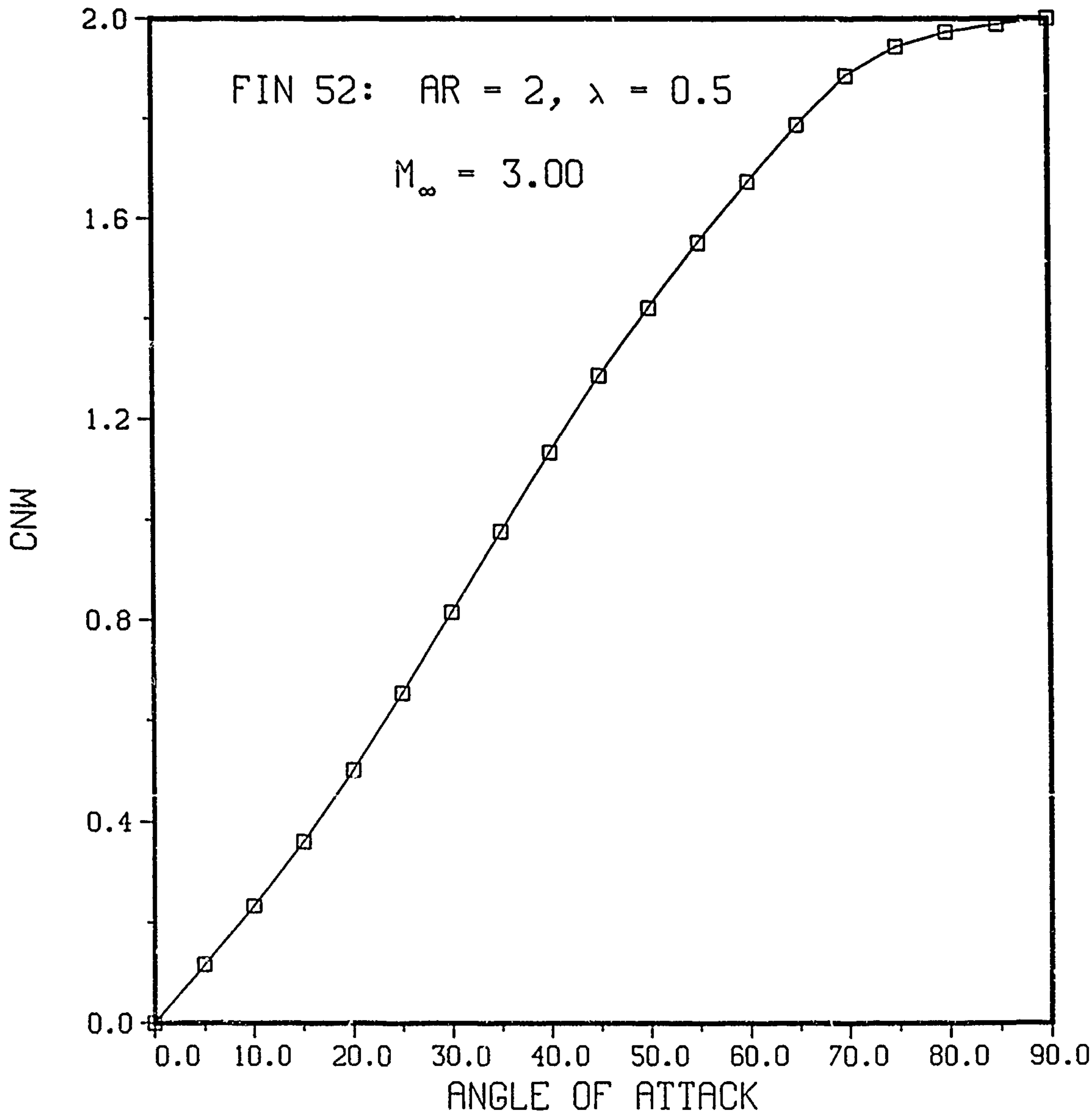

(c) $M_\infty = 3.0$

Figure 9.- Concluded.

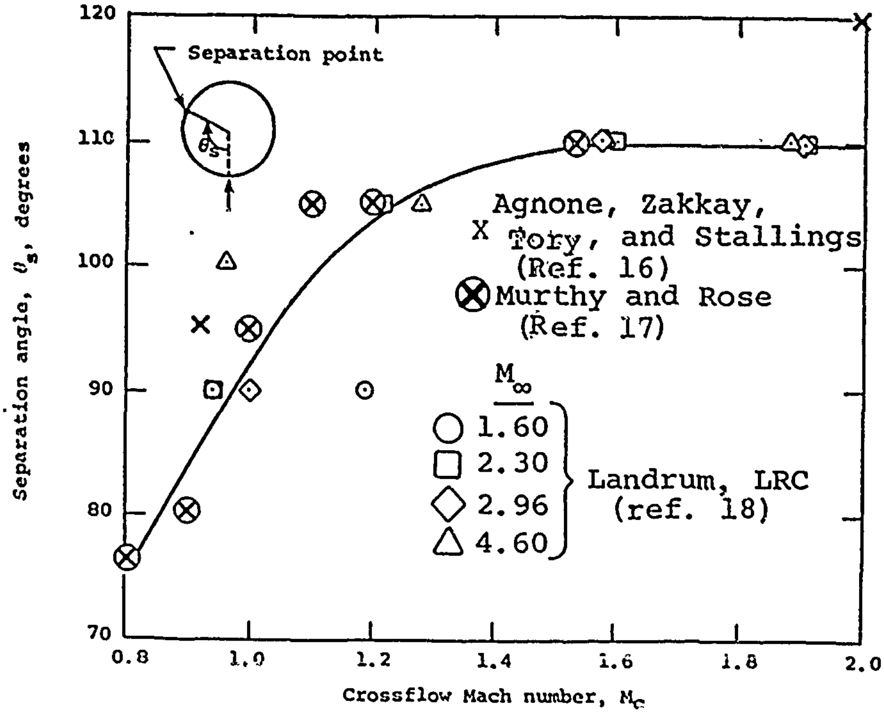

Figure 10.- Effect of crossflow Mach number on separation points on a body of revolution.

FLOW CHART OF PROGRAM - MISL3

```
PROGRAM
MISL3

    |--INPT
    |--XLEOO
    |--PROSS     ----WNGCNH
    |              |--XBAR     ----IBCIEU  ----ICSICU
    |              |                       |--ICSEVU
    |              |--YBAR     ----IBCIEU  ----ICSICU
    |              |                       |--ICSEVU
    |              |--XBARC
    |              |--YBARC
    |--CCL       ----FINTHL
    |              |--FINTHR
    |              |--FINTNL
    |              |--FINTNR
    |              |--SIMP1    ----FUN
    |--LAMIJ     ----SIMSON
    |--INTFAC    ----EQ4
    |              |--EQ5
    |              |--CHRT8
    |              |--EQ6
    |              |--EQ7
    |              |--XCPWB
    |              |--CH1416
    |--INFLU
    |--SETCNS    ----WNGCNT    ----CNT32
    |              |             |--CNT31
    |              |             |--CNT12
    |              |             |--CNT33
    |              |             |--CNT42
    |              |             |--CNT52
    |              |             |--CNT51
    |              |             |--CNT53
    |              |             |--CNT62
    |              |--WNGCND   ----CND52
    |                            |--CND51
    |                            |--CND42
    |                            |--CND53
    |                            |--CND62
    |--NOSE      ----LNTRP
    |--FINLDS    ----INTDG1
    |              |--LIN2D
    |              |--QLML     ----IBCIEU  ----ICSICU
    |              |                       |--ICSEVU
    |              |--ALFEQ    ----LNTRP
    |              |--BVTEX2   ----LNTRP
    |              |--REVFL2   ----GVEL
    |              |--INTRPD
    |              |--INTDG2
    |--FINSHD
    |--BODY3     ----VELBOD
                   |--VORADO   ----VELBOD
                   |             |--LNTRP
                   |--TRACK    ----FTRAK
                                 |--DFEQKM  ----F

END
```

Figure 11.- Subroutine calling sequence for program MISLE3.

CROSS REFERENCE MAP PAGE = 1

SUBROUTINE NAME / EXTERNAL REFERENCES	0002	ALFEQ	BODY3	BVTEX2	CCL	CH1416	CHRT8	CND42	CND51	CND52	CND53	CND62	CNT12	CNT31	CNT32	CNT33	CNT42	CNT51	CNT52	CNT53	CNT62	DFEQKM	EQ4	EQ5	EQ6	EQ7	FINLDS	FINSHD	FINTML	FINTMR	FINTNL	FINTNR	FTRAK	GVEL	IBCIEU	ICSEVU	ICSICU	INFLU	INPT	INTDG1
ALFEQ																											X													
BODY3																																								
BVTEX2																											X													
CCL																																								
CH1416																																								
CHRT8																																								
CN042																																								
CN051																																								
CN052																																								
CN053																																								
CN062																																								
CNT12																																								
CNT31																																								
CNT32																																								
CNT33																																								
CNT42																																								
CNT51																																								
CNT52																																								
CNT53																																								
CNT62																																								
DFEQKM																																								
EQ4																																								
EQ5																																								
EQ6																																								
EQ7																																								
F																						X																		
FINLDS																																								
FINSHD																																								
FINTML					X																																			
FINTMR					X																																			

(a) Page 1

Figure 12.- Subroutine cross reference list for program MISLE3.

CROSS REFERENCE MAP

SUBROUTINE NAME / EXTERNAL REFERENCES	A0002	BLFEQ	BODY3	CVTEX2	CL	CH1416	CHRT8	CND42	CND51	CND52	CND53	CND62	CNT12	CNT31	CNT32	CNT33	CNT42	CNT51	CNT52	CNT53	CNT62	DFEQKM	EQ4	EQ5	EQ6	EQ7	FINLDS	FINSHD	FINTML	FINTMR	FINTNL	FINTNR	FTRAK	GVEL	IBCIEU	ICSEVU	ICSICU	INFLU	INPT	INTDG1
FINTNL					X																																			
FINTNR					X																																			
FTRAK																																								
FUN																																								
GVEL																																								
IBCIEU																																								
ICSEVU																																			X					
ICSICU																																			X					
INFLU																																								
INPT																																								
INTDG1																										X														
INTDG2																										X														
INTFAC																																								
INTRPD																										X														
LAMIJ																																								
LIN2D																										X														
LNTRP		X		X																																				
NOSE																																								
PROSS																																								
QLML																										X														
REVFL2																										X														
SETCNS																																								
SIMP1					X																																			
SIMSON																																								
TRACK			X																																					
VELBOD			X																																					
VGRADD			X																																					
WNGCND																																								
WNGCNT																																								
WNGCNW																																								

(b) Page 2

Figure 12.- Continued.

```
            CROSS REFERENCE MAP                       PAGE =  3

           +----------+----------+----------+----------+----------+----------+----------+----------+
           | A B B C  |C C C C C |C C C C C |C C C C C |C D E E E |E F F F F |F F F G I |I I I I I |
           |0 L 0 V C |H H N N N |N N N N N |N N N N N |N F Q Q Q |Q I I I I |I I T V B |C C N N N |
SUBROUTINE |0 F D T L |1 R D D D |D D T T T |T T T T T |T E 4 5 6 |7 N N N N |N N R E C |S S F P T |
   NAME    |0 E Y E   |4 T 4 5 5 |5 6 1 3 3 |3 4 5 5 5 |6 Q       |  L S T T |T T A L I |E I L T D |
           |2 Q 3 X   |1 8 2 1 2 |3 2 2 1 2 |3 2 1 2 3 |2 K       |  D H M M |N N K   E |V C U   G |
---------- |      2   |t         |          |          |  M       |  S D L R |L R     U |U U     1 |
 EXTERNAL  |          |          |          |          |          |          |          |          |
REFERENCES |          |          |          |          |          |          |          |          |
-----------+-|-|-|-|--+-|-|-|-|--+-|-|-|-|--+-|-|-|-|--+-|-|-|-|--+-|-|-|-|--+-|-|-|-|--+-|-|-|-|--+
XBAR       |          |          |          |          |          |          |          |          |
XBARC      |          |          |          |          |          |          |          |          |
XCPWB      |          |          |          |          |          |          |          |          |
XLEOD      |          |          |          |          |          |          |          |          |
YBAR       |          |          |          |          |          |          |          |          |
           +----------+----------+----------+----------+----------+----------+----------+----------+
YBARC      |          |          |          |          |          |          |          |          |
           +----------+----------+----------+----------+----------+----------+----------+----------+
```

(c) Page 3

Figure 12.- Continued.

CROSS REFERENCE MAP PAGE = 4

SUBROUTINE NAME / EXTERNAL REFERENCES	INTDG2	INTFAC	INTRPD	LAMIJ	LIN2D	LNTRP	MISL3	NOSE	PROSS	QLML	REVFL2	SETCNS	SIMP1	SIMSON	TRACK	VELBOD	VORADD	WNGCND	WNGCNT	WNGCNW	XBAR	XBARC	XCPWB	XLEOD	YBAR	YBARC
ALFEQ																										
BODY3							X																			
BVTEX2																										
CCL							X																			
CH1416		X																								
CHRT8		X																								
CND42																		X								
CND51																		X								
CND52																		X								
CND53																		X								
CND62																		X								
CNT12																			X							
CNT31																			X							
CNT32																			X							
CNT33																			X							
CNT42																			X							
CNT51																			X							
CNT52																			X							
CNT53																			X							
CNT62																			X							
DFEQKM															X											
EQ4		X																								
EQ5		X																								
EQ6		X																								
EQ7		X																								
F																										
FINLDS							X																			
FINSHD							X																			
FINTML																										
FINTMR																										

(d) Page 4

Figure 12.- Continued.

CROSS REFERENCE MAP PAGE = 5

SUBROUTINE NAME / EXTERNAL REFERENCES	INTDG2	INTFAC	INTRPD	LAMIJ	LIN2D	LNTRP	MISL3	NOSE	PROSS	QLML	REVFL2	SETCNS	SIMP1	SIMSON	TRACK	VELBOD	VORADD	WNGCND	WNGCNT	WNGCNW	XBAR	XBARC	XCPHB	XLEOD	YBAR	YBARC
FINTNL																										
FINTNR																										
FTRAK															X											
FUN													X													
GVEL											X															
IBCIEU										X											X				X	
ICSEVU																										
ICSICU																										
INFLU							X																			
INPT							X																			
INTDG1																										
INTDG2																										
INTFAC							X																			
INTRPD																										
LAMIJ							X																			
LIN2D																										
LNTRP								X									X									
NOSE							X																			
PROSS							X																			
QLML																										
REVFL2																										
SETCNS							X																			
SIMP1																										
SIMSON				X																						
TRACK																										
VELBOD																	X									
VORADD																										
WNGCND												X														
WNGCNT												X														
WNGCNW									X																	

(e) Page 5

Figure 12.- Continued.

CROSS REFERENCE MAP PAGE = 6

SUBROUTINE NAME / EXTERNAL REFERENCES	INTDG2	INTFAC	INTRPD	LAMIJ	LIN2D	LNTRP	MISL3	NOSE	PROSS	QLML	REVFL2	SETCNS	SIMP1	SIMSON	TRACKN	VELBOD	VORADD	WNGCND	WNGCNT	WNGCNW	XBAR	XBARC	XCPWB	XLEOD	YBAR	YBARC
XBAR									X																	
XBARC									X																	
XCPWB		X																								
XLEOD							X																			
YBAR									X																	
YBARC									X																	

(f) Page 6

Figure 12.- Concluded.

```
            CROSS REFERENCE MAP                          PAGE =  1

          +-----------+-----------+-----------+-----------+-----------+-----------+-----------+-----------+
          |   A B B C | C C C C C | C C C C C | C C C C C | C D E E E | E F F F F | F F F G I | I I I I I |
          | O L O V C | H H N N N | H N N N N | N N N N N | N F Q Q Q | Q I I I I | I I T V B | C C N N N |
SUBROUTINE| O F D T L | 1 R D D D | D D T T T | T T T T T | T E 4 5 6 | 7 N N N N | N N R E C | S S F P T |
   NAME   | O E Y E   | 4 T 4 5 5 | 5 6 1 3 3 | 3 4 5 5 5 | 6 Q       |   L S T T | T T A L I | E I L T O |
          | 2 Q 3 X   | 1 8 2 1 2 | 3 2 2 1 2 | 3 2 1 2 3 | 2 K       |   D H H H | N N K   E | V C U   G |
----------|       2   | 6         |           |           |   H       |   S D L R | L R     U | U U     1 |
  COMMON  |           |           |           |           |           |           |           |           |
  BLOCKS  |           |           |           |           |           |           |           |           |
----------+-|-|-|-|-|-+-|-|-|-|-|-+-|-|-|-|-|-+-|-|-|-|-|-+-|-|-|-|-|-+-|-|-|-|-|-+-|-|-|-|-|-+-|-|-|-|-|-+
CCL       |         X |           |           |           |           |       X X | X X       |           |
CNF       | X         |           |           |           |           |   X       |           |           |
CNST      |     X X X | X X       |           |           |           |   X X     |           |     X     |
CNTLXY    | X         |           |           |           |           |   X       |           |           |
COND      |           |           |           |           |           |           |           |       X   |
          +-----------+-----------+-----------+-----------+-----------+-----------+-----------+-----------+
GEOM      |           |           |           |           |           |   X       |           |       X   |
LOS       |           |           |           |           |           |           |           |       X   |
NOSE      |           |           |           |           |           |           |           |       X   |
PREPRO    | X X       |           |           |           |           |   X       |           |           |
PROG      |     X     |           |           |           |           |           |           |       X   |
          +-----------+-----------+-----------+-----------+-----------+-----------+-----------+-----------+
REF       |     X     |           |           |           |           |   X       |           |       X   |
VORTS     |     X     |           |           |           |           |   X X     |     X X   |           |
          +-----------+-----------+-----------+-----------+-----------+-----------+-----------+-----------+


            CROSS REFERENCE MAP

          +-----------+-----------+-----------+-----------+-----------+-----------+-----------+-----------+
          | I I I L L | L M N P Q | R S S S T | V V W W W | X X X X Y | Y         |           |           |
          | N N N A I | N I O R L | E E I I R | E O N N N | B B C L B | B         |           |           |
SUBROUTINE| T T T M N | T S S O M | V T M M A | L R G G G | A A P E A | A         |           |           |
   NAME   | D F R I 2 | R L E S L | F C P S C | B A C C C | R R W O R | R         |           |           |
          | G A P J D | P 3     S | L N 1 O K | O D N N N |   C B D   | C         |           |           |
----------| 2 C D     |           | 2 S   N   | D D D T H |           |           |           |           |
  COMMON  |           |           |           |           |           |           |           |           |
  BLOCKS  |           |           |           |           |           |           |           |           |
----------+-|-|-|-|-|-+-|-|-|-|-|-+-|-|-|-|-|-+-|-|-|-|-|-+-|-|-|-|-|-+-|-|-|-|-|-+-|-|-|-|-|-+-|-|-|-|-|-+
CCL       |           |           |           |           |           |           |           |           |
CNF       |     X     |           |   X       |           |           |           |           |           |
CNST      |   X   X   |   X X     | X         |   X       |     X     |           |           |           |
CNTLXY    |           |       X   |           |           |           |           |           |           |
COND      |           |   X       |           |           |           |           |           |           |
          +-----------+-----------+-----------+-----------+-----------+-----------+-----------+-----------+
GEOM      |           |   X       |           |           |           |           |           |           |
LOS       |           |   X       |           |           |           |           |           |           |
NOSE      |           |   X X     |           |           |           |           |           |           |
PREPRO    |           |       X   |           |           |           |           |           |           |
PROG      |           |   X       |           |           |           |           |           |           |
          +-----------+-----------+-----------+-----------+-----------+-----------+-----------+-----------+
REF       |           |   X X     |           |           |           |           |           |           |
VORTS     |           |           |         X | X X       |           |           |           |           |
          +-----------+-----------+-----------+-----------+-----------+-----------+-----------+-----------+
```

Figure 13.- Common block cross reference list for program MISLE3.

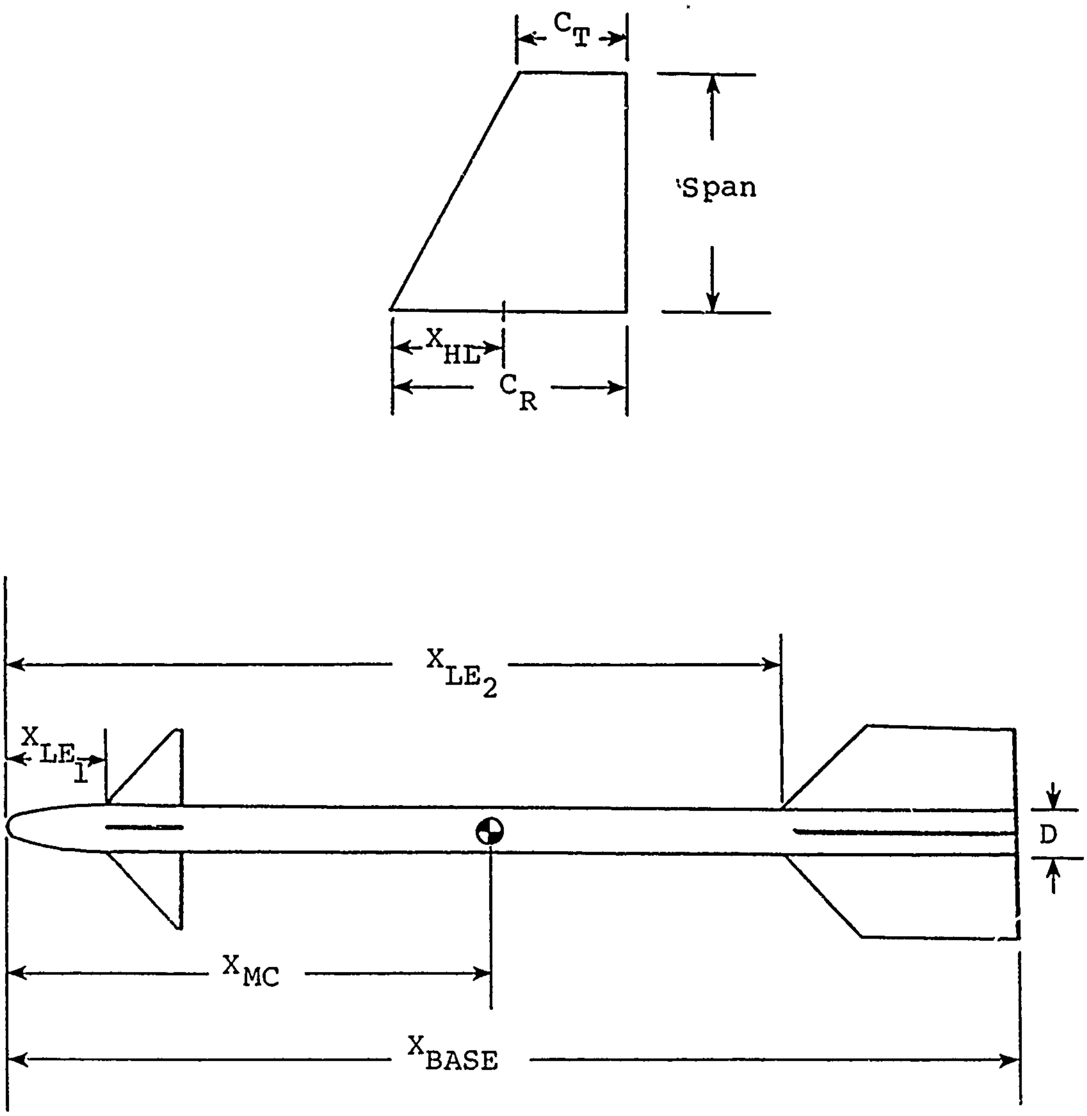

Figure 14.- Geometric inputs for program MISLE3.

```
ITEM
 NO.
-----
 (1)     2
 (2)   SAMPLE CASE 1 FOR MISLE3.  DIMENSIONS IN CENTIMETERS
       SIDEWINDER TYPE MISSILE; REF. NASA TP 2157, JUNE 1983
 (3)     2    3     1   25     1     1     F    .1ØE-Ø2    T     F     F
 (4)    14.Ø813    4.234    46.Ø4Ø     4.234     Ø.ØØØ   1Ø2.319
 (5)     7.24Ø    15.8ØØ     6.35Ø     3.338    11.123
 (6)     9.Ø4Ø    8Ø.729    1Ø.795    12.55Ø    21.59Ø
 (7)     2.ØØ     45.ØØ      Ø.ØØ      Ø.ØØ      Ø.ØØ      Ø.ØØ
         5.ØØ     45.ØØ      Ø.ØØ      Ø.ØØ      Ø.ØØ      Ø.ØØ
        1Ø.ØØ     45.ØØ      Ø.ØØ      Ø.ØØ      Ø.ØØ      Ø.ØØ
 (8)     2.5Ø
 (9)     1
(11)     1
(12)     2.ØØØØØ
(13)     31
(14)     Ø.ØØØØØ   Ø.Ø13Ø5   Ø.Ø5215   Ø.11721   Ø.2Ø8Ø3   Ø.32439   Ø.46594   Ø.63231
         Ø.823Ø5   1.Ø3762   1.27544   1.53586   1.81816   2.12157   2.44526   2.78834
         3.14988   3.52887   3.92428   4.335Ø4   4.76ØØØ   5.198Ø1   5.64787   6.1Ø834
         6.57816   7.Ø56Ø5   7.54Ø68   8.Ø3Ø75   8.52489   9.Ø2177   9.53ØØØ
(15)     Ø.ØØØØØ   Ø.ØØ6Ø9   Ø.Ø2429   Ø.Ø5437   Ø.Ø9595   Ø.14849   Ø.21136   Ø.28375
         Ø.36479   Ø.4535Ø   Ø.54881   Ø.64959   Ø.75467   Ø.86285   Ø.97289   1.Ø8358
         1.1937Ø   1.3Ø2Ø7   1.4Ø752   1.5Ø896   1.6Ø534   1.69568   1.779Ø5   1.85464
         1.9217Ø   1.97958   2.Ø2771   2.Ø6562   2.Ø9297   2.1Ø948   2.117ØØ
```

Figure 15.- Sample case 1 input.

```
ITEM
 NO.
----
 (1)     3
 (2)   SAMPLE CASE 2 FOR MISLE3.  DIMENSIONS IN INCHES
       ARMY GENERALIZED MISSILE C6T2
       REF. NEAR TR 72, AUGUST 1974.
 (3)     2    4    2   1Ø    1    1     F   .1ØE-Ø2    T    T    T
 (4)   19.635     5.ØØ     26.ØØ      5.ØØ      Ø.ØØ     52.ØØ
 (5)    3.75     12.72      2.28      Ø.25      4.ØØ
 (6)    3.5Ø     43.ØØ      3.ØØ      3.5Ø      7.ØØ
 (7)    8.ØØ      Ø.ØØ      Ø.ØØ      Ø.ØØ      Ø.ØØ      Ø.ØØ
        8.ØØ      Ø.ØØ      Ø.ØØ     15.ØØ      Ø.ØØ     15.ØØ
        8.ØØ     45.ØØ      Ø.ØØ      Ø.ØØ      Ø.ØØ      Ø.ØØ
        8.ØØ     45.ØØ     15.ØØ     15.ØØ     15.ØØ     15.ØØ
 (8)    1.3Ø      1.75
 (9)     Ø
(1Ø)    Ø.ØØ      Ø.ØØ      Ø.ØØ
        Ø.ØØ      Ø.ØØ      Ø.ØØ
        Ø.ØØ      Ø.ØØ      Ø.ØØ
        Ø.ØØ      Ø.ØØ      Ø.ØØ
        Ø.ØØ      Ø.ØØ      Ø.ØØ
        Ø.ØØ      Ø.ØØ      Ø.ØØ
        Ø.ØØ      Ø.ØØ      Ø.ØØ
        Ø.ØØ      Ø.ØØ      Ø.ØØ
```

Figure 16.- Sample case 2 input.

```
                    **************************

                        MISSILE 3 RESULTS
                         VERSION 1, 6-86

                    **************************

                   SAMPLE CASE 1 FOR MISLE3.  DIMENSIONS IN CENTIMETERS
                   SIDEWINDER TYPE MISSILE; REF. NASA TP 2157, JUNE 1983

  ***** PROGRAM CONTROLS *****
NFIN   NCOND   NMACH   NXAB   NSET   NSHED   LTAIL       E5    BSHED   OUTP   DEFLEC

  2      3       1      25      1      1       F   0.100E-02     T       F       F

  ***** REFERENCE INFORMATION *****
  SROUT        LROUT        XMC           D         XZERO        XBASE

 14.0813       4.2340     46.0400      4.2340      0.0000     102.3190

  ***** GEOMETRY INFORMATION FOR FIRST SET OF FINS *****
   SPAN         XLE          HL           CT          CR           AR          TR

  7.2400      15.8000      8.3500      3.3380     11.1230      2.0026      0.3001

  ***** GEOMETRY INFORMATION FOR SECOND SET OF FINS *****
   SPAN         XLE          HL           CT          CR           AR          TR

  9.0400      80.7290     10.7950     12.5500     21.5900      1.0592      0.5813

  ****** ATTITUDE CONDITIONS *****
  I    ALFAC      PHI    DELTA1    DELTA2    DELTA3    DELTA4

  1     2.0      45.0     0.0       0.0       0.0       0.0
  2     5.0      45.0     0.0       0.0       0.0       0.0
  3    10.0      45.0     0.0       0.0       0.0       0.0

  ***** MACH NUMBERS *****

 2.5000

  ***** NOSE GEOMETRY *****

  D(CN)/D(ALPHA) =    2.0000

XNOSE
     0.00000   0.01305   0.05215   0.11721   0.20803   0.32439   0.46594   0.63231
     0.82305   1.03762   1.27544   1.53586   1.81816   2.12157   2.44526   2.78834
     3.14988   3.52887   3.92428   4.33504   4.76000   5.19801   5.64787   6.10834
     6.57816   7.05605   7.54069   8.03075   8.52489   9.02177   9.53000

RNOSE
     0.00000   0.00609   0.02429   0.05437   0.09595   0.14849   0.21136   0.28375
     0.36479   0.45350   0.54881   0.64959   0.75467   0.86285   0.97289   1.08358
     1.19370   1.30207   1.40752   1.50896   1.60534   1.69568   1.77985   1.85464
     1.92170   1.97958   2.02771   2.06562   2.09297   2.10948   2.11700
```

(a) Page 1

Figure 17.- Sample Case 1 output.

***** MISSILE 3 OUTPUT *****

CASE 1 MACH = 2.5000 ALFAC = 2.0000 PHI = 45.0000

***** COMPONENT LOADS *****

	CX	CY	CZ	CMX	CMY	CMZ
NOSE LOADS	0.0000E+00	0.0000E+00	0.6979E-01	0.0000E+00	0.7247E+00	0.0000E+00
FIN SECTION 1 LOADS	0.0000E+00	0.0000E+00	0.5481E+00	0.0000E+00	0.3004E+01	0.0000E+00
AFTERBODY LOADS	0.0000E+00	-0.2495E-08	0.2365E-01	0.0000E+00	-0.4348E-01	0.1240E-07
FIN SECTION 2 LOADS	0.0000E+00	0.5074E-07	0.1018E+01	-0.5960E-07	-0.1163E+02	0.4414E-08
	-----------	-----------	-----------	-----------	-----------	-----------
TOTAL LOADS	0.0000E+00	0.4825E-07	0.1660E+01	-0.5960E-07	-0.7944E+01	0.4538E-08

FIN LOADINGS

FIN NO.	DELTA	AEQ	CNF	CHMF	CBMF	CRMF	XCP/CR	YCP/S
1		0.1591E+01	0.1607E+00	-0.3120E-03	0.1028E+00	0.1831E+00	0.5716E+00	0.3741E+00
2		0.1625E+01	0.1641E+00	-0.3304E-03	0.1050E+00	0.1870E+00	0.5717E+00	0.3740E+00
3		0.1625E+01	0.1641E+00	-0.3304E-03	0.1050E+00	0.1870E+00	0.5717E+00	0.3740E+00
4		0.1591E+01	0.1607E+00	-0.3120E-03	0.1028E+00	0.1831E+00	0.5716E+00	0.3741E+00
1		0.1081E+01	0.2966E+00	-0.2599E+00	0.2999E+00	0.4482E+00	0.4863E+00	0.4736E+00
2		0.1231E+01	0.3377E+00	-0.1727E+00	0.3524E+00	0.5213E+00	0.4905E+00	0.4887E+00
3		0.1231E+01	0.3377E+00	-0.1727E+00	0.3524E+00	0.5213E+00	0.4905E+00	0.4887E+00
4		0.1081E+01	0.2966E+00	-0.2599E+00	0.2999E+00	0.4482E+00	0.4863E+00	0.4736E+00

(b) Page 2

Figure 17.- Continued.

***** MISSILE 3 OUTPUT *****

CASE 2 MACH = 2.5ØØØ ALFAC = 5.ØØØØ PHI = 45.ØØØØ

***** COMPONENT LOADS *****

	CX	CY	CZ	CMX	CMY	CMZ
NOSE LOADS	Ø.ØØØØE+ØØ	Ø.ØØØØE+ØØ	Ø.2Ø91E+Ø3	Ø.ØØØØE+ØØ	Ø.2152E+Ø1	Ø.ØØØØE+ØØ
FIN SECTION 1 LOADS	Ø.ØØØØE+ØØ	Ø.ØØØØE+ØØ	Ø.138ØE+Ø1	Ø.298ØE-Ø7	Ø.7554E+Ø1	Ø.ØØØØE+ØØ
AFTERBODY LOADS	Ø.ØØØØE+ØØ	Ø.7795E-Ø8	Ø.1477E+ØØ	Ø.ØØØØE+ØØ	-Ø.2716E+ØØ	Ø.61Ø8E-Ø7
FIN SECTION 2 LOADS	Ø.ØØØØE+ØØ	Ø.ØØØØE+ØØ	Ø.283ØE+Ø1	Ø.3576E-Ø6	-Ø.3177E+Ø2	Ø.ØØØØE+ØØ
	-----------	-----------	-----------	-----------	-----------	-----------
TOTAL LOADS	Ø.ØØØØE+ØØ	Ø.7795E-Ø8	Ø.4567E+Ø1	Ø.3874E-Ø6	-Ø.2233E+Ø2	Ø.61Ø8E-Ø7

FIN LOADINGS

FIN NO.	DELTA	AEQ	CNF	CHMF	CBMF	CRMF	XCP/CR	YCP/S
1		Ø.381ØE+Ø1	Ø.3849E+ØØ	-Ø.5889E-Ø2	Ø.239ØE+ØØ	Ø.4314E+ØØ	Ø.5735E+ØØ	Ø.3631E+ØØ
2		Ø.4289E+Ø1	Ø.4332E+ØØ	-Ø.2414E-Ø2	Ø.2672E+ØØ	Ø.4838E+ØØ	Ø.5738E+ØØ	Ø.36Ø7E+ØØ
3		Ø.4289E+Ø1	Ø.4332E+ØØ	-Ø.2414E-Ø2	Ø.2672E+ØØ	Ø.4838E+ØØ	Ø.5738E+ØØ	Ø.36Ø7E+ØØ
4		Ø.381ØE+Ø1	Ø.3849E+ØØ	-Ø.5889E-Ø2	Ø.239ØE+ØØ	Ø.4314E+ØØ	Ø.5735E+ØØ	Ø.3631E+ØØ
1		Ø.2853E+Ø1	Ø.7825E+ØØ	-Ø.5747E+ØØ	Ø.789ØE+ØØ	Ø.118ØE+Ø1	Ø.4931E+ØØ	Ø.4722E+ØØ
2		Ø.3573E+Ø1	Ø.98Ø1E+ØØ	-Ø.2382E+ØØ	Ø.987ØE+ØØ	Ø.1477E+Ø1	Ø.4936E+ØØ	Ø.4716E+ØØ
3		Ø.3573E+Ø1	Ø.98Ø1E+ØØ	-Ø.2382E+ØØ	Ø.987ØE+ØØ	Ø.1477E+Ø1	Ø.4936E+ØØ	Ø.4716E+ØØ
4		Ø.2853E+Ø1	Ø.7825E+ØØ	-Ø.5747E+ØØ	Ø.789ØE+ØØ	Ø.118ØE+Ø1	Ø.4931E+ØØ	Ø.4722E+ØØ

(c) Page 3

Figure 17.- Continued.

***** MISSILE 3 OUTPUT *****

CASE 3 MACH = 2.5000 ALFAC = 10.0000 PHI = 45.0000

***** COMPONENT LOADS *****

	CX	CY	CZ	CMX	CMY	CMZ
NOSE LOADS	0.0000E+00	0.0000E+00	0.4902E+00	0.0000E+00	0.5013E+01	0.0000E+00
FIN SECTION 1 LOADS	0.0000E+00	0.0000E+00	0.2455E+01	0.0000E+00	0.1340E+02	0.0000E+00
AFTERBODY LOADS	0.0000E+00	0.1092E-08	0.6067E+00	0.0000E+00	-0.1116E+01	-0.1327E-06
FIN SECTION 2 LOADS	0.0000E+00	-0.1353E-06	0.5591E+01	-0.7153E-06	-0.6292E+02	-0.1972E-05
	-----------	-----------	-----------	-----------	-----------	-----------
TOTAL LOADS	0.0000E+00	-0.2815E-07	0.9143E+01	-0.7153E-06	-0.4582E+02	-0.2104E-05

FIN LOADINGS

FIN NO.	DELTA	AEQ	CNF	CHMF	CBMF	CRMF	XCP/CR	YCP/S
1		0.6799E÷01	0.5840E+00	-0.2971E-01	0.3589E+00	0.6509E+00	0.5778E+00	0.3594E+00
2		0.8700E+01	0.8710E+00	-0.1206E-01	0.5208E+00	0.9563E+00	0.5773E+00	0.3497E+00
3		0.8700E+01	0.8710E+00	-0.1206E-01	0.5208E+00	0.9563E+00	0.5773E+00	0.3497E+00
4		0.5799E+01	0.5840E+00	-0.2971E-01	0.3589E+00	0.6509E+00	0.5778E+00	0.3594E+00
1		0.4216E+01	0.1156E+01	-0.1716E+01	0.1304E+01	0.1882E+01	0.5171E+00	0.5280E+00
2		0.8184E+01	0.2327E+01	0.9079E-02	0.2264E+01	0.3427E+01	0.5032E+00	0.4557E+00
3		0.8184E+01	0.2327E+01	0.9079E-02	0.2264E+01	0.3427E+01	0.5032E+00	0.4557E+00
4		0.4216E+01	3.1156E+01	-0.1716E+01	0.1304E+01	0.1882E+01	0.5171E+00	0.5280E+00

(d) Page 4

Figure 17.- Concluded.

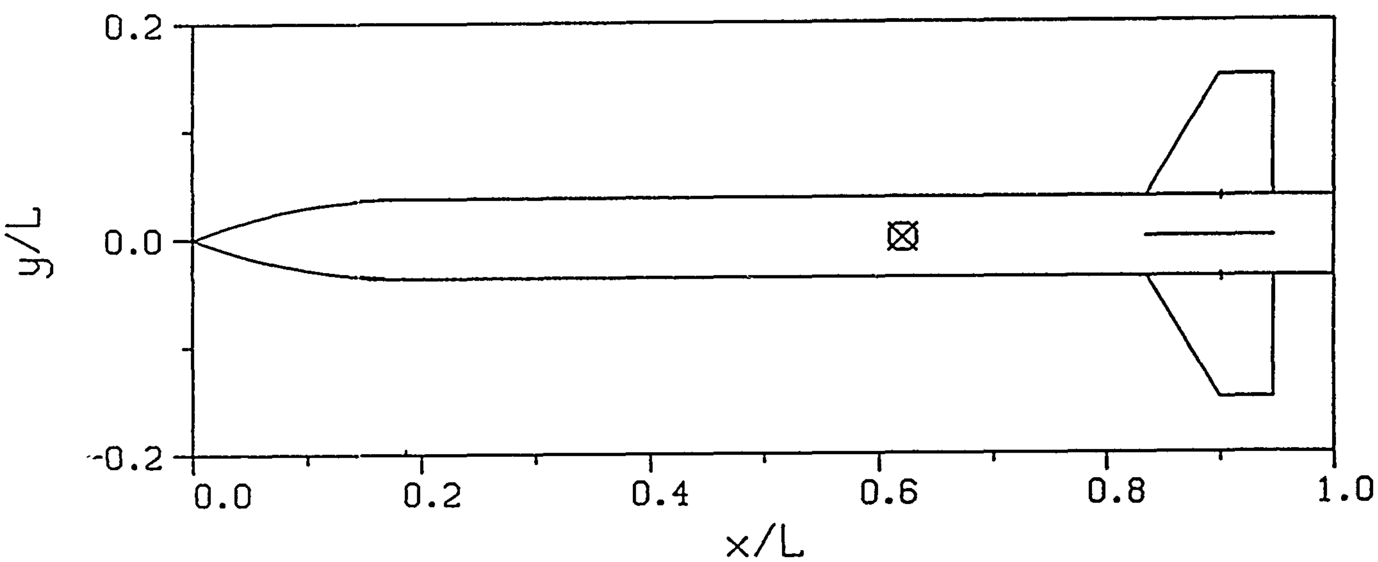

Figure 18.- Geometry for the body-tail model in Reference 27.

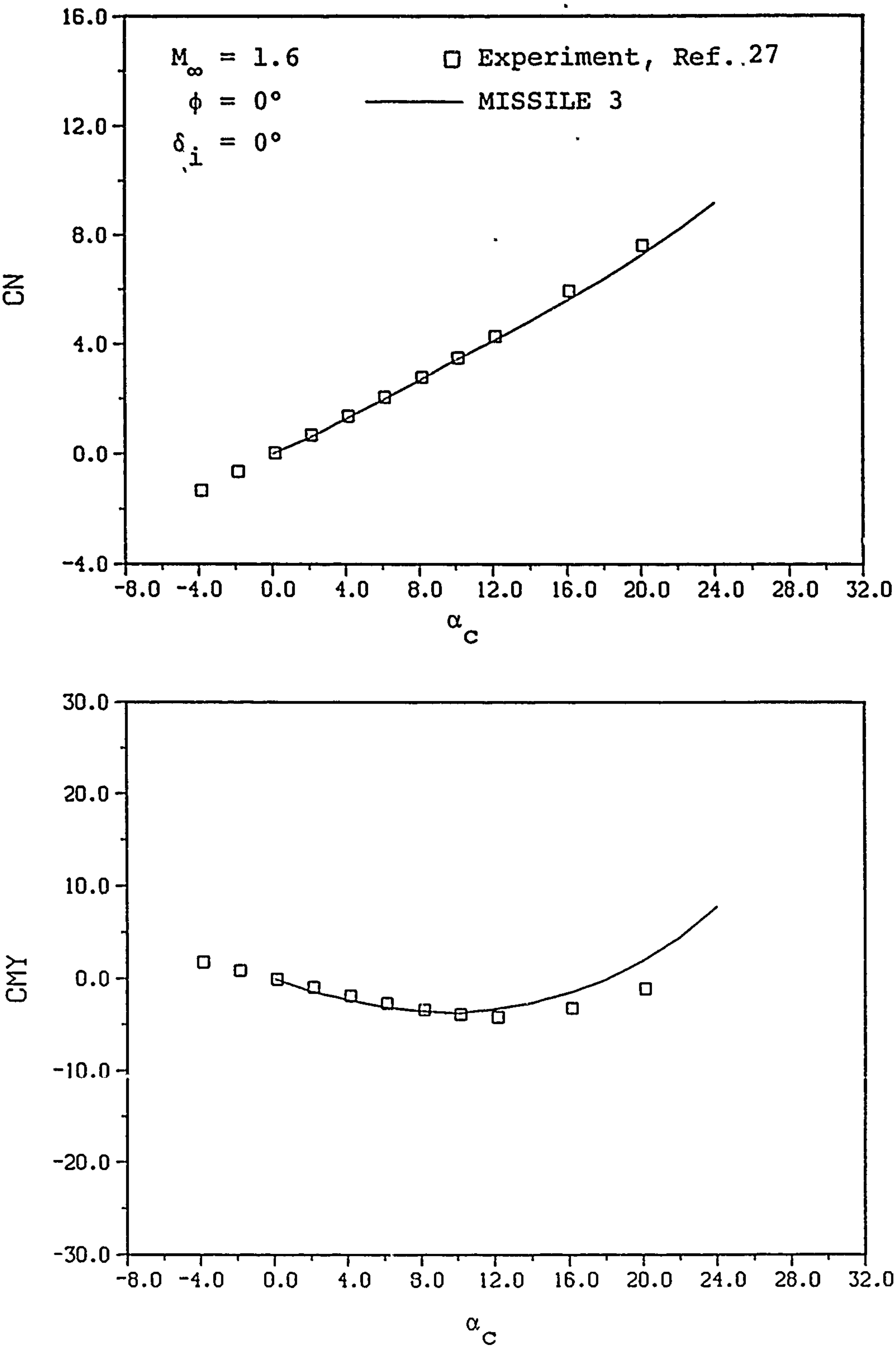

(a) Overall loads

Figure 19.- Comparison of predicted and measured aerodynamic characteristics for the body-tail model in Reference 27, M_∞ = 1.6, ϕ = 0°, δ_i = 0°.

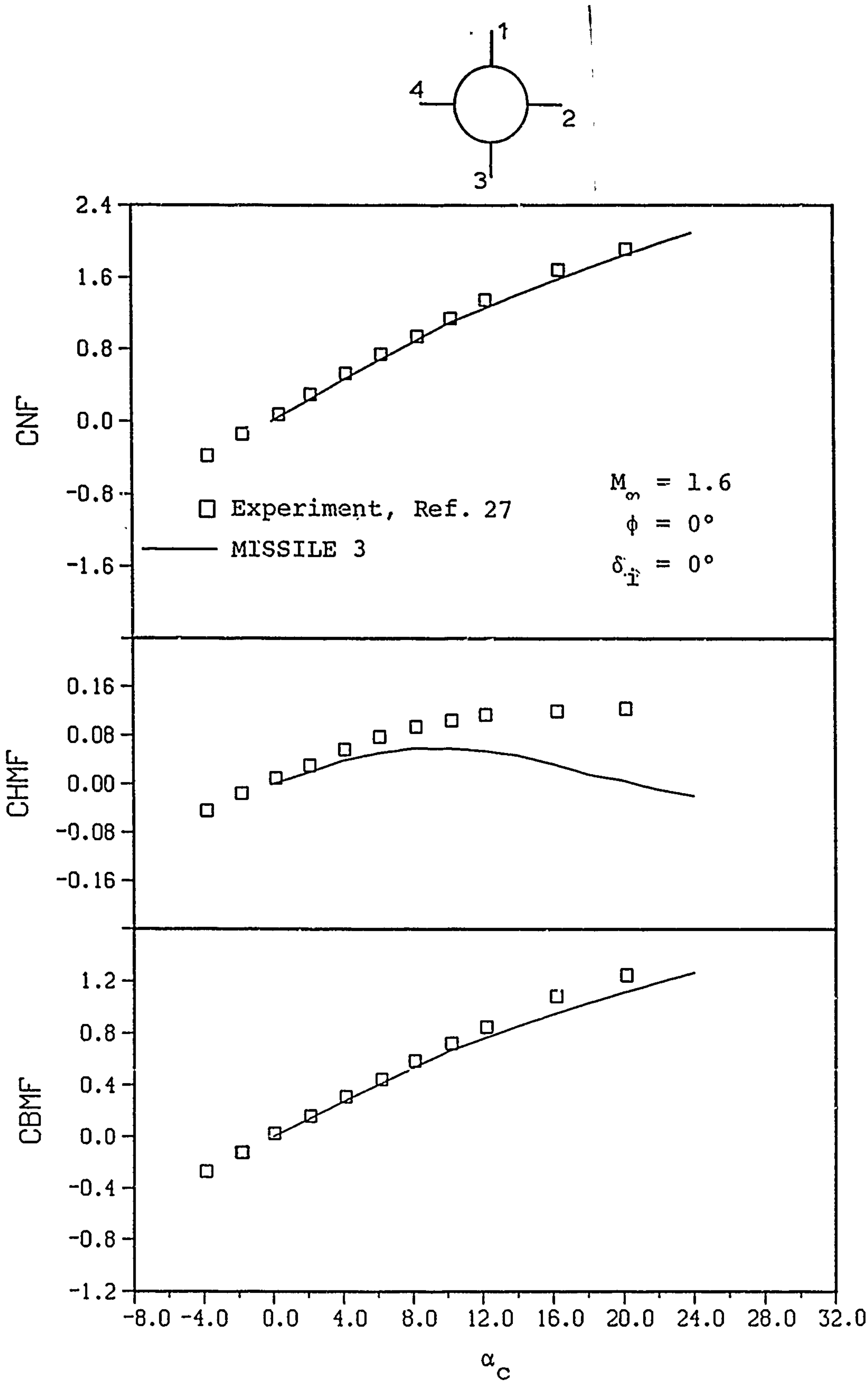

(b) Fin 2 loads

Figure 19.- Concluded.

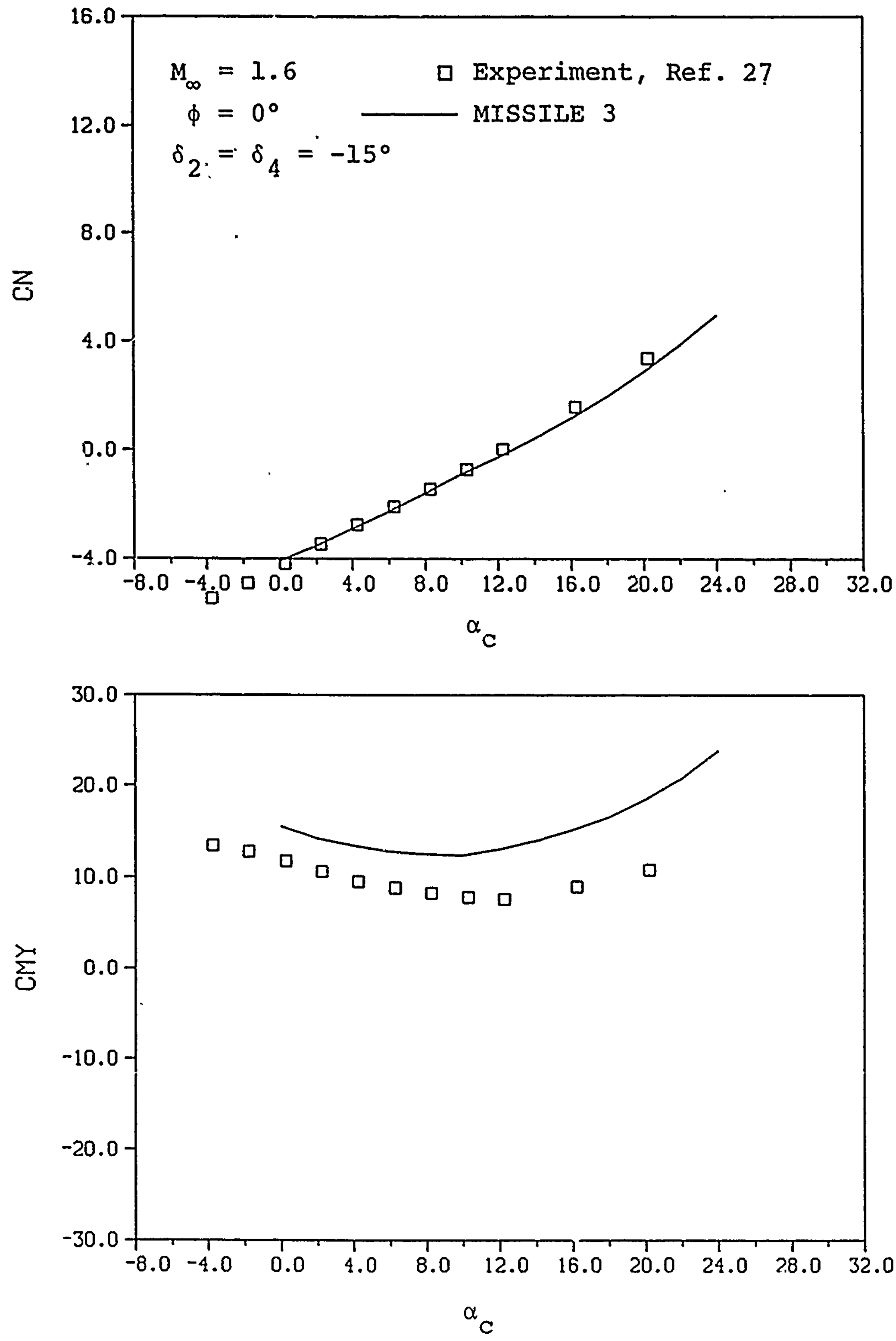

(a) Overall loads

Figure 20.- Comparisons of predicted and measured aerodynamic characteristics for the body-tail model in Reference 27, $M_\infty = 1.6$, $\phi = 0°$, $\delta_2 = \delta_4 = -15°$.

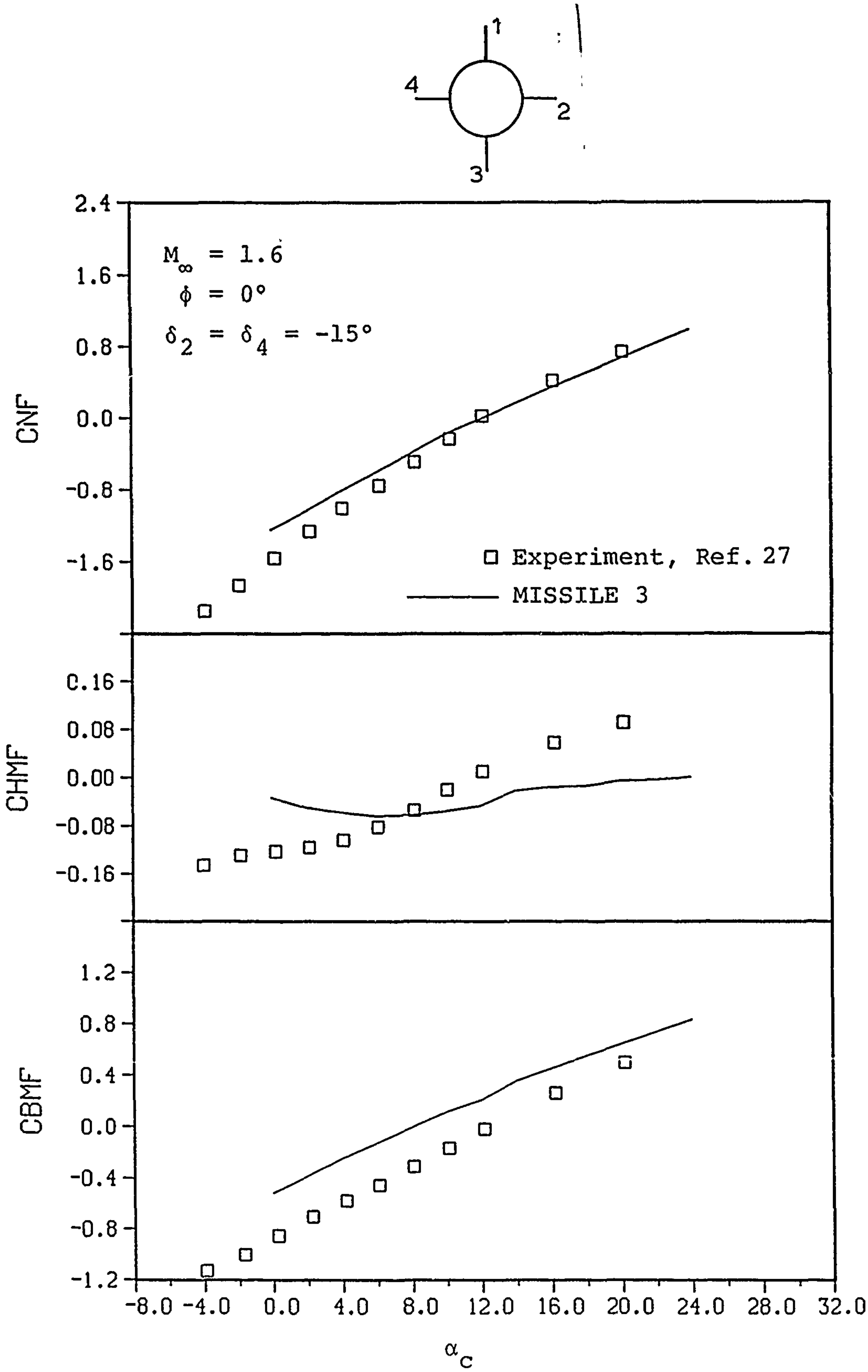

(b) Fin 2 loads

Figure 20.- Concluded.

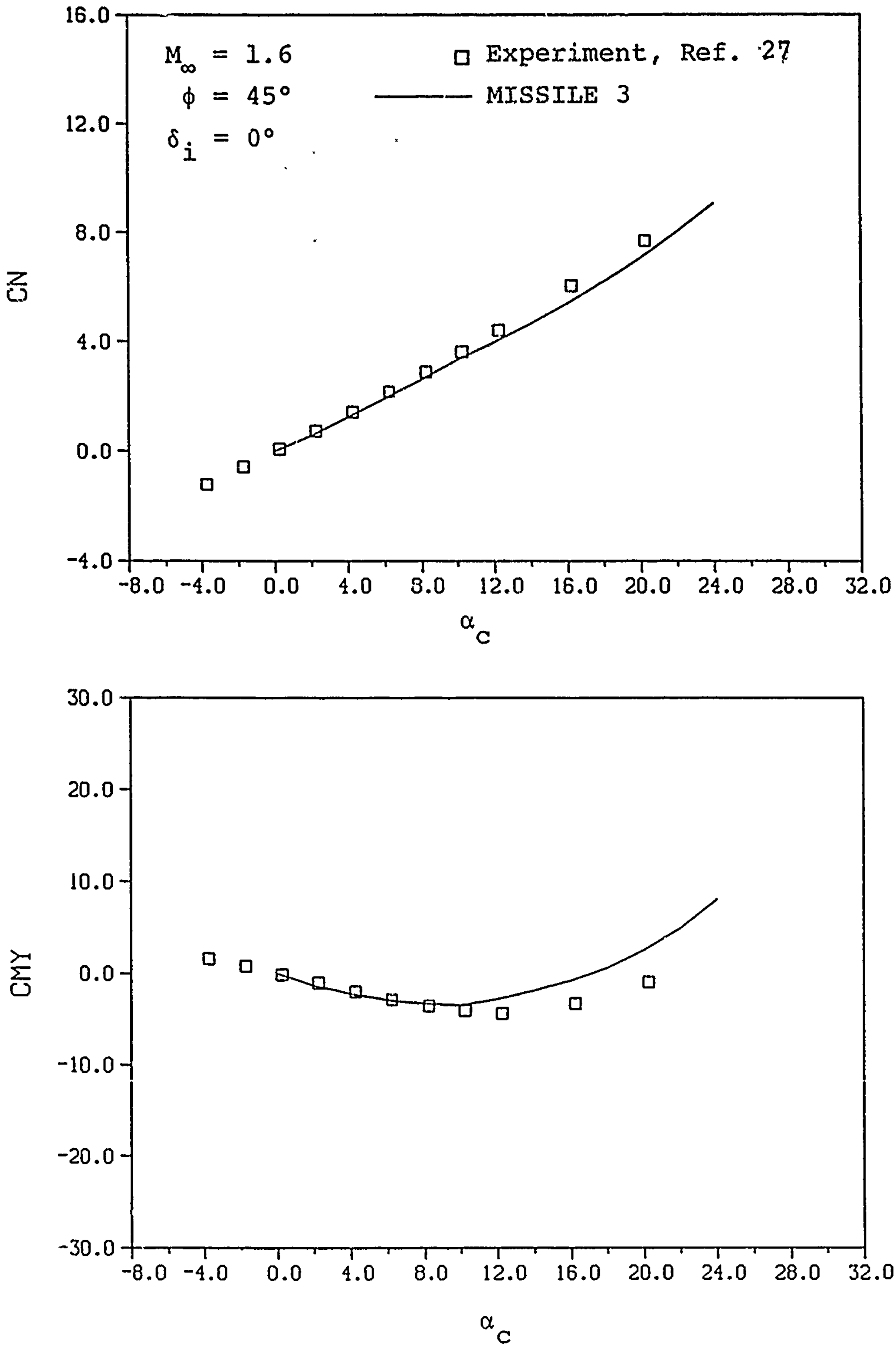

(a) Overall loads

Figure 21.- Comparison of predicted and measured aerodynamic characteristics for the body-tail model in Reference 27, $M_\infty = 1.6$, $\phi = 45°$, $\delta_i = 0°$.

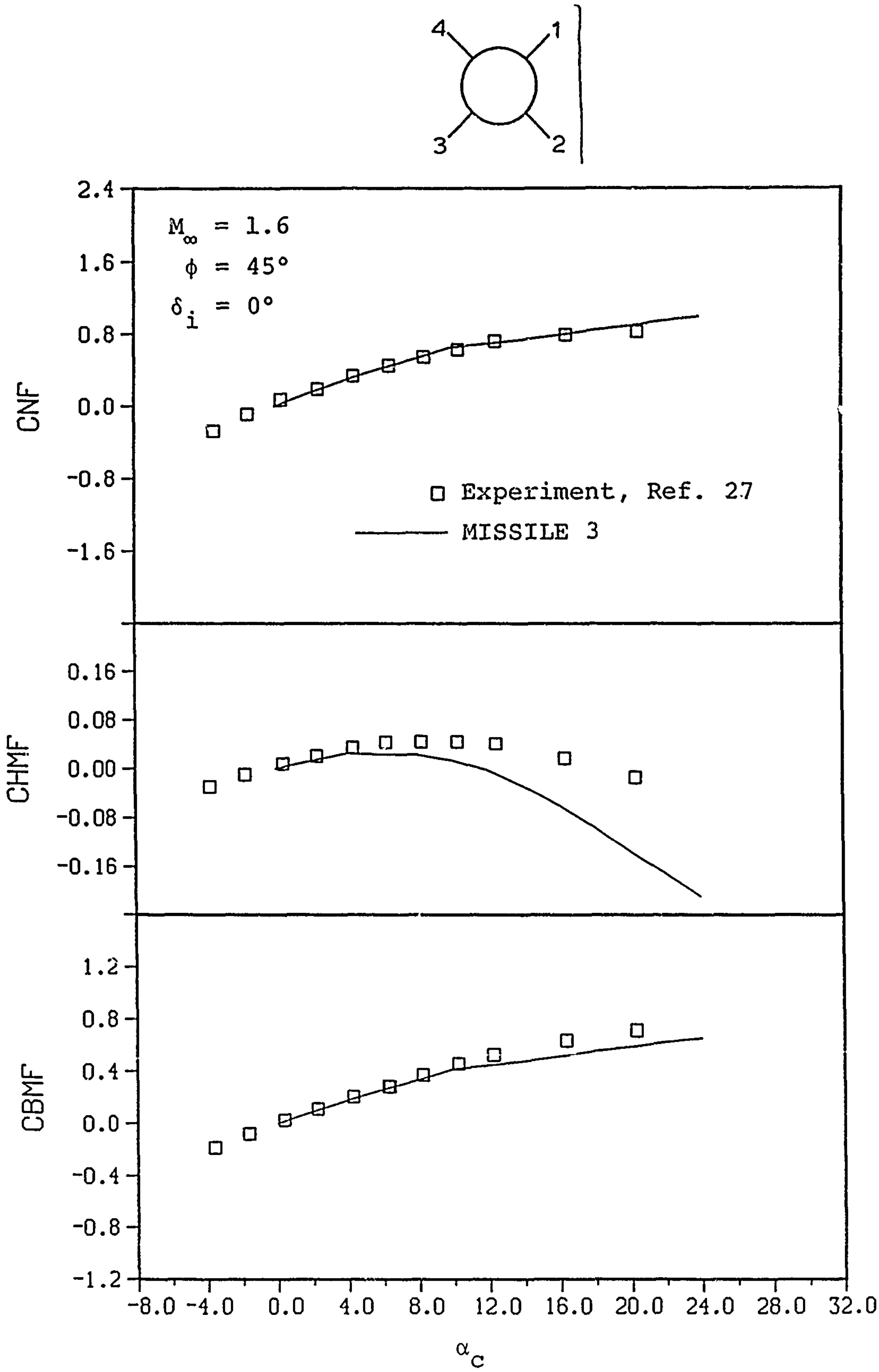

(b) Fin 1 loads

Figure 21.- Continued.

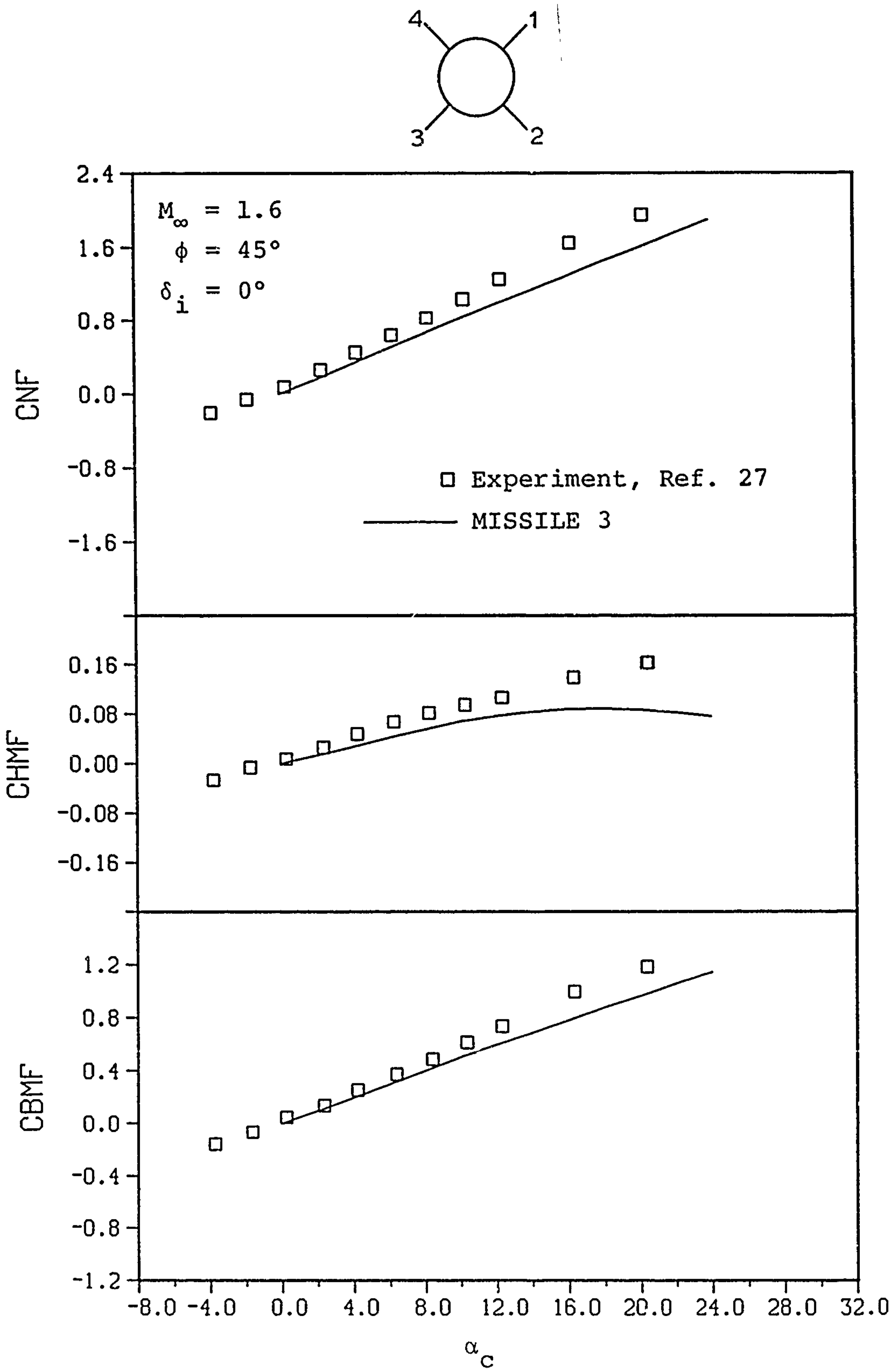

(c) Fin 2 loads

Figure 21.- Concluded.

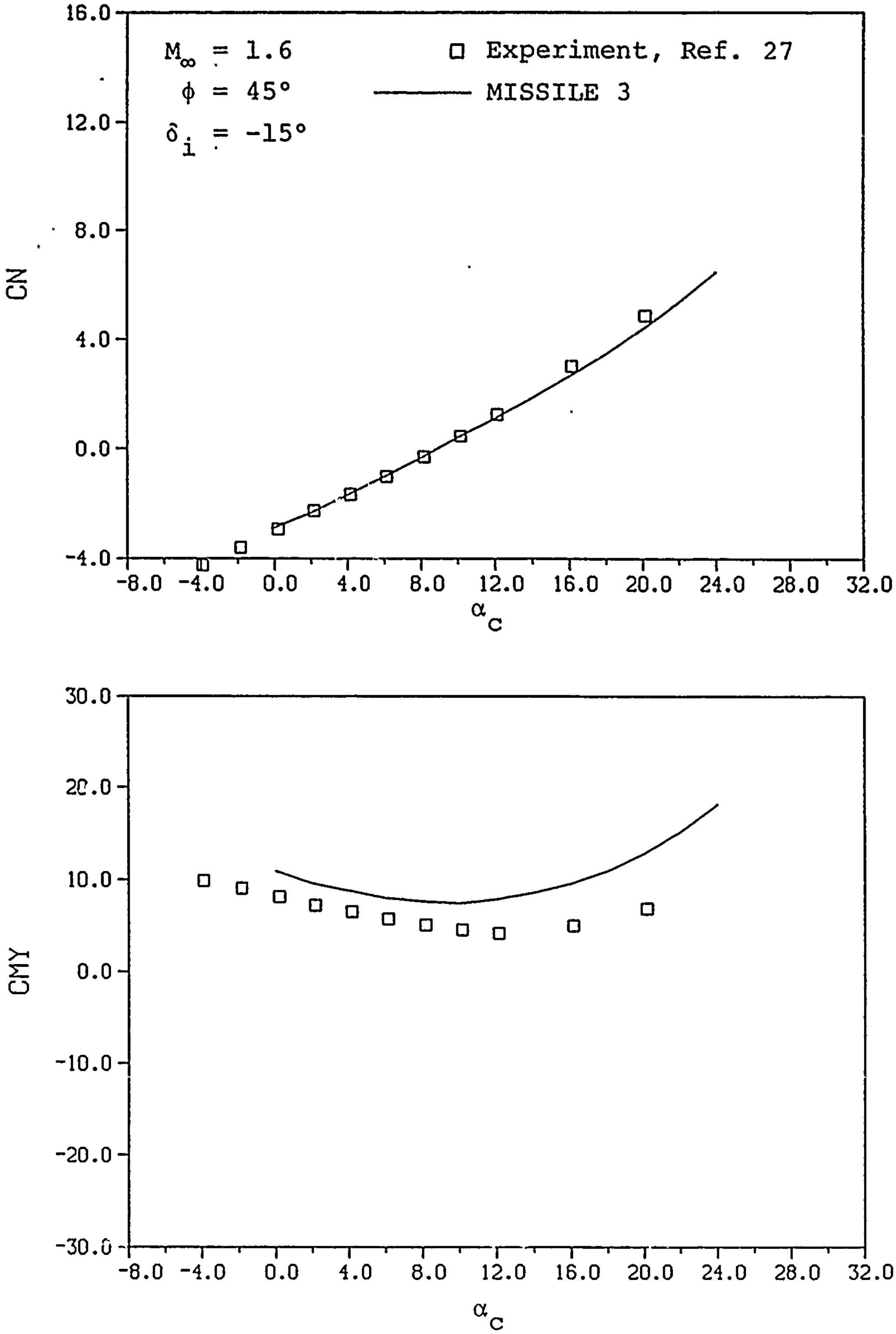

(a) Overall loads

Figure 22.- Comparison of predicted and measured aerodynamic characteristics for the body-tail model in Reference 27, $M_\infty = 1.6$, $\phi = 45°$, $\delta_i = -15°$.

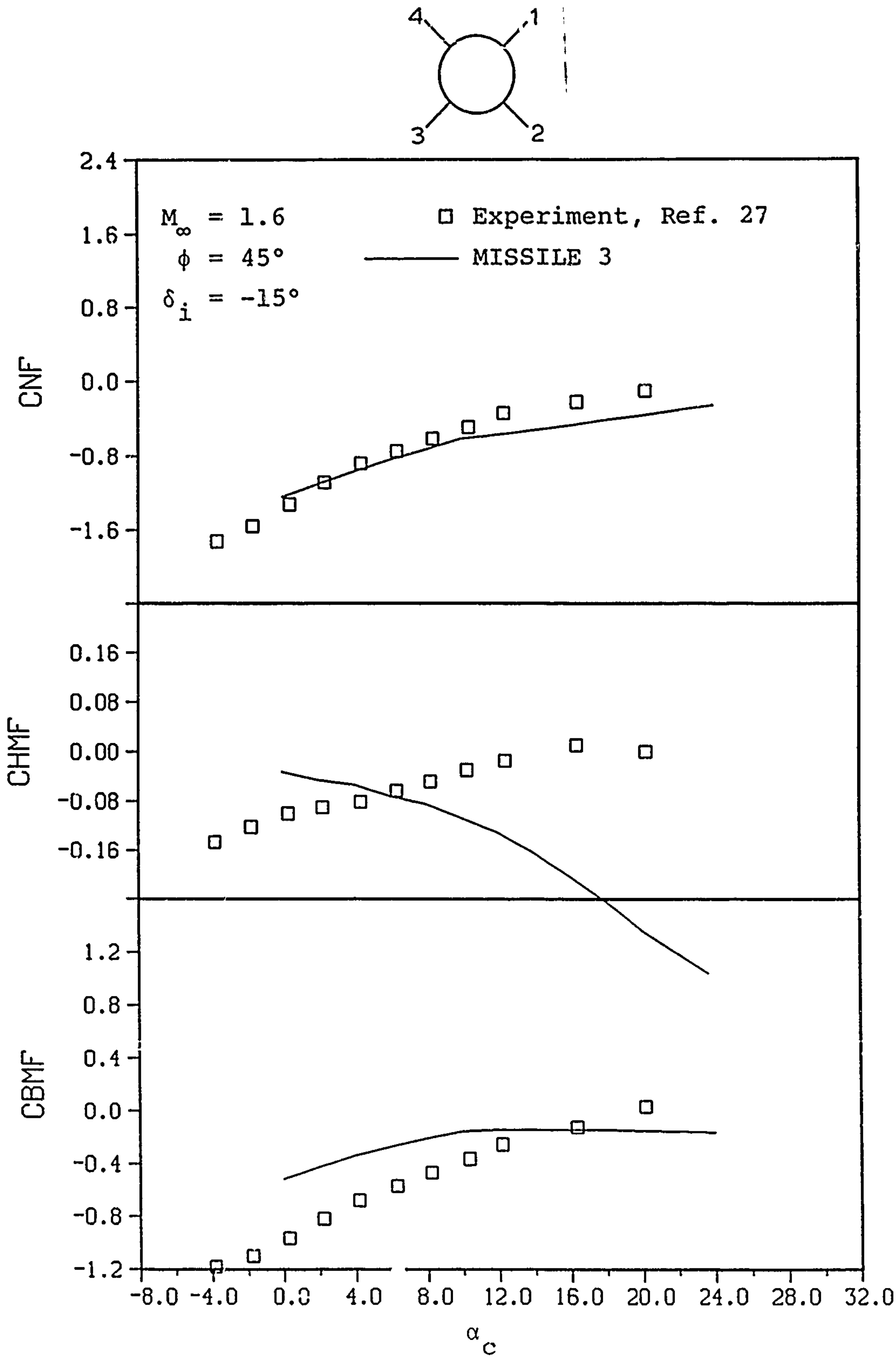

(b) Fin 1 loads

Figure 22.- Continued.

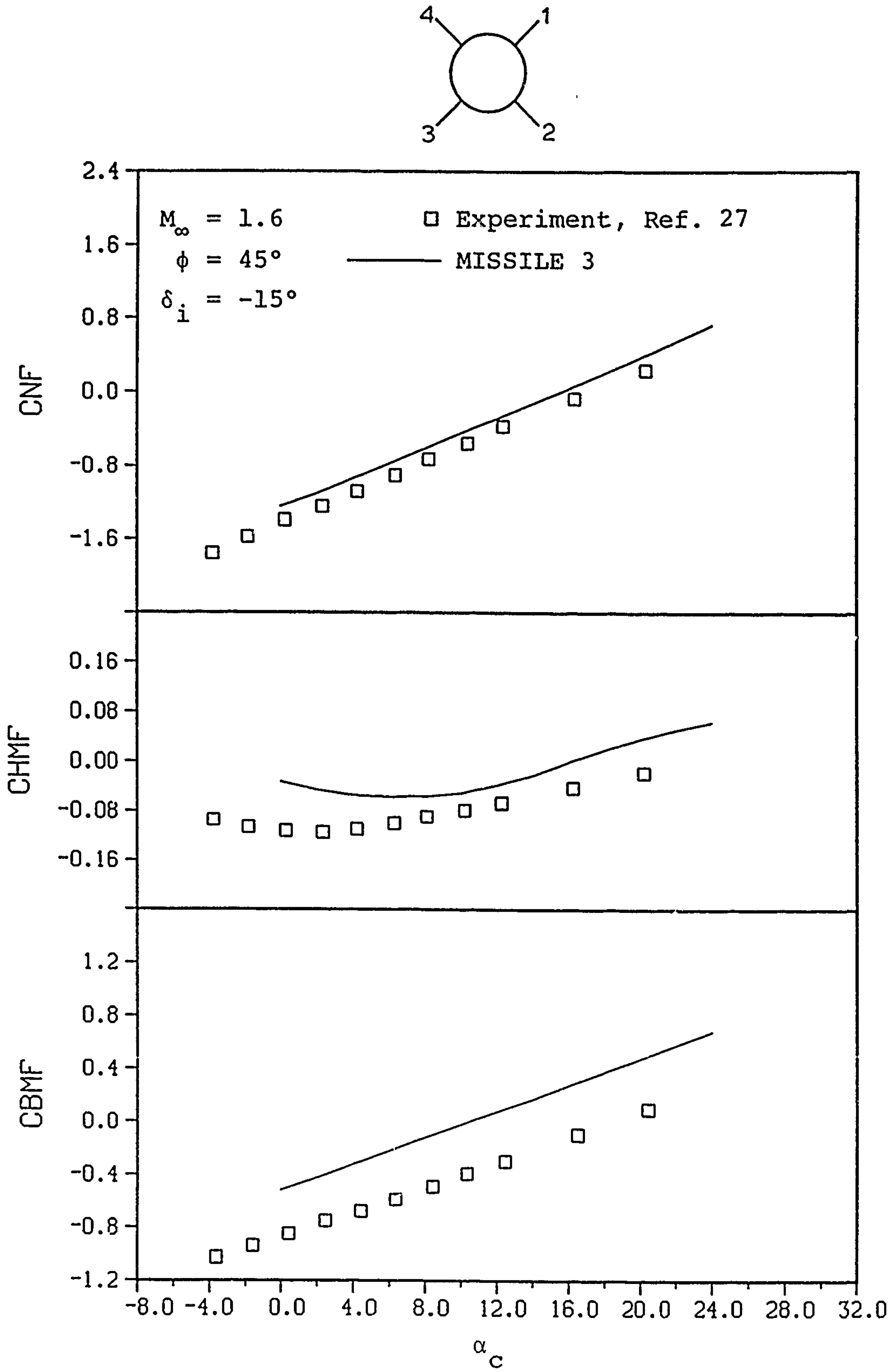

(c) Fin 2 loads

Figure 22.- Concluded.

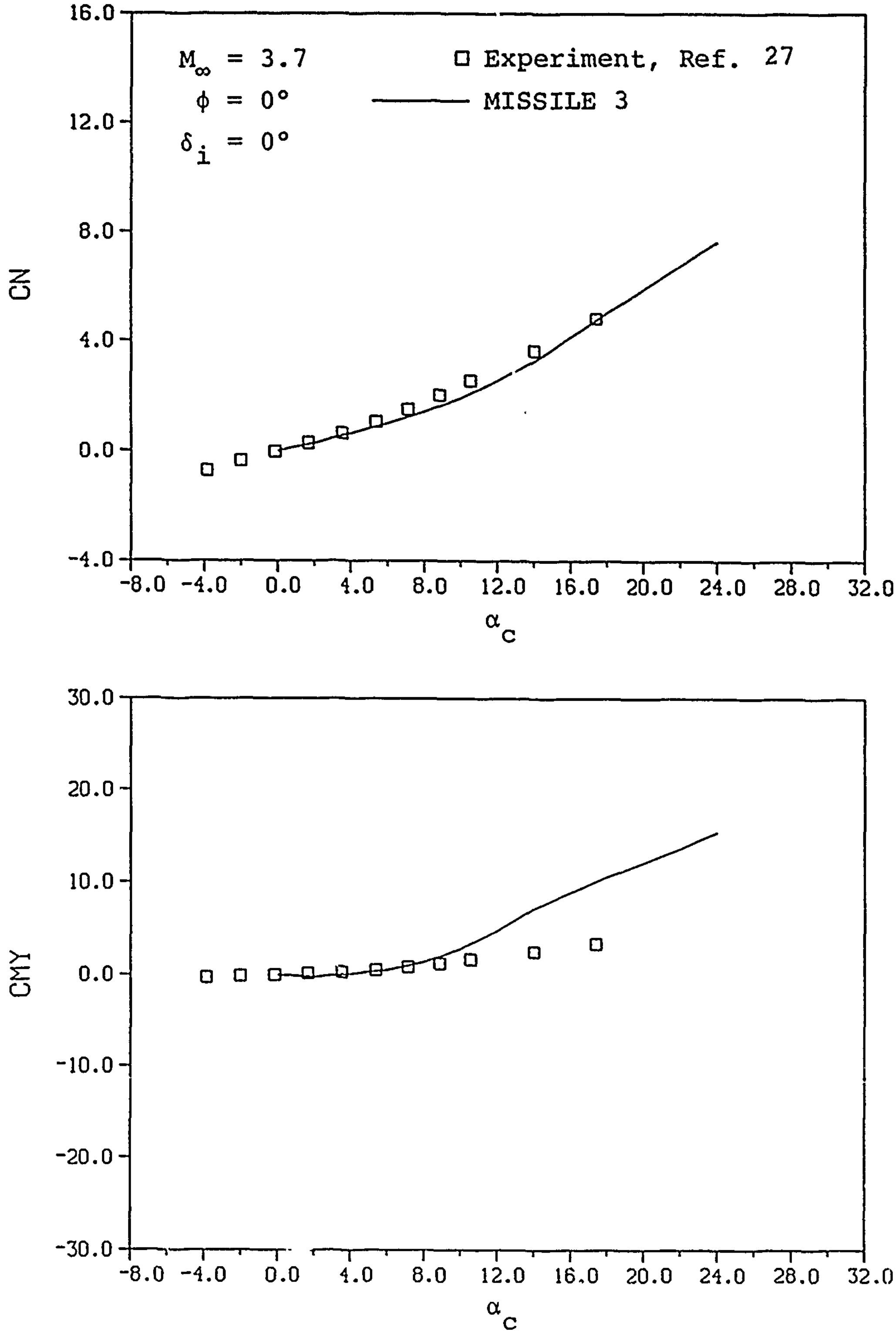

(a) Overall loads

Figure 23.- Comparison of predicted and measured aerodynamic characteristics for the body-tail in Reference 27, $M_\infty = 3.7$, $\phi = 0°$, $\delta_i = 0°$.

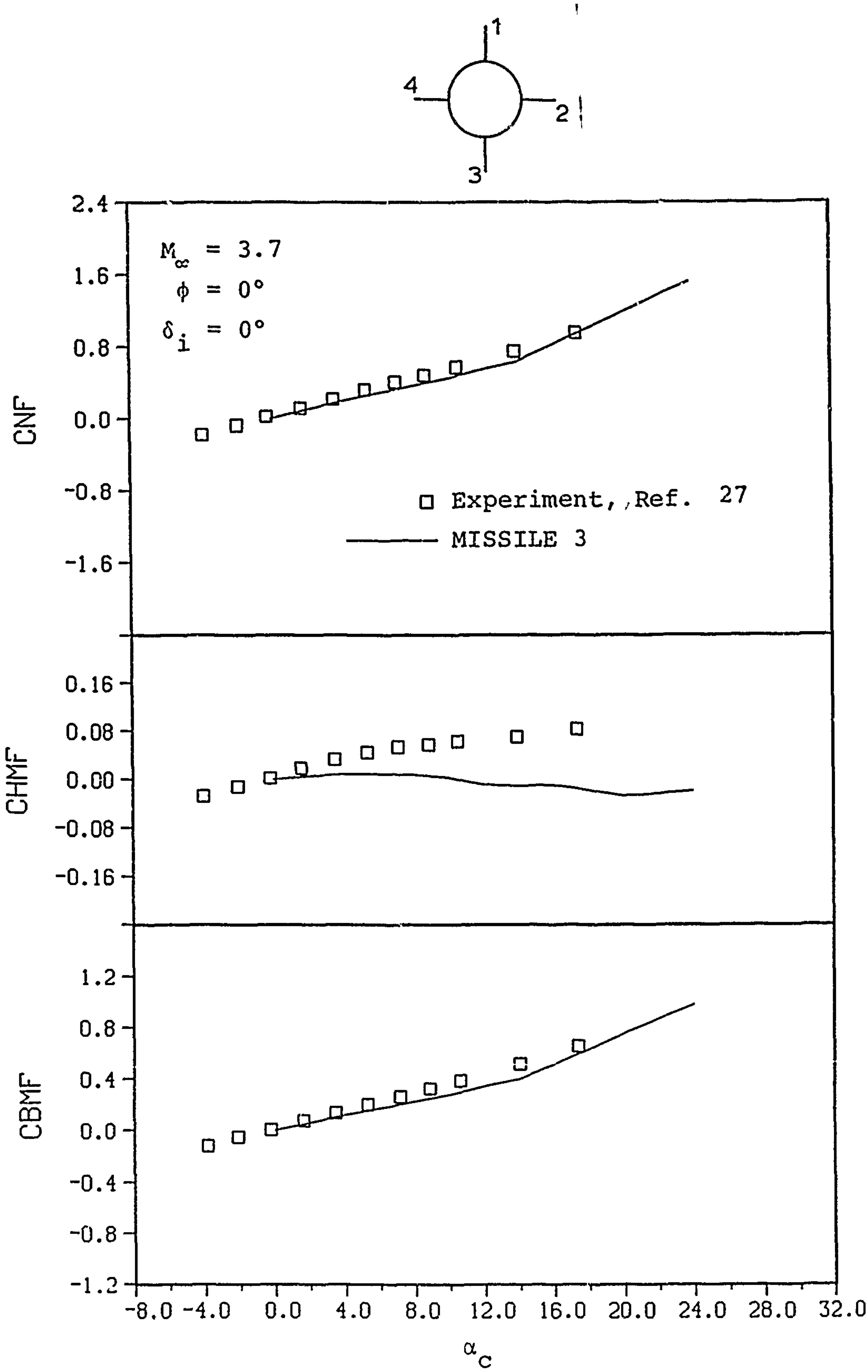

(b) Fin 2 loads

Figure 23.- Concluded.

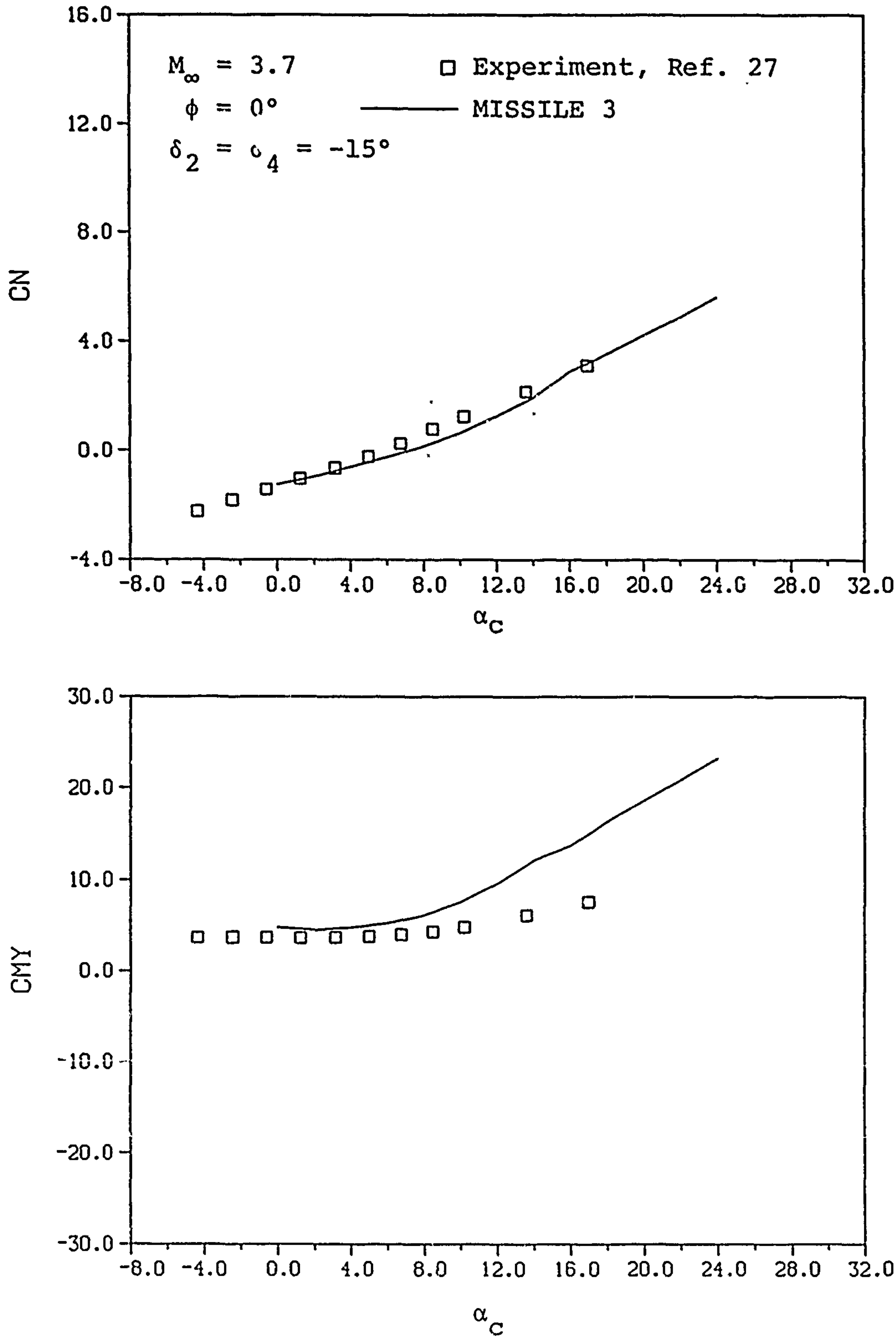

(a) Overall loads

Figure 24.- Comparison of predicted and measured aerodynamic characteristics for the body-tail in Reference 27, $M_\infty = 3.7$, $\phi = 0°$, $\delta_2 = \delta_4 = -15°$.

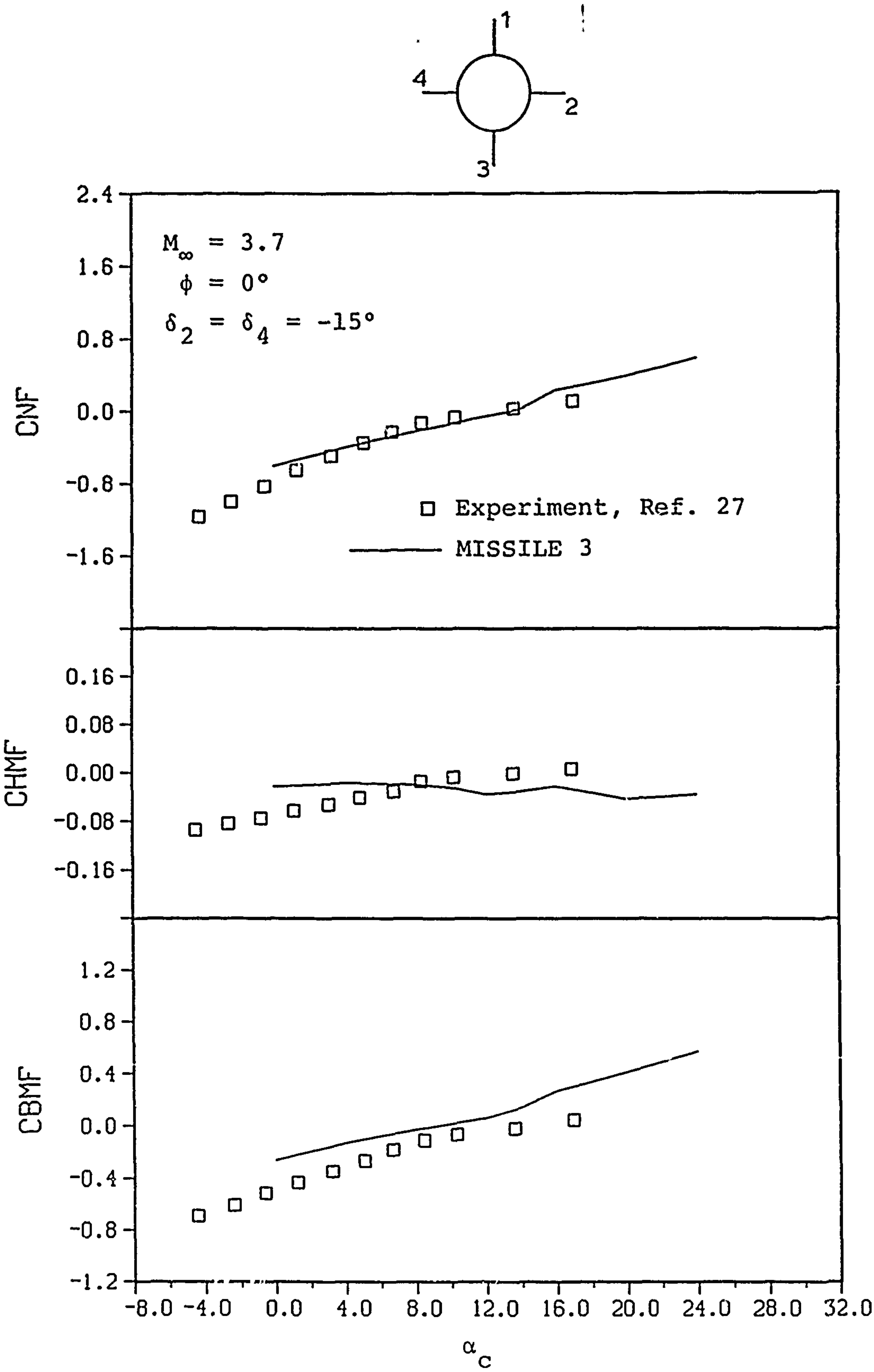

(b) Fin 2 loads

Figure 24.- Concluded.

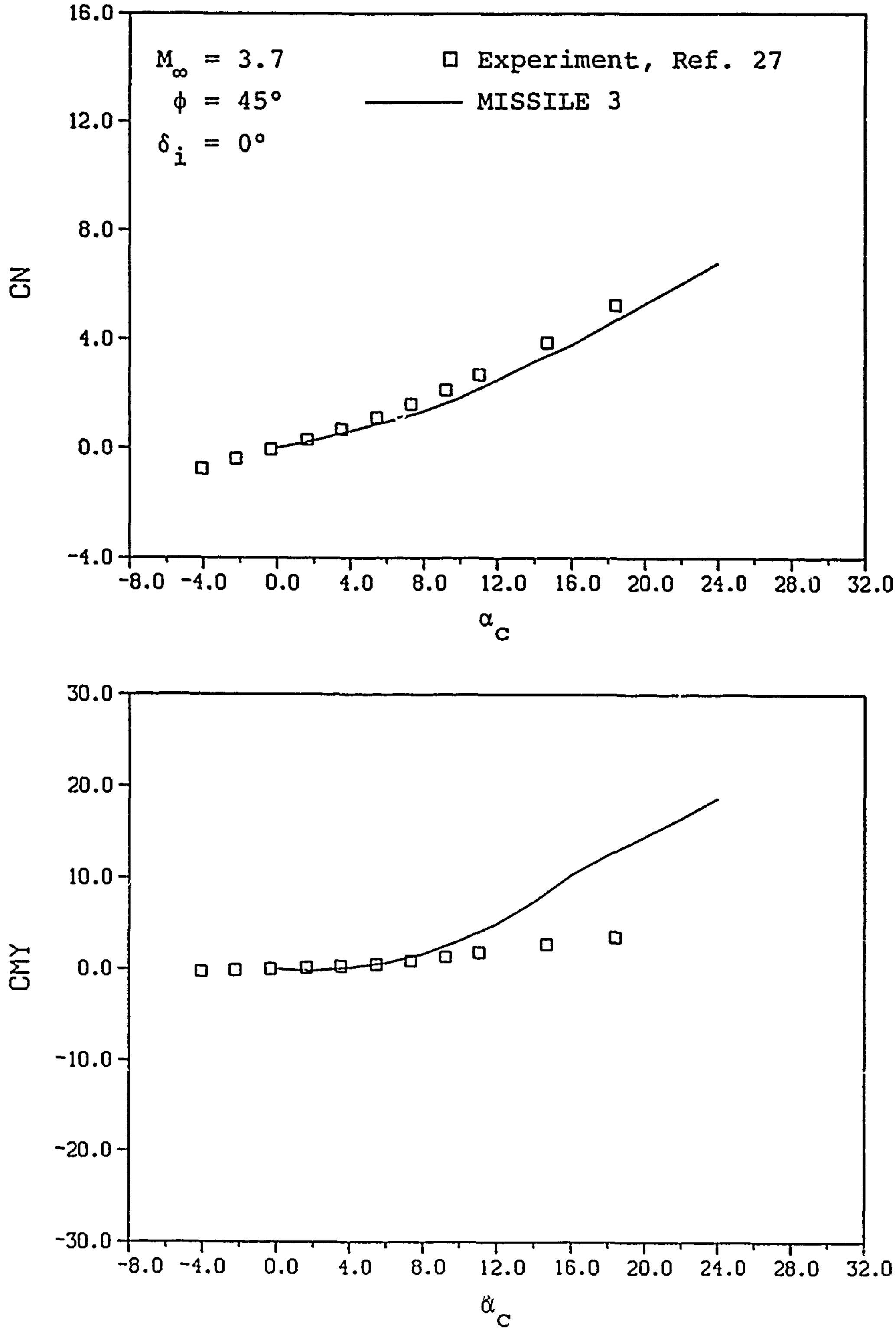

(a) Overall loads

Figure 25.- Comparison of predicted and measured aerodynamic characteristics for the body-tail in Reference 27, $M_\infty = 3.7$, $\phi = 45°$, $\delta_i = 0°$.

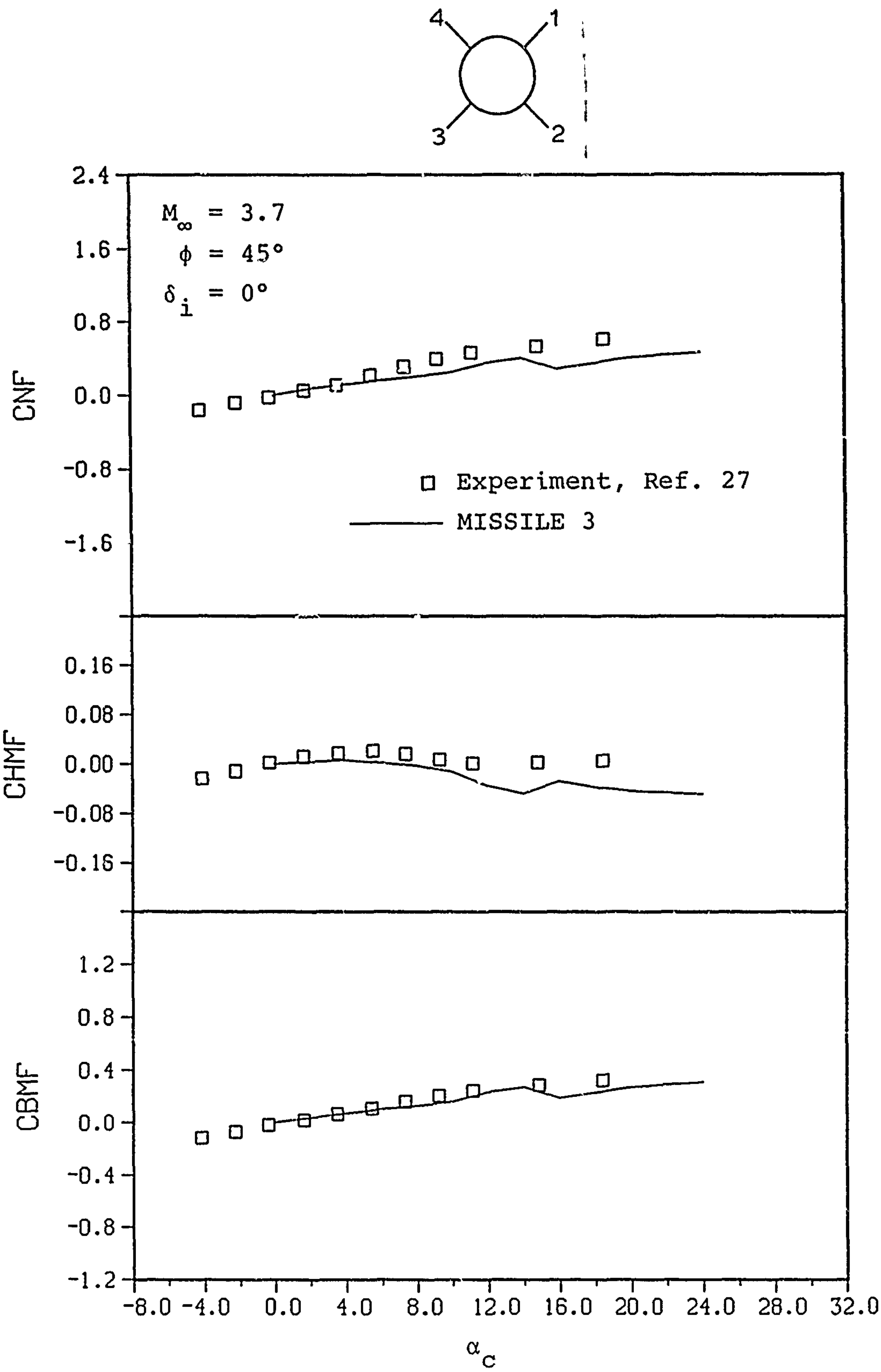

(b) Fin 1 loads

Figure 25.- Continued.

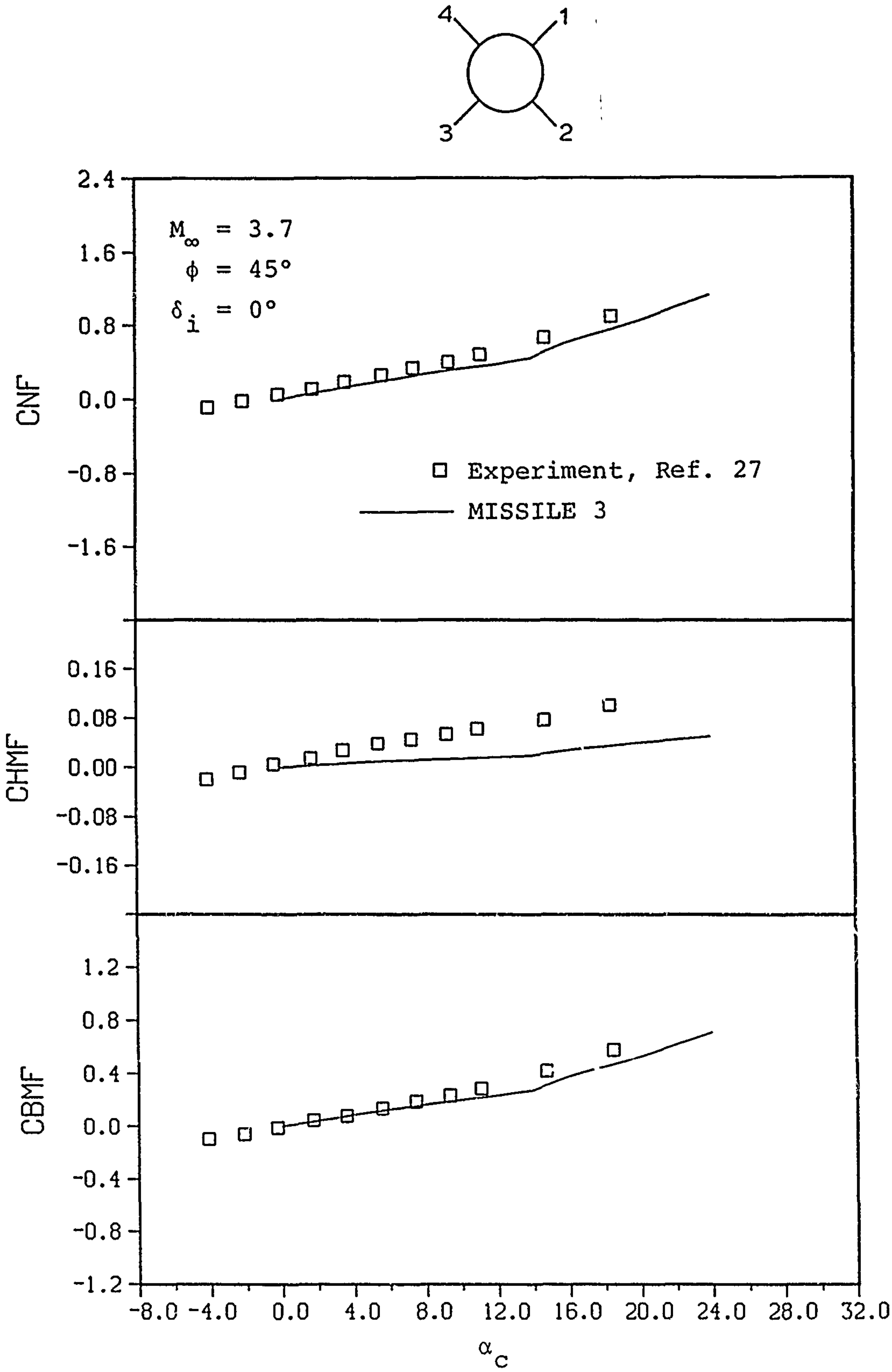

(c) Fin 2 loads

Figure 25.- Concluded.

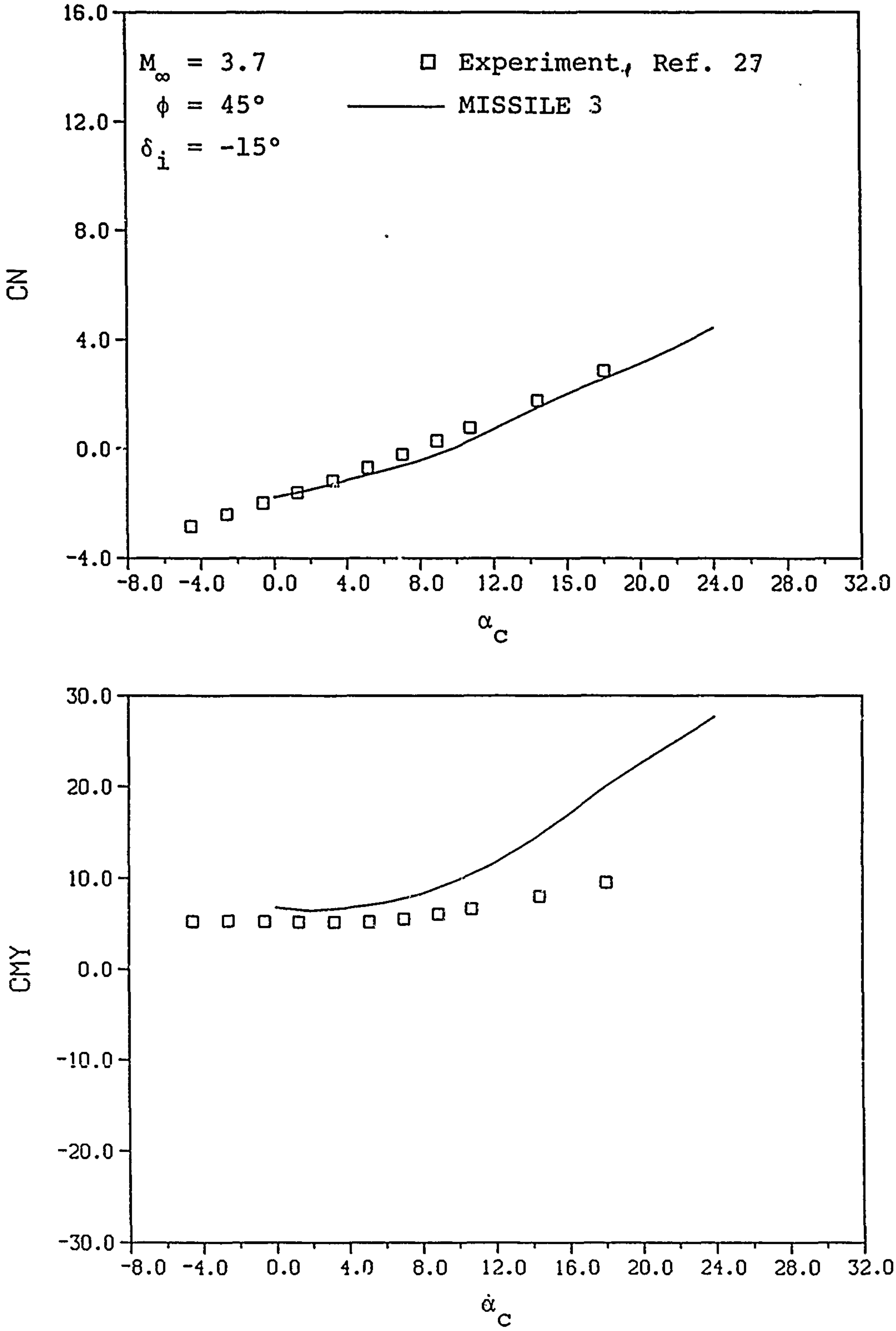

(a) Overall loads

Figure 26.- Comparison of predicted and measured aerodynamic characteristics for the body-tail in Reference 27, M_∞ = 3.7, ϕ = 45°, δ_i = -15°.

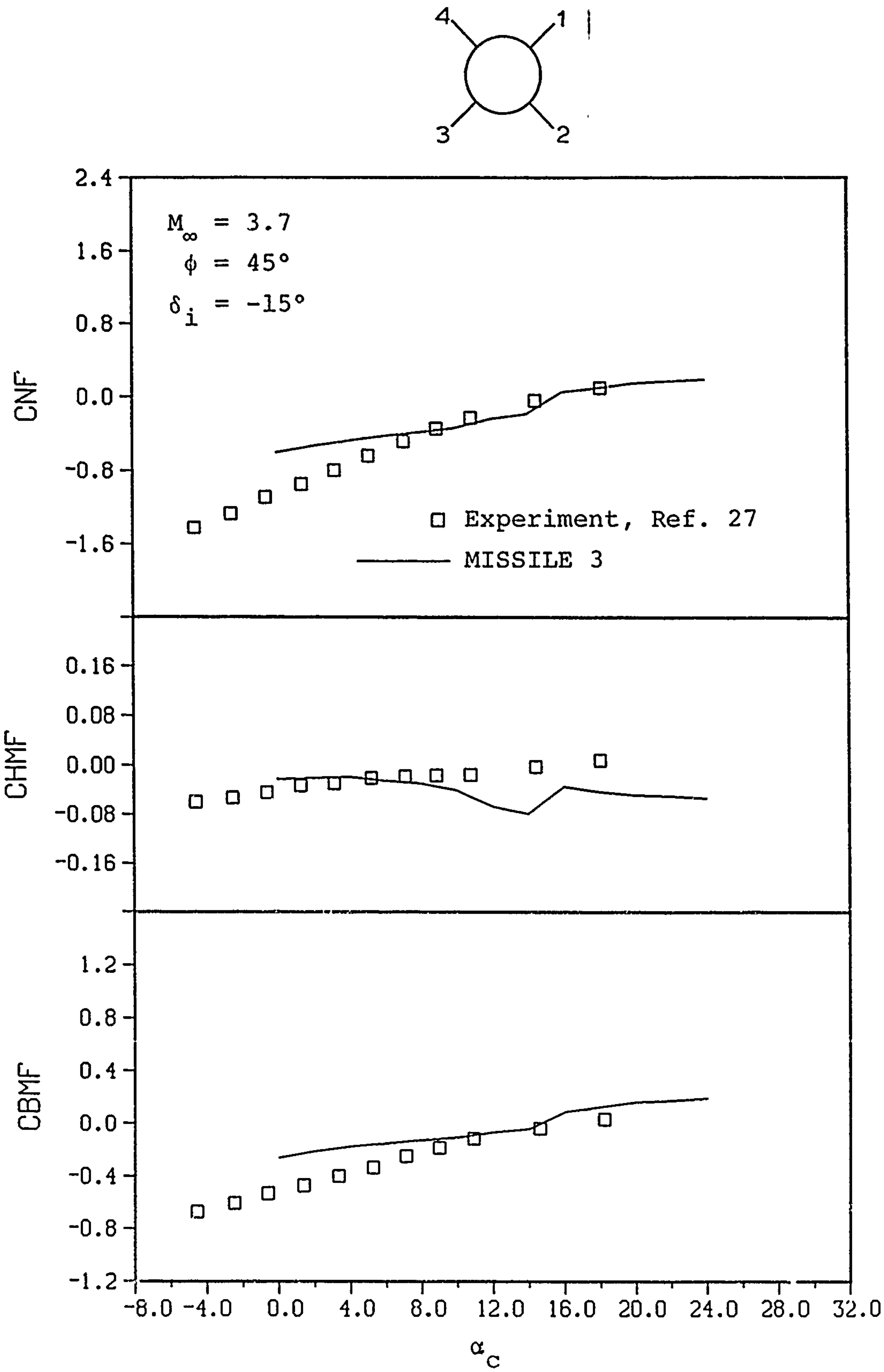

(b) Fin 1 loads

Figure 26.- Continued.

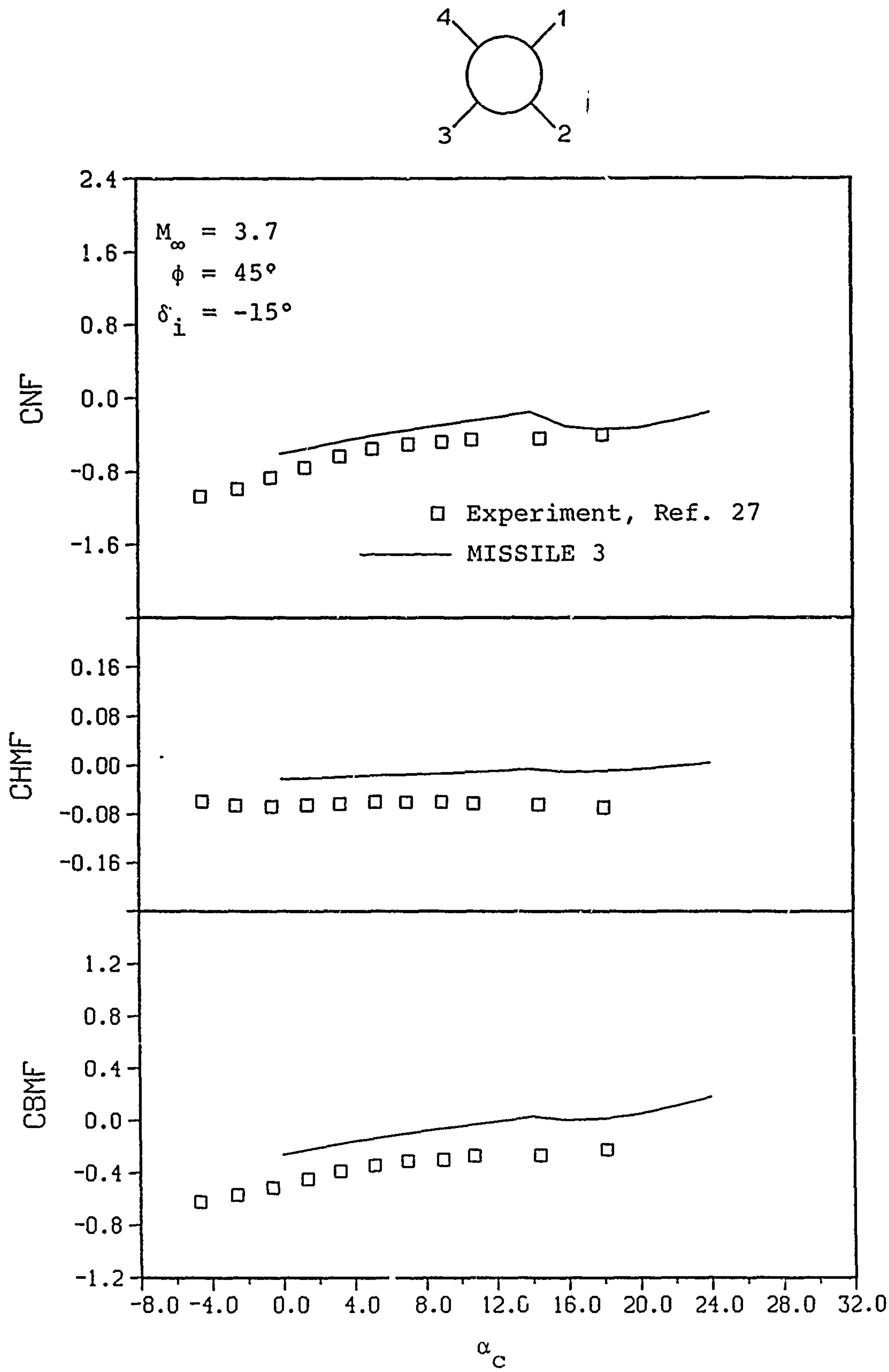

(c) Fin 2 loads

Figure 26.- Concluded.

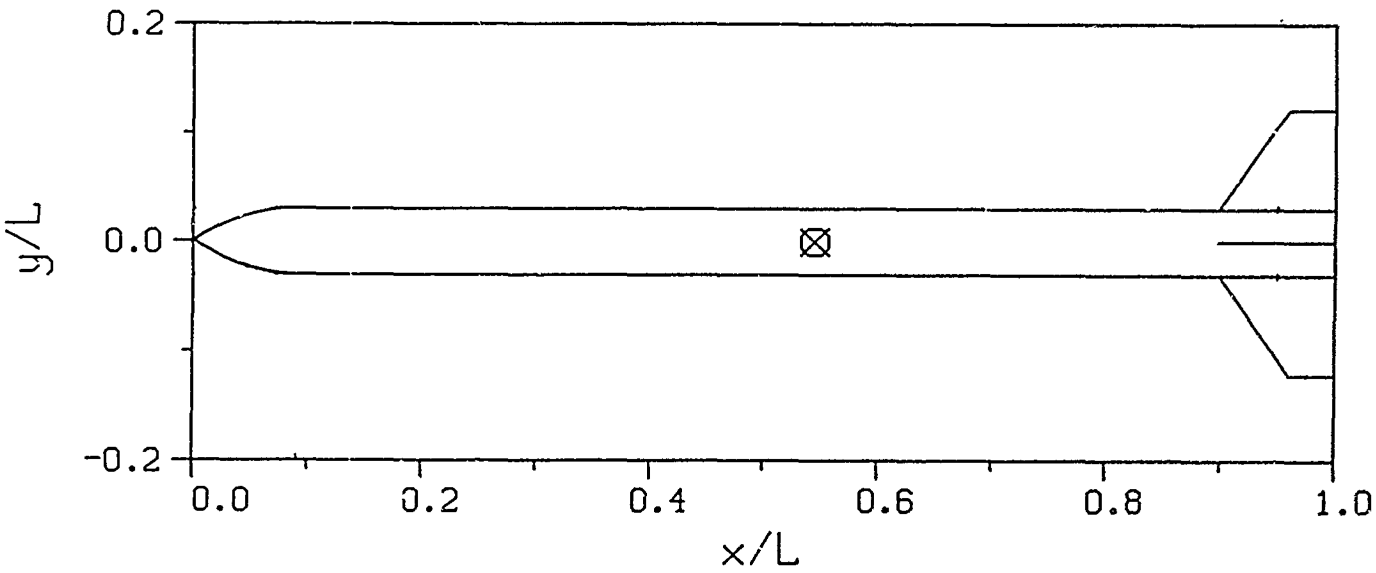

Figure 27.- Geometry for the body-tail model in Reference 28.

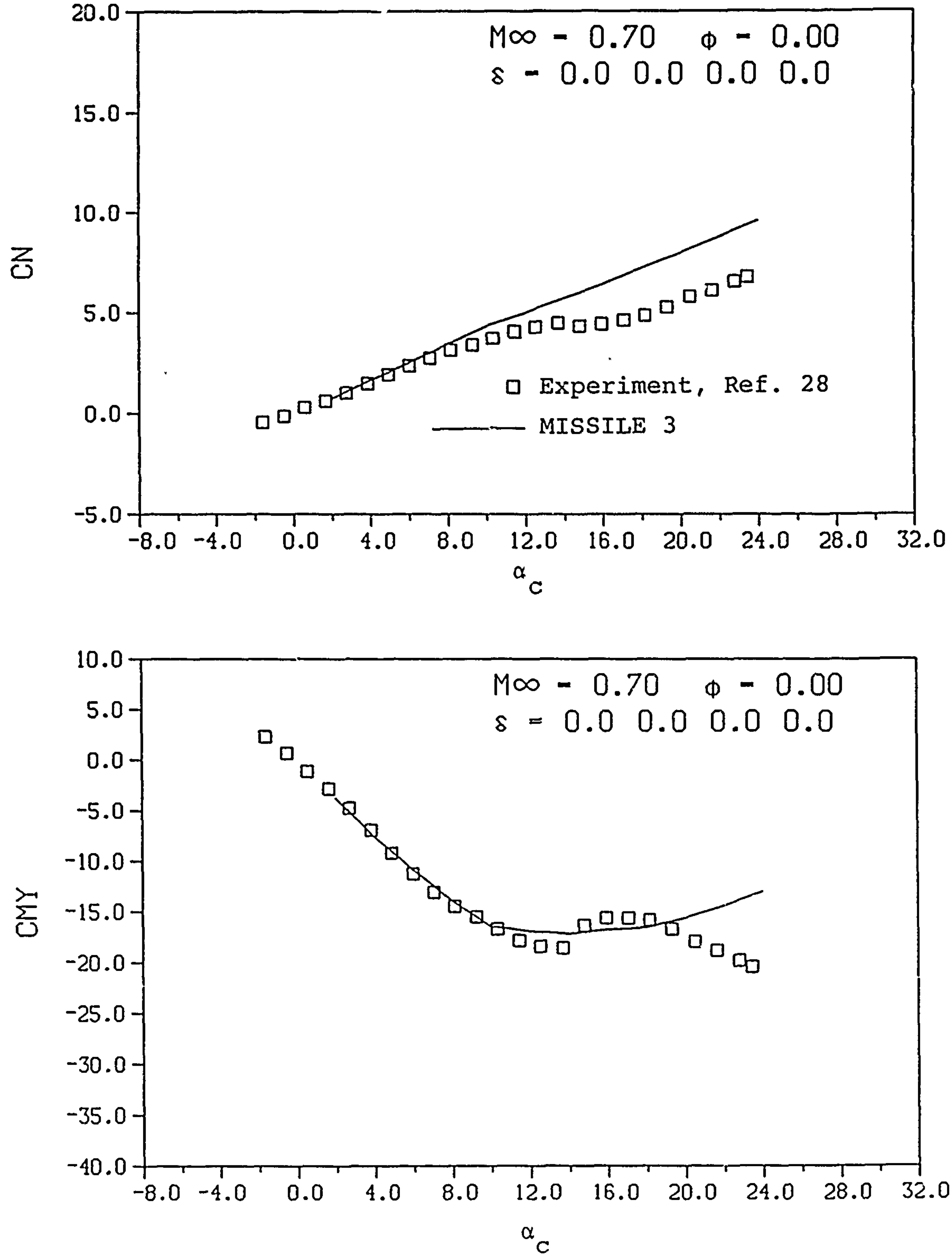

(a) $M_\infty = 0.7$

Figure 28.- Comparison of predicted and measured aerodynamic characteristics for the body-tail model in Reference 28, $\phi = 0°$, $\delta_i = 0°$.

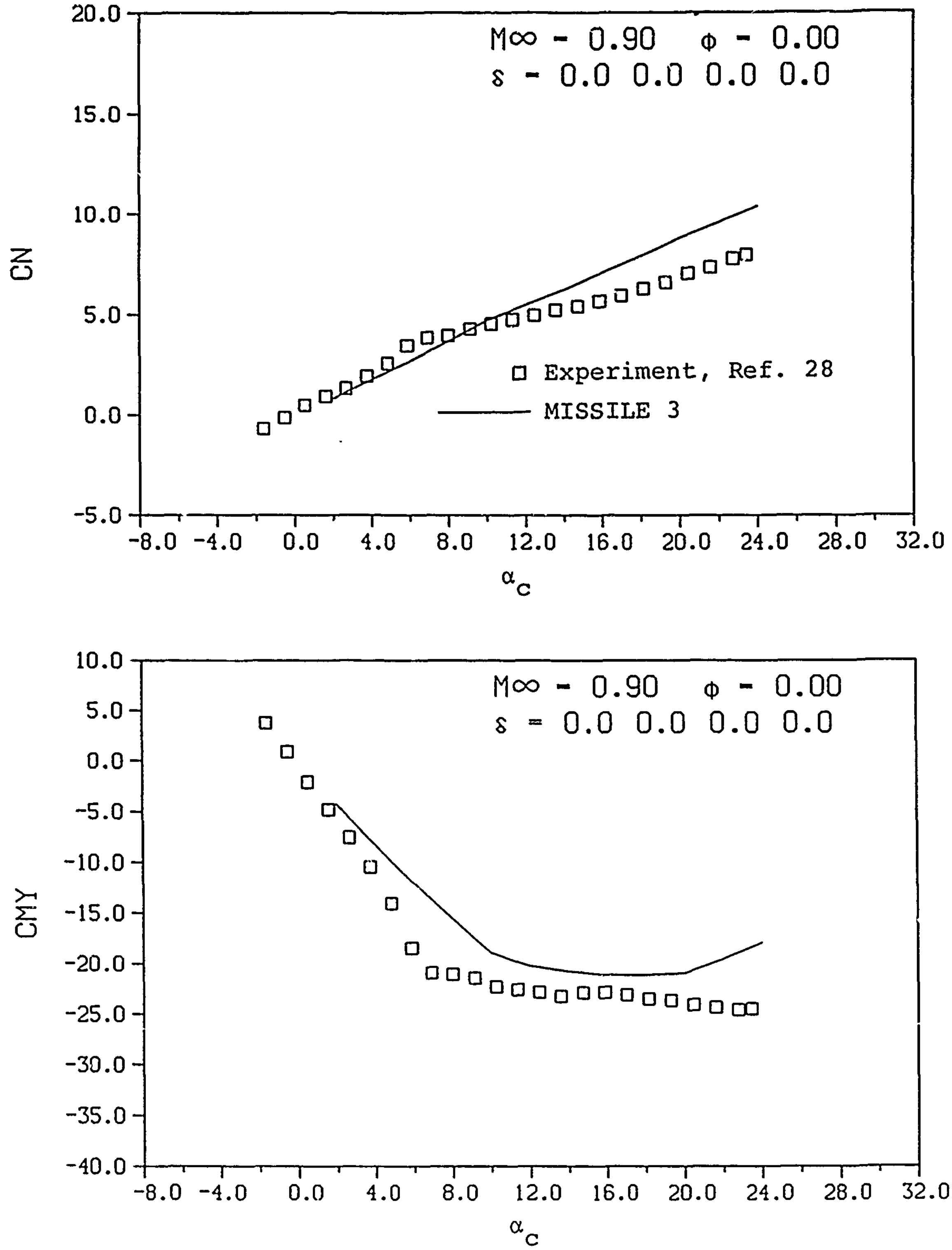

(b) $M_\infty = 0.9$

Figure 28.- Continued.

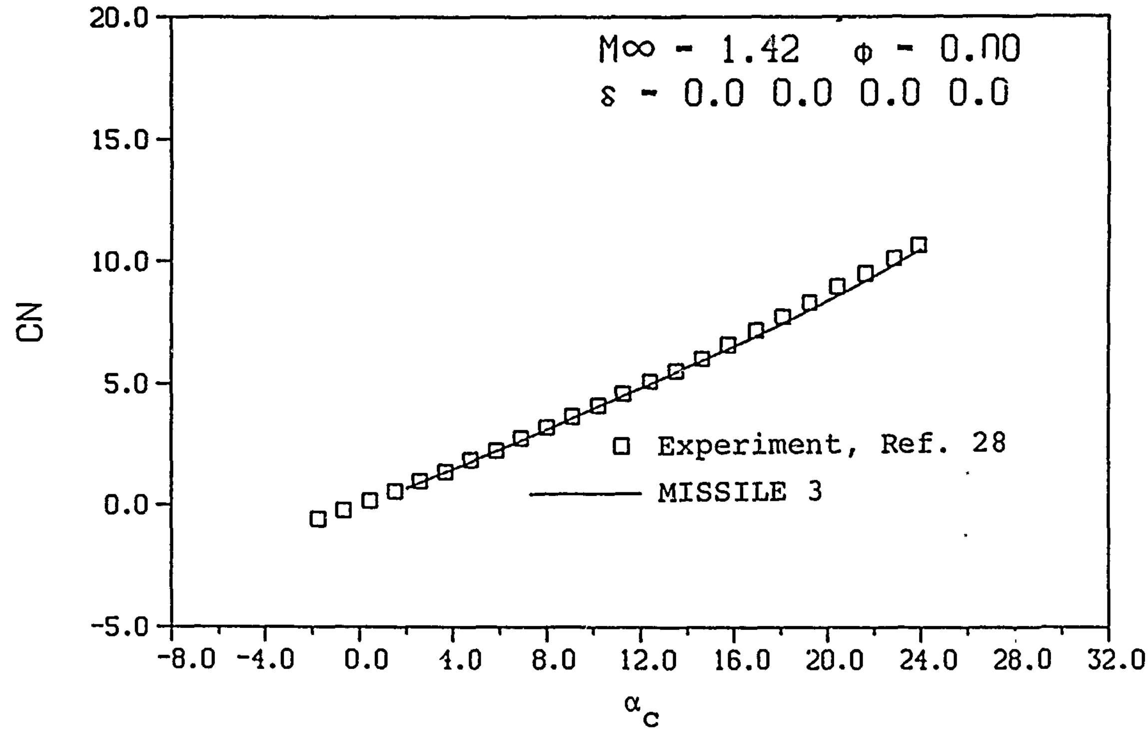

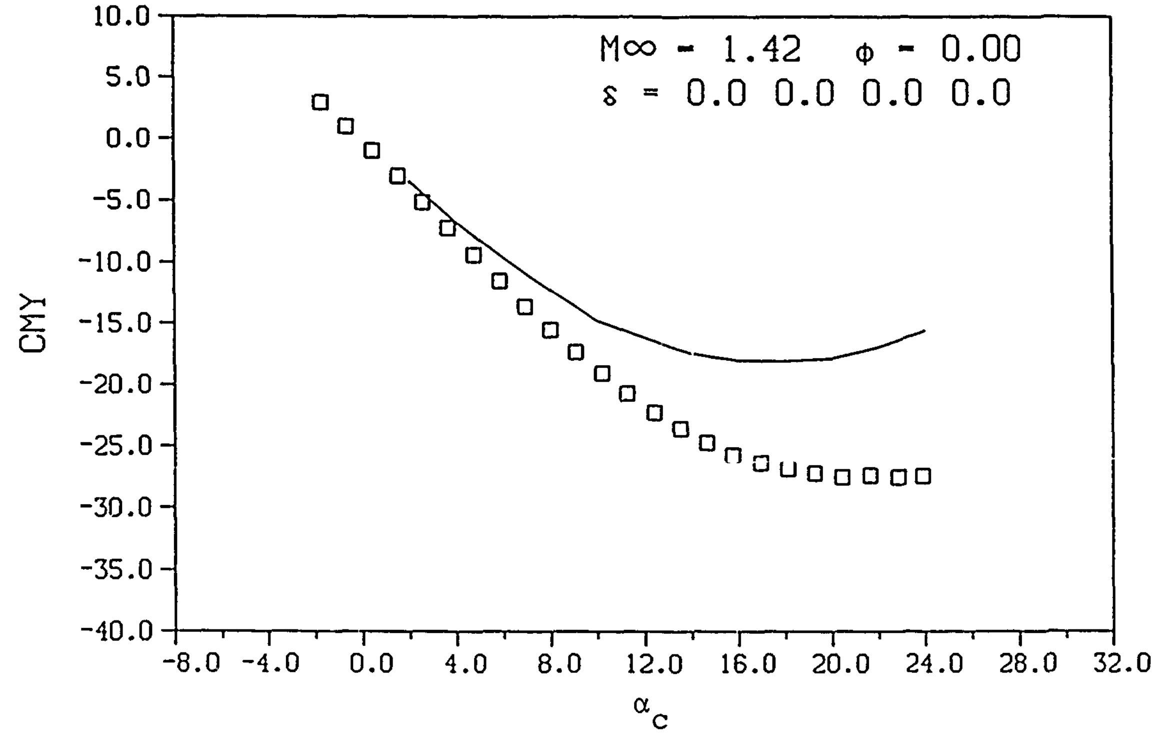

(c) $M_\infty = 1.42$

Figure 28.- Continued.

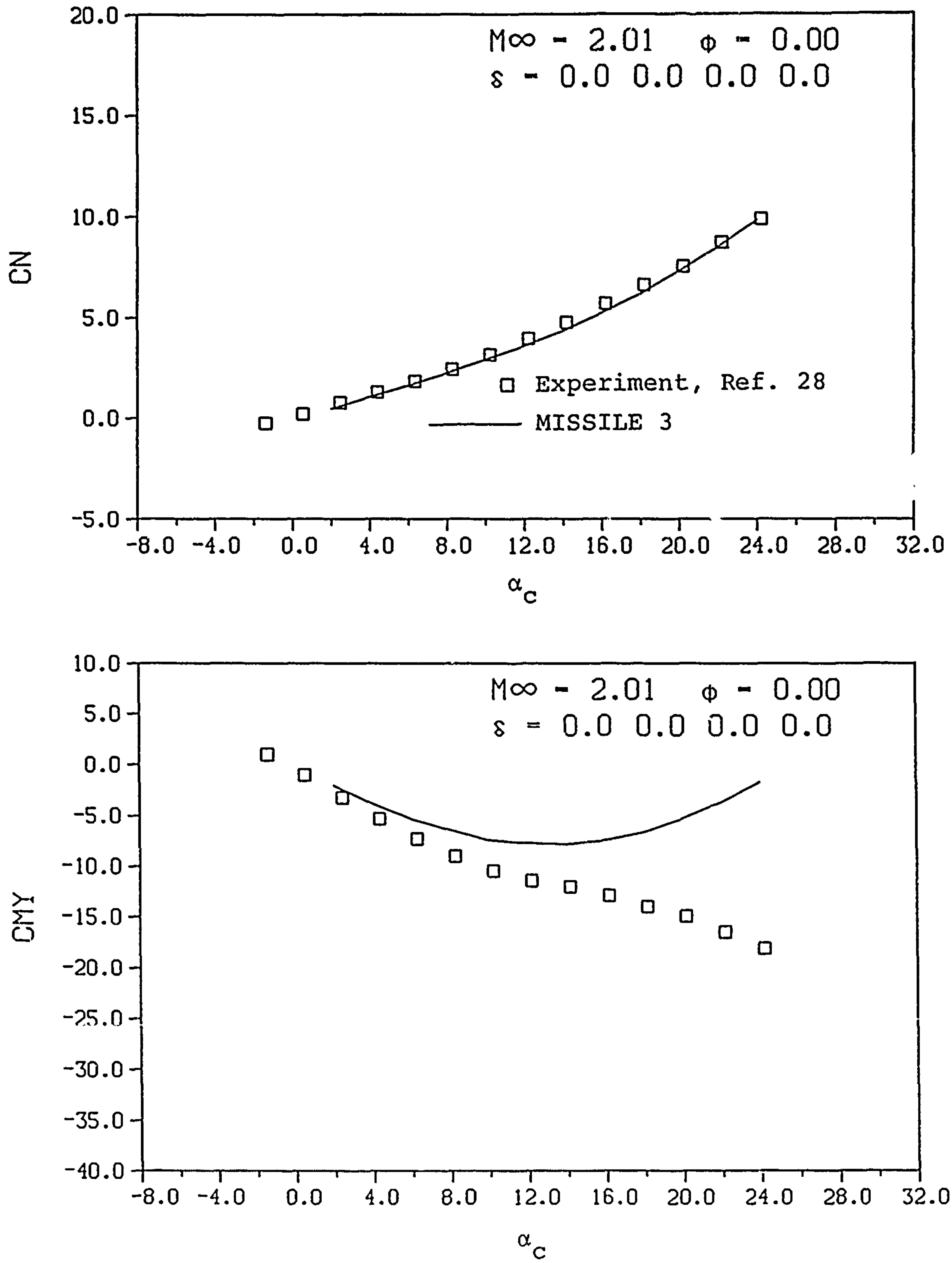

(d) $M_\infty = 2.01$

Figure 28.- Continued.

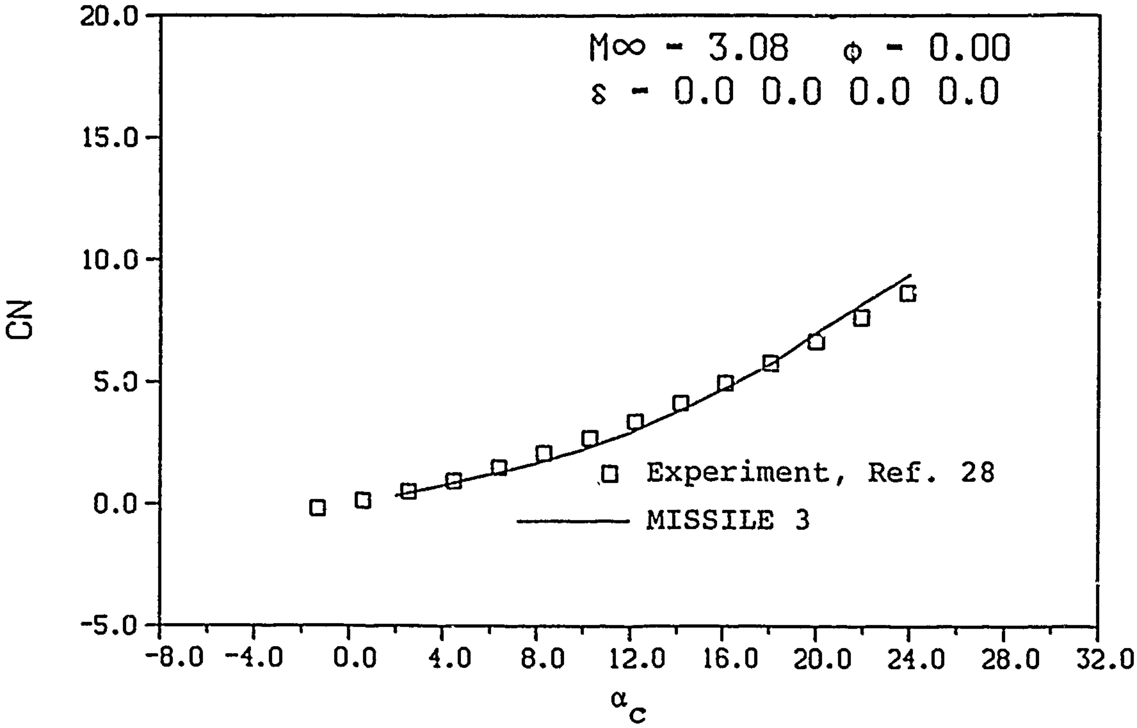

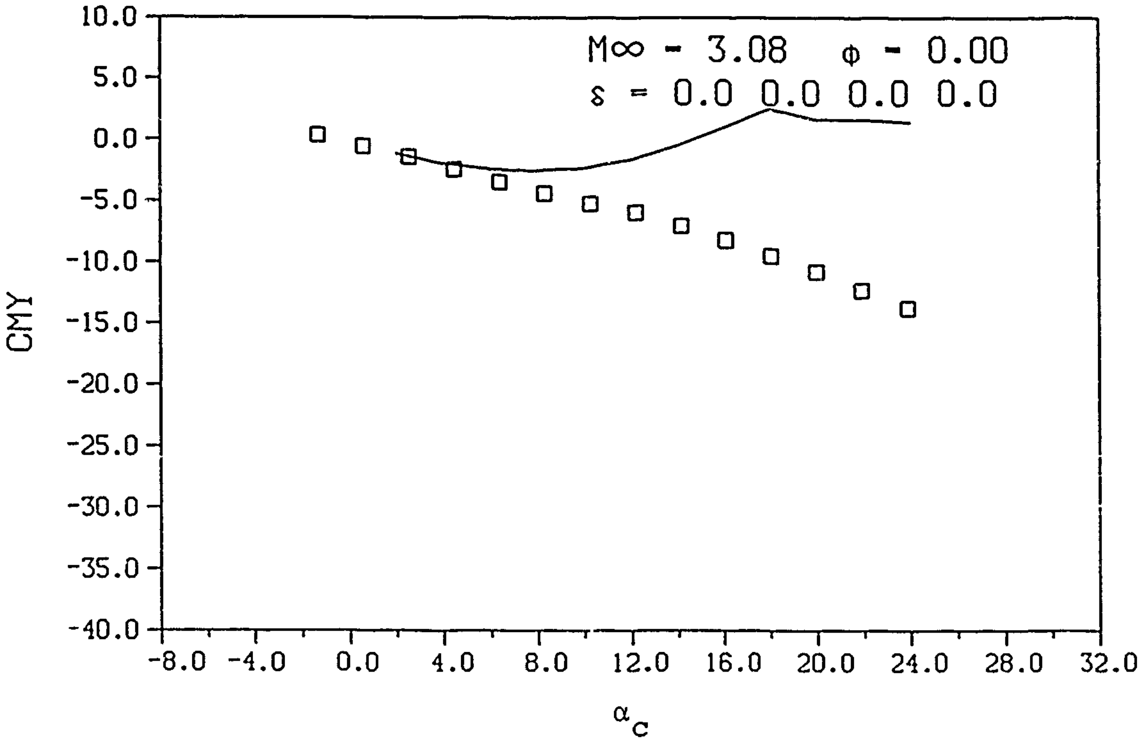

(e) $M_\infty = 3.08$

Figure 28.- Concluded.

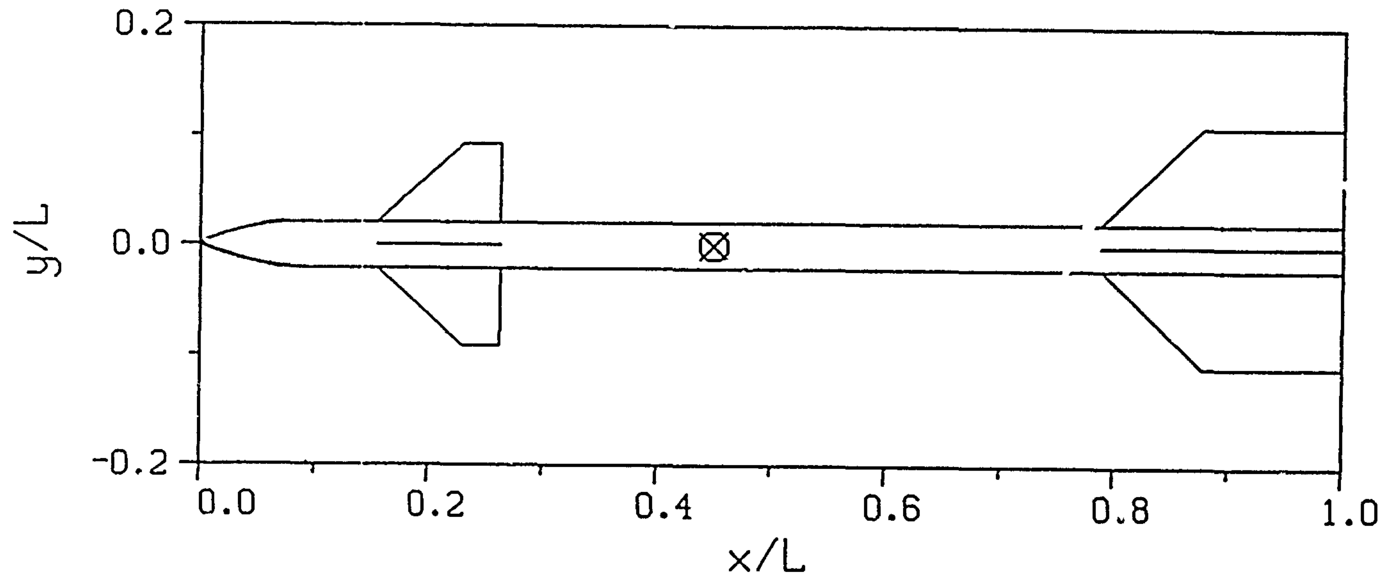

Figure 29.- Geometry for the canard-body-tail model in Reference 25.

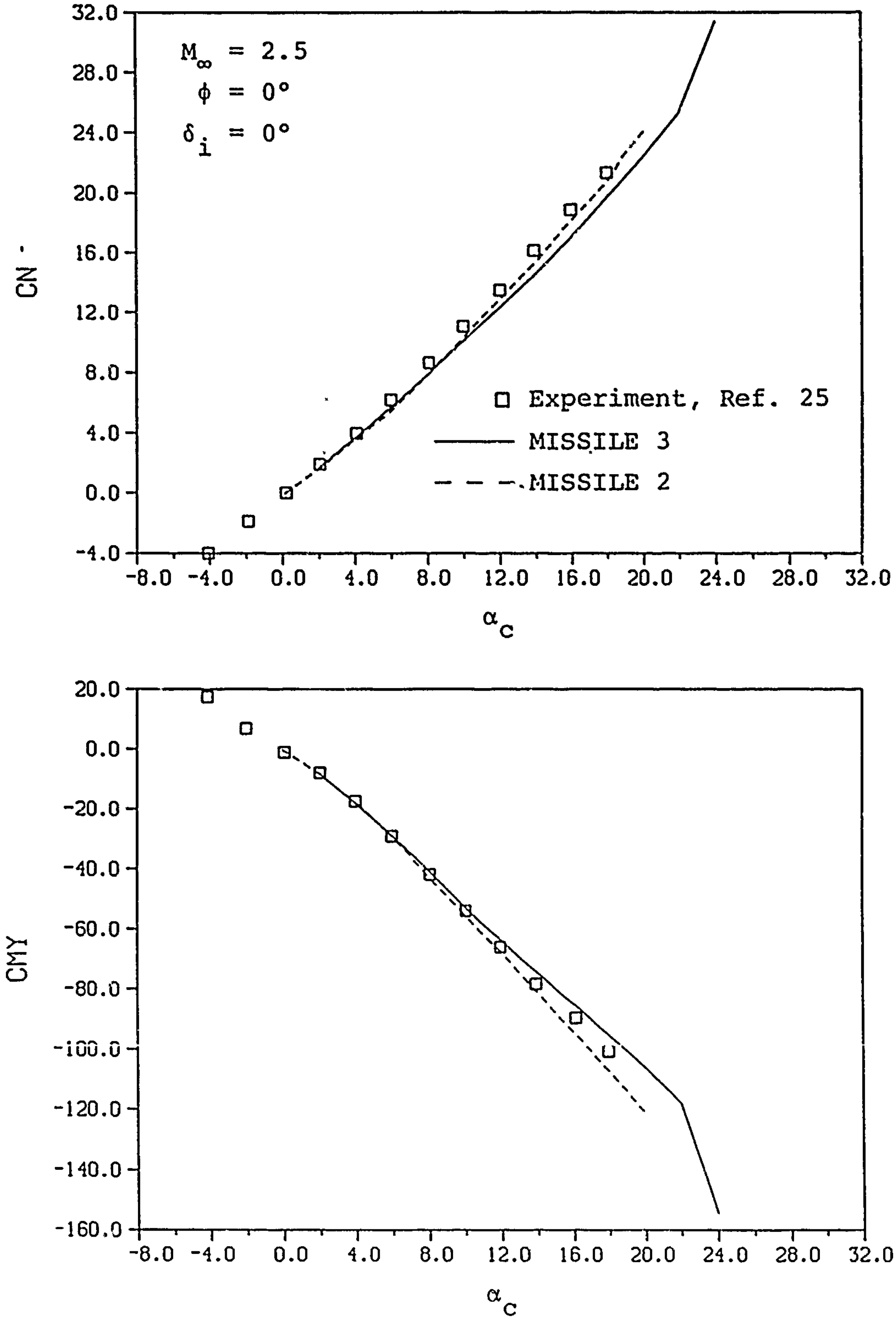

Figure 30.- Comparison of predicted and measured aerodynamic characteristics for the canard-body-tail model in Reference 25, $M_\infty = 2.5$, $\phi = 0°$, $\delta_i = 0°$.

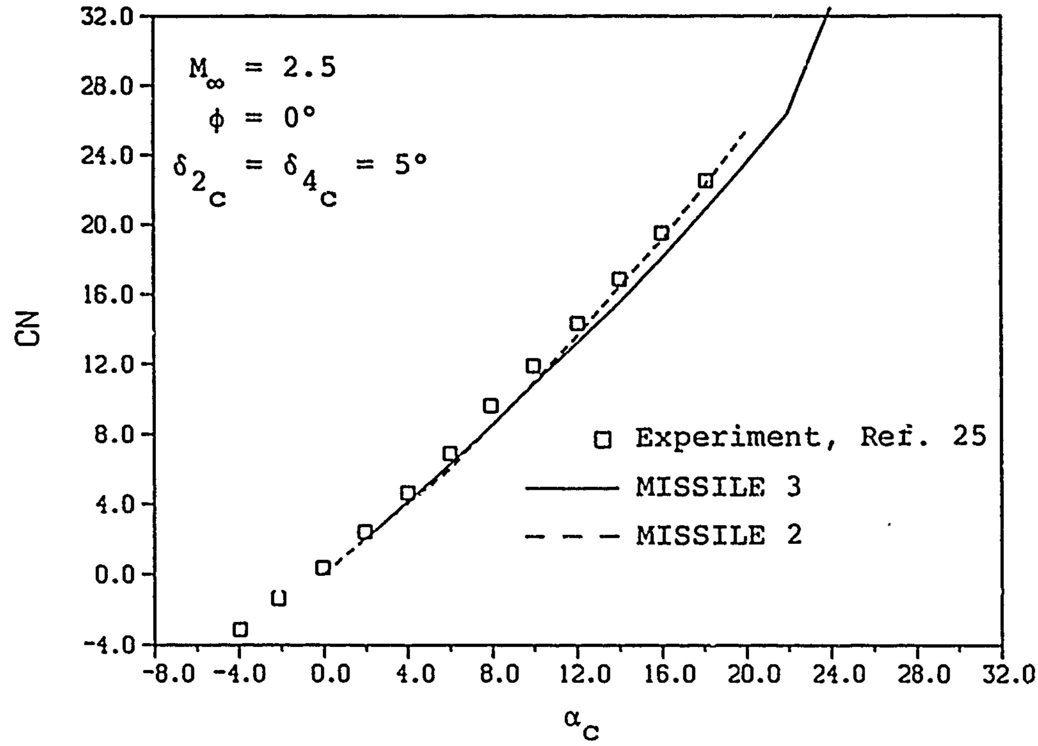

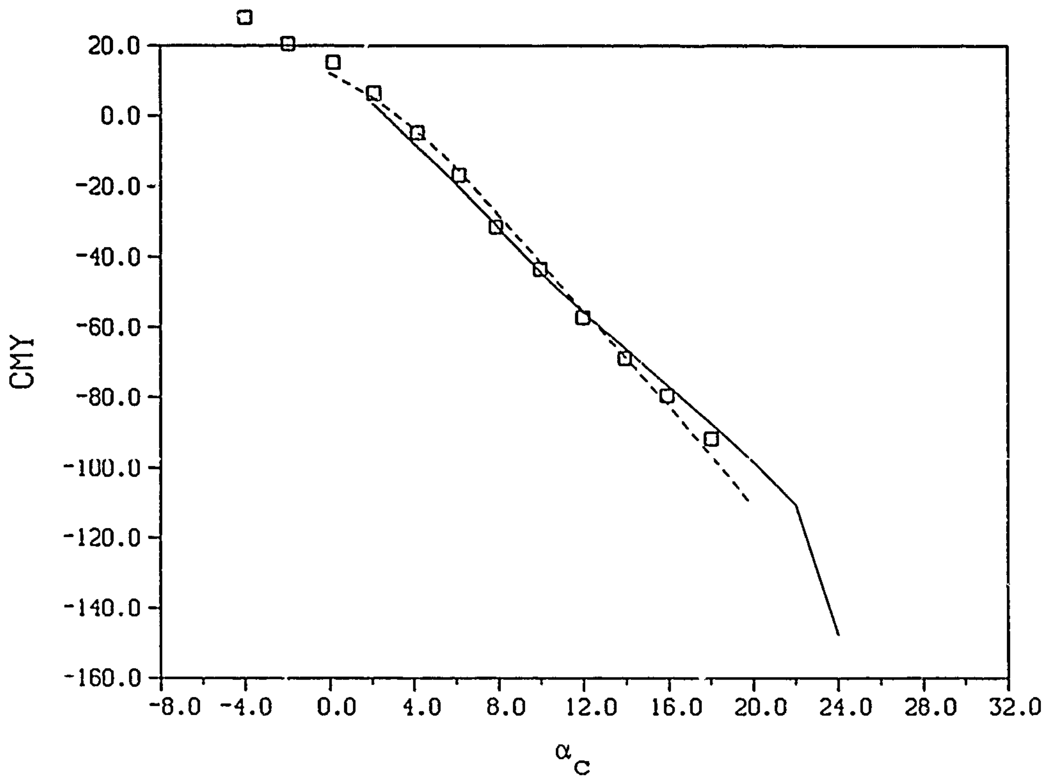

Figure 31.- Comparison of predicted and measured aerodynamic characteristics for the canard-body-tail model in Reference 25, $M_\infty = 2.5$, $\phi = 0°$, $\delta_{2_c} = \delta_{4_c} = 5°$.

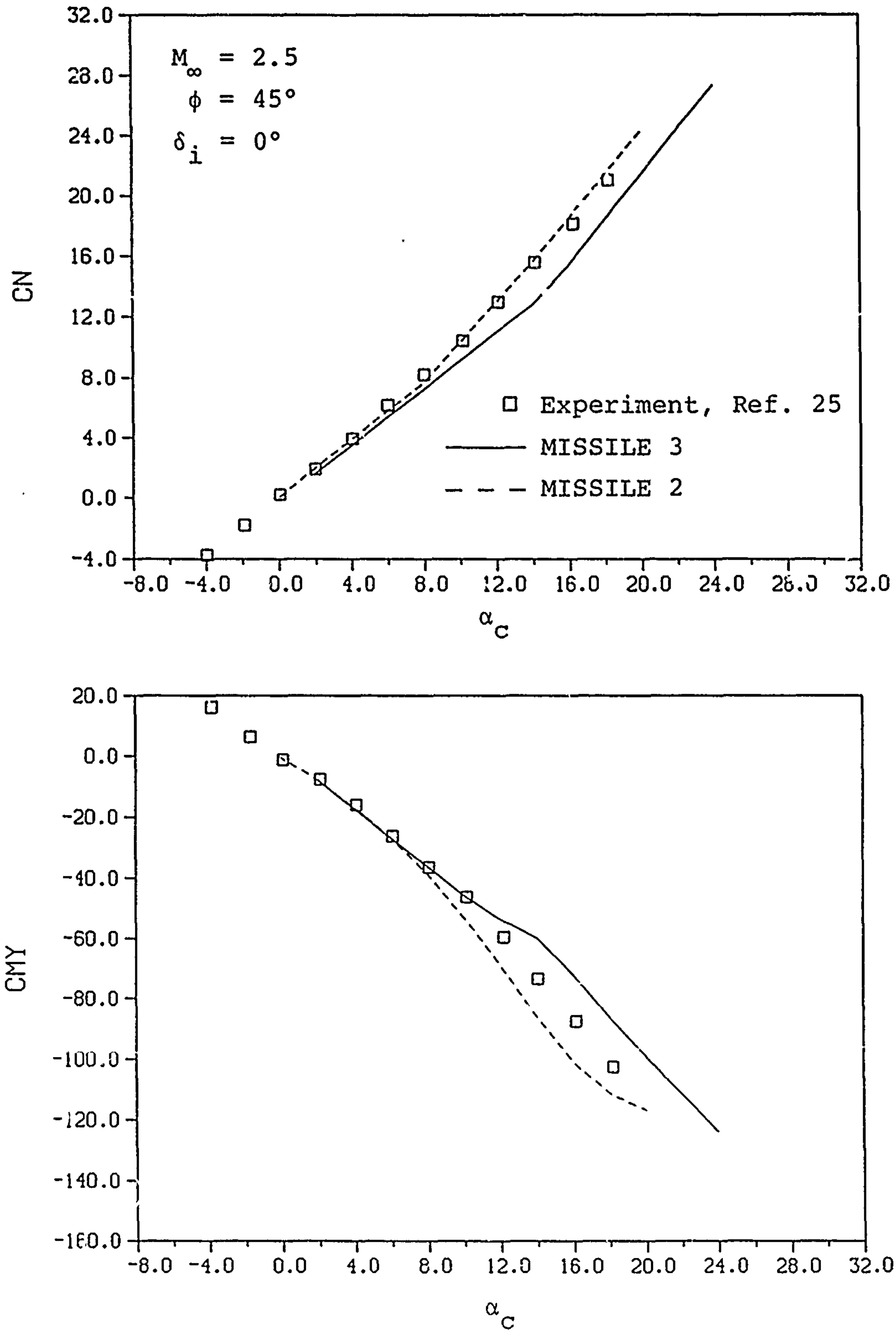

Figure 32.- Comparison of predicted and measured aerodynamic characteristics for the canard-body-tail model in Reference 25, M_∞ = 2.5, ϕ = 45°, δ_i = 0°.

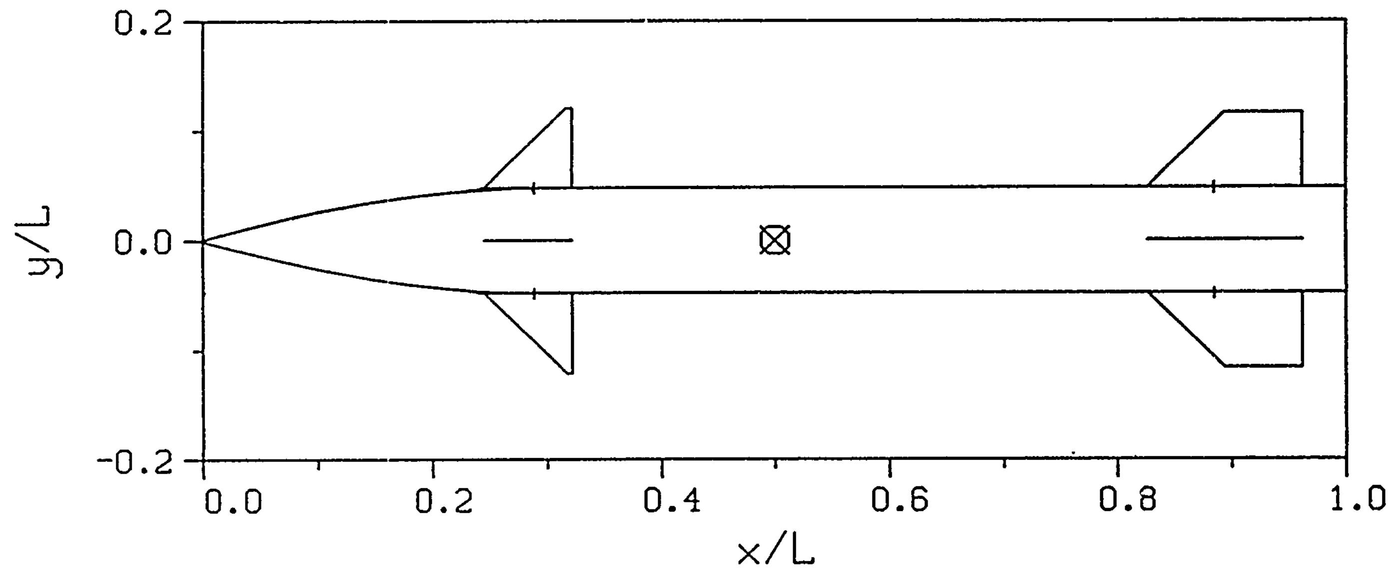

Figure 33.- Geometry for the Army Generalized Missile, Reference 26.

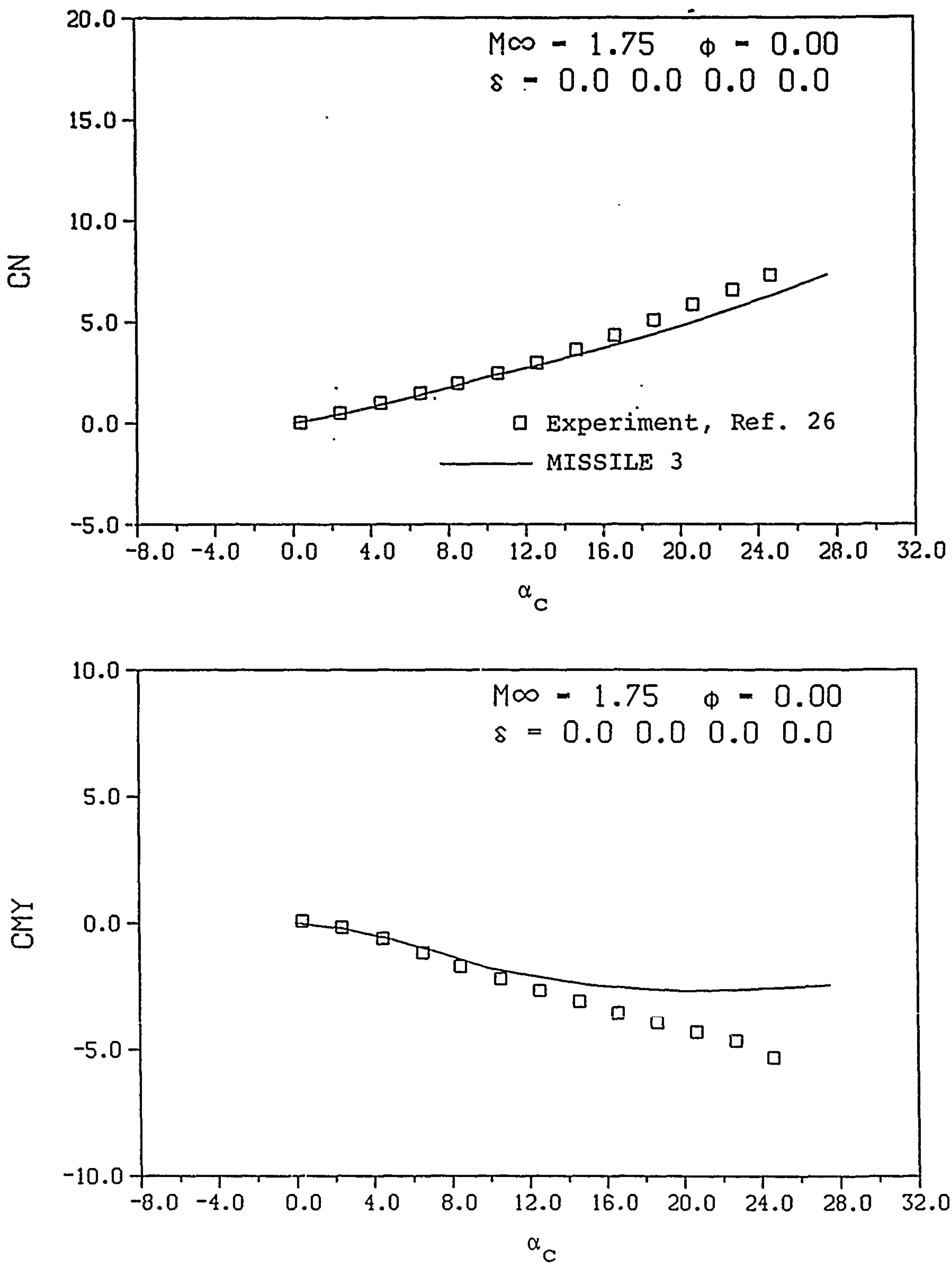

(a) Overall loads

Figure 34.- Comparison of predicted and measured aerodynamic characteristics for the Army Generalized Missile, Reference 26, $M_{\infty} = 1.75$, $\varphi = 0°$, $\delta_i = 0°$.

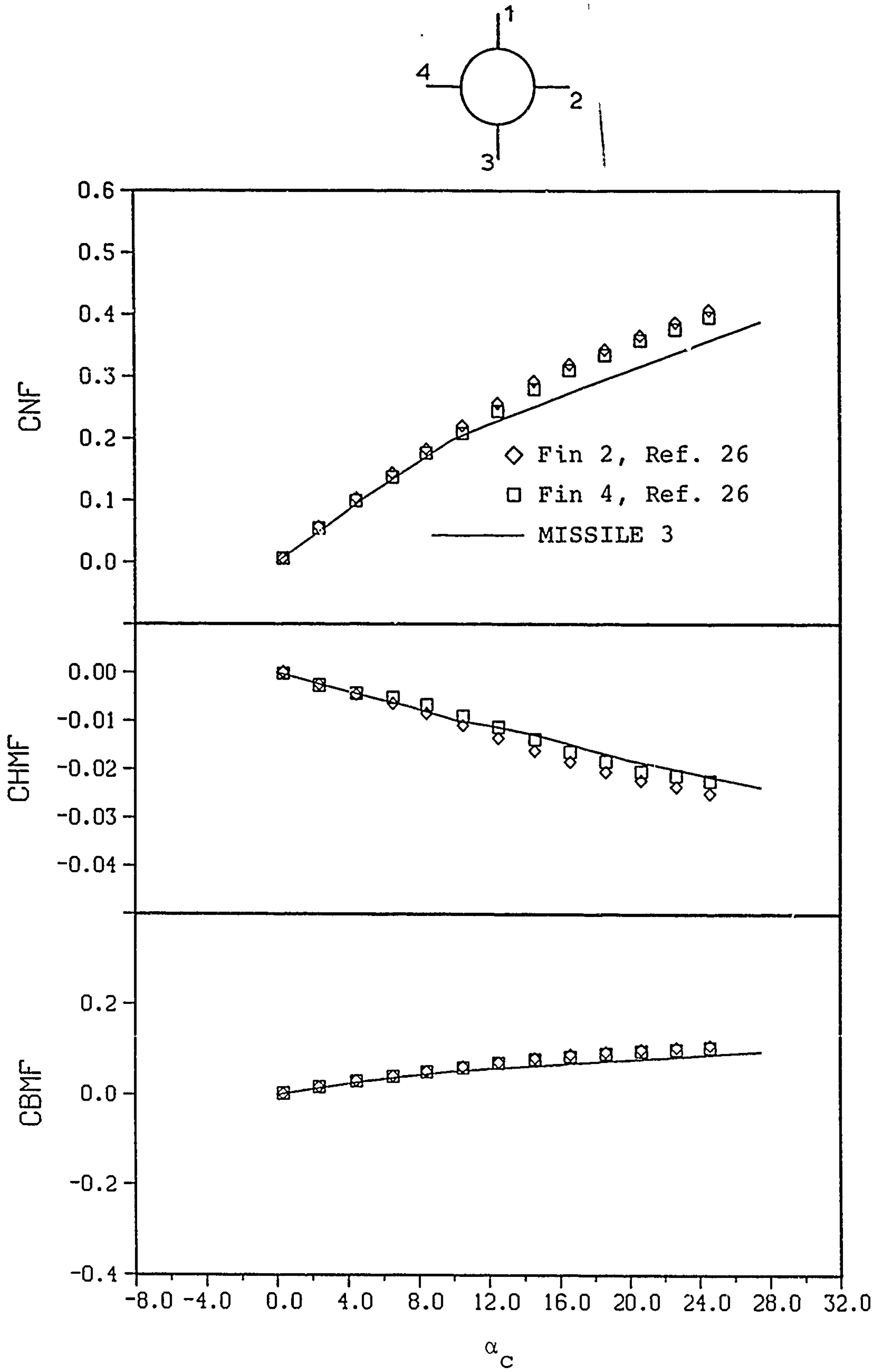

(b) Canard fin 2 loads

Figure 34.- Continued.

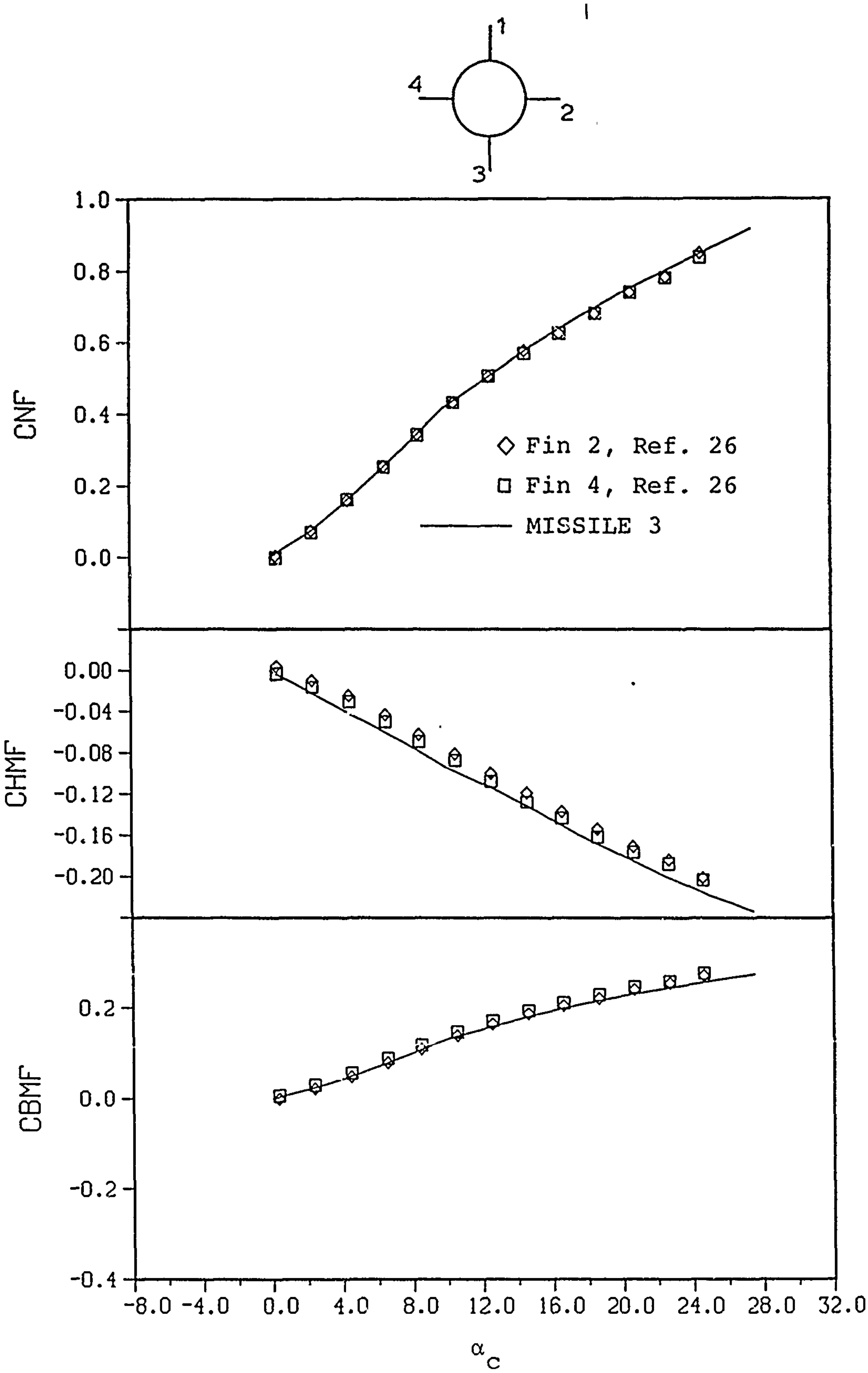

(c) Tail fin 2 loads

Figure 34.- Concluded.

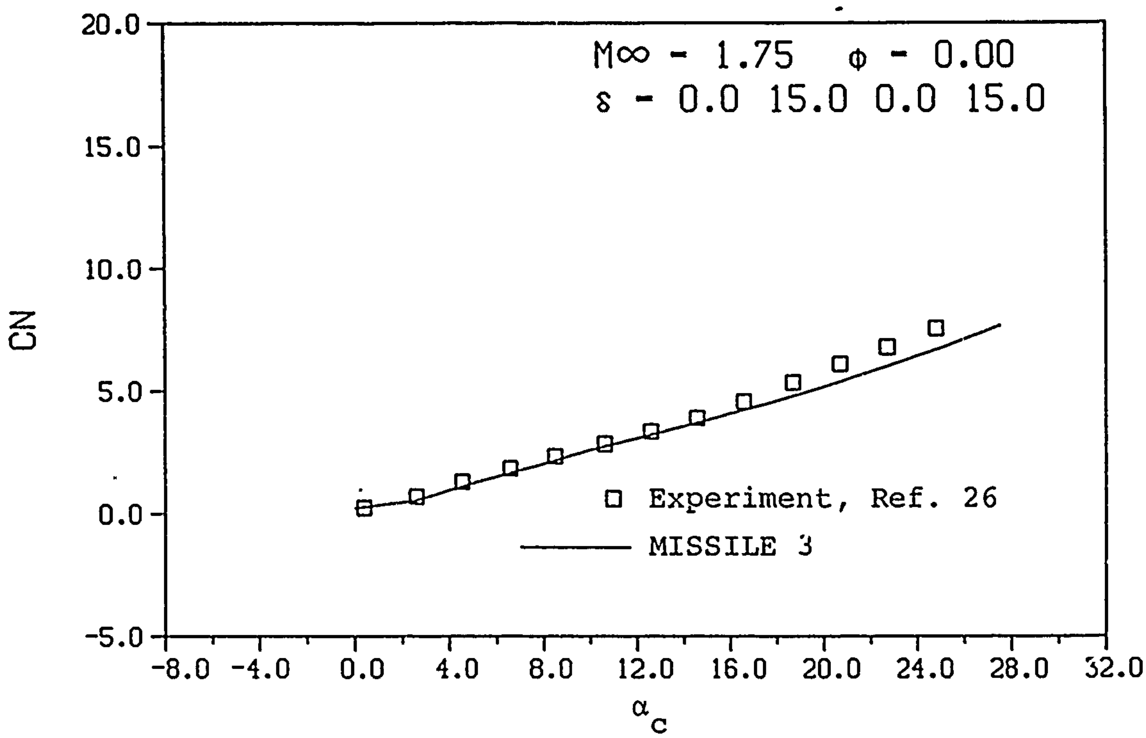

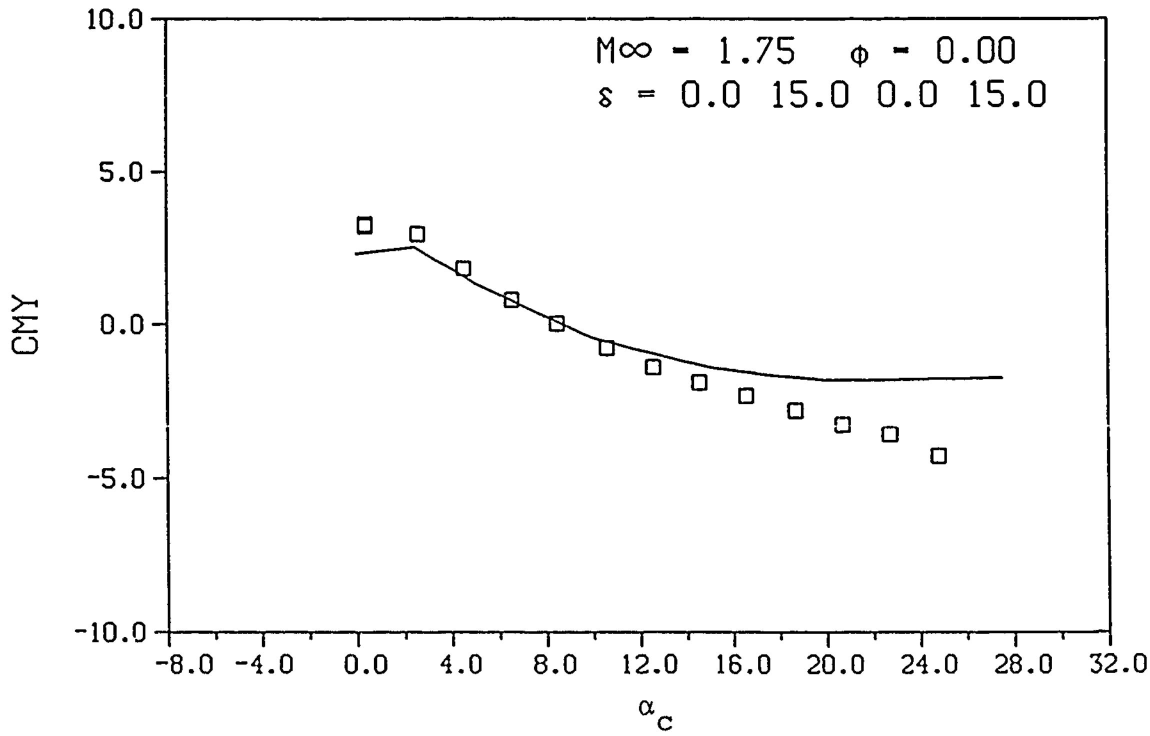

(a) Overall loads

Figure 35.- Comparison of predicted and measured aerodynamic characteristics for the Army Generalized Missile, Reference 26, $M_\infty = 1.75$, $\phi = 0°$, $\delta_{2_c} = \delta_{4_c} = 15°$.

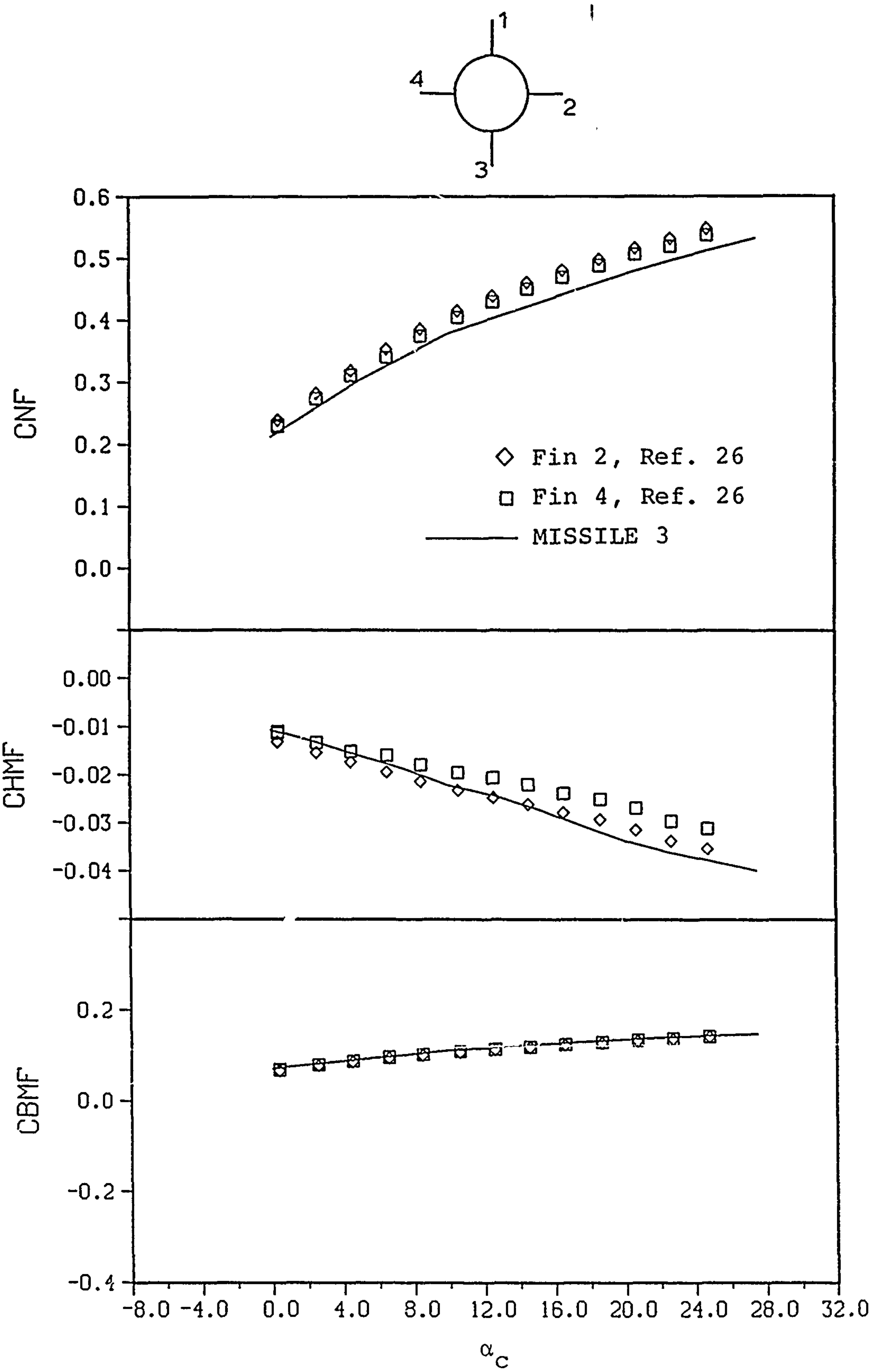

(b) Canard fin 2 loads

Figure 35.- Continued.

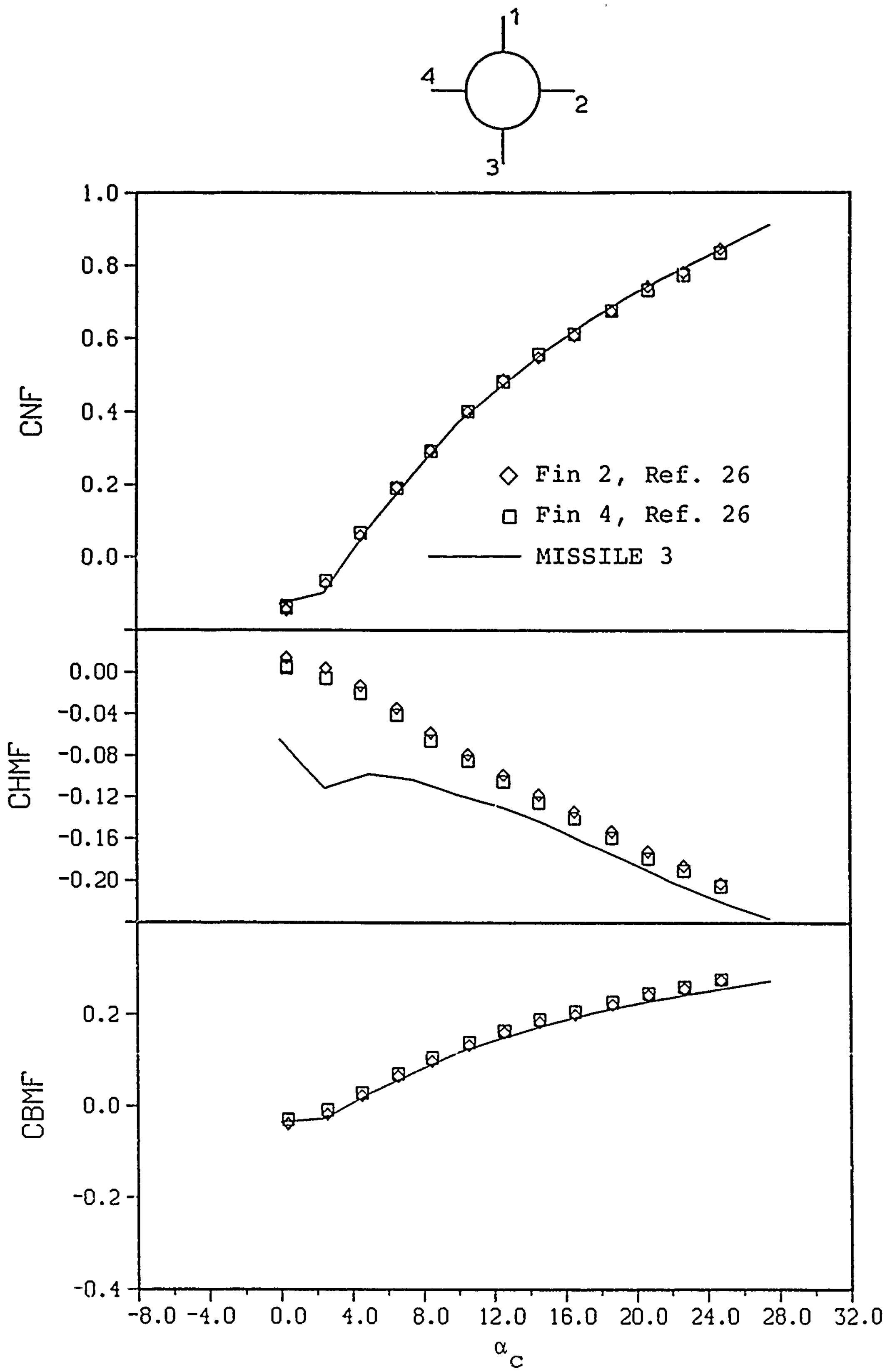

(c) Tail fin 2 loads

Figure 35.- Concluded.

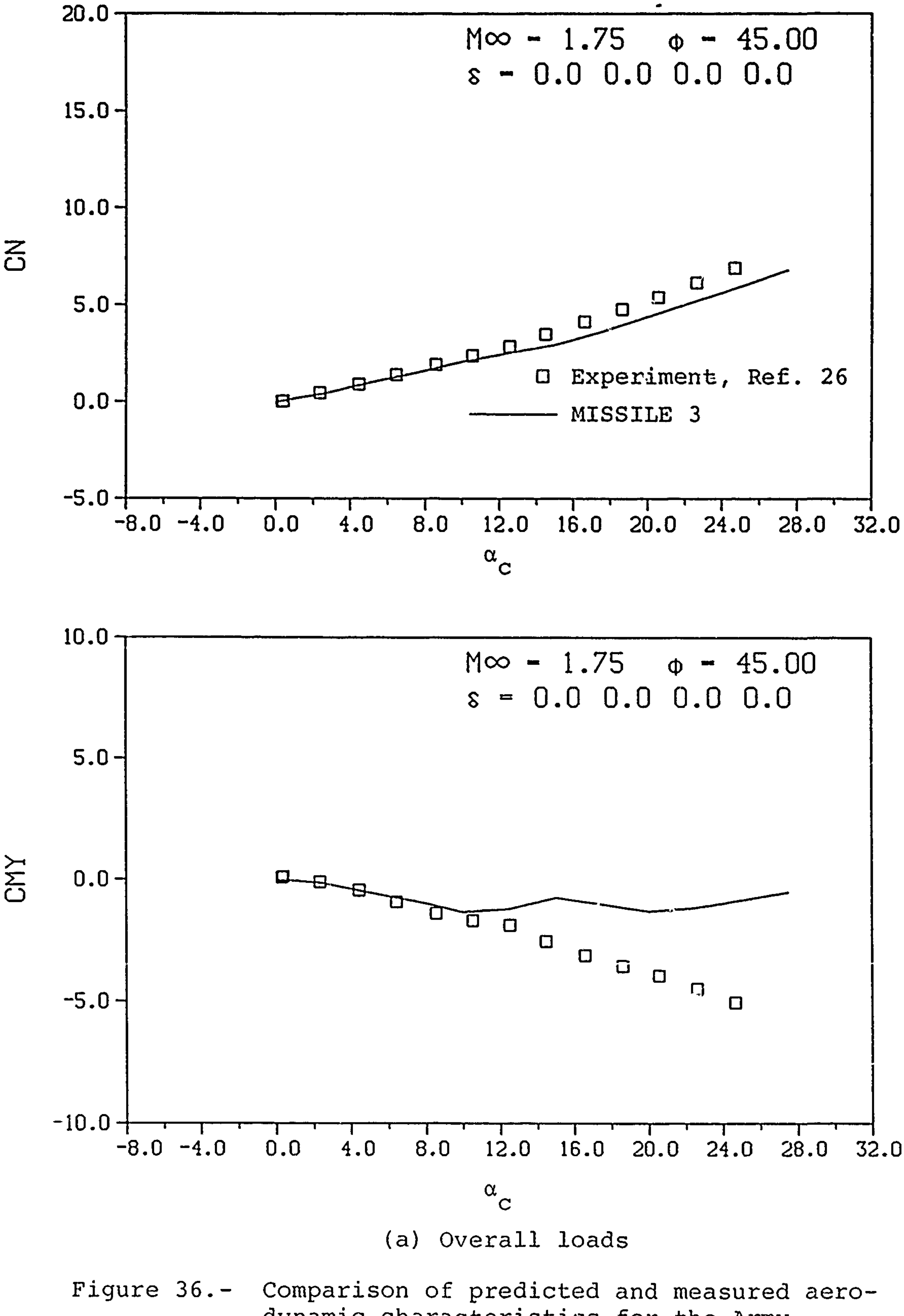

(a) Overall loads

Figure 36.- Comparison of predicted and measured aerodynamic characteristics for the Army Generalized Missile, Reference 26, $M_\infty = 1.75$, $\phi = 45°$, $\delta_i = 0°$.

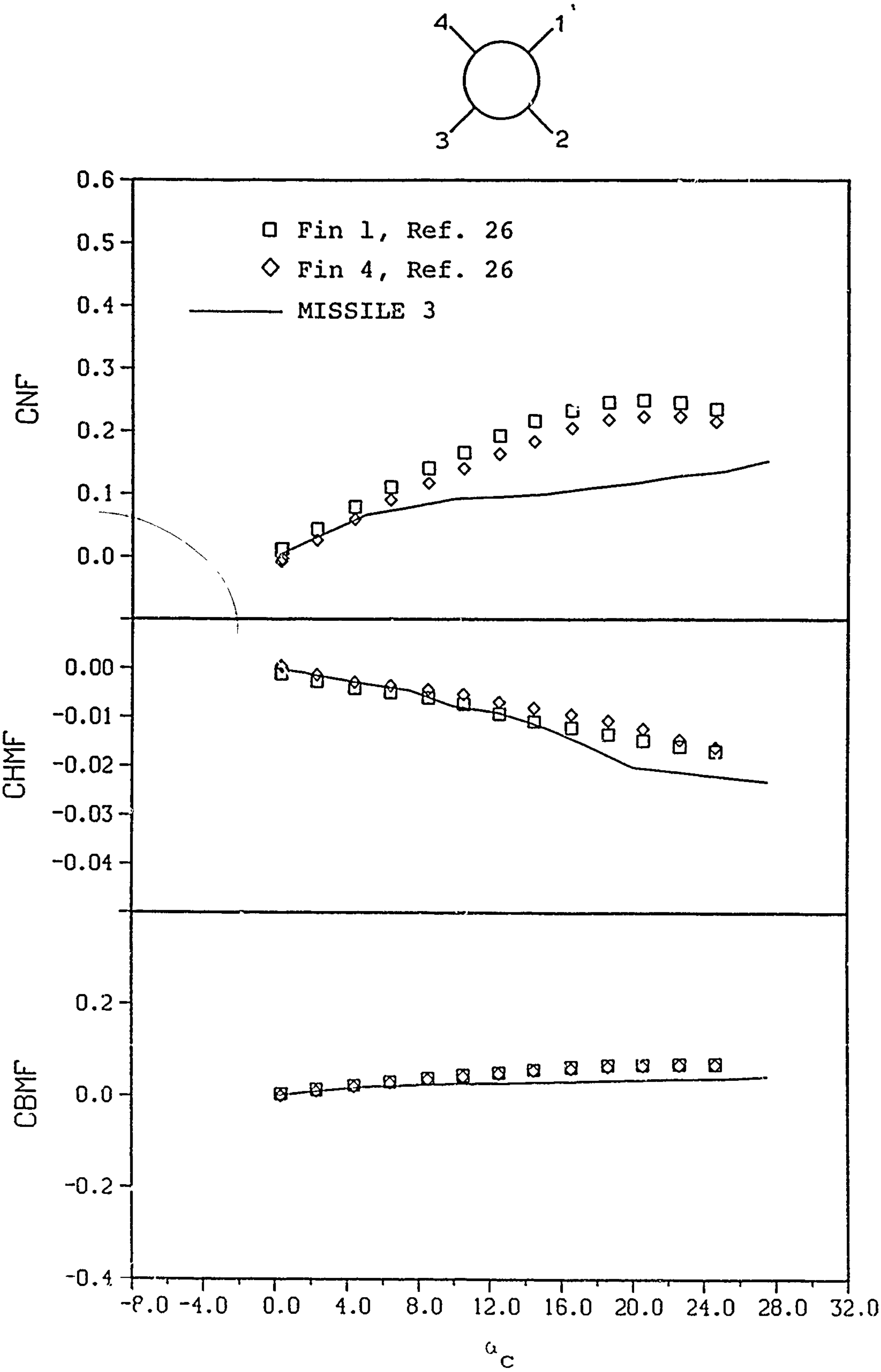

(b) Canard fin 1 loads

Figure 36.- Continued.

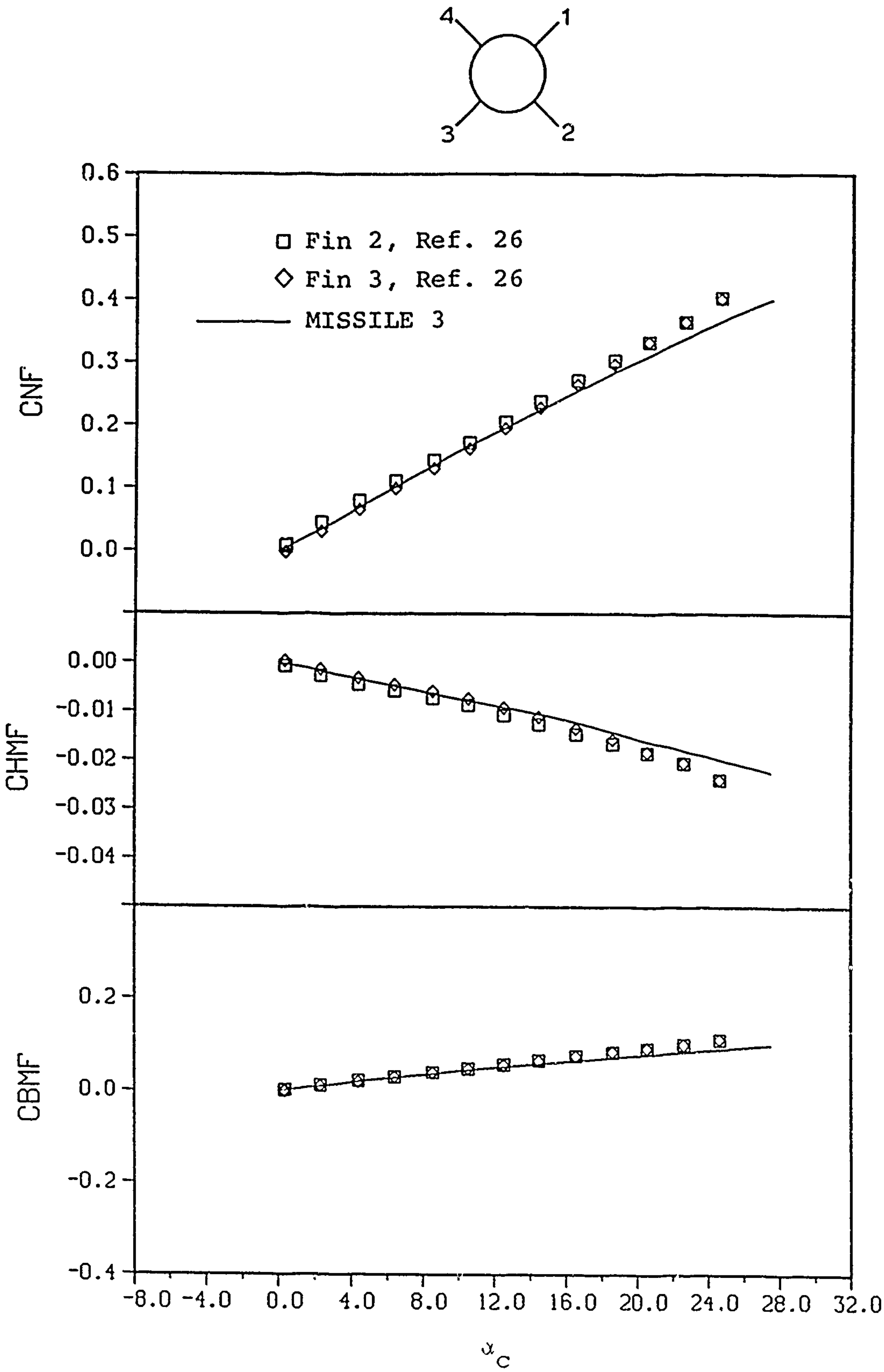

(c) Canard fin 2 loads

Figure 36.- Continued.

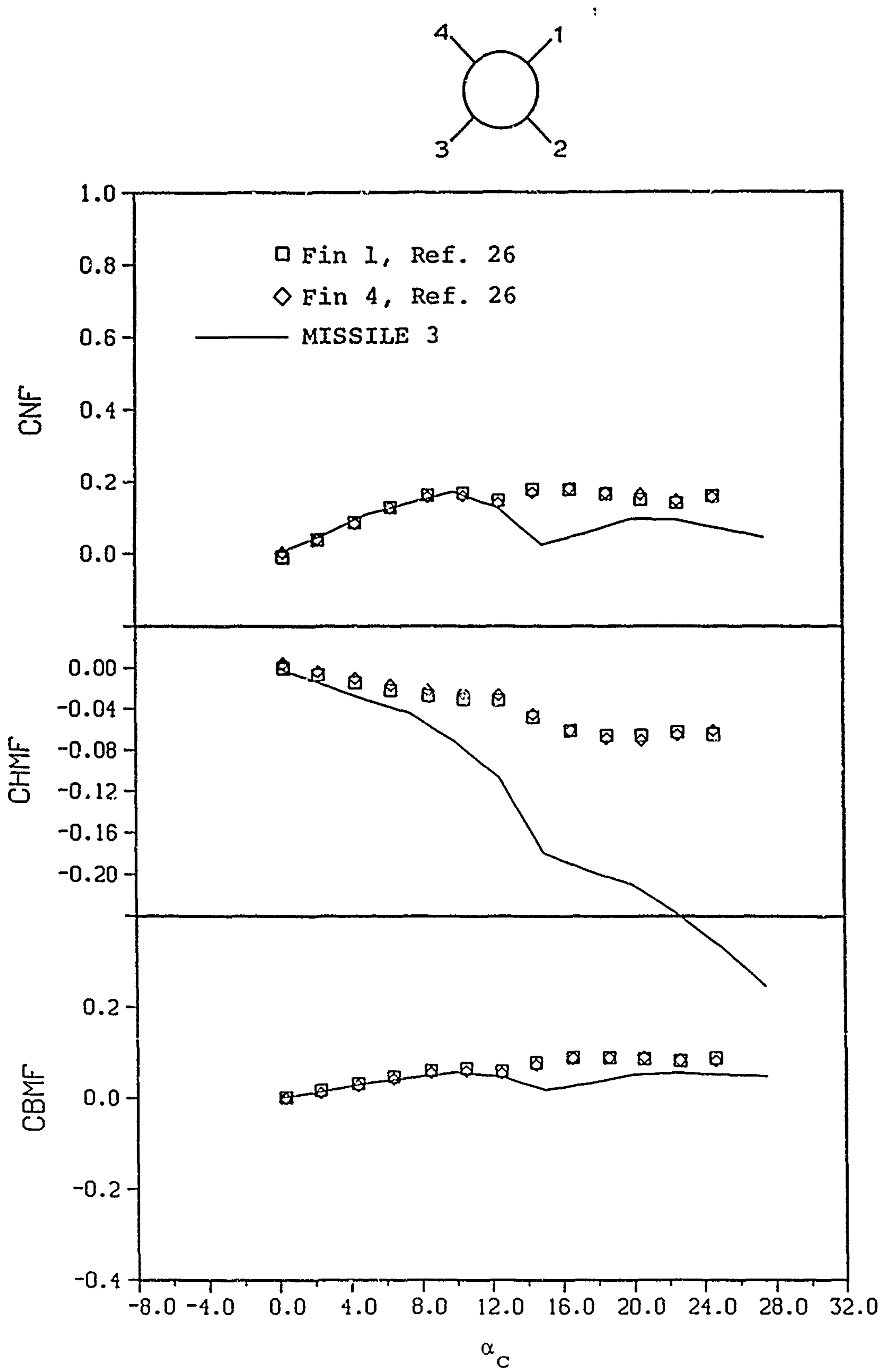

(d) Tail fin 1 loads

Figure 36.- Continued.

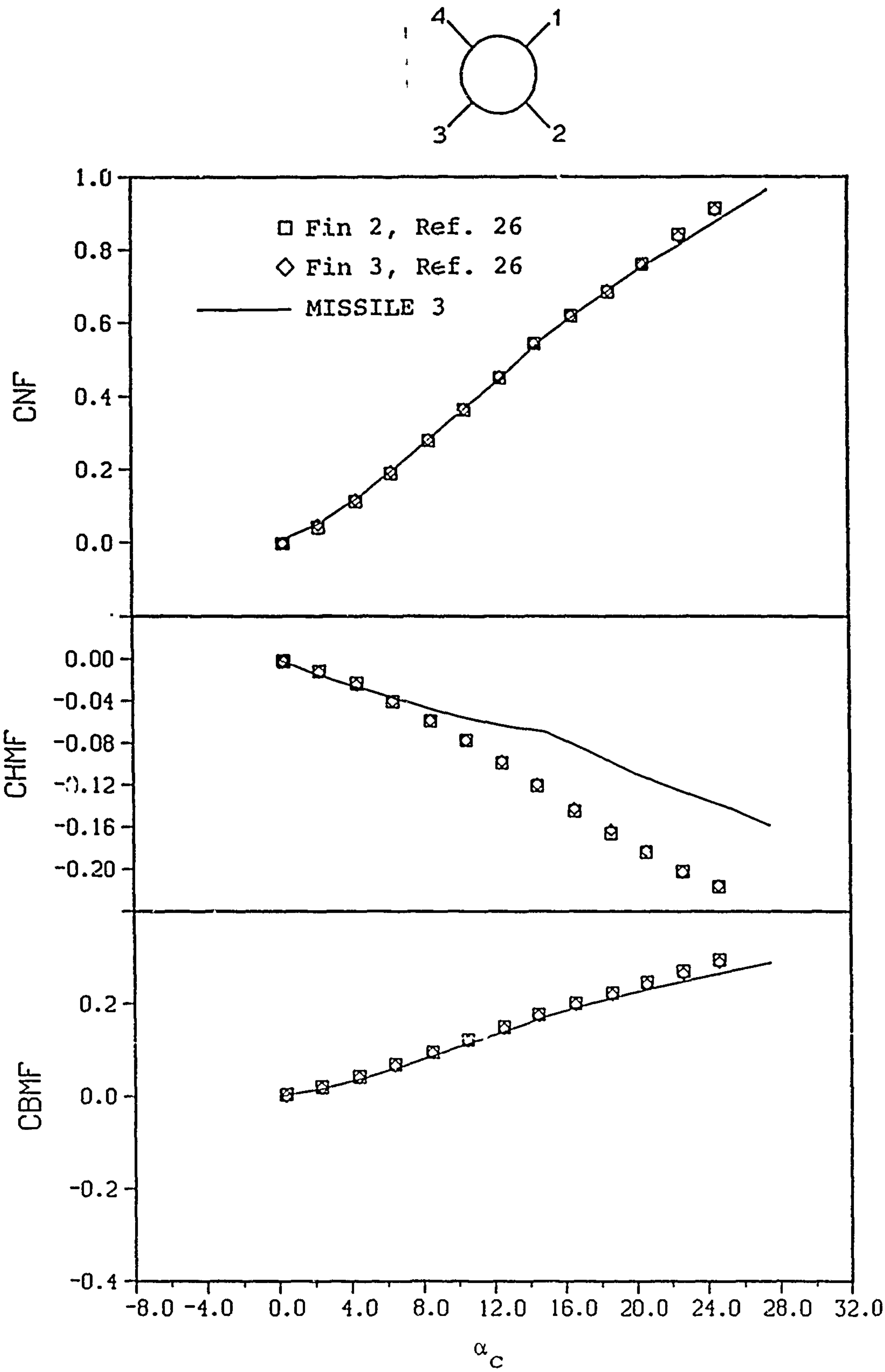

(e) Tail fin 2 loads

Figure 36.- Concluded.

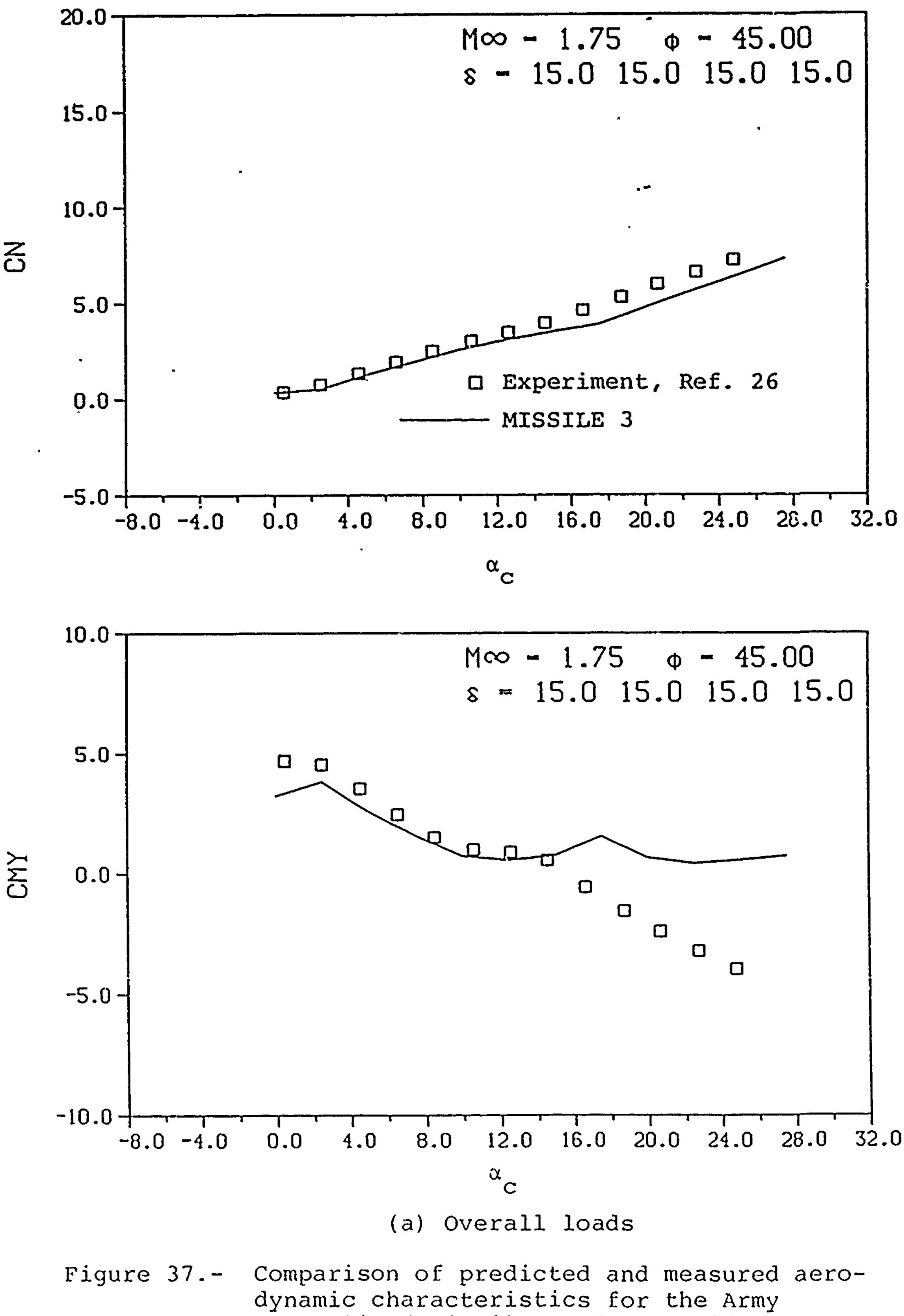

(a) Overall loads

Figure 37.- Comparison of predicted and measured aerodynamic characteristics for the Army Generalized Missile, Reference 26, $M_\infty = 1.75$, $\phi = 45°$, $\delta_{i_c} = 15°$.

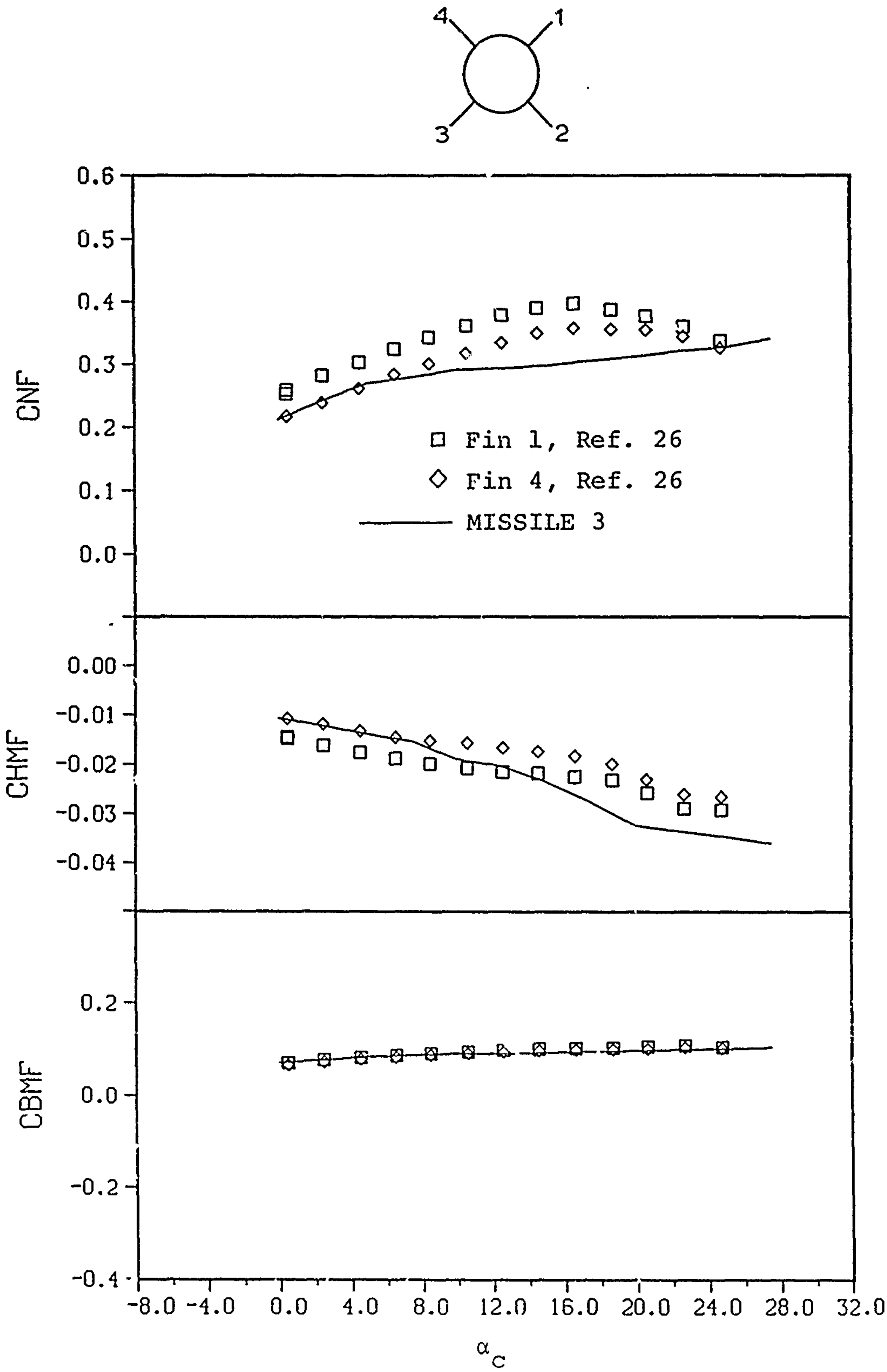

(b) Canard fin 1 loads

Figure 37.- Continued.

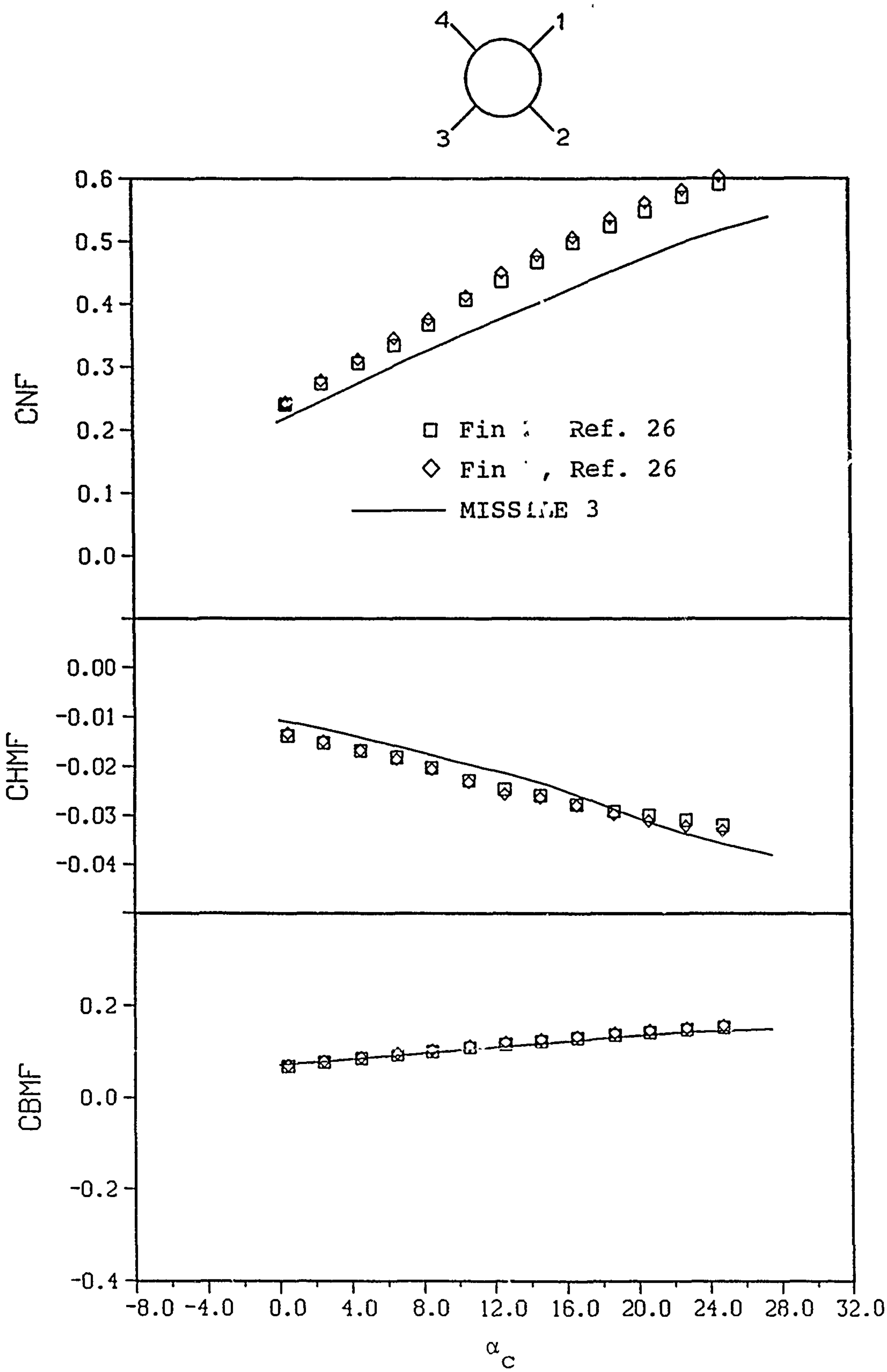

(c) Canard fin 2 loads

Figure 37.- Continued.

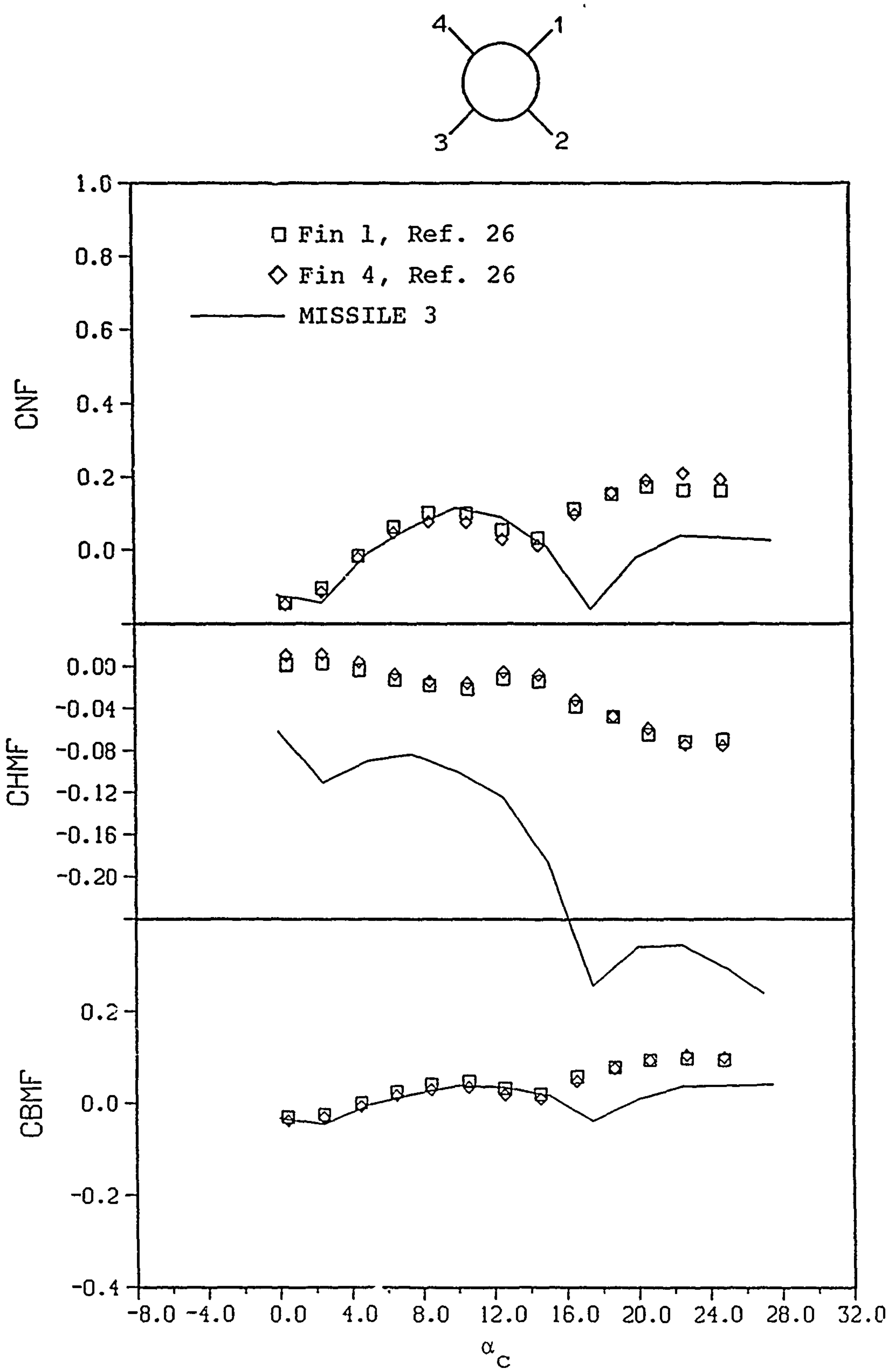

(d) Tail fin 1 loads

Figure 37.- Continued.

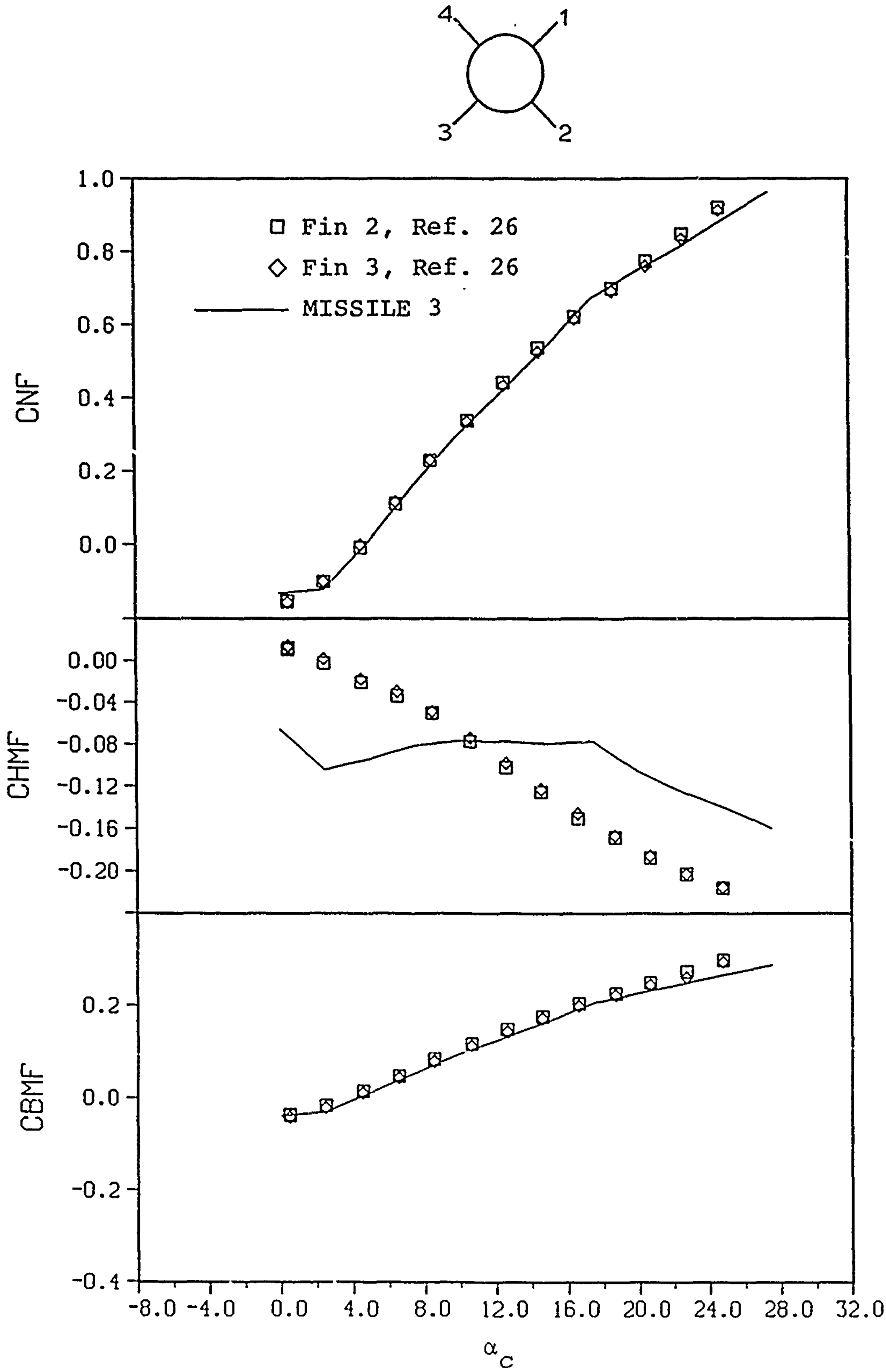

(e) Tail fin 2 loads

Figure 37.- Concluded.

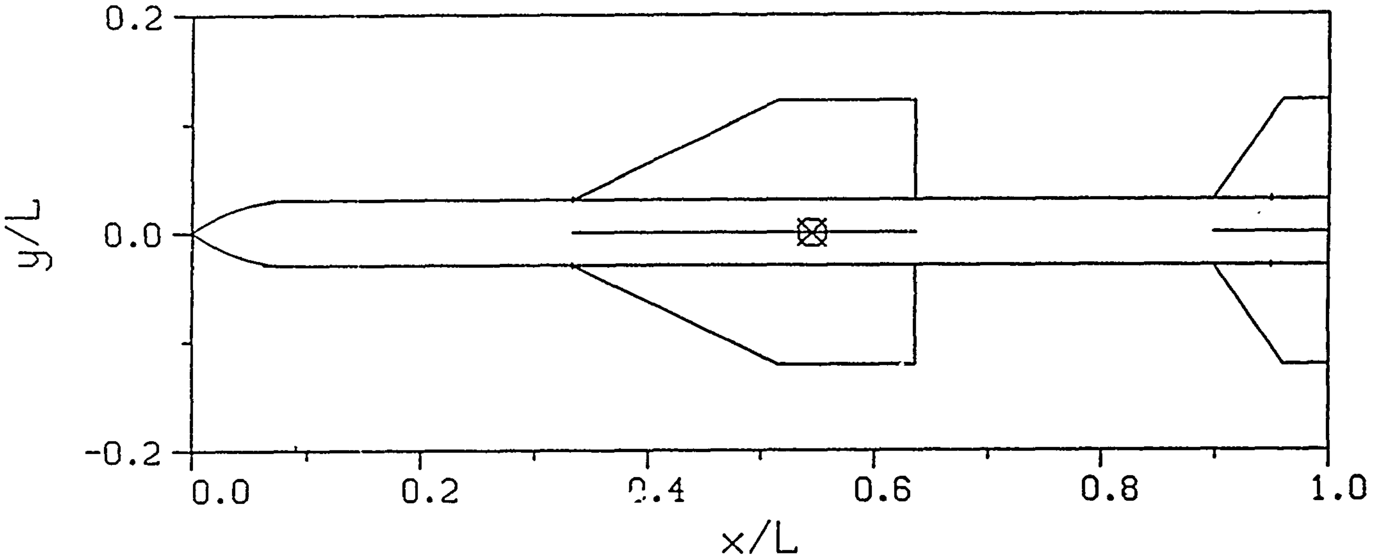

Figure 38.- Geometry for the canard-body-tail model in Reference 28.

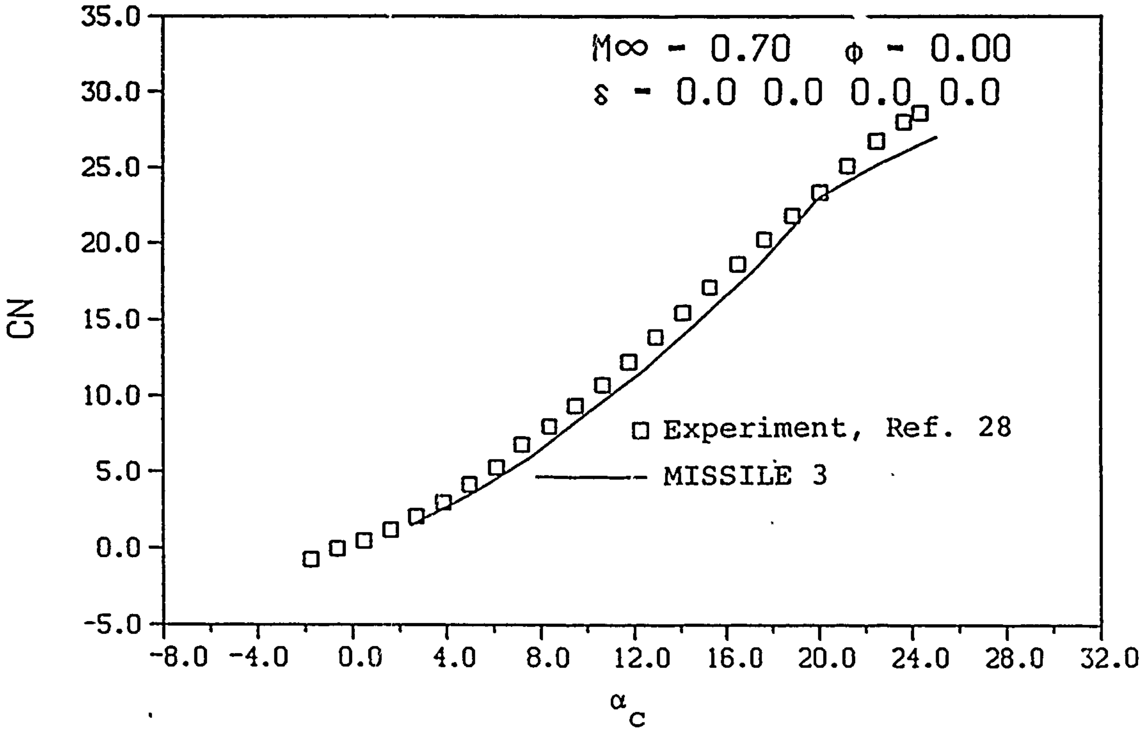

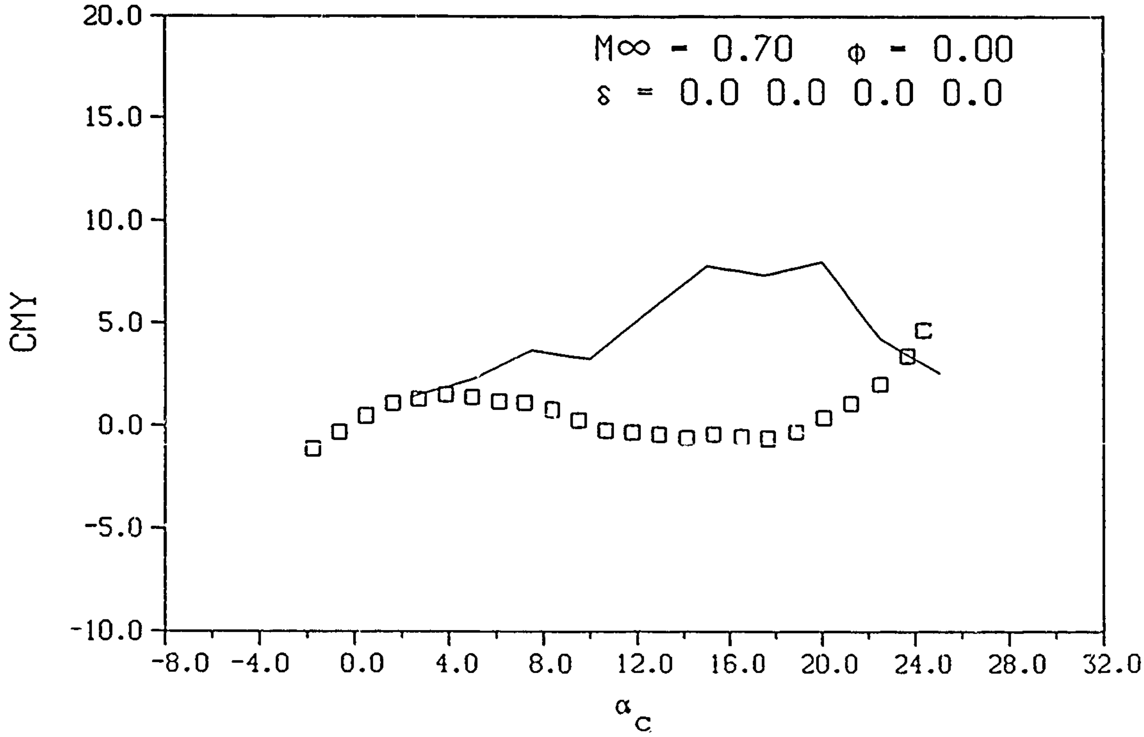

(a) $M_\infty = 0.7$, $\phi = 0°$

Figure 39.- Comparison of predicted and measured aerodynamic characteristics for the canard-body-tail model in Reference 28.

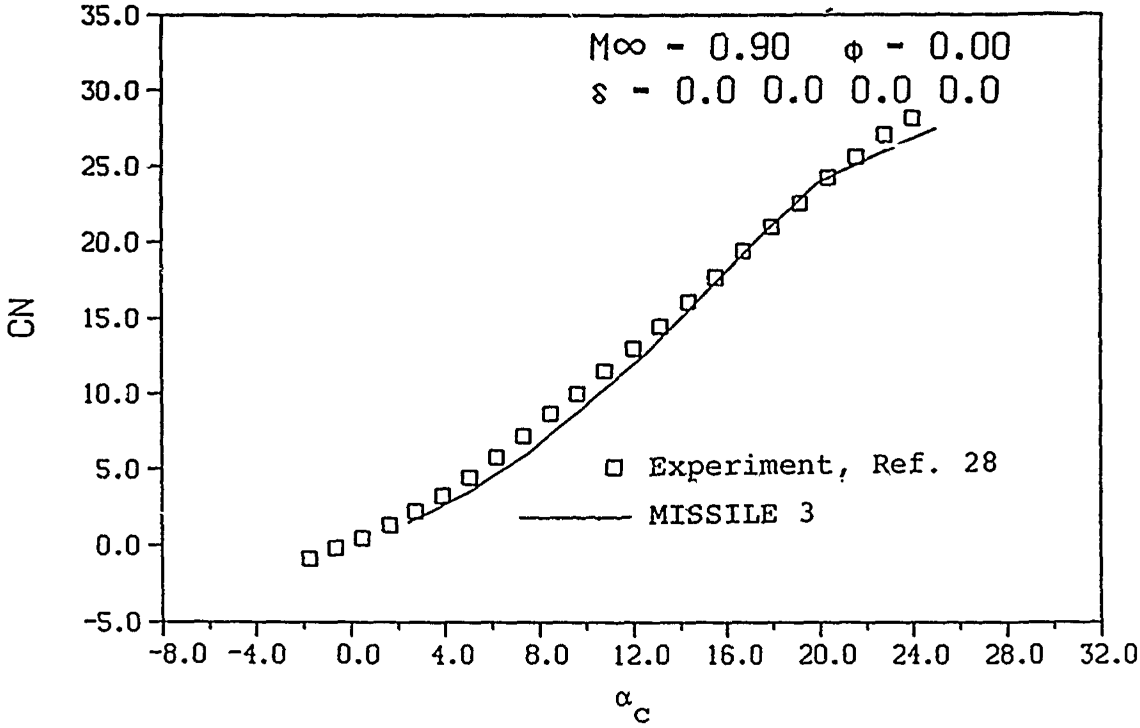

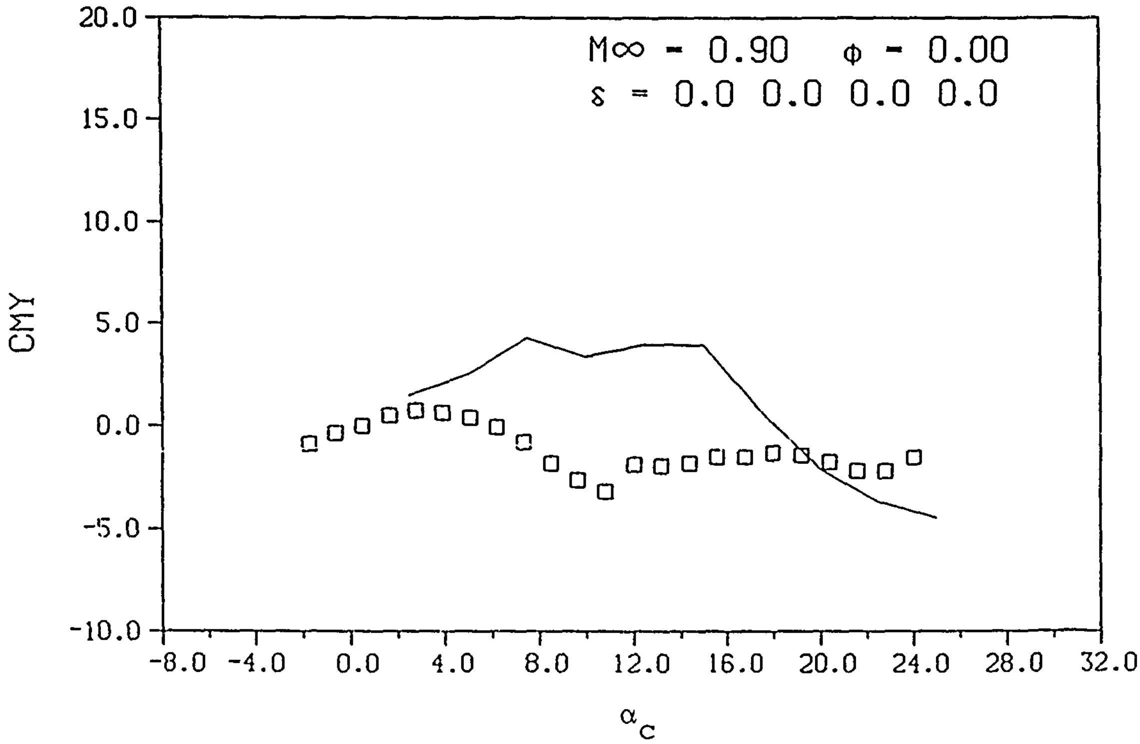

(b) $M_\infty = 0.9$, $\phi = 0°$

Figure 39.- Continued.

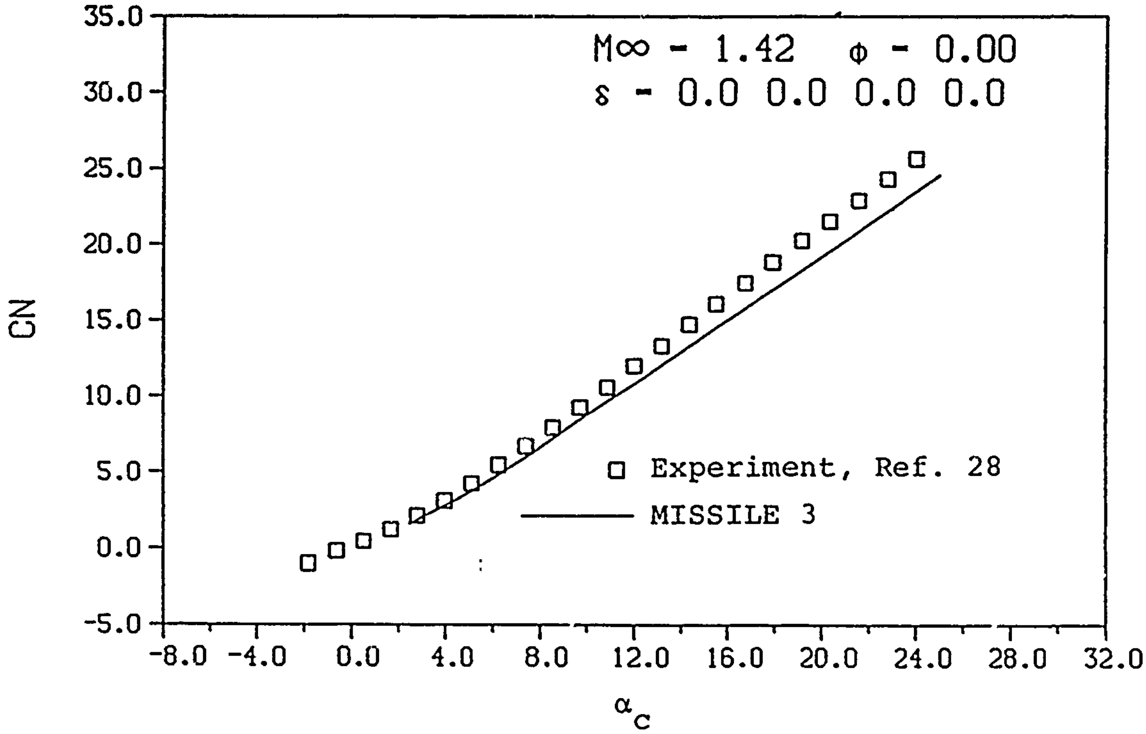

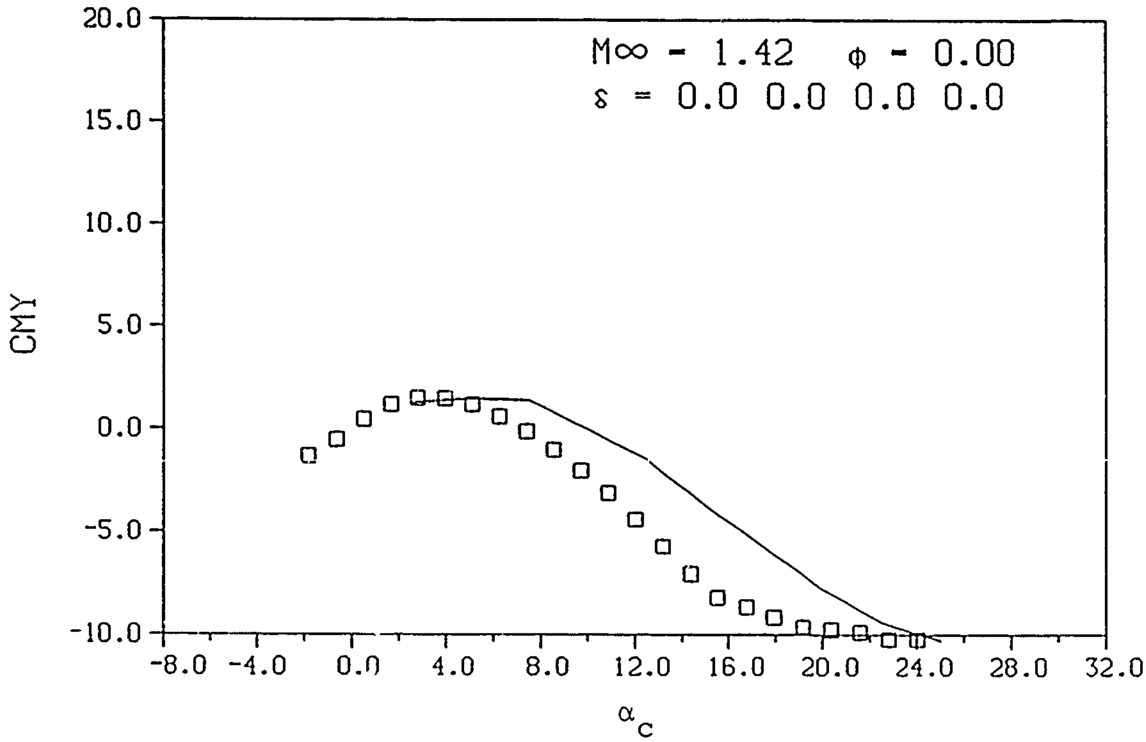

(c) M_∞ = 1.42, ϕ = 0°

Figure 39.- Continued.

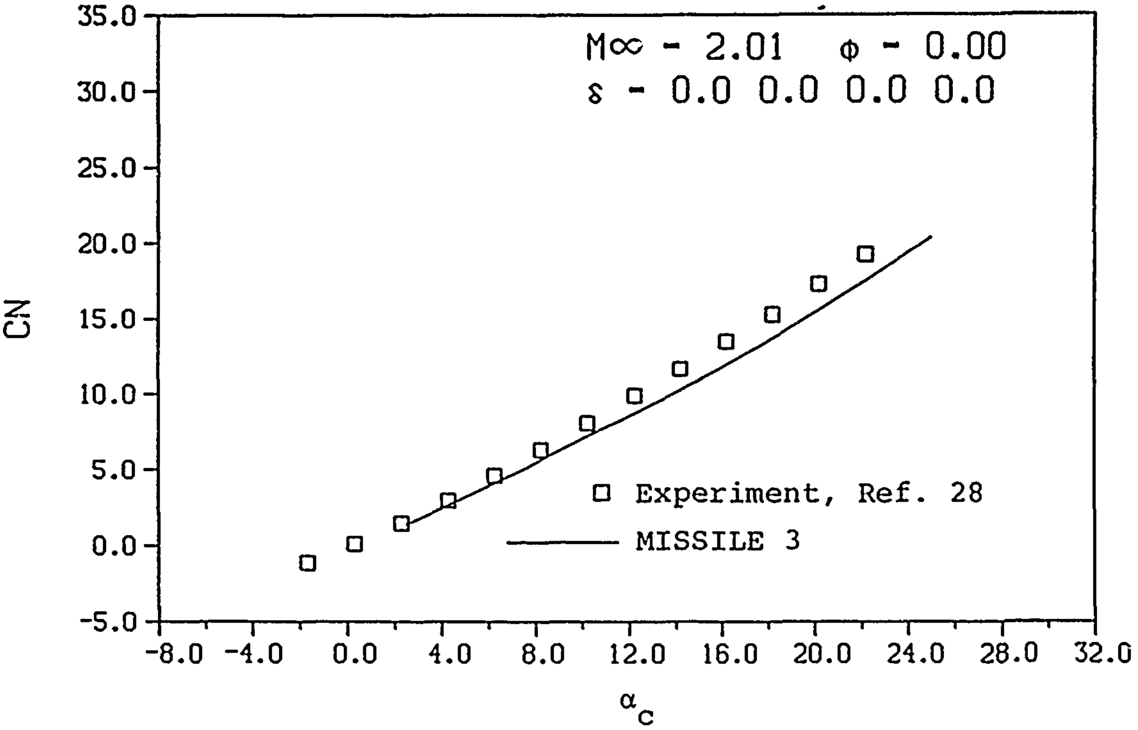

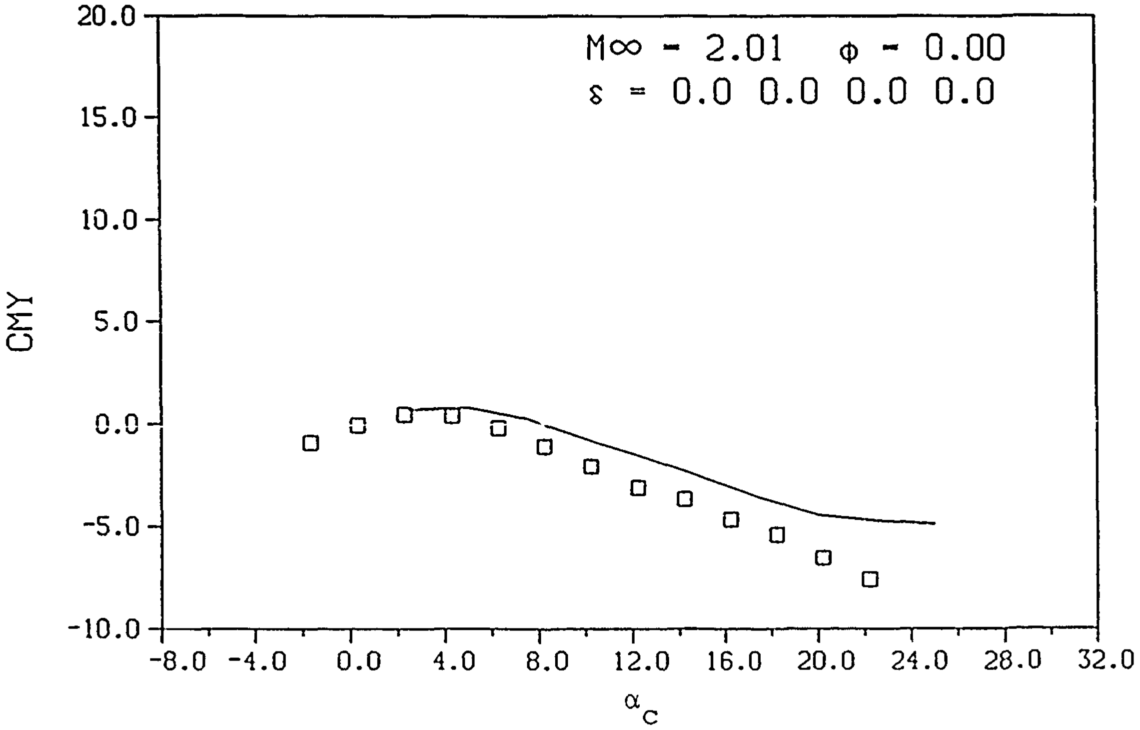

(d) $M_{\infty} = 2.01$, $\phi = 0°$

Figure 39.- Continued.

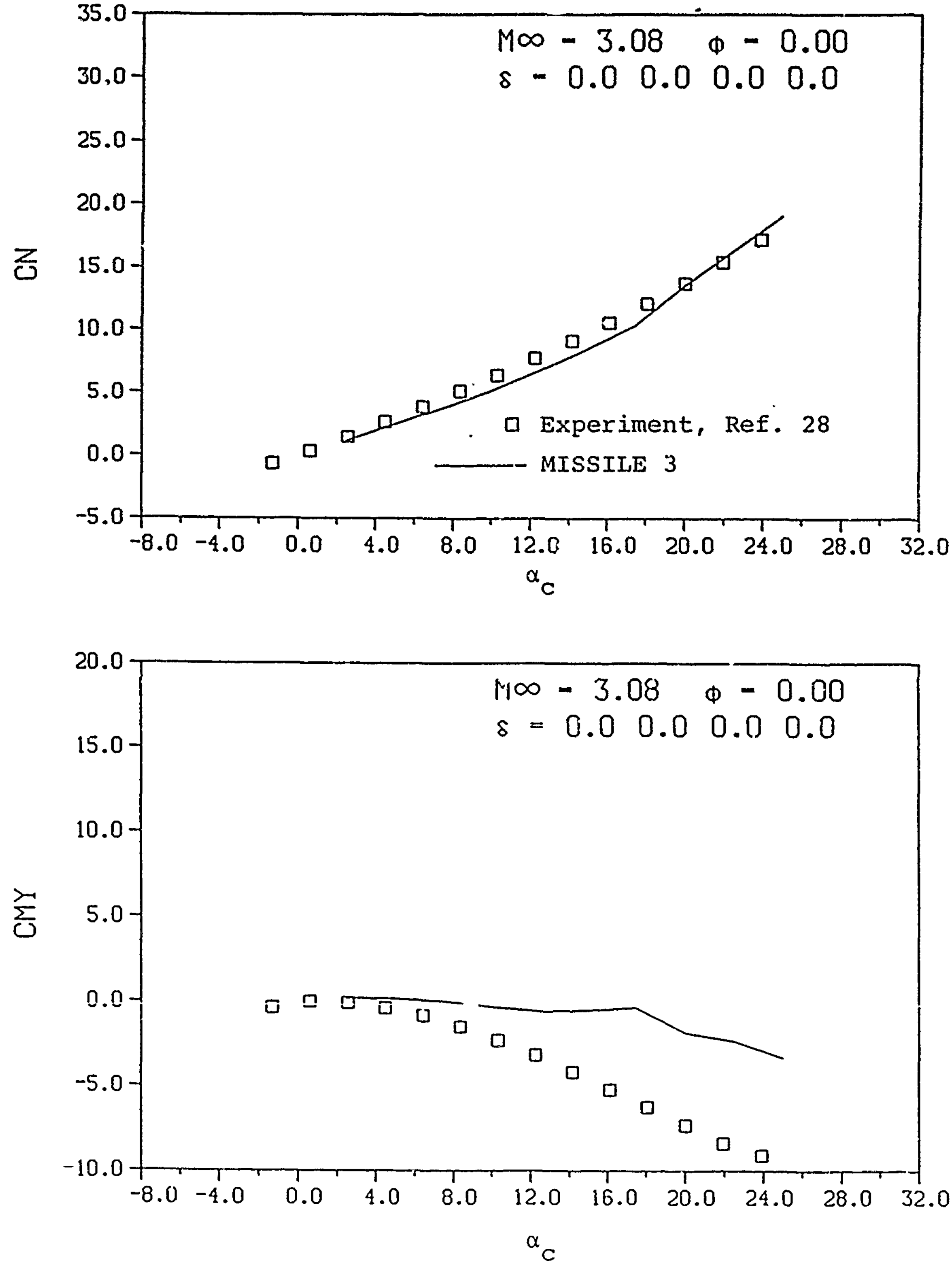

(e) $M_\infty = 3.08$, $\phi = 0°$

Figure 39.- Concluded.

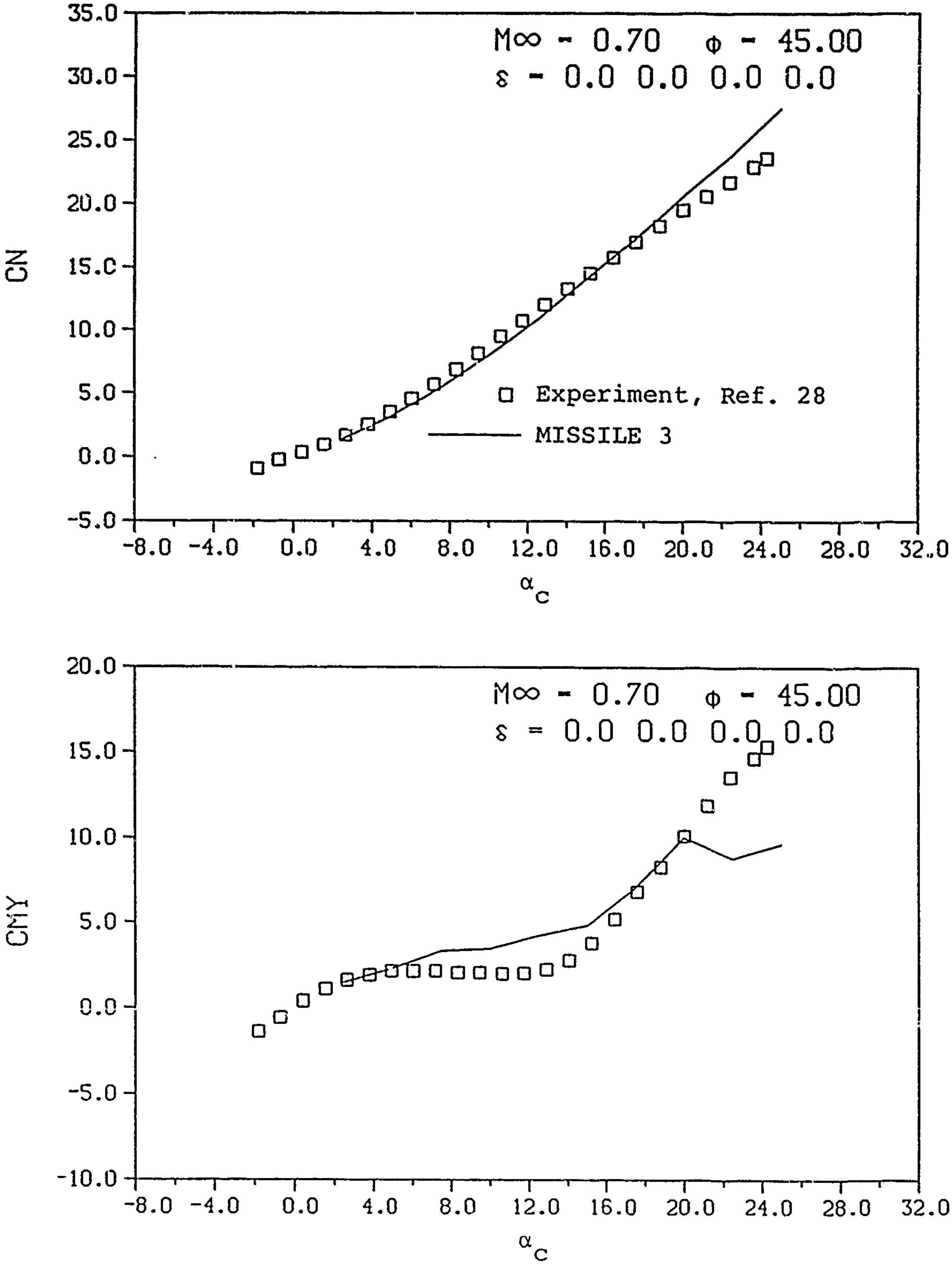

(a) $M_\infty = 0.7$, $\phi = 45°$

Figure 40.- Comparison of predicted and measured aerodynamic characteristics for the canard-body-tail model in Reference 28.

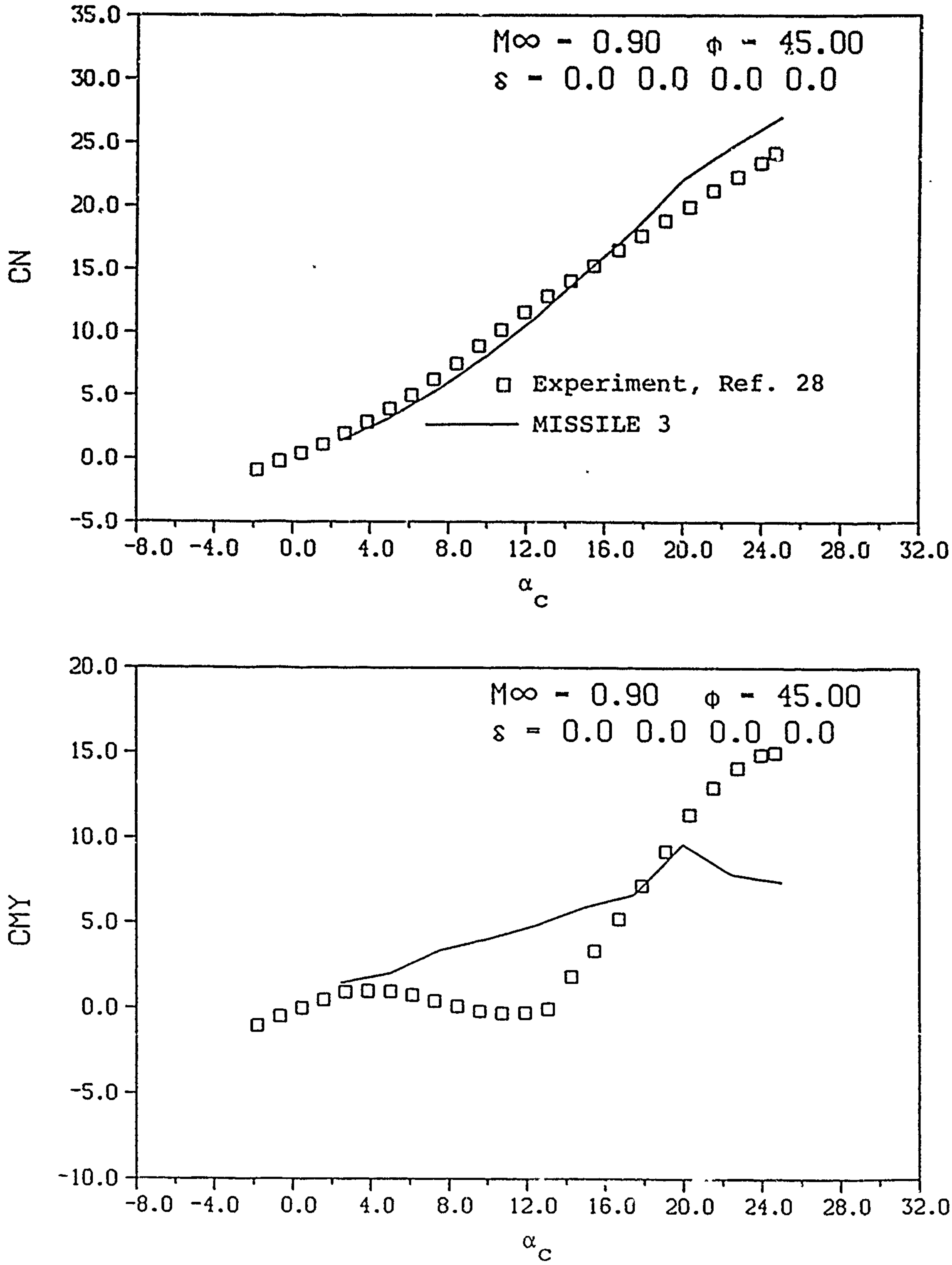

(b) $M_\infty = 0.9$, $\phi = 45°$

Figure 40.-- Continued.

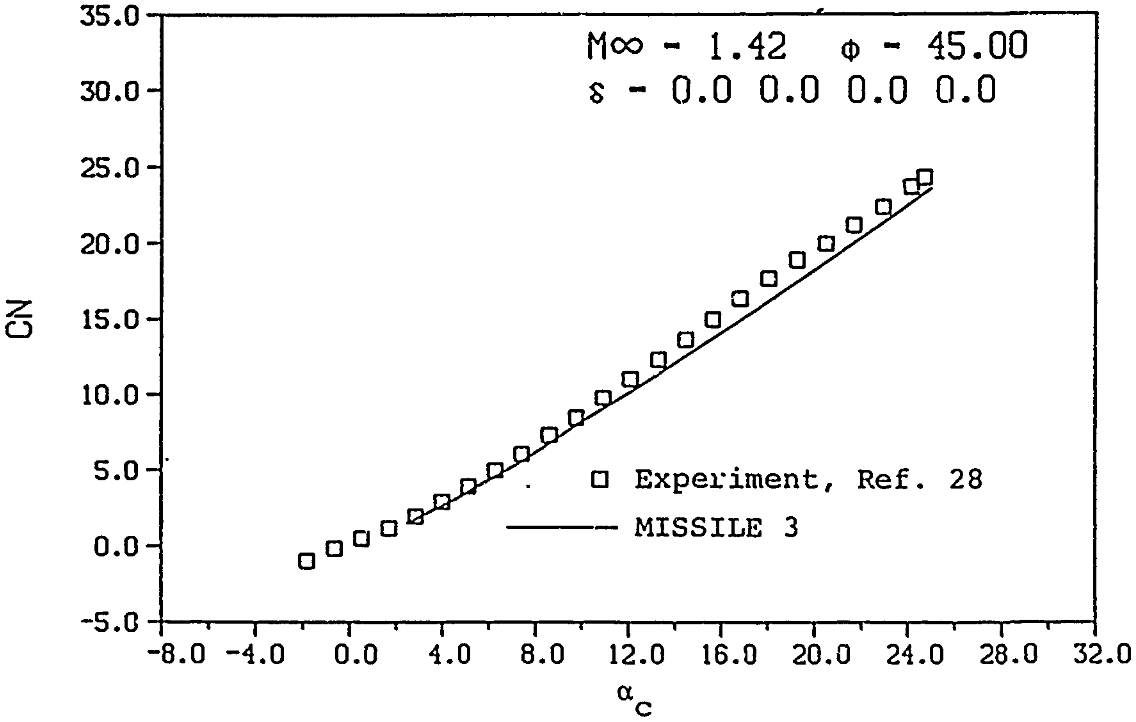

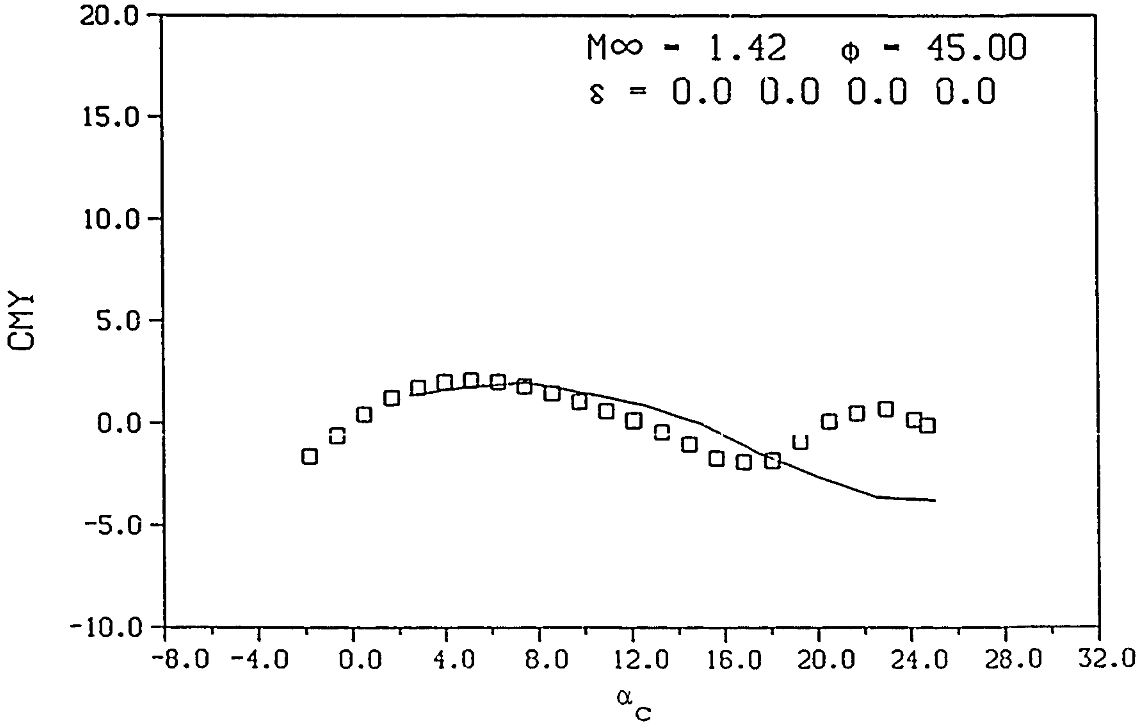

(c) $M_\infty = 1.42$, $\phi = 45°$

Figure 40.- Continued.

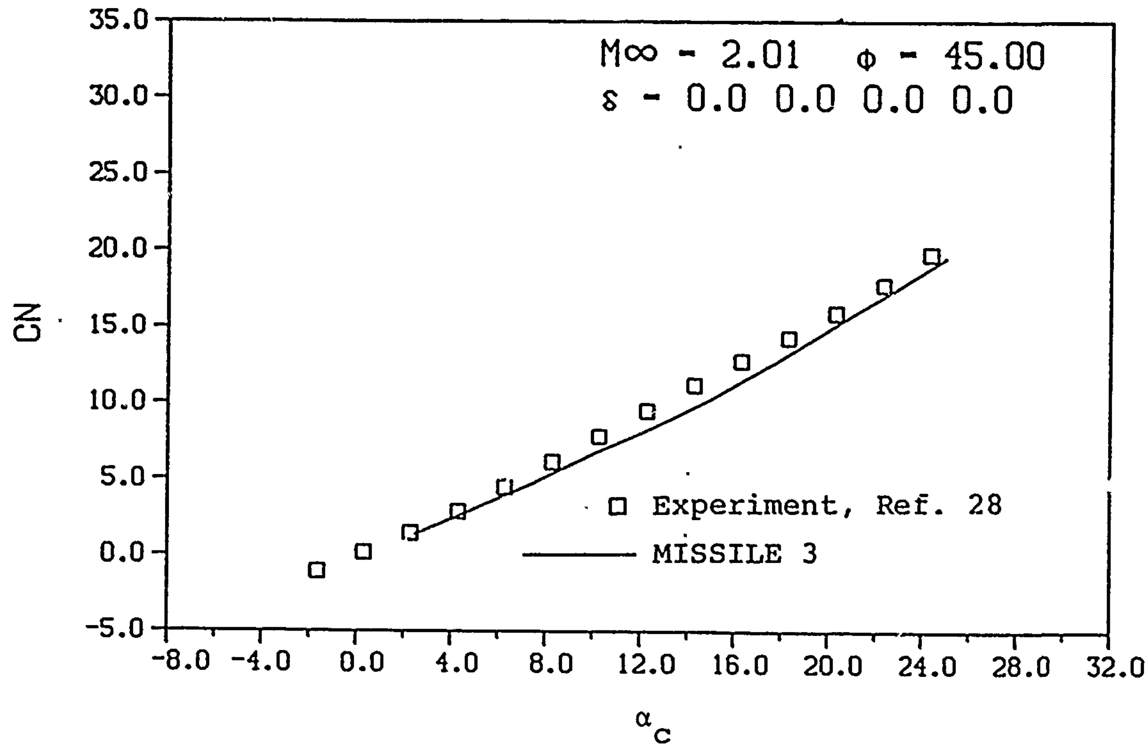

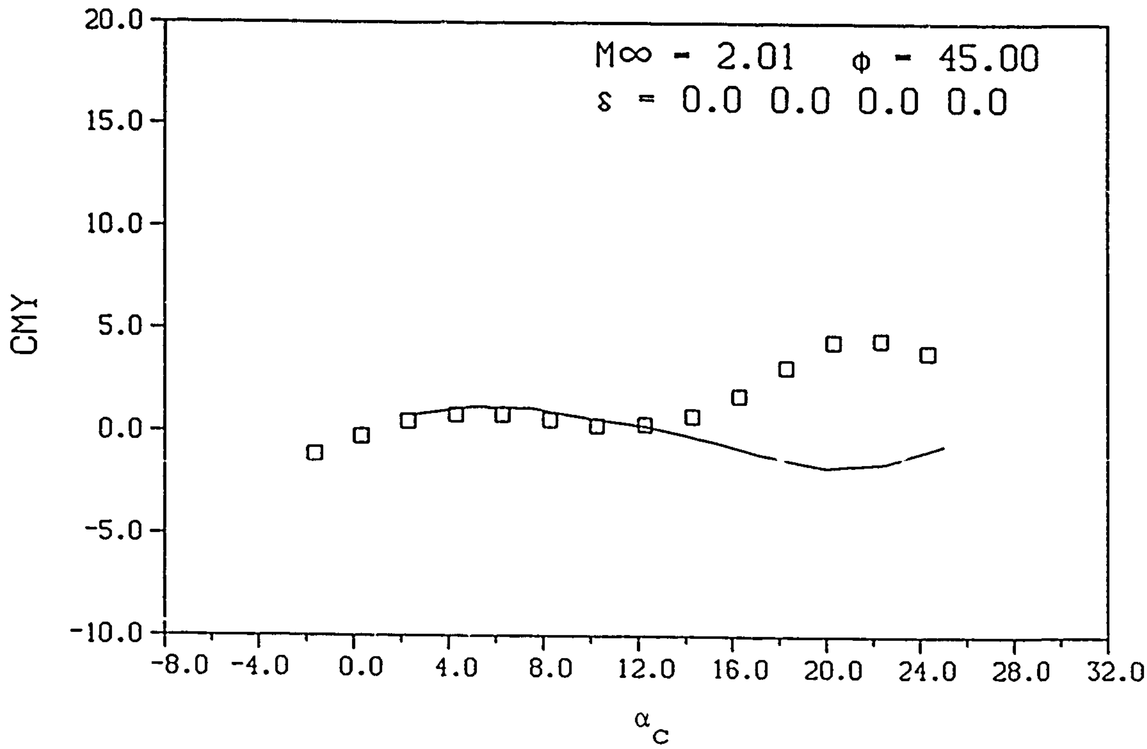

(d) $M_\infty = 2.01$, $\phi = 45°$

Figure 40.- Continued.

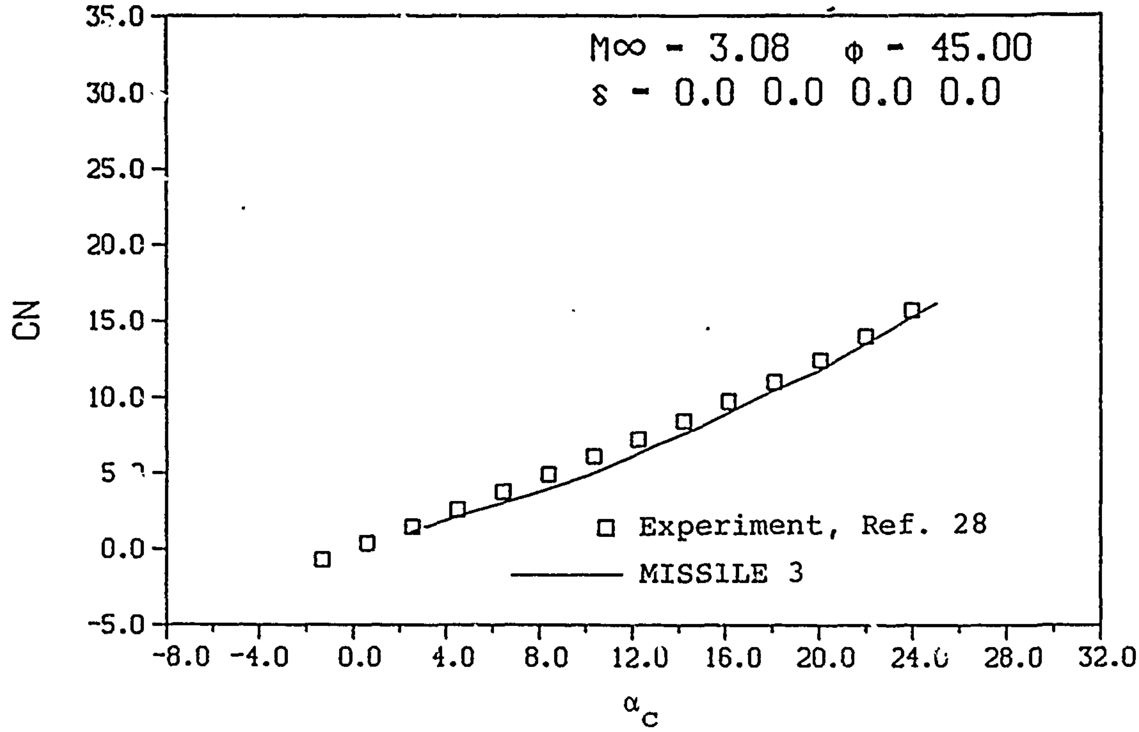

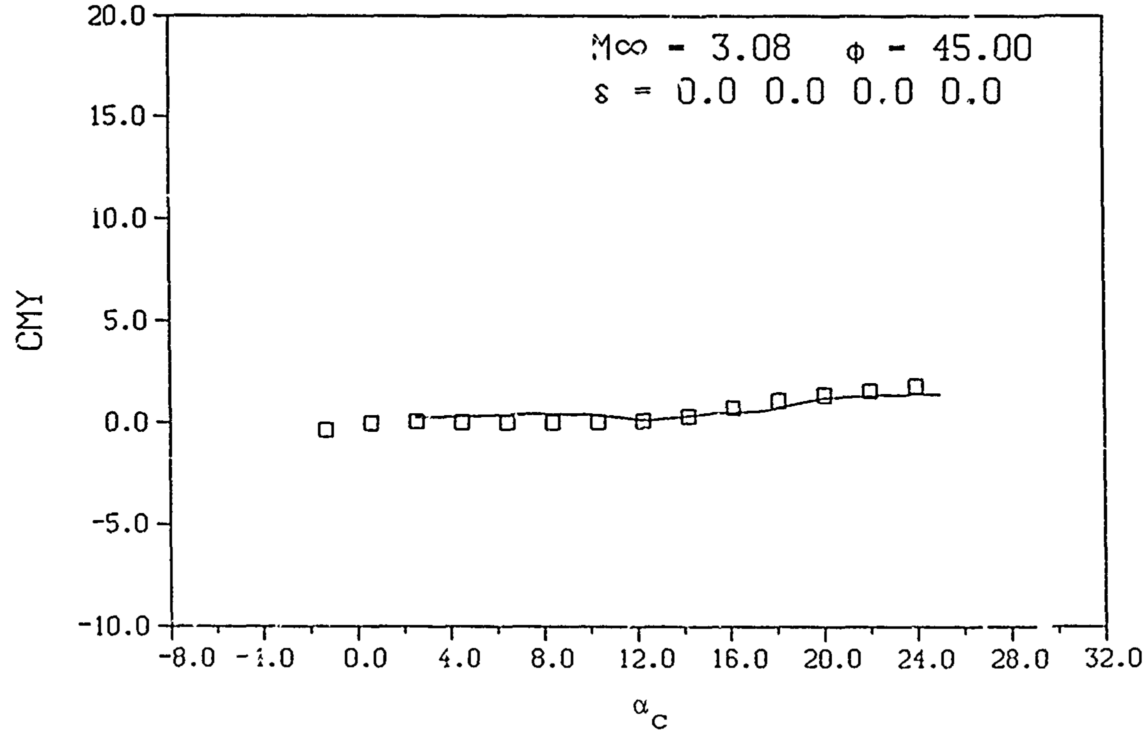

(e) $M_\infty = 3.08$, $\phi = 45°$

Figure 40.- Concluded.

APPENDIX A

Local Mach Number and Dynamic Pressure Correction

A body at angle of attack in which the crossflow Mach number, $M_\infty \sin \alpha_C$, exceeds unity experiences regions of flow where local conditions are very different from freestream conditions. For example, the presence of a bow shock wave can significantly alter local Mach numbers and dynamic pressures; therefore, a method incorporating the equivalent angle of attack approach which relies on wing alone aerodynamic characteristics in a uniform freestream requires a correction of the referenced flow conditions to account for the local flow conditions seen by the fins on the body. More detailed descriptions of this phenomena are presented in References A1 and A2.

A correction for local dynamic pressure and Mach number effects is implemented using predicted velocity components, densities, ar pressures from an Euler code. The velocity components u, v, and w, the density, ρ, and the pressure, p, are determined around a body using program SWINT. The body consists of a 3-caliber ogive nose followed by a long cylindrical section, and the flow field properties are investigated 10 diameters aft of the nose section. The following dimensionless variables are defined

$$\text{dimensions} \qquad \tilde{x} = x/l \;,\; \tilde{r} = r/l \;,\; \tilde{\phi} = \phi \qquad \text{(A1)}$$

$$\text{axial velocity} \qquad \tilde{w} = \frac{w}{U_\infty \cos\alpha} \qquad \text{(A2)}$$

(A1) Hemsch, M. J. and Nielsen J. N.: Triservice Program for Extending Missile Aerodynamics Data Base and Prediction Program Using Rational Modeling. Interim Report for Period June 18, 1982 to June 15, 1983. NEAR TR 305, Aug., 1983.

lateral velocities $\tilde{u} = \frac{u}{U_\infty \sin\alpha}$ (A3)

$$\tilde{v} = \frac{v}{U_\infty \sin\alpha} \quad \text{(A4)}$$

density $\tilde{\rho} = \rho/\rho_\infty$ (A5)

pressure $\tilde{p} = \frac{p}{\rho_\infty U_\infty^2 \sin^2\alpha}$ (A6)

Note that $\tilde{u}$, $\tilde{v}$, $\tilde{w}$, $\tilde{\rho}$, and $\tilde{p}$ are equal at corresponding points in the flow field $(\tilde{x},\tilde{r},\tilde{\phi})$ if the parameters $k_1 = \delta\cot\alpha$ and $k_2 = M_\infty \sin\alpha$ have the same values at the points. For a long (infinite) swept cylinder, $k_1 \rightarrow 0$, $\tilde{x} \rightarrow \infty$, and all of the dimensionless variables become functions of $M_\infty \sin\alpha$ only.

Considering the pressure equation, since $U_\infty^2 = M_\infty^2 \gamma p_\infty/\rho_\infty$ for isentropic flow, Equation (A6) can be written as

$$\tilde{p} = \frac{p}{\gamma p_\infty M_\infty^2 \sin^2\alpha} \quad \text{(A7)}$$

or

$$p^* = \frac{p}{p_\infty} = \gamma\tilde{p}\ M_\infty^2 \sin^2\alpha \quad \text{(A8)}$$

Since $\tilde{p} = \tilde{p}(M_\infty \sin\alpha)$ for $k_1 \rightarrow 0$, $\tilde{x} \rightarrow \infty$, Equation (A8) has the form

$$p^* = \frac{p}{p_\infty} = f(M_\infty \sin\alpha) \quad \text{(A9)}$$

(A2) Hemsch, M. J., and Mullen, J., Jr.: Analytical Extension of the MISSILE 1 and MISSILE 2 Computer Programs, March 1982, NEAR TR 272.

The normalized dynamic pressure is

$$\frac{q}{q_\infty} = \frac{\rho}{\rho_\infty}\left[\left(\frac{u}{U_\infty}\right)^2 + \left(\frac{v}{U_\infty}\right)^2 + \left(\frac{w}{U_\infty}\right)^2\right] \tag{A10}$$

Substituting Equations (A2) - (A5) into (A10) yields

$$\frac{q}{q_\infty} = \tilde{\rho}\left[\sin^2\alpha(\tilde{u}^2 + \tilde{v}^2) + \cos^2\alpha(\tilde{w}^2)\right] \tag{A11}$$

The average local dynamic pressure at a given ϕ is obtain by integrating Equation (A11) over the exposed span and dividing by the exposed span length; therefore,

$$\frac{\bar{q}}{q_\infty} = \frac{\sin^2\alpha}{s_m - a}\int_a^{s_m}\tilde{\rho}(\tilde{u}^2 + \tilde{v}^2)\,dt + \frac{\cos^2\alpha}{s_m - a}\int_a^{s_m}\tilde{\rho}(\tilde{w}^2)\,dt \tag{A12}$$

The normalized Mach number can be expressed as

$$\left(\frac{M}{M_\infty}\right)^2 = \frac{u^2 + v^2 + w^2}{\gamma p/\rho} \cdot \frac{\gamma p_\infty/\rho_\infty}{U_\infty^2}$$

$$= \frac{\rho/\rho_\infty}{p/p_\infty}\left[\left(\frac{u}{U_\infty}\right)^2 + \left(\frac{v}{U_\infty}\right)^2 + \left(\frac{w}{U_\infty}\right)^2\right] \tag{A13}$$

Substituting Equations (A2) - (A5) into (A13) yields

$$\left(\frac{M}{M_\infty}\right)^2 = \frac{\tilde{\rho}}{p^*}\left[\sin^2\alpha(\tilde{u}^2 + \tilde{v}^2) + \cos^2\alpha(\tilde{w}^2)\right] \tag{A14}$$

The average local squared Mach number is

$$\overline{\left(\frac{M}{M_\infty}\right)^2} = \frac{\sin^2\alpha}{s_m - a}\int_a^{s_m}\frac{\tilde{\rho}}{p^*}(\tilde{u}^2 + \tilde{v}^2)\,dt + \frac{\cos^2\alpha}{s_m - a}\int_a^{s_m}\frac{\tilde{\rho}}{p^*}(\tilde{w}^2)\,dt \tag{A15}$$

Note that Equation (A15) gives the average M^2 not the square of $\bar{M}$.

The following coefficients are defined for use of the SWINT-generated data base at x/D = 10.

$$A(\tilde{r},\tilde{\phi},M_\infty \sin\alpha) \equiv \tilde{\rho}(\tilde{u}^2 + \tilde{v}^2) \tag{A16}$$

$$B(\tilde{r},\tilde{\phi},M_\infty \sin\alpha) \equiv \tilde{\rho}\tilde{w}^2 \tag{A17}$$

$$C(\tilde{r},\tilde{\phi},M_\infty \sin\alpha) \equiv A/p^* \tag{A18}$$

$$D(\tilde{r},\tilde{\phi},M_\infty \sin\alpha) \equiv B/p^* \tag{A19}$$

The average values integrated over the fin span are

$$\bar{A}(a/s_m,\tilde{\phi},M_\infty \sin\alpha) \equiv \frac{1}{s_m - a}\int_a^{s_m} A(\tilde{r},\tilde{\phi},M_\infty \sin\alpha)\,d\tilde{r} \tag{A20}$$

$$\bar{B}(a/s_m,\tilde{\phi},M_\infty \sin\alpha) \equiv \frac{1}{s_m - a}\int_a^{s_m} B(\tilde{r},\tilde{\phi},M_\infty \sin\alpha)\,d\tilde{r} \tag{A21}$$

$$\bar{C}(a/s_m,\tilde{\phi},M_\infty \sin\alpha) \equiv \frac{1}{s_m - a}\int_a^{s_m} C(\tilde{r},\tilde{\phi},M_\infty \sin\alpha)\,d\tilde{r} \tag{A22}$$

$$\bar{D}(a/s_m,\tilde{\phi},M_\infty \sin\alpha) \equiv \frac{1}{s_m - a}\int_a^{s_m} D(\tilde{r},\tilde{\phi},M_\infty \sin\alpha)\,d\tilde{r} \tag{A23}$$

Using Equations (A20) - (A23), the local dynamic pressure and Mach number become

$$\frac{\bar{q}}{q_\infty} = \bar{A}\sin^2\alpha + \bar{B}\cos^2\alpha \tag{A24}$$

$$\left(\frac{\bar{M}}{M_\infty}\right)^2 \cong \overline{\left(\frac{M}{M_\infty}\right)^2} = \bar{C}\sin^2\alpha + \bar{D}\cos^2\alpha \tag{A25}$$

Tables of A, B, C, and D were created from SWINT results at x/d = 10 and the a/s_m in the data base for various crossflow Mach numbers greater than 1.0. These tables are included in MISSILE 3, and the average local dynamic pressure and Mach number are calculated from Equations (A24) and (A25), respectively.